THESIS

PHOTOSYNTHESIS IN DYNAMIC AND RAPIDLY CHANGING LIGHT: THE PHYSIOLOGY OF A CYANOBACTERIUM IN A PHOTOBIOREACTOR

Submitted by

Bjoern Andersson

Department of Biology

In partial fulfillment of the requirements

For the Degree of Master of Science

Colorado State University

Fort Collins, Colorado

Summer 2017

Master's Committee:

Advisor: Graham Peers

Marinus Pilon
Christie Peebles

ABSTRACT

PHOTOSYNTHESIS IN DYNAMIC AND RAPIDLY CHANGING LIGHT:
THE PHYSIOLOGY OF A CYANOBACTERIUM IN A PHOTOBIOREACTOR

Mass cultivation of aquatic phototrophs in photobioreactors (PBRs) has the potential to produce sustainable biofuels thus reducing net carbon emission and associated climate change. In order to make PBRs productive enough to be economically viable, the biomass accumulation rate and cell density at harvest needs to be high. However, early productivity estimates based on controlled laboratory experiments has not scaled-up to industrial size PBRs. One major reason is that the growth rates in high density, low maintenance PBRs is severely reduced compared to laboratory conditions. This is likely a consequence of the fluctuating light environment. The photophysiological response of algae or cyanobacteria to growth in outdoor PBRs has not been well characterized.

The work presented in this thesis aimed to describe the complexity of the light environment in a small-scale PBR and also the physiological response of photoautotrophs to growth in this environment. A dense culture of the cyanobacterium *Synechocystis* sp. PCC 6803 was grown in a bench-top PBR with an incident light that followed a sinusoidal function peaking at 2000 μmol photons m^{-2} s^{-1}. These conditions approximate natural sunlight. The diurnal changes in the light environment of the bench top PBR was quantified from the perspective of a single-cell, using a computational fluid dynamic approach (Chapter 1). Due to self-shading within the dense culture, single cells experienced rapid fluctuations (~6 s) between 2000 and <1 μmol photons m^{-2} s^{-1}, and on average the integrated irradiance per cell was 85% lower than the incident irradiance (mean per cell: 184 μmol photons m^{-2} s^{-1}).

We investigated the activity of photoprotective mechanisms under our realistic light environment, using pulse amplitude modulated (PAM) fluorometery and membrane inlet mass spectrometry (MIMS). Contrary to common assumption we found no evidence for net-photodamage or non-photochemical quenching (NPQ) activity *in situ* (Chapter 1). In an *ex situ* experiment we found that alternative electron transport (AET) dissipated 50% of electrons from photosystem II, preventing them from being used for carbon fixation. This indicates that AET, and not NPQ is the first photoprotective mechanism *Synechocystis* uses under dynamic and fluctuating light. These results have important applications for genetic and metabolic engineering strategies that commonly targets NPQ and photodamage as a way to boost productivity of PBRs. Since, AET caused the main diversion from linear electron transport and carbon fixation, this mechanism should be investigated as a genetic engineering strategy.

Samples were also taken to monitor the response of the transcriptome with high temporal precision around the day/night transitions (Chapter 2). The transcriptome data showed that 74% of all genes exhibited some modification in transcription across the diel cycle. In my preliminary analysis of the data (Chapter 2), I found that the major components of photosynthetic light harvesting and electron transport complexes increased in abundance during the whole light period. This is commonly observed in cultures growth under sub-saturating light intensities but not high light stress. Furthermore, few other high light stress responses were observed in the transcriptome. There was little diel variation in transcriptional activity of molecular chaperones (dnaK, hsp, groE families), proteases (ftsH and Deg families), high light inducible proteins (hli), and reactive oxygen species scavengers (superoxide dismutase and catalase peroxidase) that are responsive to high light stress. The flavodiiron proteins are considered the main player of AET in cyanobacteria and are up-regulated transcriptionally under light and inorganic carbon stress. Interestingly, there were

no increased abundance in transcripts of the flavodiiron proteins during the light period in my experiment. Assuming that transcript abundance correlates with protein abundance this could mean that either these genes are constituently expressed or that other enzymes may exist that are responsible for the AET. Further analysis of the transcriptomic data and future proteomic analysis may uncover putative genes whose transcriptional pattern indicates that they may play a role in AET under fluctuating light.

ACKNOWLEDGMENTS

To begin with I would like to thank my family for all the support throughout my two years at Colorado State University (CSU). My two daughters, June and Nina, constantly remind me that there are other important things in life besides science, believe it or not. Love from children is unconditional and boundless and the greatest antidote for stress and self-absorption. I am ever grateful to my wife and life companion Ellen for her inexhaustible support and patience. My parents and brothers in Sweden whom has supported me through my life journey. My in-laws, who drove from Nashville to Fort Collins to meet us at the airport and make sure we had a roof over our head when we landed at DIA with 10 suitcases, a four-month old, a two-year old, and 8 hours' jetlag.

My advisor Graham Peers who has been incredible generous and supportive throughout my time in his lab. Graham does not like to give you answers or instructions but pushes you seek them out for yourself. This has made me a far more independent and competent investigator today than I thought I would be at this point in my career. I also like to thank my committee members for excellent feedback and comments on my research and writing throughout the program.

The help and advised from all the students and researchers at the Peers lab has been instrumental to my achievements. Denis Jallet, who is an expert on *Synechocystis* photophysiology, taught me how to first make cultures happy and then probe them to death. Alexander Hughes, Michael A. Caballero and Michael Cantrell for assistance, advice and critical reviewing during the preparation of this thesis. David Xing for developing RNA extraction protocols and giving advice on next-generation sequencing. Our lab manager Annah Holmberg for logistical support and making 100's of liters of growth media for me. Gus Waneka helped develop microscopy and Image J protocol to measure cell sizes and he

also assisted in characterizations of the DrgA mutant in Appendix G. Prior students, Lauren F. Cole and Matthew T. Youngblood who clone the DrgA disruption vectors and did preliminary work on the mutant. Mark Layer, who is a computer wizard, wrote the fluctuating light scripts for the PAM and helped circumvent computational problems and assisted in data handling. Michael Olsen, our local glassblower, made and repaired the quartz cuvettes and the ePBR culture vessels without which I could not have conducted my research.

I came to CSU on a Fulbright scholarship and without the support of their staff throughout the application process I would probably not have made it here. I am thankful to all the staff at the office in Stockholm as well as the Institute of International Education in Denver. I am thankful to the National Science Foundation for funding me through graduate school and my research expenses. I received additional generous funding from the American-Scandinavian Foundation and Sixten Gemzeus Stiftels in Sweden, without which I would probably been forced to live in a trailer. I am also grateful to the Child Care Access Means Parents in School Program (CCAMPIS) and its employees at CSU for giving me access to affordable childcare. Lastly I would like to add that both Fulbright and the CCAMPIS program faces deep funding cuts under the current administration in Washington. I sincerely hope that this will not go into effect as they are doing wonderful work in the interest of all American citizens, not only us who benefited directly from them.

Last but not least, I would like to acknowledge the people at CSU who have contributed directly to the work presented in this thesis. Chen Shen and David S. Dandy at the Department of Chemical and Biological Engineering developed the computational fluid dynamic simulations. Michael Cantrell in the Peers lab spent countless hours setting up the membrane-inlet mass spectrometer and assisted me in collecting data using this machine. Wen Zhou at the Statistical Department guided me in establishing the system biology sampling strategy and will continue to develop statistical tools to mine the data. Seijin Park

and Kenneth F. Reardon at the Department of Chemical and Biological Engineering did a proteomic analysis that unfortunately is not yet completed but will be a valuable complement to the transcriptomic data. Many thanks and it has been a pleasure to work with all of you.

TABLE OF CONTENTS

GENERAL INTRODUCTION

1. Renewable Energy and the Next Generation of Biofuels

With many of the predicted effects of global climate change already upon us, there is an urgent need to rapidly develop net carbon-emission free energy sources. The Intergovernmental Panel on Climate Change (IPCC) has established an average global temperature increase of 0.85 C˚ since the pre-industrial era (Pachauri et al. 2014). This change has been linked to rising sea-level, melting of polar ice, changes in weather patterns, fisheries, agriculture, drought, etc., in hundreds of publications (Challinor et al. 2014; Parmesan et al. 2013; Poloczanska et al. 2013). According to the latest IPCC report published in 2014, we will experience a further warming of the planet in the range of 1.15 C˚ to 4 C˚ by the year 2100. The variable scenarios depends primarily on how much additional fossilized carbon will be released into the atmosphere (Pachauri et al. 2014). Climate change has the potential to cause the largest mass-migration in human history as individual countries or entire regions become subjected to food- and water insecurity as well as flooding. The only way to mitigate the worst-case-scenario of future climate change is to significantly cut back global greenhouse gas emissions. To accomplish this, we will have to find ways to rapidly reduce our dependence on fossil sources of fuels and energy.

To break our dependence on fossil energy we need to develop and expand renewable energy sources. The global demand for energy will increase throughout the 21st century as a consequence of increasing living standards in developing countries and population growth. In 2012, more than 80% of global energy production came from fossil sources, including oil, coal and natural gas (Bilgen 2014). Renewables energy accounted for only 2% of global energy production then, and Bilgen (2014) estimated that under a business-as-usual model this fraction will only increase to around 4% by the year 2040. However, there

is room for improvement of the current state-of-the-art production of renewable energy, and both solar and wind derived electricity are growing exponentially (Devabhaktuni et al. 2013; Pérez-Collazo et al. 2015). Given proper economic incentives and further allocations of funds towards research and development of these renewable energy sources, we have the capacity to greatly reduce the amount of energy that is derived from fossil sources today.

Biofuels form the backbone of an effort to reduce greenhouse gas emissions from liquid fuels. Although commercial production of ethanol and biodiesel from crop plants is established in a long list of countries, there are severe limitations in their scalability and effectiveness in combatting climate change. Production is severely restricted due to land-use competition with food crops and increasingly fragmented and vulnerable ecosystems (Pienkos and Darzins 2009). Moreover the release of dinitrogen oxide (N_2O), a potent greenhouse gas, during cultivation of the feedstock crops may offset any mitigating effect on climate change (Crutzen et al. 2016). Biofuel production from woody or other non-crop plant sources has therefore been explored and considerable success in chemical conversion of lignin and cellulose to biodiesel or ethanol has been achieved (Azadi et al. 2013; Han et al. 2014). These strategies broaden the feedstock spectrum of biofuel to include forestry by-products and expand the range of suitable crop-species, but ultimately land use competition with food crops and wildlife still cap scalability.

Using phototrophic microorganisms as a feedstock for biofuel has been suggested as a scalable alternative to plants and could form the backbone of the next-generation of biofuels (Nigam and Singh 2011).The potential of mass cultivation of microbial phototrophs was proposed as early as 1955 (Meier 1955) and research into production of biofuels and other chemical products have been conducted for several decades [see reviews by: (Hu et al. 2008; Pienkos and Darzins 2009)]. The use of microalgae and cyanobacteria for the production of biofuels holds great promise due to their rapid growth (Pienkos and Darzins

2009). In contrast to terrestrial crops, which generally require a growth season to yield biomass, many microalgae and cyanobacteria species can more than quadruple their biomass over the course of one day, given optimal growth conditions (Griffiths and Harrison 2009). Although mass cultivation of microbial autotrophs is aquatic, water can be recycled enabling cultivation in arid climate zones. Brackish to full saline water can also be used for cultivation depending on the species of microbial autotroph (Wijffels and Barbosa 2010). This expands the range of climate zones suitable for production beyond that of terrestrial plants. Consequently, mass cultivation of microbial autotroph using today's technology has the capacity to produce 30% of the global transportation sectors fuel, using between 2 and 50% of non-arable land depending on which continent is being considered (Moody et al. 2014).

The application of photoautotrophs to biofuel production has been hampered by a lack of scalability and productivity rates based on laboratory experiments do not scale to outdoor mass cultivation (Grobbelaar 2012). This has several reasons, including a slow growth rate in mass cultivation, culture crashes due to viral and bacterial infection, and zooplankton predation, to name a few. The time it takes a culture to double its biomass (doubling time) is often increased from 4-12 h under laboratory conditions to several days in dense, large-scale outdoor cultivation (Brennan and Owende 2010). In addition to slow growth, the biomass rarely makes up more than 1 to 5% (w/w) of the mature culture (Brennan and Owende 2010) necessitating elaborate and expensive dewatering processes (Pienkos and Darzins 2009). It is also difficult to optimize harvesting density with high quality biomass, which reduces the efficiency of the chemical conversion process (Chisti 2007; Hu et al. 2008). Contamination of zooplankton grazers can also reduce productivity and cause cultures to collapse (Mehrabadi et al. 2016). Ultimately, the slow growth rate and other production issues has non-linear effects on the overall cost of production, which translate into a final biodiesel product that currently costs 15 USD per gallon to produce (Mu et al. 2017). Considerable

research efforts have been invested into solving many of these problems including ways to increase productivity of dense cultures of algae and cyanobacteria. Yet we still understand very little about the biological mechanisms that are responsible for the retardation of growth rates.

2. Photobioreactor Design and Their Light Environments

There is currently no consensus on the most efficient design of large scale mass cultivation systems. Current systems can be roughly divided into three main design categories: 1) raceway ponds consisting of a shallow (~30 cm) elliptical circuit (up to 1 km long) mixed by a single paddle wheel (Chisti 2016), 2) thin layer cascades consisting of a series of sloping steps where the suspension flows relatively fast maintaining a depth of only a few millimeters (Masojidek et al. 2011), or 3) closed vessels of various shapes, collectively termed photobioreactors [PBRs; (Posten 2009)]. PBRs have been made in a wide variety of geometrical designs with the main goal of reducing energy and maintenance costs while maximizing the productivity of the microalgae or cyanobacteria. Common designs include tubes, flat panels and cylindrical airlift reactors (Posten 2009), but more creative and complex methods of internal illumination using LEDs or mirrors are being explored (Hu and Sato 2017; Iluz and Abu-Ghosh 2016). Thin layer cascade and very thin flat panel reactors, which have been designed with minimal fluctuations in light, have yielded the highest growth rates and the densest cultures so far (Masojidek et al. 2011; Masojidek et al. 2003), suggesting that light fluctuations causes major reduction in productivity. However, these culture conditions carry high maintenance cost, are prone to contamination, have high evaporation rates, and are hard to scale-up for industrial size production. Hence closed PBRs or open raceway ponds are more commonly used for industrial applications (see review by (Brennan and Owende 2010)).

All closed PBRs and raceway ponds create a highly variable light environment. In closed PBRs light penetrates only a few millimeters to centimeters into the dense culture,

and any scalable PBR will contain dark zones, gradients of light, and fully illuminated zones. The ratio between these zones is dictated by the surface to volume area, and engineers strive to design PBRs with large surface to volume ratios while keeping energy and maintenance costs low (Posten 2009). Another goal of PBR design has been to apply the maximum amount of mixing to increase the frequency of light/dark (L/D) oscillations under the assumption that this will boost productivity (Posten 2009). Some mixing is required to maintain gas equilibrium and prevent limitation of inorganic carbon or hyper- and hypoxia, which affects photosynthesis negatively.

For the production of sustainable biofuel especially, cells cannot be grown under artificial light since it requires more energy than it produces. Consequently, light energy has to be supplied by the sun. In addition to the fluctuations in light cells experience due to self-shading, there will be changes in the surface irradiance that are stochastic (cloud coverage and shading) or cyclical (seasonal and diurnal). One drawback of outdoor cultivation is that the light intensity cannot be controlled or optimized and will surpass the saturation point of photosynthesis, potentially causing photodamage. Photosynthetic responses to PBR growth are described in more detail in section 3 and 4. Briefly, photosynthesis in aquatic autotrophs commonly saturates at <25% the intensity of full sunlight (Macintyre et al. 2002). Consequently, the other 75% have to be dissipated in order to prevent photodamage. Due to the irregular light environment of PBRs it is thought that the cells cannot properly regulate these mechanisms resulting in either excess dissipation of light or photodamage (Posten 2009). However, the compounded complexity of variation in sun light and self-shading within PBRs has seldom been quantified and its biological effect on algae or cyanobacteria has rarely been studied.

There are mathematical frameworks that can be used to predict the light environment experienced by individual cells in PBRs. Computational fluid dynamics (CFD)

is a powerful numerical tool that can predict shear forces, mixing regimes and movement of particles in liquid or gas phase. CFD relies primarily on the Navier-Stokes equation, which accounts for velocity, pressure, temperature, density of a liquid or gas, and the effects of viscosity on flow (Hutmacher and Singh 2008). From this foundation additional chemical and physical parameters can be added depending on the research question. Originally developed for aerodynamic engineering (Jameson 1995), CFD technology is now applied to a wide variaty of industrial fields, including development of food and agricultural ventilation systems (Norton and Sun 2006) and heating/cooling systems (Patel et al. 2001). CFD simulations can also be used to address biological questions. CFD has been used to predict oxygen diffusion rates in aerobic bio-reactors (Dhanasekharan et al. 2005), the impact of shear forces on delicate human tissues grown in bio-reactors (Hutmacher and Singh 2008), and to predict cardiovascular flow (Morris et al. 2016).

Computational fluid dynamics has also been applied to optimize the design of PBRs (Barbosa et al. 2003; Huang et al. 2015; Perner-Nochta and Posten 2007). CFD enables engineers to design and test different geometrical shapes of PBRs and raceway ponds *in silico* before conducting costly large-scale experiments. This process can be applied to make predictions about the effectiveness of gas sparging, the potential shear-force damage to cells, and the mixing effects of different pumps and stirring regimes. [see review by: (Bitog et al. 2011)]. This approach can also be applied to understanding changes in light experienced by individual cells.

The light environment of PBRs is extremely complex due to self-shading within the culture and at industrially relevant densities almost all light is absorbed or scattered at a few mm distance from the illuminated surface. CFD has been used to predict the light history of single cells in PBRs, which as expected is highly variable depending on the geometrical shape of the reactors and the mechanical energy input (Barbosa et al. 2003; Huang et al. 2015;

Perner-Nochta and Posten 2007). Results from these studies indicate that, assuming binary light or dark areas, different reactors may create cell-specific Light/Dark (L/D) oscillations with frequencies spanning four orders of magnitude (10 to 0.01 s^{-1}).

Studies aimed at optimizing PBR through CFD modeling often assume that growth and photosynthetic kinetics observed under static light, or in Photosynthesis versus Irradiance curves (P-I curves), can be extrapolated to the PBRs fluctuating light environment. However, these parameters are often extracted from the literature and not investigated in tandem with the PBR investigated CFD model. PBRs are often divided into four biological light zones: 1) too dark for net-photosynthesis 2), linear response region to light, 3) high enough irradiances to saturate growth and photosynthesis, 4) high light regions where photodamage causes large reduction in photosynthetic capacity and growth (Merchuk and Wu 2003). Furthermore, engineers strive to maximize the frequency of L/D oscillations with the intent of creating what is known as the flashing light effect (Bitog et al. 2011; Hu and Sato 2017; Perner-Nochta and Posten 2007). This phenomenon will be discussed in detail in section 3, but briefly it is based on laboratory observations that growth rates under rapid L/D cycles may equal that of constant light under certain conditions (Nedbal et al. 1996; Sforza et al. 2012; Takache et al. 2015). However, as Bitog et al. (2011) pointed out there have been few collaborations between biologists and engineers to try and elucidate the metabolic and photophysiological effects of actual PBR light environments. At best, *in silico* CFD predictions are validated with growth rate observations of one species of microalgae or cyanobacteria (Barbosa et al. 2003; Huang et al. 2015). But, more often, the effect on productivity is only inferred (Moberg et al. 2012; Perner-Nochta and Posten 2007; Wu et al. 2009).

CFD simulations provide detailed information about the light environment experienced by individual cells in PBRs and offer an avenue to design experiments and

develop biological hypothesis. This information may provide a key to understanding the effects of PBR cultivation on photosynthesis and the biology of microalgae and cyanobacteria. However, this requires interdisciplinary collaboration between modelers and biologists to generate both accurate models of the light environment of PBRs and investigate its effect on photophysiology.

3. Photosynthetic Responses to Fluctuating Light

Microbial autotrophs, and their photosynthetic machinery have evolved under variable light. The photosynthetic process, which involves capturing the energy of a photon and using it to reduce inorganic compounds to generate organic matter, is an intricate process involving dozens of enzymes and cofactors. Light is captured primarily through peripheral antenna complexes (chl a/b containing light harvesting complexes in eukaryotes and phycobilisomes in cyanobacteria) and transferred to photosystem II (PSII) where charge separation occurs. During charge separation, an excited chl *a* molecule in PSII is used to reduce water, liberating a high energy electron. In linear electron transport, the free electron is then sequentially shuttled through plastoquinone, the cytochrome b_6/f complex, cytochrome c_6 (or plastocyanin in cyanobacteria), to photosystem I (PSI), generating an electrochemical gradient used for ATP synthesis. From PSI the electron is shuttled through ferredoxin and ferredoxin-$NADP^+$ oxidoreductase, and ultimately used to reduce $NADP^+$ to nicotinamide adenine dinucleotide phosphate (NADPH). ATP and NADPH is then used by the cell to, among other things, fix inorganic carbon in the Calvin-Bassham-Benson cycle (CBB cycle).

If the linear electron transport chain is saturated or blocked electrons may be trapped in PSII and cause formation of singlet oxygen and photodamage. Such a saturation or block will result in an over-reduction of the plastoquinone pool and acidification of the lumen through high H^+ translocation rates or low ATPase activity. Gene expression, protein regulation, and complex sensory and signaling pathways, queued by light receptors

(phytochromes), acidification of the lumen, and the redox state of the plastoquinone pool, interplay to avoid the formation of singlet oxygen and sequential reactive oxygen species that may cause cellular damage [see reviews by: (Foyer and Noctor 2009; Niyogi 2000; Woodson 2016)]. This has led to a highly responsive machinery that favors excessive absorption and dissipation of light over efficient utilization of light for photochemistry. This trait may make phototrophic autotrophs maladapted for efficient conversion of light energy into biomass given the rapidly fluctuating light environment of PBRs.

As described in Section 2, light fluctuates rapidly due to self-shading within the PBR and the mechanical mixing. Under outdoor conditions there is also a gradual increase/decrease in light intensities at dawn and dusk, and noon light intensities peak at irradiances much higher than most photosynthetic organism can utilize (Macintyre et al. 2002). Under supra-saturating light intensities, microbial autotrophs adapt their photosynthetic machinery over the course of hours to days by changing pigment composition (Schluter et al. 2006), reducing abundance of light harvesting complexes (Macintyre et al. 2002), exchanging the D1 protein of PSII to a homolog less susceptible to photodamage (Sicora et al. 2006), modifying the PSI/PSII ratio (Murakami 1997), and increasing the activity of the CBB cycle (Mettler et al. 2014). On shorter time scales, several rapidly inducing photoprotective mechanisms help dissipate excess light, including non-photochemical quenching (NPQ), state transitions, and modifications to linear electron flow [see review by: (Jallet et al. 2016b)]. Photosynthesis is therefore a highly dynamic and malleable process, making responses to complex light environments difficult to predict.

Photobioreactor engineers try to increase biological productivity of reactors by maximizing the frequency of L/D oscillations that individual cells are subjected to. The motive behind this is an assumption that growth rates will be increased through what is known as the flashing light effect (Bitog et al. 2011; Hu and Sato 2017; Perner-Nochta and

Posten 2007). The positive effect of fluctuation light on photosynthesis and net-growth depends on the frequency of oscillations and the intensity of the applied light and can be coarsely divided into two mechanisms. First, relatively long dark periods (seconds) allow for re-oxidation of the electron transport chain and regeneration of essential metabolites downstream of the PSI, particularly in the CBB cycle. Since intermediates in the CBB cycle may be rate limiting for photosynthesis (Mettler et al. 2014), short L/D oscillations allows growth to be maintained as under continuous light (Takache et al. 2015). By varying the frequency and duration of L/D periods of a square-wave, Takache et al. (2015) showed that growth kinetics could be maintained with dark periods up to 6 s per 12 s cycle in *Chlamydomonas reinhardtii*. A second mechanism becomes important at shorter timescales. Dark periods shorter than the slower step of linear electron transport, the reduction of the cytochrome b_6/f complex [3-5 ms; (Rochaix 2011)], have no direct impact on photosynthesis. This is because the relatively slow rate of cytochrome b_6/f reduction by plastoquinone will remain rate limiting for photosynthesis as long as dark periods are >5 ms. Under high light stress, with photosynthesis affected by photodamage and potential photoinhibition, these ms long dark periods will reduce the net amount of photons reaching the reaction center and consequently the amount of photodamage. This has been shown to increase net-growth by up to 20% in both cyanobacteria and algal species (Nedbal et al. 1996).

The flashing light effect has also been shown to impact productivity in a bench top PBR (Hu and Sato 2017; Katsuda et al. 2006; Park and Lee 2001; Sforza et al. 2012)]. However, the majority of these studies used monochromatic light of high intensity (500-2000 μmol photons m^{-2} s^{-1}), which preferentially targets the peak absorbance (Soret bands) of chlorophyll *a*. This light drives photosynthesis and photodamage much more efficiently than natural sunlight would. It also creates an environment where the cells may not be able to use all light receptors to tune gene expression and photosynthesis, since they are sensitive to

different wave-lengths of light (e.g. the Orange Carotenoid Protein, described in Section 4.5). Furthermore, none of these studies included a dark period corresponding to night or the gradual increase/decrease in irradiance associated with dusk and dawn, which oxygenic photosynthesis has evolved under for more than two billion years (Soo et al. 2017). Consequently, the relevance of the flashing light effect in scaled up mass cultivation conditions remains unknown. Recent studies have shown that, once acclimatized, neither the green algae *C. reinhardtii* nor the diatom *Phaeodactylum tricornutum* are susceptible to photodamage under sinusoidal white LED lights mimicking outdoor conditions (Cantrell and Peers in press; Jallet et al. 2016a). These findings not only challenge our current understanding of photosynthetic processes in PBRs, they invalidate the theoretical foundation of the photodamage driven part of the flashing light effect. Yet maximizing the frequency of flashing light has guided PBR design to date.

4. Metabolic Engineering of Photosynthesis as Means to Increase PBR Productivity

4.1. Mass cultivation Strategies

Metabolic engineering provides a strategy to increase productivity of existing PBRs without physical modification of the reactor. Given the difficulties designing scalable, low energy/cost PBRs with homogeneous light environments, production strains of microalgae or cyanobacteria could be adapted to variable light instead. However, the majority of metabolic engineering efforts so far have not focused on enhancing overall productivity of PBRs. Instead they aim to enhance production of specific compounds suitable for biofuel refinement, such as triacylglycerol (Tonon et al. 2002), hydrogen gas (Carrieri et al. 2008) or isoprenoids (Kudoh et al. 2014). Additional effort has been aimed at developing strains with elevated productivity of high value compounds that can be exploited commercially, or in tandem with biofuel production to reduce costs of the latter (Stephens et al. 2010). Since the overall productivity of the culture will scale linearly with production of any specific

metabolites, more effort needs to be directed towards increasing overall productivity of the culture.

Improving photosynthetic efficiency, the foundation of the production of all carbon-based compounds, has been suggested as a promising avenue to enhance productivity of terrestrial crops as well as microbial autotrophs (Murchie and Niyogi 2011; Ort et al. 2015; Peers 2014; Zhu et al. 2010a). Given that the common denominator of low productive PBRs is the irregular light environment, tuning photosynthesis to fluctuating light has the potential to greatly enhance productivity of current PBR models. There is, however, a lack of understanding of how photosynthesis and photoprotection operates under mass cultivation conditions, which is essential to direct metabolic engineering of photosynthesis.

4.2. Targeted Improvement of Photosynthesis

Targeted improvement of photosynthesis has been explored as a means to increase the growth rate of microbial autotrophs in PBRs. Photosynthetic organisms can sense both the quantity and quality of light in numerous ways including light sensing photoreceptors, the redox state of the plastoquinone pool and reactive oxygen species (Hihara et al. 2003; Hirose et al. 2013; Rochaix 2011). Manipulating these sensory and signaling pathways could be one strategy to induce a desirable acclimation state, were light harvesting, carbon fixation and energy dissipation become better tuned to the light environment of PBRs. Designing such metabolic engineering strategies will require in-depth understanding of the role of transcriptional regulators, retrograde signaling, and other signaling pathways (Rochaix 2011; Summerfield and Sherman 2007; Woodson 2016).

4.3. Increasing Carbon Fixation Efficiency

Improving the carboxylation rate of ribulose bisphosphate carboxylase/oxygenase (Rubisco) has been the holy grail of crop research for decades. However, with Rubisco being almost physically optimized for carboxylation (Tcherkez et al.

2006) this may result in relatively minor yield increases. Given that many algae and cyanobacteria have efficient carbon concentrating mechanisms, such as bicarbonate transporters and carboxysome organelles (Raven et al. 2014), and mass cultivation requires input of external CO_2 to match consumption, it is doubtful that improving carboxylation rates of Rubisco would affect productivity of these phototrophs. Even under sub-air saturated CO_2 concentrations, Rubisco does not carry out any significant amounts of energetically wastefully oxygenation in *Synechocystis* sp. PCC 6803 [*Synechocystis* from here on] (Young et al. 2011). This suggests Rubisco may not be a viable target for metabolic engineering in algae and cyanobacteria.

Under optimal nutrient and light conditions carbon fixation is often the growth limiting step of algae and cyanobacteria (Behrenfeld et al. 2004). However, the rate limiting steps of the CBB-cycle will likely depend on enzymes other than Rubisco (Farquhar et al. 1980). Given the physical differences between PBRs and crop plant cultivation, metabolic strategies to enhance carbon fixation in PBRs require unique approaches. Since light is supplied in short burst of supra-saturating light in PBRs, maximizing the rate of the CBB-cycle to utilize the maximum amount of photons during these short event could be a successful metabolic engineering strategy. It would be critical to evaluate the effect of such an engineered strain under realistic PBR light environments since the phenotype may not develop under static light.

4.4. Reducing Light Harvesting Capacity

Reducing light harvesting in individual cells has been one effective way to increase microalgae and cyanobacteria productivity under excess light. Reducing light harvesting capacity of individual cells allows for deeper penetration of light into the PBR, giving a larger fraction of the total cell population access to it. Similar approaches to reduce the canopy effect in crop plants have been explored (Ort et al. 2011) although successful

engineering strategies have not yet been achieved in field experiments (Ort et al. 2015). Reducing light harvesting capacity has, however, been successfully exploited in PBRs, perhaps as a consequence of the extreme magnitude of the shading effect (Kirst et al. 2014).

In cyanobacteria, reducing the size of the peripheral light harvesting antenna (phycobilisome) of individual cells of *Synechocystis* sp. PCC 6714 has successfully increased the overall productivity of the culture. A mutated strain lacking the phycocyanin encoding gene, which forms rods extending out from the core of the phycobilisome, has truncated phycobilisomes causing photosynthesis to saturate at higher irradiances (Nakajima and Ueda 1997) and less photodamage to occur compared to wild type (Nakajima et al. 1998). The authors later developed a theoretical framework predicting a five-fold increase in productivity under field conditions (Nakajima and Itayama 2003). Kirst et al. (2014) used a different phycobilisome truncation strategy in *Synechocystis* to increase productivity by 57% at a constant light flux of 2000 μmol photons m^{-2} s^{-1} and an industrially relevant cell density.

Similar observations as in cyanobacteria have been made in green algae. For instance, disruption of chlorophyll biosynthesis in *C. reinhardtii* yielded a reduction in the abundance of light harvesting complexes and an elevated photosynthetic capacity on a chlorophyll *a* basis (Kirst et al. 2012). In this paper the authors did not test if the mutant was competitive to wild type in terms of productivity under simulated light conditions of mass cultivation. However, using a forward genetics screen of *Chlorella sorokiniana* strain*s* with truncated light harvesting antennas, Cazzaniga et al. (2014) found a 30% increase in productivity under outdoor conditions in one of their screened mutants. Truncating the size of the light harvesting antenna appears to be a viable method of enhancing productivity, but the discrepancies between theoretical and observed gains in terms of productivity highlights the need to evaluate future strains under realistic mass cultivation conditions.

4.5. Modifying Non-Photochemical Quenching.

In the truncated light harvesting mutants it is assumed that as smaller fraction of the light captured by a cell is being dissipated as heat. Another avenue to increase productivity is to directly target light dissipation mechanisms (Kromdijk et al. 2016; Murchie and Niyogi 2011; Ort et al. 2015; Zhu et al. 2010a). In microalgae and cyanobacteria, photosynthesis and growth commonly saturates between 100 and 500 μmol photons m^{-2} s^{-1} (Du et al. 2016; Macintyre et al. 2002), which is significantly lower than at solar noon (~2000 μmol photons m^{-2} s^{-1}). Consequently, the 75-95% of photons that are not utilized for photochemistry must be dissipated through other mechanisms or they will cause formation of singlet oxygen and other reactive oxygen species causing photodamage.

Non-photochemical quenching is a prevailing mechanism in most eukaryotic microalgae but is lacking in many cyanobacteria species (Campbell et al. 1998). qE, the rapidly adjustable component of NPQ, is induced by the disassociation of light harvesting complexes from the PSII reaction center followed by quenching by a zeaxanthin containing Light- Harvesting Complex Stress-Related (LHCSR) protein in green algae (Peers et al. 2009). This neutralizes exciton of the quenched light harvesting complex as heat and the system enters a quenched state, where most of the light energy absorbed by light harvesting complexes is dissipated as heat instead of serving photochemistry. This function is analogous to the PsbS protein in plants (Li et al. 2000). Cyanobacteria on the other hand, have a radically different light harvesting complex consisting of phycobiliproteins and no chlorophyll pigments (Elmorjani et al. 1986). The phycobilisome was long thought to be incapable of rapidly inducible NPQ (Campbell et al. 1998), but in 2006 a carotenoid-containing protein (OCP) capable of quenching phycobilisomes was characterized in the model cyanobacterium *Synechocystis* (Wilson et al. 2006). OCP acts as a dual photoreceptor/energy quencher and in contrast to plants and algae, where acidification of the

lumen of the chloroplasts induces qE (Li et al. 2000; Peers et al. 2009), rapidly inducible NPQ is regulated by the perceived intensity of blue light in *Synechocystis* (Wilson et al. 2006). The induction and relaxation kinetics depends primarily on the relative abundance of OCP and a Fluorescence Recovery Protein (FRP), two proteins that compete for access to the quenching site of the phycobilisome (Boulay et al. 2010; Gwizdala et al. 2013). As a consequence, cyanobacterial NPQ cannot be induced by red actinic light, commonly used in pulse amplitude modulated (PAM) fluorometery (Schreiber et al. 1986), which may have delayed the discovery of rapidly inducible NPQ in cyanobacteria.

Non-photochemical quenching has proven to be an essential photoprotective mechanism during abrupt changes in light intensity. The NPQ induction kinetics is much faster than the relaxation kinetics, and tuning these two processes has proved to be an effective way to induce crop plant productivity in *Nicotiana tabacum* in field trials (Kromdijk et al. 2016). Similar engineering of NPQ in production strains of microalgae and cyanobacteria has been suggested as a path to improve productivity of PBRs (Melis 2009; Radakovits et al. 2010). Disruption of OCP in thin PBRs under natural sunlight did increase growth rates of the mutant, suggesting that this may be a feasible strategy under certain growth conditions (Peers 2015). Interestingly, there are very few *in situ* NPQ activity measurements under realistic PBR light environments to support this idea. Studies where NPQ has been suggested to play a pivotal role in photoprotection base their conclusions largely on observations of NPQ capacity derived from P-I curves, not actual *in situ* measurements [eg: (Berteotti et al. 2016; Masojídek et al. 2003; Yarnold et al. 2016)]. On the contrary, it was recently shown that NPQ plays a minimal role in photoprotection in the diatom *P. tricornutum* under a sinusoidal light/dark regime, mimicking outdoor conditions (Jallet et al. 2016a). The lack of evidence for the role of NPQ in mass cultivation acclimated

microalgae or cyanobacteria suggests that engineering efforts may not produce desired results in scaled PBRs.

4.6. Modifying Other Photoprotective Mechanisms

There are other strategies by which algal and cyanobacterial photoinhibition or energy dissipation may be modified. Protection from reactive oxygen species may limit effects of photodamage, and upregulation of antioxidants has been explored as one possible avenue to achieve this (Shigeoka et al. 2002). This strategy could be applied in PBRs that have demonstrated photodamage occurring *in situ*, such as super-thin tubular reactors with focused light reaching up to 6000 μmol photons m^{-2} s^{-1} (Masojídek et al. 2003). However, these strategies assume that there is significant photodamage occurring in PBRs, which may not be the case under realistic light conditions or in photobioreactors with different geometries (Cantrell and Peers *in press*; Jallet et al. 2016a).

State transitions are another mechanism that microalgae and cyanobacteria use to redistribute reducing power between the two photosystems (Kirilovsky et al. 2014; Minagawa 2011). State transitions balance excitation pressure between PSII and PSI based on the mobility of the associated antennae. Consequently, this mechanism can be used to skew the ATP/NADPH production ratio or dissipate exciton through cyclic electron transfer around PSI. In contrast to eukaryotes – where state transitions are relatively slow and play a photoprotective role under high light – cyanobacteria use state transitions to optimize photon utilization under low light, in a very rapid process (Emlyn-Jones et al. 1999; Kirilovsky et al. 2014). In cyanobacteria, state transitions are regulated by the redox state of the plastoquinone pool (Mullineaux and Allen 1990). When the plastoquinone pool is oxidized (low light intensities or wavelengths targeting PSI preferentially), relatively more phycobilisomes associate with PSII, causing a high fluorescence state (State I). When the plastoquinone pool becomes reduced (high light intensities or wavelengths targeting PSII preferentially), some

phycobilisomes associate with PSI to maintain a balanced electron flow through the electron transport chain (State II). The effect of fluctuating light on state transitions has not been investigated, but – given the gradients in light intensity and quality within PBRs – cells likely oscillate rapidly between the two states.

Alternative electron transport (AET) is another potential photoprotective strategy that so far has been an overlooked target for metabolic engineering [but see (Peers 2014)]. The reason for this may be that the underlying mechanisms are not well understood and difficult to characterize experimentally (Bailleul et al. 2017). In green algae the Plastid Terminal Oxidase (PTOX) and flavodiiron proteins are capable of carrying out a Mehler-like reaction where electrons are ultimately donated to oxygen at various different points of linear electron transport, instead of being used to reduce $NADP^+$ (Chaux et al. 2017; Mcdonald et al. 2011). However, there is currently a lack of evidence that these pathways are operational as a photoprotective mechanisms [but see (Houille-Vernes et al. 2011)] partly because of difficulties in disentangling the plastid and mitochondrial oxygen consumption under illumination.

Cyanobacterial AET has been studied in greater detail than eukaryotes. In cyanobacteria, both respiratory and photosynthetic electron transport occur within the thylakoid membrane (Lea-Smith et al. 2016) allowing respiratory terminal oxidases to participate in AET. AET may serve two functions in the cell: 1) dissipating energy as a photoprotective mechanism or, 2) increasing the ATP production relative to NADPH which allows energy demanding molecular work to be done while carbon fixation is saturated or blocked. In terms of photoprotection under high or fluctuating light, cyanobacteria utilize several enzymes capable of carrying out Mehler-like reactions, including two terminal oxidases that also function in respiration (Ermakova et al. 2016), flavodiiron proteins targeting PSII (Bersanini et al. 2014; Zhang et al. 2012) and flavodiiron proteins operating

downstream of PSI. In *Synechocystis*, AET activity may dispense up to 70% of the electrons flowing through the electron transport chain under highly stressful conditions such as carbon limitation and min-scale fluctuations in growth light (Allahverdiyeva et al. 2013; Ermakova et al. 2016; Shimakawa et al. 2015). Despite a growing understanding of the molecular complexity of cyanobacterial AET under various laboratory light regimes, little is known about how these mechanisms operate under natural or industrially relevant light conditions. Given that AET has been shown to consume 70% of the electrons from PSII (Allahverdiyeva et al. 2013; Ermakova et al. 2016; Shimakawa et al. 2015) this mechanism should be considered in metabolic engineering projects.

5. System Biology Approaches to Understand Responses to PBR Environments

Global changes in gene expression, protein abundance, and metabolic fluxes provide a holistic view of cellular responses to environmental conditions. In terms of applied development of production strains of algae and cyanobacteria these methods can be used as discovery tool to find putative gene targets for metabolic engineering or infer effects of disruption of specific genes. System level studies can also provide understanding of regulatory processes and metabolic responses to certain stressors associated with PBR growth. Most studies so far have focused on transcription and isolated events associated with PBR growth, such as high light exposure (Muramatsu and Hihara 2012; Summerfield and Sherman 2007) abrupt switches in light (Mettler et al. 2014), autotrophic to heterotrophic changes (Kurian et al. 2006; Saha et al. 2016), nutrient limitation (Fuszard et al. 2013; Wang et al. 2015), inorganic carbon limitation (Battchikova et al. 2010), and oxygen super-saturation (Ludwig and Bryant 2011). All of these studies investigate the response to a single-step change in the environment and these conditions to not represent what happens in the real world.

From studies that coupled transcriptomic and proteomic analysis, we know that post transcriptional modifications are prevalent in biology. Consequently, the transcriptome has been shown to be a poor predictor of protein abundance in *Escherichia coli* (Taniguchi et al. 2010), *Saccharomyces cerevisiae* (Griffin et al. 2002), *C. reinhardtii* (Mettler et al. 2014) and the cyanobacterium *Prochlorococcus sp* MED4 (Waldbauer et al. 2012). System level responses should therefore ideally be conducted on several levels, not just transcription, and integrate physiological experiments for the most informative observations. Mettler et al. (2014) provide an excellent example of this while integrating transcriptomics, proteomics, and metabolomics with photophysiological measurements in *C. reinhardtii.* Using this approach, the authors illustrated how the flux through the CBB-cycle is modified at different light intensities in the short term, enabling more efficient carbon fixation at higher light. This was accomplished through quantification of both the enzymes and metabolites in the CBB-cycle combined with knowledge of the Michaelis Menten kinetics of the various reactions. The authors showed that the CBB-cycle may be limited by abundanc of metabolites and not enzyme, and that glyceraldehyde 3-phosphate (GAP) was potentially limiting the overall reaction. However, most studies do not go into this depth of analysis and too many are confined to only studying transcriptional responses.

Transcription and protein synthesis of key enzymes respond rapidly to stressors in cyanobacteria and microalgae. Shift in light intensities or depletion of inorganic carbon causes major responses in as little as 15 min (Gill et al. 2002; Muramatsu and Hihara 2012). While, some studies claim to detect changes in protein abundance following only 30 min of stressor application (Hong et al. 2014; Mühlhaus et al. 2011) only a handful of genes were found to change in such a short time raising concerns of type II statistical error creating false discoveries. In response to the depletion of inorganic carbon the proteome is largely modified within 6 h, and continues to change for up to 72 h (Battchikova et al. 2010). The vast majority

of proteomic studies in cyanobacteria and algae do not include temporal resolution but compare different acclimatized states [e.g. (Fuszard et al. 2013; Förster et al. 2006; Kurian et al. 2006; Pandhal et al. 2007)]. Even fewer studies have looked at gradual increases in environmental stimuli's, such as those associated with diurnal changes in light intensities.

Changes in light have a profound impact of transcription in photosynthetic organisms. For instance, it affects 75% of all gene transcript levels in *C. reinhardtii* (Zones et al. 2015). Yet in algae and cyanobacteria, the effect of light has mainly been studied through two-step experiments where a culture was taken from a low light or dark acclimatized state to a supra-saturating light (Ludwig and Bryant 2011; Muramatsu and Hihara 2012; Summerfield and Sherman 2007). By large, these studies have corroborated what we already know from decades of photophysiology research: transcript abundance of pigment and light harvesting complexes goes down while genes involved in photoprotection, proteases, heat-shock protein, reactive oxygen species scavenger goes up. This enable cells to harvest less light energy, dissipate a larger fraction of what light is harvested, as well as prevent and repair photodamage. Few novel mechanisms aside from the role of transcriptional regulators and sigma factors have generally been found this way.

Complex shifts in metabolism have only recently been investigated in algae and cyanobacteria. Diurnal changes from autotrophic to heterotrophic growth – associated with a day and night cycle – has for example been analyzed on a transcriptional level (Angermayr et al. 2016; Beck et al. 2014; Saha et al. 2016). These studies suggest that aside from genes directly involved in photosynthesis, diurnal regulation of catabolism, inorganic nutrient acquisition and protein synthesis are important under cyclic light/dark growth. For example, there is a strong diel regulation of the transcriptional activity of various nutrient transporters which likely mirror energy conservation. Macro-nutrients transporters, whose assimilation requires relatively large amounts of energy, are upregulated during the day while transcripts

of micro-nutrients transporters amass during the night (Saha et al. 2016). Species that have diurnal cycles of cell division also synchronizes DNA replication and mitotic division to the night, and focus on photosynthesis and growth during the day (Zones et al. 2015).

Circadian rhythm regulates transcription on a diurnal basis in many, but not all, phototrophs (Xu et al. 2011). In *Synechocystis*, the main regulation of light response is mediated through the redox state of the PQ pool (Hihara et al., 2003), and not circadian rhythms (Beck et al.2014). Gene members of the *kai* gene family known to regulate circadian rhythm in other phototrophic organism are transcriptionally active but have apparently lost much of their influence over global transcription in *Synechocystis* (Beck et al. 2014). Kucho et al. (2005) came to a slightly different conclusion showing that 2-9% of the genes oscillated in a circadian fashion in *Synechocystis*, and Layana and Diambra (Layana and Diambra 2011) estimated that only 164 out of 3,600 genes were under circadian control. The latter study found that certain genes related to catabolism and respiration are maintained under circadian control and upregulated in the afternoon, in preparation for the onset of darkness. This suggests that *Synechocystis* prioritizes circadian control of heterotrophic metabolism whereas light queues autotrophic responses.

There have been few, if any, system level studies of microbial autotrophs under outdoor-condition or natural sunlight, likely due to the high risk of contamination and difficulties with quenching of transcription and cell extraction outside of the laboratory environment. Labiosa et al. (2006) did use a sinusoidal light regime peaking at 400 μmol photons m^{-2} s^{-1} and followed transcriptional changes with 2 h resolution. Their main finding was that that DNA and cell replication transcripts amass at night. Neither these authors, nor those of other diurnal studies (Angermayr et al. 2016; Beck et al. 2014; Saha et al. 2016), discuss or present results regarding transcription of genes involved in photoprotection. Given that light is known to vary significantly in aquatic environment due to diurnal movement of

the sun, position of cells in the water column, cloud coverage, and shading from competing autotrophs, cyanobacteria and microalgae have likely evolved respond to dynamic changes in light. Understanding system biology responses to realistic outdoor light environments can help us understand fundamental metabolic responses to growth in both PBR and natural light environments. This information will be useful in both the design of productive PBRs and engineer strains of algae and cyanobacteria that can grow faster in them.

6. Outlook

The objective of this thesis was to gain a fundamental understanding of how photosynthetic and photoprotective processes operate in cyanobacteria under simulated conditions of mass cultivation. Based in the current literature I hypothesized that rapid and dynamic fluctuation in light would cause induction of NPQ and/or photodamage to cells during mass cultivation. To better understand how the cells orchestrates their response to these dynamic changes in light, I also followed changes in the transcriptome across a day-cycle.

To test my hypothesis, I needed to recreate a light environment of a PBR in a laboratory setting. I used a commercially available bench-top PBR (Lucker et al. 2014) and dense cultures of *Synechocystis* to create a fluctuating light environment that is similar to outdoor PBRs. *Synechocystis* has been a model organism for photosynthesis for decades. It has a small and well annotated genome [3660 putative protein coding genes: (Kaneko et al. 1996)] making it is a suitable systems biology model for photosynthesis and central carbon metabolism in phototrophs. Due to its relatively simple metabolic network and amenability to genetic modification, cyanobacteria are excellent candidates for metabolic engineering towards enhanced productivity under mass cultivation conditions and production of industrial compounds (Angermayr et al. 2015; Kaneko et al. 1996; Koksharova and Wolk 2002). By

using *Synechocystis* I can both test my hypothesis in a well characterized organism and generate information which apply to industrially relevant production strains.

I used computational fluid dynamics to quantify the light environment experienced by individual cells over time. I illustrate how this knowledge can be applied to gain biological insight into physiological mechanisms and stressors associated with growth under these conditions. I also develop a frame-work for how to use information about the light history of a cell in a PBR to design future experiments through application of the predicted light history in *ex situ* experiments. Finally, I conducted systems level measurements of the transcriptome and proteome to investigate broad metabolic responses associated with dynamic and realistic changes in light.

CHAPTER 1: THE USE OF A CELL-SPECIFIC LIGHT ENVIRONMENT MODEL TO EVALUATE THE IMPACT OF RAPIDLY FLUCTUATING LIGHT ON THE PHYSIOLOGY OF *SYNECHOCYSTIS* SP. PCC 6803

Summary

Individual cells of cyanobacteria or algae are supplied with light in a highly irregular fashion when grown in photobioreactors (PBRs). These conditions coincide with significant reductions in growth rate compared to static light environments commonly used in laboratory experiments. This loss of productivity could be due to reduction in photosynthetic capacity or photoprotective responses. To investigate this, we grew a dense culture of the model cyanobacterium *Synechocystis* sp. PCC 6803 under a sinusoidal light regime in a bench-top PBR (the Phenometrics ePBR). We used a computational fluid dynamics model to predict that cells experienced rapid fluctuations (~6 s) between 2000 and <1 μmol photons m^{-2} s^{-1}, due to vertical mixing and self-shading. The daily average light exposure of a single cell was 180 μmol photons m^{-2} s^{-1}. Physiological measurements across the day showed no *in situ* non-photochemical quenching or photoinhibition. Yet the growth rate of the dense ePBR culture was 85% lower than during light limited exponential growth. An *ex situ* experiment showed that 50% of electrons derived from PSII were diverted to alternative electron transport. Collectively our results suggest that modification of non-photochemical quenching may not increase productivity of cyanobacteria in PBRs with rapidly changing light. Instead, our results suggest that tuning the rate of alternative electron transport and increasing the processing rates of electrons downstream of photosystem I are potential avenues to enhance productivity.

1. Introduction

Targeted improvement of photosynthetic efficiency has been suggested to form the basis for the next generation of improved biofuel and crop strains (Ort et al. 2015; Zhu et al. 2010b). Optimization of dissipation of light energy is one potential avenue to achieve this goal and modification to photoprotection has been shown to boost biomass production of *Nicotiana tabacum* by 30% in field trials (Kromdijk et al. 2016). Photosynthesis however is an intricate process that directly involves dozens of enzymes and cofactors. Gene expression, protein regulation, and complex sensory and signal pathways interplay to tune photosynthetic efficiency and avoid the formation of reactive oxygen species that cause cellular damage (see reviews: (Foyer and Noctor 2009; Niyogi 2000; Woodson 2016)). To find suitable photosynthetic enzyme targets in microbial autotrophs we must first understand how these processes operate under realistic light environments of mass cultivation.

Microbial autotrophs have evolved under light regimes that bear little resemblance to those of mass cultivation where light is supplied in a highly irregular fashion. In photobioreactors (PBR) light fluctuates on a seasonal and diurnal basis, but also at a much faster time-scale due to the high density of the culture, which causes self-shading (Posten 2009). From the perspective of a single photosynthetic cell the latter translates into rapid fluctuations between full sunlight and darkness throughout the day. Little is known about how this light environment affects the photophysiology of microbial autotrophs due to our limited understanding of the pattern of light fluctuations in PBRs. This is compounded by the difficulties of studying photosynthesis *in situ* in these large-scale reactors.

Computational fluid dynamics (CFD) offers a high precision method of tracking the movement of gases and liquids (Jameson 1995). CFD has been used to optimize heterotrophic bioreactors by predicting nutrient mixing and gas exchanges (Devarapalli et al. 2009; Dhanasekharan et al. 2005; Hutmacher and Singh 2008). More recently, CFD studies

have predicted scalability and velocity fields of autotrophic raceway ponds (Liffman et al. 2013; Prussi et al. 2014) and the light environment of closed tubular and air lift PBRs (Barbosa et al. 2003; Huang et al. 2015; Perner-Nochta and Posten 2007). These studies predict that light-dark (L/D) oscillations are highly variable in closed PBRs, ranging from 10 to 0.01 s^{-1}, depending on reactor design. A limited set of studies have investigated the effect of such rapid L/D fluctuation on photosynthesis and they suggest that 1000 to 0.1 s^{-1} oscillations may actually benefit productivity through recycling of rate limiting metabolites in the Calvin-Bassham-Benson cycle (Takache et al. 2015) and reduced photodamage (Nedbal et al. 1996). Aside from aiding in the design of new reactors, CFD offers a refined method to predict light and mixing environments in existing reactors, and it provides a novel framework of testing their effects on photosynthesis and other cellular functions.

In addition to the rapid fluctuations in light caused by self-shading, outdoor PBRs experience a gradual increase/decrease in light intensities at dawn and dusk. At noon, light intensities peak at irradiances much higher than the light harvesting capacity that any photosynthetic organism can sustain. Phototrophs have evolved several photoprotective mechanisms to dissipate this excess light, including non-photochemical quenching (NPQ) and modification to linear electron flow [see review by (Derks et al. 2015; Jallet et al. 2016b)].

The orange carotenoid protein (OCP) is responsible for photoprotective NPQ in phycobilisome containing cyanobacteria. OCP is induced proportionally to the blue light intensity and not in response to acidification of the lumen (Wilson et al. 2006). State transitions is another NPQ mechanism that cyanobacteria use to redistribute light energy between the two photosystems through physical movement of the phycobilisome. Cyanobacteria use state transition to optimize photon utilization under low light (Emlyn-Jones et al. 1999). The process is regulated by the redox-state of the plastoquinone pool and is very

rapid, occurring within seconds of changes in light conditions (Mullineaux and Allen 1990; Mullineaux and Emlyn-Jones 2005).

Cyanobacteria also have a complicated electron transport chain downstream of photosystem II (PS II) since both respiratory and photosynthetic electron transport occurs within the thylakoid membrane (Lea-Smith et al. 2016). This enables electrons to be diverted from linear electron transport to reduce oxygen at various points, which is used as photoprotection or to modify the ATP:NADPH production ratio (Chaux et al. 2017; Ermakova et al. 2016) under excess light or inorganic nutrient limitation (Bailleul et al. 2017). Several enzymes are capable of carrying out these Mehler-like reactions in cyanobacteria, including two terminal oxidases (Ermakova et al. 2016), and flavodiiron (flv) proteins. Flv protein can operate either directly downstream of PSII (Bersanini et al. 2014; Zhang et al. 2012) or PSI (Allahverdiyeva et al. 2013; Mustila et al. 2016). Despite a growing understanding of the molecular complexity of cyanobacterial photoprotection under various laboratory light regimes, very little is known about how these mechanisms operate under industrially relevant light conditions.

Understanding the complex interactions between dynamic light and photo-physiology is crucial to metabolic engineering of cyanobacteria and algae. Cyanobacteria are excellent candidates for metabolic engineering for enhanced production of biofuels and other industrial compounds due to their relatively simple structure, metabolic network, small genome, and amenability to genetic modification (Angermayr et al. 2015; Kaneko et al. 1996; Koksharova and Wolk 2002). This study aims to answer three questions: 1) how does the light environment of a photobioreactor change on a diurnal basis from the perspective of a single cell? 2) how do these light changes affect photosynthesis and culture productivity? 3) which photoprotective mechanisms are active *in situ*? To this end, we grew the model cyanobacterium *Synechocystis* sp. strain PCC6803 at an industrially relevant density in one of

the most commonly used bench-scale PBR: the Phenometrics environmental PBR (ePBR). We used CFD to model the cell-specific light environment of the ePBR and monitored rates of cell division and carbon accumulation. Finally, we measured NPQ activity across the day *in situ* and subjected cultures to the predicted light model *ex situ* to investigated photophysiological responses to the rapidly changing light environment.

2. Materials and Methods

2.1. Culture Conditions and Growth Estimates

A glucose tolerant strain of the model cyanobacterium *Synechocystis* sp. PCC6803 (*Synechocystis* from here onwards) gifted from the National Renewable Energy Laboratory (NREL, Dr. Jianping Yu) was grown axenically for the experiment described below. Cultures were maintained in BG-11 media (Stanier et al. 1971) modified with 10 mM TES-NaOH buffer (pH 8), 2 mM Na_2CO_3, and elevated concentration of phosphate (0.106 M K_2HPO_4). All chemicals used were laboratory grade and purchased from either Fisher® or Sigma-Aldrich®.

2.1.1. Culture Conditions and Experimental Design

A 200 mL pre-culture was grown in 500 mL Erlenmeyer flasks in a Percival incubator at atmospheric CO_2, 30°C, and 12/12-h, 50 µmol photons m^{-2} s^{-1}/dark (Phillips F17T8/TL841/ALTO light tubes), on a rotating board at 100 rpm agitation for 1 week. The pre-culture was used to inoculate a custom made glass vessel in an Environmental Photobioreactor v1 (ePBR, Phenometrics, East Lansing MI) to a final volume of 500 mL. The culture was sparged with 0.5 L min^{-1} 1% CO_2 enriched air, and constantly stirred at 500 rpm. The surface light intensity was set to a 12 h sinusoidal function peaking at 2000 µmol photons m^{-2} s^{-1} (Jallet et al. 2016a). For detailed information on the spectral properties of the LED, see Lucker et al. (2014) and for the custom made glass vessel see Fig. A1.

To approximate conditions of mass cultivation we maintained the ePBR culture at a density corresponding to linear growth throughout the experiment. The culture was grown un-diluted in batch mode for 4 days before being diluted to a density in mid-linear growth phase at the end of the 4th day. After that the culture was switched to semi-continuous growth mode through daily dilutions for at least 36 h prior being sampled between the 7th and 10th incubation day. Depending on the type of sample collected 5-13 sample points were taken, replacing an exact volume of 200 mL of the vessel each day. We chose this sampling scheme for two reasons: 1) it maintained the culture density, volume (i.e. distance between surface and LED light), and hence the light environment within the ePBR stable, 2) it allowed us to sample large volumes of culture (up to 10% of total volume per sampling time) without depleting experimental replicates.

When describing diurnal time points of the ePBR we use Zeitgeber Time (ZT) based on circadian rhythm as described in (Van Alphen and Hellingwerf 2015). Throughout the paper we refer to diurnal time points as ZT (i.e hours past dawn), e.g. ZT-1 corresponds to one h pre-dawn and ZT6 six h past dawn (or solar noon).

2.1.2. Culture Density, Cell Count and Size Measurements

Cell density was measured using a BD Accuri™ C6 Flow Cytometer (Agilent Technologies). At each time point, two technical 25 µL samples were diluted 1:40 in pre-filtered (0.45 µm) BG-11. Pigment containing cells, which constituted >95% of all recorded particles, were gated from non-viable particles using chl *a*/phycobilisome auto-fluorescence (640 nm excitation and 675±25 nm emission detection). Because we used a semi-continuous cultivation method, we calculated doubling time based on an equation that accounted for the number of cells being extracted from the vessel, as well as any small net-changes in cell density.

$$\text{Doubling time (h)} = \left(\frac{(C_{t1} - C_{t0}) + \Sigma\left(N_{\text{cells removed}}\right)/V}{C_{\text{mean}} \times (t_1 - t_0)} \right) \quad \text{(Eq. 1)}$$

C_{t1} is the cell density at the end time point, C_{t0} the initial cell density, t_1 and t_0 specific time of daily measurements (i.e. 24 h in-between), $N_{cells\ removed}$ the quantity of cells removed during sampling, V the constant volume of the vessel (0.5 L), and C_{mean} the average density of the culture between C_{t1} and C_{t0}, including measurements in-between. It is important to note that this doubling time is specific to the density used is this experiment (OD_{750} of 0.73) since cells were growing linearly.

Cell volumes (referred to as bio-volume from here on) were measured microscopically in 26 samples collected across one day from two experimental replicates. A one mL sample was centrifuged (× 5000 g, 5 min) and the pellet was re-suspended in 100 µL BG-11 and frozen at -20°C. Within 48 h samples were thawed and imaged at 800 × resolution using a Leica 5000 light microscope with a Hamamatsu C4742-95 digital camera. The area of >500 cells per samples were analyzed using ImageJ version 1.51 (Abràmoff et al. 2004) and converted to bio-volume assuming a spherical cell shape. The measured bio-volume was used to calibrate the forward scatter (FSC-A) measurment of the flow cytometer (linear regression, $R^2 = 0.56$, N = 26), which was used to track changes in cell size across the experiment.

The *in vivo* absorption at 750 nm (OD_{750}) was monitored in 1:10 diluted sample, using a Cary 60 UV-Vis Spectrometer. The OD_{750} was used as a proxy for culture density in the modeling of the cell-specific light environment (see Section 2.2.2 below).

2.1 Modeling the Cell-Specific Light Environment of the ePBR

2.2.1. Tracking Cell Movement Using Computational Fluid Dynamic Modeling[*]

Computational fluid dynamics (CFD) was used to simulate the movement of neutrally buoyant, 2 µm diameter particles in the ePBR. The shape of the vessel (see Fig. A1), speed of the rotation bar, sparging gas flow rate, and Reynolds number all affect the movement of the multiphase media and suspended particles. All governing equations and

[*] *Note from the author; parts of this section was written by Chen Shen as part of his dissertation.*

boundary conditions were modeled within the ANSYS Fluent framework. The model was validated using high-speed camera video recording of the movement of neutrally buoyant beads (1 mm diameter) in the ePBR vessel under the defined culture conditions (see Section 2.1.1). It was also validated against published results for similar systems (Luo and Al-Dahhan 2011; Perner-Nochta and Posten 2007).

To accurately simulate the physics of both bubble and liquid motion, a multiphase volume of fluid (VOF) model with an Euler-Euler approach was employed, whereby the two phases are treated as continua and it is assumed that the total volume fraction of each phase is constant (summing to unity) and continuous with respect to space and time. Conservation principles for mass and momentum are then applied to obtain the pointwise governing equations for the simulation. The standard k-ε model was selected for this simulation, with a pressure based solver to simulate the turbulence effect arising from the rotational motion of the stir bar and the introduced bubble column. This turbulence model includes two equations, one for turbulent kinetic energy k and the other for the specific dissipation rate ε. To predict the trajectories of individual *Synechocystis* cells in response to the bubble column and stir bar, the unsteady state discrete phase model (DPM) was employed. The shape of the cyanobacteria may be approximated as spherical, and thus a spherical drag law may be applied to calculate the drag force on any particle.

An important observation during the development of the CFD model was that the diameter of the modeled particles plays an important role in accurately predicting the cells trajectories. We found that the trajectories vary significantly when the size of the particles are changed within the software (data not shown). When the size is large enough (diameter of about 80 μm) we found that the trajectories are smoother and particles accumulated in the top half of the ePBR. To circumvent this limitation of the software we develop the UDF so that

the trajectories of the cells can be well predicted and the particles will not escape to the gas phase.

Particle motion was subsequently predicted using the three-dimensional flow field. A total of 6204 particles were introduced into the liquid phase with uniform spacing, 27.0 s after flow is initiated by the stir bar and air addition; it was independently confirmed that the flow field is fully developed by this time. Once the individual cell trajectories were predicted a supplemental Matlab code, developed for this study, was applied to perform statistical analysis on the data. The frequency for the particles to reach the surface and bottom of the ePBR as well as the time intervals between these events were calculated with 1 ms resolution to analyze the pattern of the light environment experienced by the cyanobacteria over the course of a 24 h period.

2.2.2. Vertical Light Extinction in the ePBR

In order to understand the light environment within the ePBR we conducted measurements on a culture at an OD_{750} between 0.85 and 0.62. We observed a degree of variability of photosynthetic active radiation (PAR) across the surface (1000±500 µmol photons m^{-2} s^{-1}) that depended on the distance from the center, but for the model we assumed that the surface light intensity was homogeneous. The PAR was measured at six discrete depths in the culture vessel at ½ radius distance from the center (surface, 1, 2, 4, 8, and 23 cm depth), using a spherical light meter (ULM-500, Walz Universal). The light environment within the ePBR was modeled assuming a one-dimension vertical extinction of light with culture depth. The average light intensity at a specific depth were used to calculate the absorption coefficient using Beer-Lambert Law as described in (Lee 1999).

$$A_x = \frac{\log 10\ (I_0/I_x)}{C \times D} \qquad \text{(Eq. 2)}$$

I_x is the light intensity at depth x, I_0 the light intensity at the surface, A_x the calculated absorption coefficient at depth x, C the density of the culture (in OD_{750}), and D is

the depth in cm. Measurements were repeated at four different culture densities spanning the range of densities recorded during the experiment (Table C1). We observed that the absorption coefficient decreased with increasing depth (Table C1), so Eq. 2 was modified to include two absorption coefficients: one that govern the light extinction in the deep part of the reactor and another close to the surface.

$$I_x = 10^{\left(\log_{10}\left[I_0\times\left(\frac{D}{Dmax}\right)\right]-A_{4cm}\times C\times D\right)} + 10^{\left(\log_{10}\left[I_{(o)}\times\left(1-\frac{D}{Dmax}\right)\right]-A_{23cm}\times C\times D\right)} \quad \text{(Eq. 3)}$$

A_{4cm} and A_{23cm} are the absorption coefficients calculated based on the light intensity measured at 4 cm and 23 cm depth, respectively, and D_{max} the depth at the bottom of the vessel (23 cm)

2.2.3. A Synthesized Model of the Cell-Specific Light Environment of the ePBR

The methods described in the section above allowed us to model both the diurnal and rapid (ms resolution) fluctuating in incident light that an individual cell is subjected to as it mixes in the ePBR. This was accomplished by synthesizing the vertical light extinction model (Eq. 3) with the sinusoidal change in surface light intensity given in Jallet et al. (2016a), and the vertical tracking of a single cell over the course of 24 h, using the CFD model (Section 2.2.1). This generated a high resolution model of the light intensity perceived by a single cell over the course of a day, which is referred to hence forward as the cell-specific light environment.

2.3. Physiological Measurements

2.3.1. Chlorophyll a and Total Carotenoid Quantification

The absorption spectra of pigments in 100% methanol was recorded using a Cary 60 UV-Vis spectrometer (Agilent Technologies). 0.01% Tween-20 was added to a 1.5 mL sample which was centrifuged at 5000 g for 5 min and the resulting pellet was dissolved in methanol and pigments were extracted over-night at -20°C. Chlorophyll a (chl *a*) concentrations in the extract were calculated according to previous methodology (Ritchie

2006) and the total carotenoid content was deconvoluted from chl *a* using previously published equations (Wellburn 1994). The ratio of total carotenoids to chl *a* was calculated on a g per g basis.

2.3.2. Total Organic Carbon and Nitrogen Content

To estimate rates of carbon accumulation in the culture, total organic carbon (TOC) and nitrogen (TN) was analyzed using a Shimadzu TOC-L Laboratory TOC Analyzer. We used the method described in (Caballero et al. 2016), with modifications to the cell harvesting protocol as described below. A 1.5 mL culture sample was centrifuged in acid washed (10% HCl) Eppendorf tubes at 5000 × g for 5 min. The pellet was washed in 1 mL ice cold 0.041 N NaCl solution (isotonic to BG-11) with 0.01% Tween-20 and the cell density of the washed cells was measured using flow cytometry. Cells were centrifuged a second time (× 5000 g, 5 min), the supernatant was removed, and the pellet was immediately frozen and stored at -80°C. Preliminary experiments determined that the additions of Tween did not impact our TOC estimates (data not shown).

2.3.3. Pulse Amplitude Modulated Chlorophyll a Florescence, Net-Oxygen Evolution and Rapid Oxygen Versus Irradiance Curves

The photosynthetic capacity of *Synechocystis* was assayed using a combination of Chl *a*/phycobilisome florescence and oxygen evolution measurements. A Walz DUAL-PAM 100 fluorometer equipped with a custom-made, aluminum cuvette holder and a FireSting OXROB10 probe connected to a FiresSting Optical Oxygen Meter was used to detect chl *a*/phycobilisome fluorescence and changes in oxygen concentration mirroring net-oxygen evolution and dark consumption rates. The oxygen probe was calibrated against air saturated and anoxic BG-11, which was instigated through the addition of sodium sulfite which rapidly reacts with and consumes molecular oxygen. We utilized the ePBR's white LED light as actinic light source to more closely approximate conditions of the ePBR. In

tandem the measuring light (620 nm) and saturating pulses (300 ms, 10,000 µmol photons m^{-2} s^{-1}, 654 nm) of the PAM was used to monitor F_0' and elicit F_M'. F_0 corresponds to the florescence of cells in darkness, whereas F_M is measured during the saturating flash. The aluminum cuvette holder was maintained at 30°C through internal circulation of heated water from a Isotemp water bath (Fisher Scientific).

Rapid light curves were generated using a range of relevant light intensities (2.5, 15, 21, 47, 56, 92, 119, 125, 165, 356, 600, 950, 1200, 1400 µmol photons m^{-2} s^{-1}) using one min intervals (Macintyre et al. 2002). 50 mL samples were pulled from the ePBR at specific time points and pre-incubated under low white light (20 µmol photons m^{-2} s^{-1}) in a 250 mL Erlenmeyer flask for 10 min to relax NPQ and other rapidly relaxable photoprotective mechanisms. Measurements were taken on a 1.5 mL subsample enriched with 10 mM sodium bicarbonate in a cylindrical quartz cuvette. Dark respiration rates and estimations of F_0 was measured during an initial 5 min dark treatment after which the actinic light intensities were applied in an incremental fashion.

Light response parameters were calculated as described in (Eilers and Peeters 1988), where P_{max} corresponds to the maximum rate of photosynthesis, E_k the irradiance saturation index, and α the linear coefficient of the light limited slope. For the purposes of defining the optimal irradiance for photosynthesis ($E_{optimum}$) and the half-point saturation of photosynthesis ($P_{max\text{-}half}$) we used the Wait-In-Line model, as described in Steele (1962), using the Excel calculations provided by Ritchie (2008).

2.3.4 Non-Photochemical Quenching versus Irradiance

The fluorescence trace collected during the P-I curves was used to quantify the level of non-photochemical quenching at specific irradiances. Each light step was ended with a saturating pulse and the non-steady state NPQ was estimated as the relative quenching of F_M through the equation [$1\text{-}F_M'/F_M$; (Wilson et al. 2006)]. We choose not to use traditional NPQ

calculations like the Stern-Volmer equation, since cyanobacteria has a different quenching mechanism than plants and most algae (Kirilovsky 2007). A representative example of a fluorescence trace is shown in Fig. B1A.

2.3.5. Chlorophyll Fluorometery of in situ Physiology

The quantum yield of photosystem II (F_V/F_M) was measured as an indicator of photoinhibition or modifications to the redox state of the plastoquinone pool. Within 30 s of removing a sampling from the ePBR, F_V/F_M was measured using a Satlantic FIRe Fluorometer (Kolber et al. 1998). This system utilizes a blue excitation light (excitation at 450 nm, emission measured at 678 nm), which dampens the interference of *Synechocystis's* phycobilisome fluorescence by targeting the soret band unique to the chl *a*'s absorption spectra (Elmorjani et al. 1986; Vernotte et al. 1992). F_0 corresponds to the fluorescenser of cells in darkness and a 400 ms single turnover flash (27,500 µmol photons m^{-2} s^{-1}, 475 nm) was used to elicit F_M.

Since cyanobacteria has a different light harvesting antenna and quenching mechanism than eukaryotes, standard NPQ parameters, such as the Stern-Volmer equation, are invalid. However, the two best characterized NPQ components, state transition and orange carotenoid protein (OCP) depended quenching, are activated under low and high light respectively and can therefore be induced through different actin light treatments. We used a Walz DUAL-PAM 100 fluorometer with a red measuring light (620 nm) to estimate quenching of chl *a*/phycobilsome fluorescence and distinguish between orange carotenoid protein dependent quenching (OCP-quenching) and state transition.

In cyanobacteria, state transition is a rapid (ms to s scale) low light adaptive response regulated by the redox state of the plastoquinone pool (Mullineaux and Emlyn-Jones 2005). The maximum variable fluorescence due to state transition (State-quenching) was based on the low blue light (26 µmol photons m^{-2} s^{-1} of 430 nm) acclimatized state (State I;

high fluorescence) versus the dark acclimatized state (State II; low fluorescence). An example of a fluorescence trace is shown in Fig. B1B with the equation State-quenching=($1-F_{Md}/F_M$) describing the capacity for state transition.

Orange carotenoid protein dependent quenching of fluorescence is a high light induced photoprotective mechanism and it was elicited as described in (Wilson et al. 2006), using a red measuring light (620 nm), with modification described below. The *in situ* level of quenched fluorescence (F_{M60}) was based on the measured F_M' 60 s after the sample was extracted from the ePBR, including a treatment with 10 s of low blue actinic light treatment (26 μmol photons m^{-2} s^{-1} of 430 nm) to promote state I transition. F_M was based on the maximum recovery of F_M' under continued low blue actinic light treatment. Thus the level of *in-situ* OCP dependent quenching ($OCP_{in\ situ}$-quenching) was estimated as $OCP_{in\ situ}$ quenching=($1-F_{M60}/F_M$) according to the fluorescence trace shown in Fig. B1C. The maximum capacity for fluorescence quenching was measured by applying a strong blue actinic light (880 μmol photons m^{-2} s^{-1}) for 7 min and recording the maximum quenching of F_M' (F_{Mq*}). The maximal capacity for fluorescence quenching was calculated as OCP_{max} quenching=(F_{Mq*}/F_M). In this paper we consider fluorescence parameter based on measurements taken within 1 min of removing the sample from the ePBR to represent *in situ* conditions, which was validated by the relatively slow relaxation kinetics of OCP_{max} quenching (see Fig. B1C).

2.3.6. Quantification of Oxygen Production and Consumption ex situ Using Membrane Inlet Mass Spectrometry

We designed an experiment to investigate the physiological response of *Synechocystis* to the predicted cell-specific light environment of the ePBR. By applying a fluctuating light treatment *ex situ* we could synchronize a population of cells to the unique cell-specific conditions of the ePBR, as predicted by our cell-specific light model. We used

the actin lights of the Dual-PAM to recreate the light environment of a single-cell using one-part blue (430 nm) to two-parts red (635 nm). We selected a representative five min section of the CFD model (see Fig. D2) and modified the surface light intensity according to the time of day (see Table D1). We used membrane inlet mass spectrometry (MIMS) to partition between illuminated rates of oxygen production and consumption (Allahverdiyeva et al. 2013; Ermakova et al. 2016).

A QMS-100 (Pfeiffer Vacuum) fitted with a 0.2 μm thickness silicon membrane, was used to partition between oxygen production ($^{16}O_2$ derived from H_2O) and consumption ($^{16}O_2$ and $^{18}O_2$ producing H_2O). The design of the MIMS and PAM set-up can be seen in Fig. D1. A 25 mL culture sample was centrifuged (3220 g × 10 min) and the cell pellet was re-suspended in BG-11+10mM HCO_3 to a chl *a* concentration of 15 ug mL^{-1}. 2 mL of the culture was incubated in the MIMS and the dissolved oxygen concentration was reduced to approximately 25% of atmospheric saturation through equilibration with 100% N_2 gas. The removed oxygen was replaced with pure isotopic $^{18}O_2$.

The isotopic enrichment process was conducted under dim light (>5 μmol photons m^{-2} s^{-1}) and took 10 min. After that dark respiration was measured for five min followed by a three min static light treatment, and four loops of the five min fluctuating light treatment (see Appendix D for description of fluctuating light treatment). Due to the small volume of the cuvette and the continuous consumption of gases by the MIMS, there was a significant net-extraction of dissolved gases (ca. 30% per h). To account for this abiotic consumption of gases and changes in partial pressure we normalized the oxygen trace to Argon (mz 40) based on equations published by Bailleul et al. (2017). Oxygen evolution (gross-photosynthesis) and consumption (respiration and alternative electron transport) during the different treatments was calculated as previously described in Beckmann et al. (2009).

2.4. Statistics

All data used for the statistical analysis were gathered from independent experimental replicates and analyzed using Sigma Plot (v 1.3, Systat Software Inc.). Repeated measurement analysis of variance (RM-ANOVA), with time as the fixed variable, was used to analyze diurnal changes in physiological variables of the ePBR cultures. A 1-way ANOVA was used to compare response variables between different growth conditions. Temporal and treatment differences were further analyzed using Tukey's post-hoc test. Samples with $p<0.05$ were considered statistically different and data are shown as averages ±1 standard deviation (SD) throughout the text. F-statistics are presented with the degree of freedoms between groups (time points or treatments) followed by the total degrees of freedoms (between measuring-points) as $F_{df(\text{time points}, df(\text{measuring-points})}$.

3. Results

3.1. Growth Rate and Productivity

We conducted experiments on batch cultures of *Synechocystis* in the ePBRs to establish growth traits. The culture grew at an initial exponential rate of 12.5±1.0 h^{-1} (N=6) but as it became denser, and the light penetration was reduced, it entered linear growth phase at around 0.5×10^8 cells mL^{-1} (Fig. 1.1A). The culture grew linearly from that point onwards until it entered stationary phase at 8×10^8 cells mL^{-1}, most likely due to inorganic nutrient depletion (Fig. F1A).

Based on the batch growth observation we set the experimental density of the semi-continuously grown ePBR cultures at mid-linear growth and maintained it at $1.4\times10^8\pm0.1\times10^8$ cells mL^{-1} (N=90) during the experimental sampling (day 6-7: Fig. 1.1A). This corresponded to an OD_{750} of 0.73. The pH of the ePBR cultures was well below that of the buffered medium throughout the experiment (7.5±0.07, N=58) and the final density was four times lower than those observed in stationary phase (Fig. F1A), suggesting that the ePBR culture was growing linearly due to light limitation. The doubling time at this specific density

was 75±22 h, a 10-fold increase compared to exponential growth (7.9±0.72 h; Fig. 1.1B). The doubling time did not change significantly between day 6 and 7 (Fig. 1.1B), suggesting that the culture had acclimatized to the experimental conditions.

3.2. Modeling the Cell-Specific Light Environment of the ePBR

We wanted to understand the scale of temporal changes in the light environment from the perspective of a single-cell, which changes rapidly due to intense mixing and self-shading. To this end we used computational fluid dynamics (CFD) coupled with *in situ* measurements of the light intensity in the ePBR to generate a high resolution model of the cell-specific light environment.

3.2.1. Computational Fluid Dynamics[†]

Computational fluid dynamics (CFD) was used to track the movement of simulated cells in an ePBR over time. The movement of a single cell was highly stochastic on the second scale but over the course of several min a repetitive pattern emerged as cells were moved due to the stir bar and the high sparging rate, causing them to spin upwards along the edges of the vessel and sink down the middle (Fig. 1.2). To further understand the driving forces that moved the suspended particles, we looked at the velocity contours and vectors of four horizontal and one vertical cross section (Fig. 1.3). The results show that there are strong rotational motions in the horizontal plane due to the activity of the stir bar (Fig. 1.3B) A high-velocity region (up to 0.3 m s^{-1}) was observed in the depth region (9, 14, 19 and 23 cm depth), as shown in the cross sections of Fig. 1.3A and D, which is caused by the rising bubbles. The velocity magnitude is higher near the outside boundary of the vessel than at the center since the angular velocity is similar in each cross section. It can also be seen that the velocity near the boundary gets higher when it is near the stir bar at the bottom (Fig. 1.3C) and the mean velocities of cross section one through four are 0.122, 0.155, 0.175, and 0.204 m s^{-1},

[†] *Note from the author; parts of Section 3.2.1 was written by Chen Shen as part of his dissertation*

respectfully, while the overall mean velocity in the ePBR is 0.153 m s^{-1}. These results suggest that the fluid rotates with a higher angular velocity at the bottom than it does at the surface. This is reasonable because the angular momentum is transferred by the stir bar at the bottom and dissipated as the fluid moves away from the stir bar. The vessel is also slightly cone shaped which means that more volume exists near the surface than the bottom of the vessel, diluting the rotational energy.

The velocity profile in the vertical cross section show that the fluid has a stronger convection motion in the vertical direction (Fig. 1.3D), causing the particles to approach the surface along the sides and sink down in the center. The CFD model also showed that the rising bubble column caused occasional disturbances when particles were rapidly lifted towards the surface, or shifted to a downwards convection before reaching the surface.

We corroborated the *in silico* modeling results with high-speed camera recordings of 1 mm in diameter neutrally buoyant beads. A video showed that the bubble column and rotational momentum predicted by the CFD model cells could be seen *in situ* as well (Fig. A1; Supplemental Video 1). Special attention was made to the CFD model of the gas inlet, which due to the surface tension allow the gas phase to collects in the tube near the inlet. Once the gas phase becomes large enough, a bubble is formed, leaves the inlet and navigates the liquid phase and finally enters the headspace of the vessel. Although the shape of the inlet and the merging behavior of the bubbles near the inlet has been simplified, the shapes and behaviors of the bubbles and the gas-liquid interface are captured well (Supplemental Video 1). The location where the bubbles hit the interface of the wall is also comparable to the simulated result suggesting that the bubble column was accurately modeled.

3.2.2. The Cell-specific Light Environment

The vertical light environment of the ePBR changed dramatically with only 1% of the surface light remaining at half the maximum depth of the vessel (Fig. 1.4A). Most commonly, cells could be mixed from the surface to the bottom of the vessel, or vice versa, in 0.8 to 6.4 s (Fig. A3B, and Fig. 1.4B). Due to the exponential extinction of light, the impact of this movement on the cell-specific light exposure was exacerbated (Fig. 1.4C). Based on the CFD model, cells oscillated between darkness (>10 cm depth; <1.5% of surface PAR), in the bottom of the vessel, to the surface zone (<2 cm depth; >30% of surface PAR) with an average frequency of 0.17 s^{-1} (or one light exposure every 6 s). The average surface event lasted for only 0.7 s and the average time a cell went into the lower half of the ePBR (<1.5% of surface PAR) was 2.6 s. The maximum length of a surface event that happened at least every h was 6 s whereas dark events with a length between 6 to 12 s occurred on average every 7 min (Fig. A3).

The light model was integrated with the diurnal change in surface light intensity. This illustrates how the cell-specific light environment is highly dynamic across the day (Fig. 1.4). At ZT6 (6 h past dawn or solar noon). The model predicted that the 10 min average cell-specific light exposure was around 300 µmol photons m^{-2} s^{-1} including brief exposures to irradiances up to 2000 µmol photons m^{-2} s^{-1} as cells reached the surface (Fig. 1.4D). Across the whole day the cell-specific light intensities were around 10-15% of the surface PAR, when averaged across a 10 min period (Fig. 1.4D). When integrated across the full 12 h light-period of the day, the cell-specific photon-flux was 180 µmol photons m^{-2} s^{-1}. If supplied as static light in Erlenmeyer flasks, such an intensity enabled *Synechocystis* to grow at its maximum capacity, which is 10-times faster than what we observed in the ePBR (Fig. F1B). This suggests that the rapidly changing light environment causes a major reduction in the capacity of *Synechocystis* to utilize photons efficiently for growth.

3.3. Diurnal Changes in Cell Physiology

3.3.1. Diurnal Changes in Pigmentation, Bio-volume and Cell Division Rate

To understand the diurnal changes in cell growth and photophysiology we measured changes in cell size, division rate and pigment composition across the day. We were particularly interested in the changes between heterotopic and autotrophic metabolism and focused on the transition from darkness to light and light to darkness, around ZT0 and ZT12. The cell population displayed a small, but statistically significant, change in the average size across the day, ranging between 1.5 and 1.7 μm^3 (Fig. 1.5A) Cells size appeared to follow the surface light intensity and by ZT3 the average cell was significantly larger than at ZT0 (see Table E1 for detailed statistical results).

An important acclimatization response to shifting light intensities in cyanobacteria is modification to the pigment composition and light harvesting capacity. However, chl *a* content per unit bio-volume did not change significantly in the ePBR culture at any point during the day (Fig. 1.5B), and chl *a* was maintained around 12 fg chl *a* [μm^3 bio-volume]$^{-1}$. There was a minor, but statistically significant, diurnal modification in the total carotenoid:chl *a* ratio, which covary with the sinusoidal change in surface irradiance, albeit skewed toward the morning (Fig. 1.5C).

3.3.2. Diurnal Changes in Total Organic Carbons and Nitrogen Content

The cell-specific total organic carbon content (TOC) changed in a sinusoidal pattern following the illumination and closely resembled the changes in bio-volume. The TOC content was significantly larger between ZT3 and ZT11.75 than at other times of day ($p<0.001$, Table E1), and at ZT6 the TOC content peaked at 0.65 pg TOC cell^{-1}(Fig. 1.5D). The TOC:TN ratio did not change on a diurnal basis and was maintained at 5.1±0.45 (N=68). When the diurnal changes in carbon content were integrated with the cell division rate it showed that the culture accumulated 3.5±0.1 mg TOC L^{-1} h^{-1} during the daytime (Fig. 1.5E).

Across the whole day the productivity of the culture was 35±3 mg TOC L^{-1} day^{-1} or 9.0±0.7 g TOC m^{-2} day^{-1} when normalized to the surface area of the reactor. Interestingly there was -3.769±2.46 mg TOC L^{-1} day^{-1} net-loss of TOC between ZT11 and ZT13 (Fig. 1.5E), which was significantly larger than than during the latter part of the night (-0.465±0.660 mg TOC L^{-1} day^{-1}; ZT13-ZT24). This loss was driven both by a small (statistically non-significant) reduction in the average TOC content per cell (Fig. 1.5D) but mainly by an arrest in cell divisions.

3.3.3. Diurnal Changes in Photosynthetic Efficiency

Photosynthesis versus irradiance (P-I) curves reveal information about the state of the photosynthetic machinery (Macintyre et al. 2002). We observed no diurnal change in the shape of the P-I curves (Fig. 1.6A) or the fitted parameters (Table 1), suggesting that a robust photosynthetic machinery was maintained regardless of surface light intensities. The chl *a* normalized P_{max} was around 500 µmol O_2 [mg chl *a*]$^{-1}$ h^{-1} and the saturation index (E_k) was reached at 500 µmol photons m^{-2} s^{-1} (Table 1). Since we observed no statistical changes in the P-I parameters, we pooled all measurements (15 response curves and 210 individual measuring points), and defined the saturation point of photosynthesis ($P_{half\text{-}max}$) and the optimum irradiance for photosynthesis ($E_{optimum}$) using the Wait-In-Line model (Steele 1962). $P_{half\text{-}max}$ was reached at 250 µmol photons m^{-2} s^{-1} wheras the optimal irradiance for photosynthesis $E_{optimum}$ occurred at 1050 µmol photons m^{-2} s^{-1}.

We integrated the parameters of the Wait-In-Line model of the P-I curve with the cell-specific light exposures model (Section 3.2) to illustrate how the cell-specific light environment of the ePBR can be expected to affect photosynthesis (Fig. 1.7A). Summed across the illuminated part of the day the cells spent more than half the time at light intensities below the compensation point of photosynthesis (net-respiring). Only one third of the day were spent at light intensities within the linear response range of photosynthesis

(>compensation point, < $P_{half\text{-}max}$) and less than 30 min of the day was at supra-saturating light intensities (>$E_{optimum}$, Fig. 1.7A). However, during these 30 min of supra-saturating light exposure (>1050 µmol photons m^{-2} s^{-1}), supplied mainly as <1 s flashes spread out across the day (Fig. 1.4), the cells recived ~40% of their daily photons dose (Fig. 1.7B). Another ~40% of the integrated photon flux was supplied in the non-linear response range (>$P_{max\text{-}half}$, <$E_{optimum}$), and could not be used with maximal efficiency either, assuming that *ex situ* observations translate to *in situ* conditions.

3.3.4. Diurnal Changes in Non-Photochemical Quenching

Non-photochemical quenching (NPQ) in *Synechocystis* is a complex interaction between state transitions, orange carotenoid protein dependent quenching (OCP-quenching) and various other quenching mechanisms. Fluorescence changes monitored during our P-I curves suggested an initial level of fluorescence quenching, which was most likely state transition related given the low light intensities (>50 µmol photons m^{-2} s^{-1}), followed by OCP-quenching induction, initiated at around 350 µmol photons m^{-2} s^{-1} (Fig. 1.6B). However, the level of *in-situ* OCP-quenching in the ePBR culture was very low across the day (>0.02 quenching of F_M), and did not change significantly on a diurnal basis (Table 2, p=0.073).

The maximum capacity for OCP-quenching, induced through application of seven min of strong blue light (880 µmol photons m^{-2} s^{-1}), was significantly higher in the morning (ZT1 and ZT3; 0.484–0.433) than midday or the afternoon (0.411–0.408, Table 2, p>0.001). The F_M' did not fully recover under subsequent dim blue light illumination (residual quenching: 0.09±0.5%, N = 14), suggesting that state transition, photodamage, and/or an OCP independent mechanism may have contributed to the maximal quenching (Fig. B1C). Due to the rapid induction and reversion of state transitions, this parameter cannot be measured *in situ* using our methodology, but the capacity for state transition *ex situ* was significantly higher at ZT1 than midday or the afternoon (Table 2, p>0.001). Collectively these results

show that the OCP-quenching capacity was highest in the morning when the PAR intensity was increasing, but that NPQ did not become significantly active *in situ* across the day.

3.3.5. Diurnal Changes in the Maximal Quantum Yield of Photosystem II

In our experiments the *in situ* maximal quantum yield of photosystem II (F_v/F_M) varied between 0.45 and 0.52 throughout the day (Fig. 1.8). There was a pronounced increase/decrease in F_v/F_M during the transition from dark to light and from light to dark (Fig. 1.8), from about 0.48 to 0.53. Interestingly, the major driver of this change was a modification to F_M and not F_0 (data not shown), suggesting that changes in the redox state of the plastoquinone pool was not the main driver, but rather changes in the size of the antenna and/or functional PSII abundance. There was also a small, but statistically significant, reduction in F_v/F_M around the peak surface light intensity (from about 0.53 to 0.50 at ZT6 and ZT9).

3.3.6. Effects of Fluctuating Light on Oxygen Evolution and Consumption Ex Situ

To investigate the activity of photoprotective mechanisms under fluctuating light we programed the Dual-PAM flurometer's actinic light to replicate the modeled cell-specific light environment of the ePBR. A combination of two-part red (654 nm) and one-part blue (430 nm) light was used in accordance to the CFD model. Using ePBR acclimatized cultures we measured chlorophyll fluorescence as well as illuminated oxygen production and consumption rates during the treatment, mimicking the light at various ZT time points. At ZT0.25 the maximum light intensity was 130 µmol photons m^{-2} s^{-1} with long periods of darkness and an integrated photon flux of 18 µmol photons m^{-2} s^{-1}. At noon the treatment peaked at a maximum light intensity of 2000 µmol photons m^{-2} s^{-1} and an integrated photon flux of 284 µmol photons m^{-2} s^{-1} (see Table D1).

The fluorescence trace showed some initial quenching of F_M in the first few min of actinic light (Fig. 1.9). After that a repetitive pattern in F_M' emerged between the five min

loops during the rest of the treatment, with lower values during more dark dominated period and higher values at periods of rapid actinic light flashes (Fig. 1.9). Given the rapid changes in F_M' this was most likely due to continuous state transitions. The yield of PS II (YII) oscillated between 0 and 0.2 indicating that the majority of PSII reaction centers shifted between open and closed in the rapidly changing light of the ePBR (Fig. 1.9).

The *ex situ* fluctuating light treatment caused profound alterations to oxygen fluxes based on simultaneous measurements of illuminated oxygen evolution and consumption using MIMS. As predicted by the P-I curves were $E_{optimum}$ was reached at 1050 µmol photons m^{-2} s^{-1}, gross oxygen evolution did not scale linearly to the integrated light exposure (Fig. 1.10A), which doubled between ZT1 and ZT2, and ZT2 and ZT6. This was also seen as a 30-40% reduced capacity for gross oxygen evolution in fluctuating versus static light within the same biological sample (see Fig. D4). In the fluctuating light oxygen evolution peaked at ZT6 (212±19 µmol O_2 [mg chl *a*]$^{-1}$ h^{-1}), which was only 25% that of the maximum capacity under constant white light at an intensity of 1000 µmol photons m^{-2} s^{-1} (800 µmol O_2 [mg chl *a*]$^{-1}$ h^{-1}). The rate of light-dependent oxygen consumption also increased from -25±5 to -106±15 µmol O_2 [mg chl *a*]$^{-1}$ h^{-1} between ZT0.25 and ZT6 (Fig. 1.10B). Light-dependent oxygen consumption rates were higher than dark respiration recorded using the Firesting probe (-15 to -20 µmol O_2 [mg chl *a*]$^{-1}$ h^{-1}; Table 1), indicating that the light-dependent oxygen consumption was due to light induced alternative electron transport. It appeared that the high light intensities during the brief flashes of light were not the main driver of light-dependent oxygen consumption, since both static and fluctuating light yielded similar rates of light-dependent oxygen consumption in the same biological replicate (Fig. D4B).

Between ZT2 and ZT10, when cells are supplied with the majority of photons, light-dependent oxygen consumption accounted for around 50% of the electrons passing

through the electron transport chain, reducing net photosynthesis to <106 μmol O_2 [mg chl *a*]$^{-1}$ h^{-1} (Fig. 1.10C). In the early morning and evening an even greater proportion of electrons where diverted to oxygen, maintaining net-photosynthesis close to the compensation point. Together these *ex situ* results suggest that a combination of light induced alternative electron transport, and an inability to harvest photons during the brief (>1 s) supra-saturating light flashes reduces the photosynthetic efficiency of *Synechocystis* in the ePBR.

4. Discussion

4.1. Diurnal Changes in the Cell-specific Light Environment and Growth Rates

One of our experimental goals was to generate and describe a light regime similar to closed industrial photobioreactors (PBRs). We further aimed to quantify temporal changes in the light intensity perceived by individual cells and study its effect on growth, photosynthesis and photoprotective mechanisms. To do so we used the ePBR, which was originally designed to mimic a raceway pond in terms of depth and illumination (Lucker et al. 2014). However, we operated the ePBR differently than the original authors who allow only brief bursts of mixing every 10 to 15 min. In contrast we mixed and sparged the ePBR continuously to generate a rapid mixing regime that more closely resembles closed tubular or airlift photobioreactors (Posten 2009). To compensate for the differences in cross section/depth (1-10 cm in closed PBRs vs 20-30 cm in raceway ponds) we maintained our culture at circa 10 times lower concentration than scaled PBRs (Brennan and Owende 2010), allowing deeper light penetration.

The computational fluid dynamics (CFD) model showed that individual cells in our ePBR treatment were subjected to a time-integrated photon flux of 180 μmol photons m^{-2} s^{-1} across the day. If supplied as static light this would saturate growth of *Synechocystis* (Du et al. 2016). We also showed that cultures grown under static light of the same integrated photon flux as in the ePBR (12/12h, 180 μmol photons m^{-2} s^{-1}/dark) grew 10 times faster (Fig. F1).

Collectively this shows that the rapidly fluctuating light environment has a profound negative impact on the capacity of *Synechocystis* to utilize photons efficiently to support growth and biomass accumulation.

The slow growth of *Synechocystis* in the ePBR was starkly different from exponential growth under common laboratory conditions [e.g.: (Du et al. 2016; Ermakova et al. 2016; Wilson et al. 2006)], but resembled rates reported for PBR field experiments [doubling time of 1-10 days is normal; (Brennan and Owende 2010)]. Our culture density was only 0.076±0.01 g TOC L^{-1}, which assuming that 50% of the biomass consists of carbon (Kim et al. 2011), translates into 0.15 g dry weight L^{-1}. This is significantly lower than most industrial PBRs which are usually maintained at between 1 to 10 g dry weight L^{-1} (Brennan and Owende 2010). However, most PBRs are designed with a cross section that is only a few centimeters thick, whereas the ePBR is 23 cm deep. Hence the surface to volume ratio of PBRs are generally around 50 m^{-1} (Posten 2009) whereas the ePBR has a ratio of only 7.5 m^{-1}. This means that significantly less light reaches the cells in the bottom of the ePBR than in an industrial PBR, given equal culture density. Thus our low experimental density compensated to some degree for the depth of the ePBR. When normalized to the surface area, we saw growth rates of 9 g TOC m^{-2} day^{-1} (18 g dry weight m^{-2} day^{-1}), which is within the range reported for various closed PBRs [10-40 g dry weight m^{-2} day^{-1} (Brennan and Owende 2010)]. By applying a rapid mixing regime we also moved cells in and out of the illuminated part of the ePBR with an average frequency of 0.17 s^{-1} comparable to reports for industrial scale tubular and airlift PBRs [10 to 0.01 s^{-1} (Barbosa et al. 2003; Huang et al. 2015; Perner-Nochta and Posten 2007)]. Although the range of conditions in industrial size PBRs are highly variable, the ePBR system can facilitate characterization of *Synechocystis* photophysiology under industrially relevant conditions.

Our CFD model illustrates the stochastic and dynamic light environment perceived by cells in PBRs. Yet the effect of rapidly fluctuating light on photosynthesis has mainly been investigated through highly controlled L/D flash experiments using square-wave treatments of supra-saturating (500 to 2000 μmol photons m^{-2} s^{-1}) monochromatic light. These studies have shown that under L/D oscillation around 100 s^{-1} growth rates may be maintained, or even slightly elevated compared to constant light, due to reduction in photodamage (Nedbal et al. 1996). Square-wave L/D oscillations >0.1 s^{-1} may also have a positive impact on culture productivity by allowing regeneration of essential metabolites downstream of the electron transport chain during dark periods (Takache et al. 2015). Growth rates in scaled-down PBRs, have also been shown to correlate with the frequency of L/D oscillations under static surface light (Huang et al. 2015). As the frequency of L/D oscillations decreases to <0.1 s^{-1} there appears to be little effect on the growth of the autotrophic cultures, and growth rates shift to correlate with surface intensity or duration of the light period (Barbosa et al. 2003). However, in addition to using unrealistic square-wave light conditions, these studies were performed under either static high or low light and did not include diurnal fluctuations in light associated with outdoor conditions.

In contrast to these results, we observed a 10-fold decrease in growth rate under our fluctuating light conditions compared to growth under constant light in Erlenmeyer flasks (Fig. F1), suggesting that realistic growth fluctuations in light have a detrimental effect on culture productivity. This can likely in part be explained through the amount of time the cells spent at different light intensities. The cell-specific light model showed that 6 h out of the 12 h daytime was spent below the compensation point for photosynthesis (Fig. 1.7). Only a combined 2.5 h per daytime was spent above the $P_{half\text{-}max}$ (250 μmol photons m^{-2} s^{-1}) where photosynthesis is operating at a high rate in the photo-acclimatized culture. This light was delivered to the cells as a few thousand flashes per 12 h daytime and were most often less

than 1 s long (Fig. A3). This is likely not enough time to sustain metabolic processes across the relatively long periods (1-6) spent below the compensation point. Our results suggest that the boost in productivity associated with flashing light may be an artifact of controlled laboratory conditions and not applicable to current state of-the-art photobioreactors grown under natural light conditions.

4.2. Diurnal Changes in Photosynthetic Capacity

The photosynthetic capacity of the ePBR culture was robust across the day, as illustrated by the P-I response (Fig. 1.6, Table 1). Interestingly the TOC normalized P_{max} was twice as high in the ePBR culture as in exponentially growing cells under both static low or high light (30 and 400 µmol photons m^{-2} s^{-1}, Table F2). Such an elevated P_{max} suggests that the ePBR culture had optimized the capacity to process electrons downstream of PSI (Behrenfeld et al. 2004), likely in an effort to maximize the utilization of photons harvested during the intense but brief flashes (Yarnold et al. 2016).

We observed diurnal changes in the F_v/F_M but the magnitude of these changes was small (0.53 to 0.50 during the illuminated period). It is very important to distinguish between fluorescence parameters collected using red or blue measuring lights since the former excites phycobilisomes and chl *a*, whereas the latter only targets chl *a*. This has important impacts on the amplitude of the F_v/F_M parameters and abilities to detect phycobilisome related quenching mechanisms such as state transitions and OCP-quenching. We used a blue measuring light to investigate the quantum yield of PSII (F_v/F_M) and our results (0.53 to 0.50 during the illuminated period) are within the range reported for other cyanobacteria species that have been probed with a blue measuring light under nutrient replete conditions and low light intensities (Hwang et al. 2008; Li et al. 2012; Liu and Qiu 2012; Ritchie 2008). This suggests that very little, if any, photoinhibition to PSII occurred *in situ* in the ePBR. This stands in contrast to observations in the green algae *Chlamydomonas reinhardtii* where 0.1 s^{-1}

simulated L/D oscillation caused photodamage and reduced growth rates (Yarnold et al. 2016). This may be explained by the fact that an individual cell only spent a total of 30 min per 12 h daytime, and that this was not sufficient time to cause major photodamage. The sharp increase/decrease in F_v/F_M around dawn and dusk (Fig. 1.6) likely coincides with state transitions (Behrenfeld and Kolber 1999; Richier et al. 2012). Collectively our observations suggest that the cells have acclimatized to the oscillating light environment, maintain a robust photosynthetic machinery across the day, and experience minimal photoinhibition.

4.3. Diurnal Changes in Non-Photochemical Quenching

Non-photochemical quenching is one mechanism used by autotrophs to harmlessly dissipate photons when supplied in excess of their photosynthetic capacity. The NPQ mechanism is often suggested to be important under light conditions associated with mass cultivation (Berteotti et al. 2016; Posten 2009) and tuning NPQ directly, or indirectly through reduction of the antenna size, has been suggested as an avenue of genetic engineering toward high productivity strains (Melis 2009; Radakovits et al. 2010). Interestingly, there have been few actual measurements of NPQ *in situ* in PBRs. Measurements that are published are primarily based on P-I curves and thus capture the NPQ capacity and not the *in situ* activity (Berteotti et al. 2016; Masojídek et al. 2003; Yarnold et al. 2016).

In our P-I curves we observed that OCP dependent NPQ in the ePBR acclimatized culture was not induced *ex situ* until around 300-500 µmol photons m^{-2} s^{-1} (Fig. 1.6B and Fig. B1A). We used a red measuring light to detect OCP dependent NPQ, which occurs at the level of the phycobilisome. The white LED of the ePBR was used as actinic light to better mimic *in situ* conditions. Given that the predicted 10 min average cell-specific photon flux never got above 400 µmol photons m^{-2} s^{-1} (Fig. 1.4C), we would expect that at any given time only a very small fraction of cells, that recently spent more than normal time close to the surface, would induce OCP-quenching *in situ*. Additionally, a larger portion of

the blue light, which activates OCP dependent quenching, is filtered out from the total PAR by at least 2 cm depth and below (Fig. D3A), reducing the likelihood that NPQ becomes induced in any given cell. When we measured *in situ* quenching of fluorescence within the ePBR culture we could not detect significant induction at any point throughout the day (Table 2). This illustrates how the CFD modeling together with the P-I data could be used to accurately predict responses of photoautotrophs to growth in different PBRs. These results raise important questions about our current understanding of NPQ and its role in photoprotection under nutrient replete and realistic industrial light environments.

The regulation of rapidly inducible NPQ is very different between cyanobacteria and microalgae. Chloroplast containing eukaryotes regulates NPQ through acidification of the lumen (Oxborough and Horton 1988) whereas OCP acts as a dual photoreceptor/quencher and blue light intensity regulates its activity (Wilson et al. 2006). It is possible that other cyanobacterial or microalgal species induce NPQ at lower light intensities, and depending on the design of the reactor the irradiance threshold for NPQ may be reached at some point throughout the day. We have previously observed that disruption of OCP increased growth rates of *Synechocystis* in thin PBRs in greenhouses (Peers 2015), suggesting that NPQ induction will occur if the light intensities are high enough. On the other hand, we did not observe induction of NPQ *in situ* in the ePBR using the model diatom *Phaeodactylum tricornutum* (Jallet et al. 2016a). These contrasting observations collectively illustrate that it cannot be assumed that NPQ is induced under high and fluctuating light. Regarding the experiments in this Chapter it did not appear that NPQ was responsible for the low rates of biomass accumulation we observed in *Synechocystis* under our experimental conditions.

4.4. Diurnal Changes in Alternative Electron Transport

We measured oxygen consumption and evolution *ex situ* under the predicted CFD model of the cell-specific light history. We emphasize that the absolute rates of oxygen

fluxes need to be interpreted cautiously since we used the dichromatic actinic light (654 nm and 430 nm) of the PAM flourometer during the fluctuating light experiment. These two wavelengths specifically target the peak absorption of chl *a* and phycobiliproteins (see Fig. D3) and therefore drive photosynthesis more efficiently than the white light of the ePBR does (α of 1.23±0.05 compared to 3.72±0.27 for the white LEDs of the ePBR; Table D2). Unfortunately, the software associated with the white LED of the ePBR could not be program to response fast and accurately enough to recreate the cell-specific light environment. If we had accesses to white LEDs we would have preferred to use them and we suggest that future studies should strive to use broad spectrums of light similar to natural sunlight during similar experiments. With these limitations in mind, our main conclusions are based on the relative rates of light-dependent oxygen consumption and gross oxygen evolution.

Alternative electron transport (AET) is an important photoprotective mechanism in cyanobacteria (Ermakova et al. 2016). Cells may induce AET as a means to modify their ATP to NADPH ratio and generate more energy that can be used for basal metabolic rather than reductive power for carbon fixation (Bailleul et al. 2017). Unlike OCP-quenching we observed light-induced oxygen consumption, or AET, when we subjected ePBR cultures to the predicted cell-specific light environment *ex situ*. Based on the MIMS quantification, light-dependent oxygen consumption dispensed 50% of the electrons flowing through the electron transport chain. This is a similar amount relative to what has been observed under highly stressful conditions such as carbon limitation and for min scale fluctuations in growth light (Allahverdiyeva et al. 2013; Ermakova et al. 2016; Shimakawa et al. 2015). Under artificially fluctuating light conditions, mutants lacking either of the flavodiiron heterodimers (Flv2/4 and Flv1/3) or the cytochrome bd quinol oxidase experience severely reduced growth phenotypes and photo-bleaching (Allahverdiyeva et al. 2013; Lea-Smith et al. 2013; Zhang et al. 2012). In combination with our results, this suggests that AET, and not NPQ, is the

photoprotective mechanism cyanobacteria first use to cope with dynamic and fluctuating light. By using AET instead of NPQ the cells also have the additional benefit of creating a proton motive force that can be used to generate ATP for molecular work hat does not require NADPH, such as transporter activity.

Very little is known about what regulates mechanisms of AET. Since the redox state of the plastoquinone pool exerts a strong influence on global transcription (Hihara et al. 2003) and regulates NPQ in chloroplasts (Oxborough and Horton 1988) it may influence the activity of AET too. Given that the light environment changes in short (1-6 s) but frequent (350 h^{-1}) exposure to light intensities below the compensation point for photosynthesis (Fig. A3B), this likely leads to rapid oxidation of the plastoquinone pool, as suggested by the fluctuations in Y(II) [Fig. 1.9], which could induce transcription of genes associated with respiration or activation of terminal respiratory oxidases. Conversely, short pulses of excess light would reduce the plastoquinone pool that could lead to the activation of enzymes(s) involved in photoprotective AET. Regardless of the mechanism, tuning AET through genetic manipulation may potentially be a successful way to increase carbon fixation and growth of *Synechocystis* in PBRs. Based on our physiological data we cannot pinpoint the enzyme(s) involved in AET. However, observations in Chapter 2 seek to address the transcriptional responses associated with growth in rapidly changing light which could provide a first step in manipulating AET for increased photosynthetic productivity.

4.5. Conclusions

In our experiments we isolated the effects of dynamic and rapidly changing light and showed that it did not induce NPQ *in situ* and there was no indication of photoinhibition. This stands in contrast to common perceptions that the light environment in PBR inevitably induces excess NPQ and causes photodamage in PBRs (Berteotti et al. 2016; Bitog et al. 2011; Kirst et al. 2012; Posten 2009; Shigeoka et al. 2002). Much of our understanding of

high light stress and photo-acclimatization in algae and cyanobacteria comes from experiments where cells are acclimatized to low light intensities for dozens of generations and suddenly subjected to high light (Förster et al. 2006; Hihara et al. 2001; Muramatsu and Hihara 2012). This may not reflect long-term photo-acclimatization to growth in PBRs, as our data suggests. If our results extend to other species and scaled PBRs it indicates that attempts at tuning NPQ through genetic engineering (Berteotti et al. 2016) may have little effect on the productivity of the PBR. Attempts at reducing photodamage through reactor-design (Posten 2009), rapid fluctuations in light (Nedbal et al. 1996) or genetic engineering (Shigeoka et al. 2002) may also be misguided efforts. Instead our data suggests that more focus should be devoted to exploring whether AET can be manipulated to increase productivity of PBRs. This has the potential to create strains of phototrops with elevated growth rates of phototrophs that are adapted to the unique conditions associated with PBR cultivation.

In mass cultivation conditions with less fluctuating light, such as thin PBRs or less dense cultures, it is still possible that NPQ can be targeted to increase productivity (Masojidek et al. 2003; Peers 2015). The discrepancies between different studies may be solved through better models and observations of cell-specific light histories in commercial state-of-the-art PBRs. This would generate a benchmark of what light conditions we strive to adapt future production strain to. Future genetic engineering attempts should be evaluated against a given bench-marked light environment. *in situ* measurements of NPQ in WT should also accompany these engineering attempts to illustrate the feasibility of the approach.

Under industrial conditions in PBRs photoautotrophs may face a multitude of different stressors aside from high light, including low concentrations of inorganic carbon, limitations in inorganic nutrients, viral and bacterial parasitism, and predation. All of these stressors likely interact with light and change the dynamics of photoprotection and photodamage. We suggest that future studies should begin incorporating additional stressors

into experiments using realistic light environments. This will give insight into how dynamic changes in light intensities interact with other stressors to shape how photosynthesis and photoprotective mechanisms function.

In this study we characterized the cell-specific light environment of the bench-top ePBR, which to our knowledge is the first time this is done for a commercial bench-scale PBR. We stress that future studies regarding strain productivity, metabolic engineering, and stressors associated with mass cultivation in PBR, should incorporate more realistic light environments into their experimental design. The fact that we observed such a drastic reduction in growth rate at higher densities in the ePBR suggests that there are major metabolic differences between cells grown in dynamic and rapidly changing light versus static light.

5. Tables

Table 1.1. Parameters derived from the rapid photosynthesis versus irradiance curves. Differences between time points were analyzed using 1-way RM-ANOVA (N=3) and were non-significant for any of the five parameters. Chl *a* concentration was 3±0.5 µg mL^{-1}.

P-I parameters on chl *a* basis

ZT (h)	Dark respiration (µmol O_2 [mg chl *a*] h^{-1})	Compensation point (µmol photons m^{-2} s^{-1})	α (µmol O_2 [mg chl *a*] h^{-1})/ (µmol photons m^{-2} s^{-1})	P_{max} (µmol O_2 [mg chl *a*] h^{-1})	E_k (µmol photons m^{-2} s^{-1})
0.25	-17.1±8.6	11.7±6.50	1.29±0.15	482±68	374±62
2	-19.1±8.6	9.32±8.32	1.22±0.17	483±64	403±105
6	-15.7±8.6	9.33±6.03	1.23±0.05	527±17	429±31
10	-14.5±9.9	6.33±7.77	1.31±0.17	467±64	363±89
11.75	-18.8±10.5	9.00±9.50	1.42±0.26	469±32	341±88
$F_{4,8}$ (p)	*0.138 (0.963)*	*0.311 (0.863)*	*1.29 (0.352)*	*1.29 (0.352)*	*2.87 (0.095)*

Table 1.2. Relative quenching of maximum fluorescence and its origin. See Section 2.2.5 and Fig. B1 for derivation of parameters. Briefly a PAM fluorometery with a red measuring light (620 nm) and blue actinic light (430 nm) was used to derive *in situ* (>60s after removal of culture from ePBR) and capacities for fluorescence quenching. Data is shown as relative quenching of maximum fluorescence. Differences between time points were analyzed using 1-way RM-ANOVA (N=3). Letters denote significant differences between time points. Chl *a* concentration was 3±0.5 µg mL^{-1}

	Fractional quenching of fluorescence		
ZT Time (h past dawn)	*In situ* $OCP_{in\ situ}$-quenching	Maximal OCP capacity OCP_{max}-quenching	State transition quenching capacity (State-quenching)
1	0.00±0.00	$0.484±0.014^{a}$	$0.274±0.035^{a}$
3	0.020±0.010	$0.433±0.016^{abc}$	$0.240±0.021^{ab}$
6	0.015±0.011	$0.408±0.015^{bc}$	$0.223±0.020^{b}$
9	0.010±0.001	$0.411±0.013^{c}$	$0.230±0.013^{b}$
11	0.011±0.003	$0.408±0.013^{c}$	$0.234±0.011^{b}$
$F_{4,8}$ (p)	*3.25 (0.073)*	*10.6 (0.003)*	*9.58 (0.004)*

7. Figures

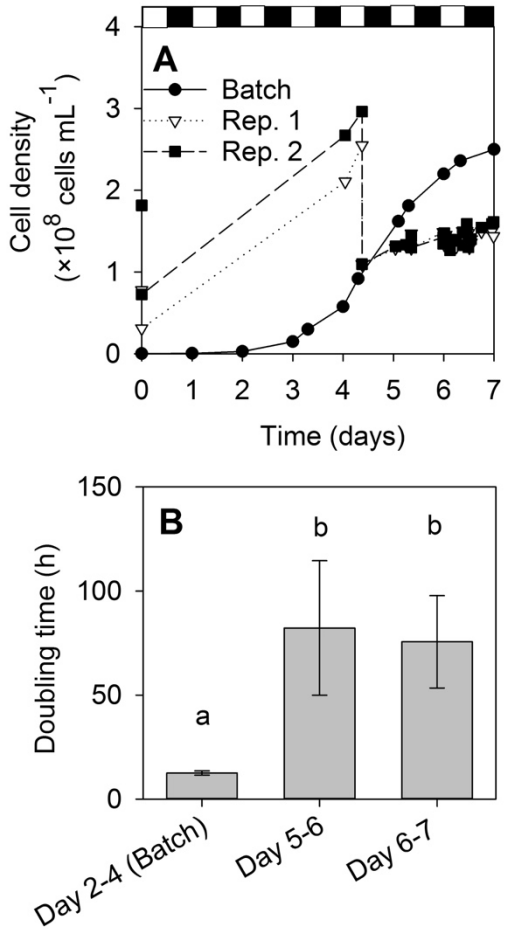

Figure 1.1. Growth curves, experimental densities and growth rates. A) example of batch culture grown in the ePBR under sinusoidal light (Batch) and during the semi-continuous cultivation experiment. Note that the cell densities drop at specific sampling points, B) comparison of doubling times during low density exponential growth (Batch exp.) and the first day of semi-continuous growth (day 5-6) and the sampling day (day 6-7). Differences in growth rates were analyzed using 1-way ANOVA, $F_{2,15}=17.311$, $p<0.001$.

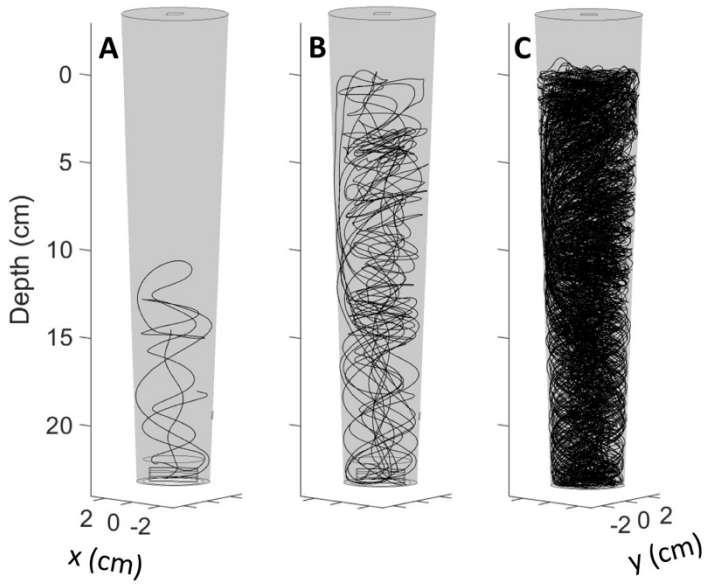

Figure 1.2. *In silico* tracking of a particle (single cells) in the ePBR using computational fluid dynamic. Tracking of the position of a single particle (cell) is shown for different periods of time. A) 6 s, B) 60 s, C) 600 s. *[Note from the author; figure credit Chen Shen as part of his dissertation]*

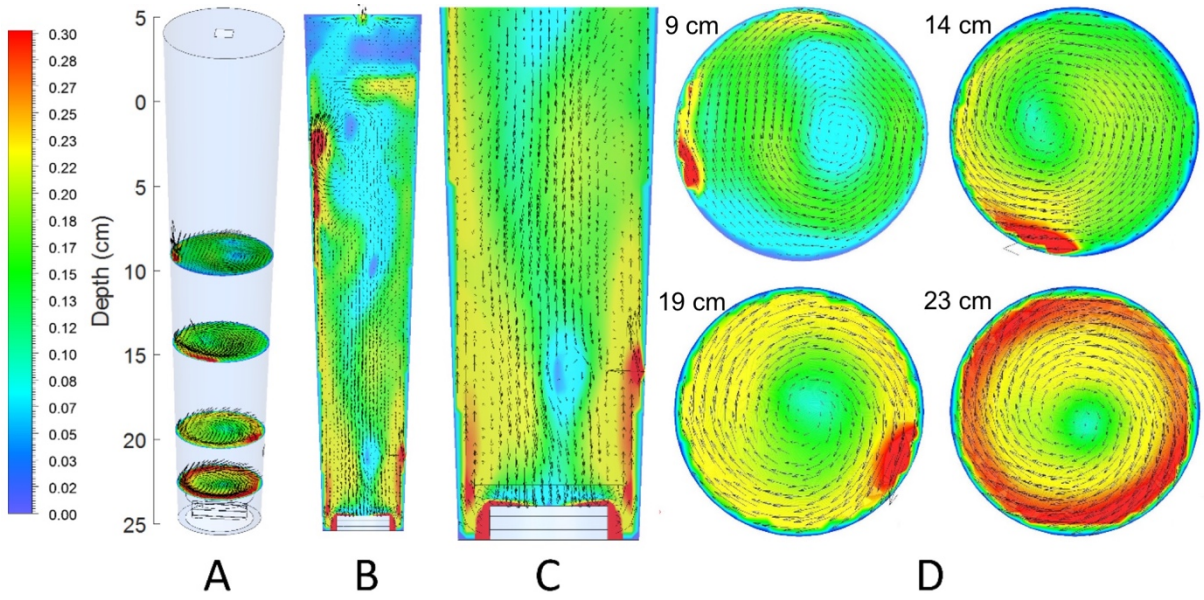

Figure 1.3. A Snapshot of the computational fluid dynamic model showing instantaneous velocity vectors and contours of the ePBR vessel. A) four different horizontal cross sections illustrated in the ePBR, B) vertical cross section, C) close-up of to lower half of the ePBR with stir bar in white and red zone to the right coinciding with the entry point of the bubble stream, and D) vertical overviews or the transects shown in A. Color indicate velocity of fluid in m s^{-1} and vector arrows show direction. *[Note from the author; figure credit Chen Shen as part of his dissertation]*

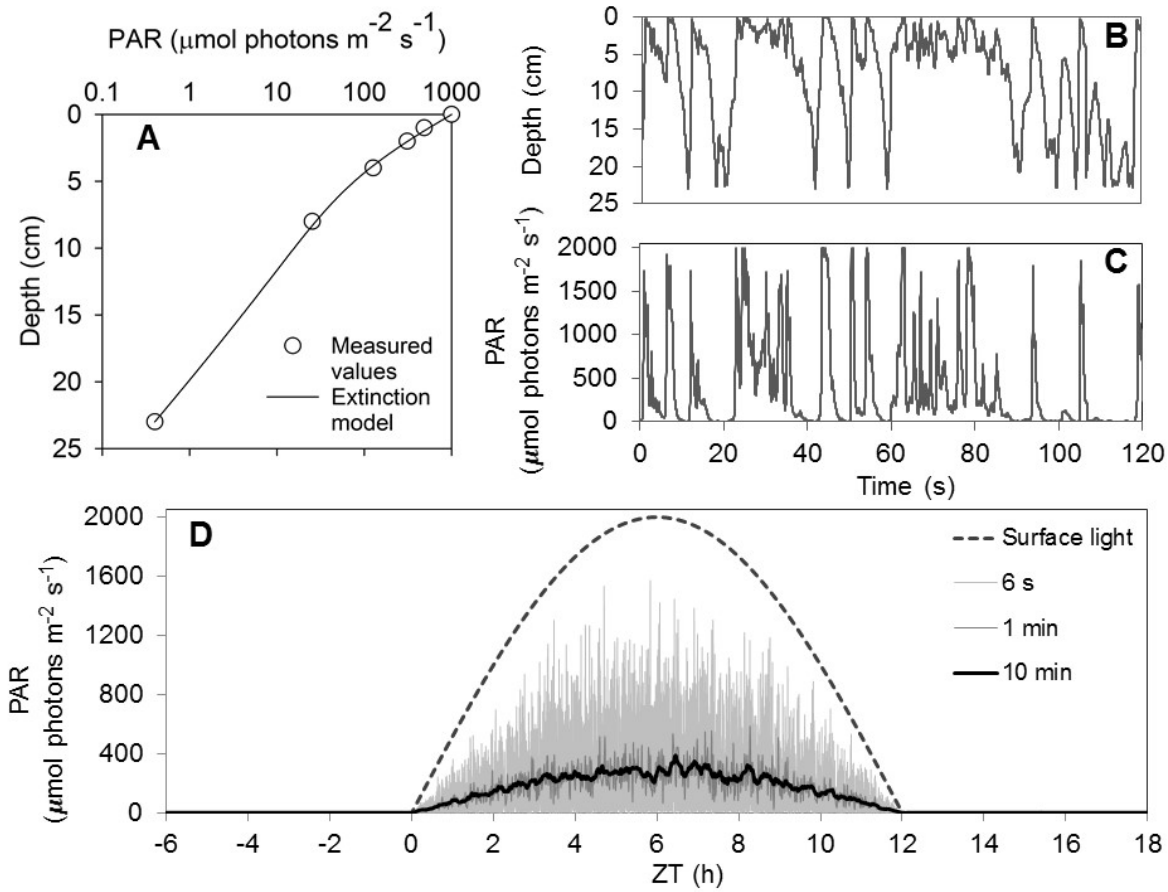

Figure 1.4. Diurnal changes in the cell-specific light environment. A) Light extinction through the ePBR vessel measured at six discreet depths and modeled based on Eq. 3 (Section 2.4). B) computational fluid dynamic results showing the vertical position of a single cell in the ePBR during two min, C) the vertical position in panel C translated to cell-specific light environment using the surface light intensity at ZT6 and the light extinction model shown in panel A, and D) the cell-specific light environment model across a day, including diurnal changes in surface light intensity. For clarity only running averages of 6 s, one min, and 10 min are shown.

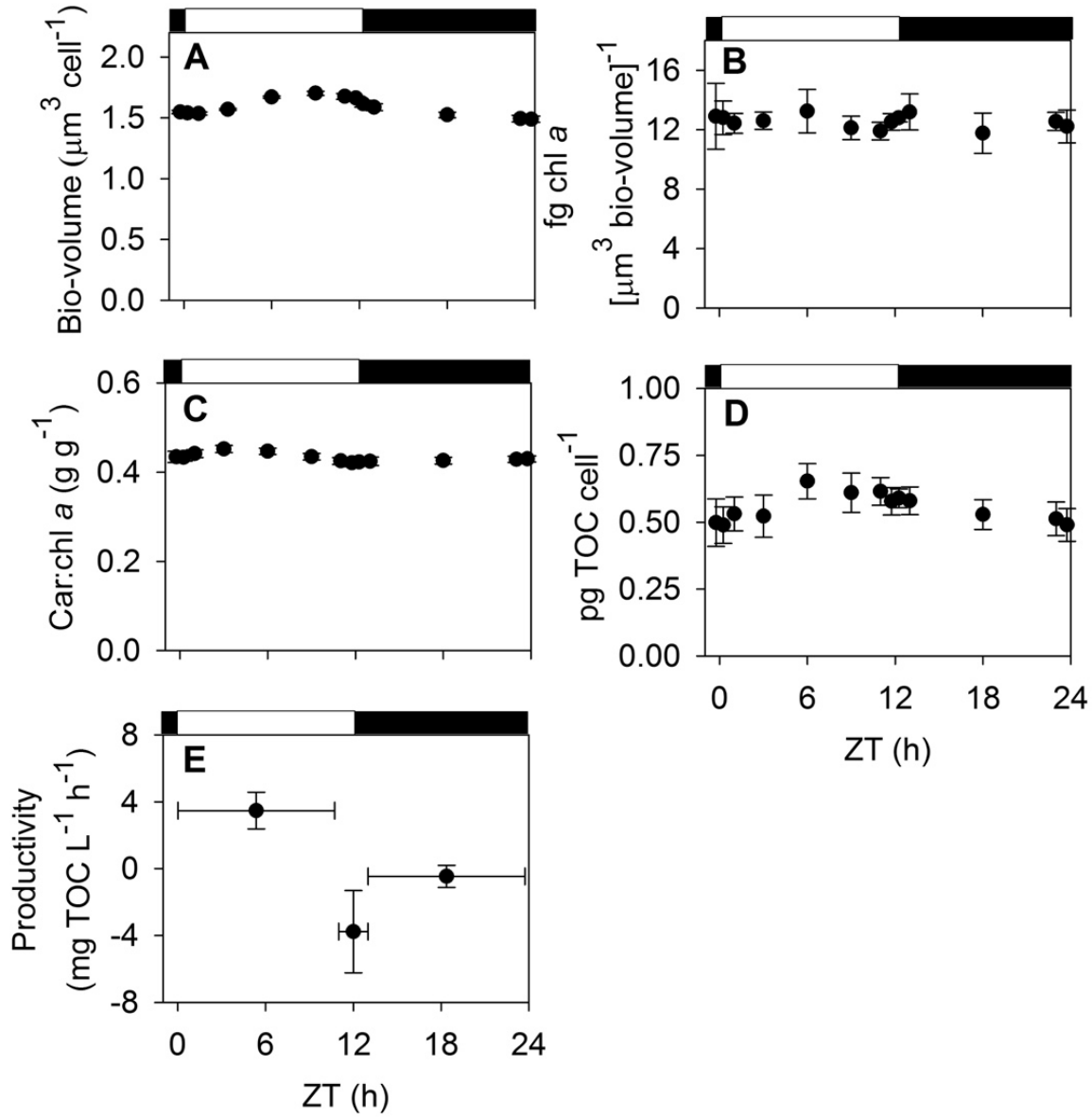

Figure 1.5. Diurnal changes in cellular properties. A) average cell bio-volume ($F_{12,60}=116$, $p<0.001$), B) chlorophyll *a* density per bio-volume (n.s., $F_{12,59}=1.11$, $p=0.366$), C) total carotenoid:chl *a* ratio ($F_{12,59}=38.5$, $p<0.001$), D) cell-specific total organic carbon (TOC) content ($F_{12,60}=4.521$, $p<0.001$), E) productivity described as TOC accumulation per volume culture ($F_{2,10}=26.6$, $p<0.001$). Differences between time points were analyzed using RM-ANOVA (N=5-6). For clarity we have provided results from the statistical analysis between time points in a separate table (Table E1). Vertical error bars show SD and horizontal bars in E illustrates the temporal range encompassed in the averages.

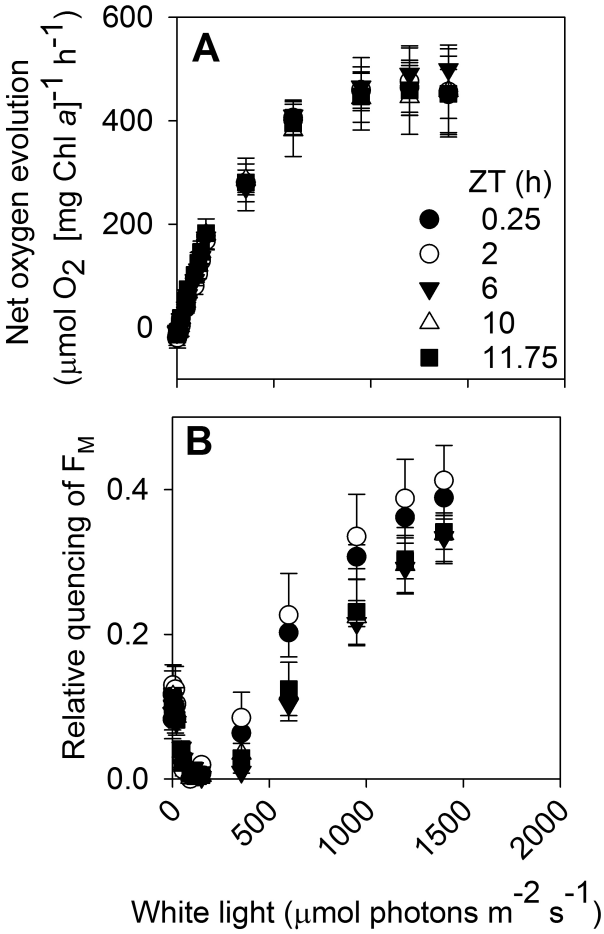

Figure 1.6. Photosynthesis versus irradiance curves. A) net-oxygen production measured with a Firesting oxygen probe, B) relative quenching of fluorescence calculated as described in Section 2.3.4. The white LED growth lights of the ePBR was used as actinic light source. Shown are averages±SD (N=3) for A, and averages and range for B (N=2). Chl *a* concentration was 3±0.5 μg mL^{-1} during the measurements.

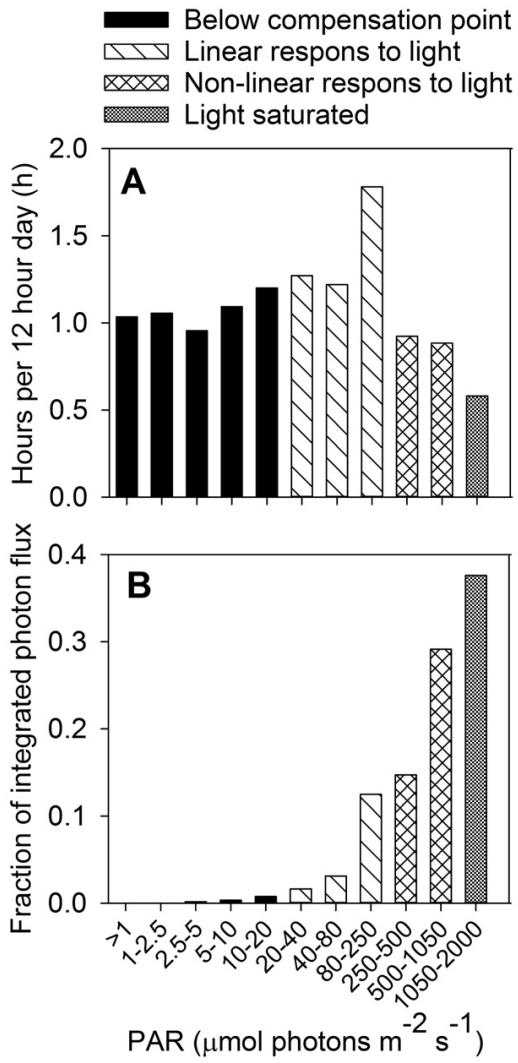

Figure 1.7. Integration of the cell-specific light environment with P-I parameters. A) accumulation of time a cell was predicted to spend at different light intensities throughout the day, B fraction of integrated daily photon flux they receive at each light intensity. Categories are based on pooled analysis of all diurnal P-I curves (N=15 response curves and 210 data points) using the Wait-In-Line model as described in (Ritchie 2008). Black bars; time spent below the compensation point, striped bars; time spent in the linear response range ($<P_{half-max}$), checked bars; time spent in the non-linear response range ($>P_{half-max}$; $<E_{optimum}$), and gray bars; time spent in saturation ($>E_{optimum}$).

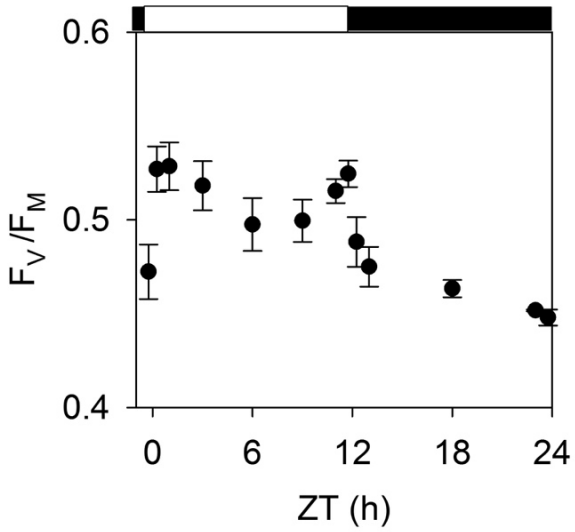

Figure 1.8. *In situ* quantum yield of photosystem II (F_v/F_M) measured using a blue excitation light (450 nm). Shown are averages±SD. Differences between time points were analyzed using RM-ANOVA ($F_{12,47}=45.5$, $p<0.001$). Results from the statistical analysis between time points are shown in a separate table (Table E1).

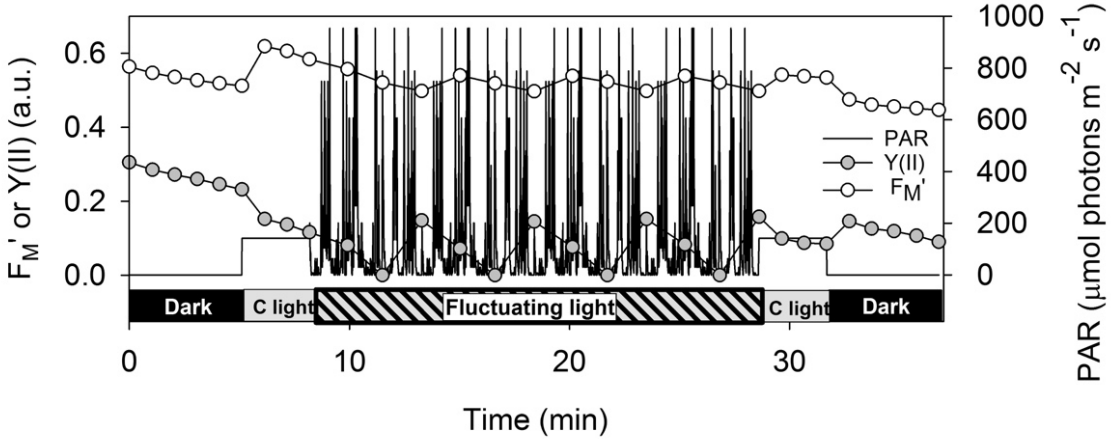

Figure 1.9. Chlorophyll fluorescence during the *ex situ* fluctuating light treatment. Example of a representative sample at ZT2. Maximal fluorescence (F_M') and the yield of photosystem II [Y(II)] is shown along with the changes in light intensity across the treatment. Saturating pulses were applied every 60 s during constant light/dark and every 100 s during fluctuating light. Chl *a* concentration was 15 ug mL^{-1}.

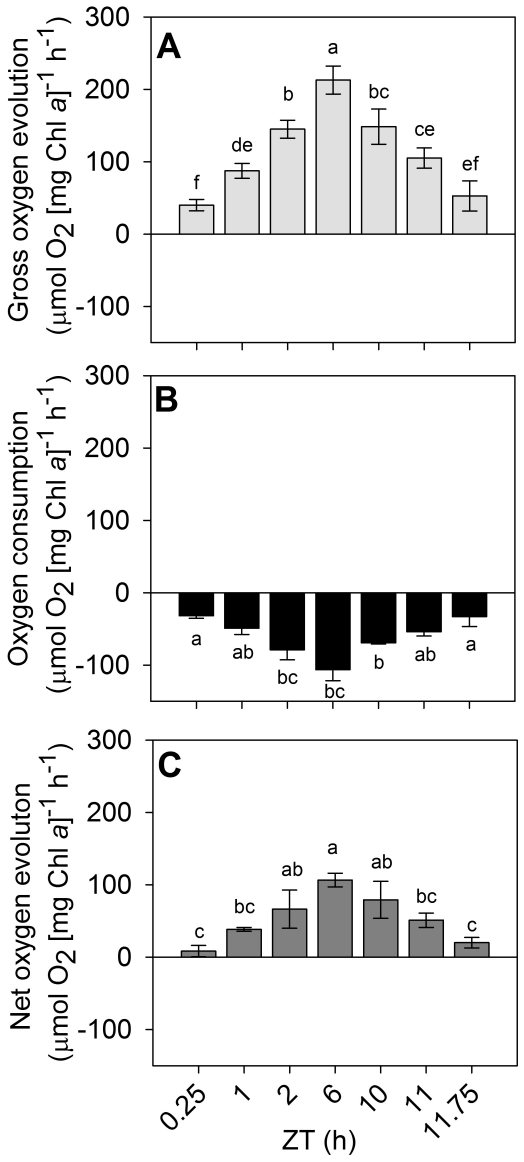

Figure 1.10. Illuminated rates of oxygen evolution and consumption during the *ex situ* fluctuating light experiment. The light treatment was based on to the cell-specific light environment model, applied using blue (430 nm) and red (640 nm) LEDs of the Dual-PAM and measurements were collected using MIMS (see Table D1 for information on maximum and integrated photon flux at different ZT times). A) gross oxygen evolution corresponding to photosynthesis, B) light-dependent oxygen consumption, corresponding to respiration and alternative electron transport, and C) net oxygen evolution (evolution + consumption). Temporal differences in evolution, consumption and net-photosynthesis were analyzed using 1-way RM-ANOVA with $F_{6,12} = 34.6$, 21.0, and 14.3, respectively, and <0.001 for all three parameters. Chl *a* concentration was 15 μg mL^{-1}.

CHAPTER 2: THE TRANSCRIPTOME OF *SYNECHOCYSTIS* SP. PCC 6803 SUGGESTS FEW LIGHT STRESS RESPONSES UNDER GROWTH IN A REALISTIC LIGHT ENVIRONMENT OF A PHOTOBIOREACTOR: A PRELIMINARY STUDY

Summary

Microbial autotrophs perform photosynthetic growth under variable light intensities. During outdoor mass cultivation changes in light can be rapid and unpredictable. This is due to a combination of changes in solar irradiance and self-shading with the cultivation system. To explore how a photosynthetic cyanobacterium acclimatize to a dynamic and rapidly changing light environment, I grew the model cyanobacterium *Synechocystis* sp. PCC 6803 under a sinusoidal light regime in bench-top photobioreactors. The light environment and physiological responses are described in Chapter 1. Chapter 2 presents data associated with the transcriptional responses over a day/night cycle. I sampled the transcriptome with high resolution (30 min) around the transition periods of dusk and dawn, and less frequently around mid-day and during the night. I did not see any transcriptional indications of photodamage or other common indicators of high light stress, despite observing a very slow growth rate. Transcript abundance of genes related to light harvesting, photosynthetic electron transport, and pigment synthesis was significantly higher across the day compared to the night. There was no change in photosynthetic capacity across the day (Chapter 1) suggesting that this regulation is used primarily to sustain growth, which occurs during the day. Transcripts encoding chaperones, proteases, reactive oxygen species scavengers, and high light inducible proteins were not upregulated during the day. Genes involved in photoprotective mechanisms such as the orange carotenoid protein and flavodiiron proteins were not upregulated throughout the day. These two sets of observations, in combination with *in situ* measurements of non-photochemical quenching and the quantum yield of photosystem

II (Chapter 1), challenge the perception that rapidly changing light causes major stress on microbial autotrophs grown in mass cultivation.

1. Introduction

Mass cultivation of aquatic phototrophs in photobioreactors (PBRs) has the potential to produce sustainable biofuels thus reduce carbon emission and dampen climate change (Moody et al. 2014). This has not been realized because the technology has been hampered by a lack of scalability in terms of growth rate and productivity from benchtop to industrial scales (Grobbelaar 2012). Growth rates based on laboratory experiments decrease 10-fold in large-scale cultivation systems (Brennan and Owende 2010). Aquatic autotrophs have evolved under light regimes that bear little resemblance to that of PBRs, which may explain this reduced productivity. Light fluctuates rapidly in PBRs due to self-shading and differently designed reactors may create cell-specific light/dark oscillations with frequency from 10 to 0.01 s^{-1} (Barbosa et al. 2003; Huang et al. 2015; Perner-Nochta and Posten 2007). Compounded on this fluctuation is a gradual increase/decrease in light intensities at dawn and dusk. At noon light intensities peak at irradiances much higher than any photosynthetic organism can utilize, which may cause photoinhibition and decreased productivity.

Photosynthetic organisms are acutely responsive to changes in light. Gene expression, protein regulation, and complex sensory and signal pathways, queued by both light receptors and the redox state of the plastoquinone pool, interplay to avoiding the formation of reactive oxygen species causing cellular damage [see reviews: (Foyer and Noctor 2009; Jallet et al. 2016b; Niyogi 2000; Woodson 2016)]. Responses to changes in light have mainly been studied through single shifts between one constant irradiance to another. When the light changes from low to higher intensities, microbial autotrophs adapt their photosynthetic machinery over the course of hours to days by changing pigment composition (Schluter et al. 2006), reducing the abundance of some light harvesting

complexes (Macintyre et al. 2002), exchanging the D1 protein of PSII to a homologue less susceptible to photodamage (Sicora et al. 2006), up-regulating photorepair mechanisms (Muramatsu and Hihara 2012), modifying the PSI/PSII ratio (Murakami 1997), and increasing the activity of the Calvin-Bassham-Benson cycle [CBB cycle; (Mettler et al. 2014)]. On shorter time scales several rapidly inducible photoprotective mechanisms help dissipate excess light energy, including non-photochemical quenching (NPQ), state transitions, and modification to linear electron flow [see review by:(Derks et al. 2015)]. Photosynthesis is therefore a highly dynamic and malleable process and responses to complex light environment are difficult to predict. Little is known about how these mechanism operate under naturally or industrially dynamic light environments.

Diurnal changes in global transcription in microbial autotrophs, associated with day and night cycles, have only recently been analyzed with some temporal resolution (Angermayr et al. 2016; Beck et al. 2014; Saha et al. 2016; Zones et al. 2015), and few studies have incorporated dynamic changes in light intensities [but see Labiosa et al. (2006)]. These studies have suggested that there may be light stress associated with the onset of light under a square-wave cycle (Angermayr et al. 2016) but little evidence of this was seen under dynamic light (Labiosa et al. 2006). However, in the latter study light intensities peaked at only 400 μmol photons m^{-2} s^{-1} on the surface of the culture vessel and when self-shading was incorporated cells experienced only an average 31 μmol photons m^{-2} s^{-1} at that time, which is probably too low to induce photodamage.

Metabolic engineering of aquatic phototrophs has been explored as a strategy to enhance biofuel precursor productivity of PBRs. Various strategies involving disruption of central carbon metabolism have been explored as avenues to enhance the quality of the biomass (Carrieri et al. 2008; Gründel et al. 2012; Kudoh et al. 2014; Tonon et al. 2002; Work et al. 2010). Targeted improvement of photosynthesis has been explored to increase the

photosynthetic rate of photoautotrophs (Ort et al. 2015; Zhu et al. 2010b). Indeed, reducing the cell-specific light harvesting capacity have resulted in higher productivities in the lab (Cazzaniga et al. 2014; Kirst et al. 2014; Nakajima and Ueda 1997). Additionally, attempts at tuning photoprotective mechanisms have also yielded some promising results (Berteotti et al. 2016; Peers 2015). However, a better understanding of the metabolic and photosynthetic responses to growth in dynamic PBR light environment is essential to guide future metabolic engineering strategies to increase carbon fixation and partitioning to biofuel precursors.

Synechocystis has a small and well annotated genome [~3600 genes: (Kaneko et al. 1996)] making it is a suitable system biology model for photosynthesis and central carbon metabolism in phototrophs. Due to it relatively well characterized photosynthetic structure, metabolic network, and amenability to genetic modification, it is also a promising candidate for metabolic engineering towards enhanced productivity under mass cultivation and production of industrial compounds (Angermayr et al. 2015; Kaneko et al. 1996; Koksharova and Wolk 2002). The small impact of circadian rhythm on transcription also makes *Synechocystis* a suitable model to study how dynamic and fluctuating light affects global transcription. In *Synechocystis* sp. PCC6803 (*Synechocystis* from here onwards) the main regulation of light response is driven by the redox state of the plastoquinone pool (Hihara et al., 2003), and not circadian rhythms (Beck et al. 2014). Consequently, light itself can be largely isolated as the driver of transcription and metabolic processes in this species.

Since photosynthetic microbes face high light intensities under mass cultivation, it is widely assumed that photodamage and photoprotection reduces the productivity of cultures (Berteotti et al. 2016; Ort et al. 2015; Posten 2009). However, there is little experimental evidence for this. In Chapter 1, I showed that NPQ was not an active photoprotective mechanism under rapidly fluctuating light. Furthermore, the quantum yield of photosystem II (F_V/F_M) did not change across the diel period, indication little net-

photodamage. However, it is still possible that there is some degree of photodamage occurring but that the cells can cope with it through upregulation of photorepair mechanisms. To investigate this, I measured changes in global transcription across the diel cycle. I hypothesized that if light is a stressor during growth in dynamic light, I would detect a transcriptional induction of stress responsive genes once a certain threshold of irradiance is reached in the morning. I expected increased transcription in genes related to photorepair mechanisms, reactive oxygen species scavengers, and photoprotective mechanisms, similarly to what has been observed during constant high light stress (Muramatsu and Hihara 2012). To this end, I grew *Synechocystis* at high density in a bench top photobioreactor under a sinusoidal light regime mimicking solar changes in light intensity. Under this changing light environment I investigated diurnal changes in global transcription with high temporal resolution around the transition from light to dark and dark to light.

2. Materials and Methods

2.1. Growth Conditions and Experimental Design

A glucose tolerant strain of the model cyanobacterium *Synechocystis* sp. PCC6803 originating from the National Renewable Energy Laboratory (NREL) was grown axenically for the experiment described below (gift of Dr. Jianping Yu). Cultures were maintained in BG-11 media (Stanier et al. 1971) modified with a 10 mM TES-NaOH buffer (pH 8) and elevated concentration of phosphate (0.106 M K_2HPO_4). All chemicals used were laboratory grade and purchased from either Fisher® or Sigma-Aldrich® unless specified.

Cultures were grown under a diurnal light regime with sinusoidal light mimicking natural changes in sun light throughout a day (Fig. 1.4). White LED lights with a broad spectrum across the photosynthetically active radiation (PAR) range was used to approximate sun light (see light spectrum in Fig. D3). The cultivation conditions have been described in detail elsewhere (see Chapter 1). Briefly, the cells were acclimatized and grown

in a custom made glass vessel of the Environmental Photobioreactor v1 (ePBR, Phenometrics, East Lansing, MI) at a volume of 500 mL. See Lucker et al. (2014) for a description of the ePBR and Appendix A for a description of the glass vessel. The culture was sparged with 1% CO_2 enriched air at a rate of 0.5 L min^{-1} to avoid inorganic carbon limitation. The day length was 12 h per 24 h period and I will refer to time points using Zeitgeber (ZT) time throughout this chapter (Van Alphen and Hellingwerf 2015), which starts the 24 h period at dawn. A semi-continuous cultivation strategy allowed for sampling of up to 15% of the total culture volume without depleting experimental replicates. The culture was maintained at a high density in mid-linear, light limited, growth, at $1.4\times10^8\pm0.1\times10^8$ cells mL^{-1} (N=90) during the experimental sampling.

Due to self-shading within the culture the cells experienced rapid fluctuations in light between the dark bottom of the reactors and the surface (Fig. A3). These cell-specific fluctuations in light has been quantified and are described in detail in section 3.2. of Chapter 1. In summary a single cell was only subjected to about 15% of the surface PAR over a 1 min period but experienced constant fluctuations between >1 and up to 2000 µmol photons m^{-2} s^{-1} on a second time-scale.

End point samples of each biological replicate were streaked on two different 1% agar plates containing either BG11 + 10 mM glucose or Luria Broth (LB). The plates were incubated at 30°C and 20 µmol photons m^{-2} s^{-1} for 1 week and screen for contamination. No contaminations were observed in any of the experimental replicates used for further analysis.

2.2. Sampling Design

I aimed to capture diurnal changes in the transcriptome and potential light stress responses. Since changes from light to dark, or vice versa, is known to have the most profound effect on the transcriptome of *Synechocystis* onder a diel cycle (Beck et al. 2014;

Saha et al. 2016) I designed my sampling strategy around ZT0 and ZT12 (Table 1). Around these key events I collected RNA samples at ± 15 min and 1 h. I also sampled at ZT3 (mid-morning), ZT6 (zenith), ZT9 (mid-afternoon), and at ZT18 (middle of the dark period). I collected time-series samples from 6 biological replicates and randomly excluded two biological replicates per time point for downstream RNAseq analysis.

2.3. Sampling for RNA

I used the sample method developed by Young et al. (2011) to rapidly quench transcription and RNA degradation during the sampling. A quenching slurry was prepared by storing 25 mL phosphate buffer saline (PBS) in 50 mL Falcon tubes at -24°C for 50 min prior sampling. Within 30 s of pulling a 25 mL sample from the ePBR, the culture was quenched to < 2°C through mixing with the frozen PBS slurry. Cells were pelleted through centrifuged at 2°C (10 min at 3220 g) and re-suspended in *Trizol*® and stored at -24°C for < 1 month. The time from sampling to fixation was never more than 20 min and the cells were maintained at below 2°C during the entire process. A total of 25 mL culture (~15 mg wet-weight biomass) was used for each RNA extraction.

2.4. RNAseq

RNA was extracted from samples frozen in *Trizol*® (Thermo Fischer Scientific, Fair Lawn, NJ) using chloroform and isopropyl alcohol following the manufactures instruction. Genomic DNA was depleted through a 30 min incubation at 37°C with TURBO™ DNase (Thermo Fischer Scientific). Large (>200bp) RNA molecules were purified on silica columns (RNeasy ™ mini kit, Qiagen, Valencia, CA.). Succesfull DNA depletion was confirmed through RT- and nonRT qPCR, were RT reaction yielded consistently >10 lower ct value for the cytochrome b_6/f complex (petB, primers shown in Table 2). The RNA integrity was measured using an Agilent 2200 TapeStation and the median, automatically calculated RNA integrity number (RINe) was 8.5, but ranged from 7.5

to 9.9. Manual inspection of bands showed no signs of ribosomal degradation but the software miss-assigned ribosomal peaks occasionally, likely due to the unusual RNA species found in *Synechocystis* (Beck et al. 2014).

RNAseq was carried out using the Illumina® HiSeq 4000 platform at Duke Center for Genomic and Computational Biology. Ribosomal RNA was depleted using Ribo-Zero rRNA depletion kit for Gram-Negative Bacteria (Illumina, Inc, San Diego, CA) and stranded cDNA was created using the KAPA Stranded mRNA-Seq Kit (Kapa Biosystems, inc. Wilmington, MA) according to the manufacturers instruction, excluding the initial oligo dT selection step. The 48 samples were multiplexed across two sequencing lanes rendering an average 15 million reads per sample (for sample specific information see Table H1).

Reads were aligned to Cyanobase reference genome of *Synechocystis* sp. PCC6803 (Kaneko et al. 1996) using CLC workbench (v. 10.0.1, Qiagen, Aarhus, Denmark). The genome sequence, protein annotations, and GO-terms were downloaded from Cyanobase (on May 24th, 2017: http://genome.annotation.jp/cyanobase/Synechocystis). In total ~90% of all reads mapped to genome, with between 40 and 70% of the read mapping to two non-coding RNAs: a transfer mRNA (tmRNA, ssrA) and the ribonuclease P subunit (RnpB, slr1469). These RNA species are components of the ribosomes (De La Cruz and Vioque 2001) and displayed diurnal oscillation in abundance and was therefore excluded from further analysis to not skew the normalization. Reads Per Kilobase of transcript per Million mapped reads (RPKM) were consequently calculated based only on putative protein coding genes (Mortazavi et al. 2008).

2.5. Statistics

Four biological replicates per time points was analyzed (Table 1) except for one timepoint (ZT-0.25). Statistical analysis of the RNAseq data was performed on RPKM values by CLC

workbench. Principle components analysis (PCA) was performed on the whole putative protein coding transcriptome scale to visualize broad trends and was used as a quality control for variation between biological replicates. Diurnally changes in gene expression was tested using Analysis of Variance (RM 1-way ANOVA) with Bonferroni correction for type II statistical errors. Only genes with a corrected p value < 0.05, and with more than a one-fold change in transcription between one or more time points and the grand mean, were analyzed further.

3. Results

3.1. Growth Conditions and Experimental Design

The growth patterns and photophysiology of *Synechocystis* under the experimental conditions have been described in detail in Chapter 1. In summary the sampled culture grew very slowly with a doubling time of 75±22 h, which was almost 10-fold slower than the maximum exponential growth rate of dilute cultures under 12h/12h 180 μmol photons m^{-2} s^{-1}/dark cycle (7.9±0.72 h). Based on an *in silico* prediction of the light history of cells in the ePBR, cells experienced the same integrated photon flux under these two conditions. The photosynthetic capacity did not change across the day and there were no evidences of photoinhibition (Chapter 1). Non-photochemical quenching (NPQ) was not an active photoprotective mechanism *in situ*, but significant amounts of photosynthetic reductant derived from PSII were diverted back to oxygen through alternative electron transport (AET; Chapter 1).

3.2. General Transcriptional Patterns

I detected transcripts associated with 98.8% of the predicted open reading frames in the *Synechocystis* genome (Table 4). The only genes not detected were transposable elements and hypothetical proteins, which may mirror transcriptionally silent genes or genomic differences between the reference genome and my strain of *Synechocystis*. I found

statistically significant changes in the transcript abundance of 2699, or 74% of the predicted genes (Table 4). This is similar to the green algae *Chlamydomonas reinhardtii* grown under a square wave diel cycle (Zones et al. 2015).

Principal Component Analysis (PCA) compares changes in multiple variables using the minimal numbers of vectors, which is useful to illustrate the magnitude of transcriptional changes between large datasets (Wold et al. 1987). The PCA of the complete *Synechocystis* transcriptome showed that the largest global shifts in the transcriptome occurred in the time frame of 15 min before and after dawn or dusk (around ZT0 and ZT12; Fig. 2.1). The two major axes of the PCA separated the samples along a light/dark (PC 1, explaining 43% of the variability) and morning/afternoon (PC 2; explaining 21% of the variability) gradient (Fig. 2.1). There were very small changes in global transcript abundance between ZT18 and ZT23.75/-0-25 (later part of the night) but otherwise individual time points clustered distinctly from one another.

The variability between biological replicates (N=4) were generally small. Fig. 2.2 shows standard deviations in a few randomly selected genes involved in photosynthesis (A) and other metabolic processes (B). For clarity, I have refrained from including error bars in the rest of the figures but show only significantly changing transcripts (see section 2.5). Do to time constraints I limited my analysis on the genes involved in photosynthesis, photo-repair, photoprotection and acquisition of inorganic nutrients needed to sustain growth.

3.3. Inorganic Carbon and Nitrogen Uptake

The transcriptional response in carbon concentrating mechanisms did not indicate any inorganic carbon limitation. *Synechocystis* has an efficient carbon concentrating system. Ribulose-1,5-bisphosphate carboxylase/oxygenase (Rubisco) operates within a carboxysome structures with elevated pCO_2 in its immediate vicinity, and inducible bicarbonate transporters transport HCO_3- across the cell-membrane (Raven et al. 2014).

Transcript abundance of the plasma membrane bicarbonate import system changed on a diel basis (cmp operon) but was not upregulated during the light period (Fig3. A). Additional transcripts in the low CO_2-inducible, high affinity CO_2 uptake system, cupA and cupB, did not change significantly in abundance (Table H2). I did however observe that genes essential for the carboxysome function were induced by light, including internal carbonic hydrogenases (ecaB and slr1347), and certain structural and assembly genes (ccm operon Fig. 2.3B). I also observed that the genes encoding for the carbon concentrating subunits of the NADH dehydrogenase (ndhF3, ndhF4 and ndhD4) were upregulated between 4 and 8 fold during the light period (Table H2).

Photosynthetic organisms need to import additional inorganic nutrients including nitrogen, phosphorus and potassium to support growth. In the growth media inorganic nitrogen is supplied as nitrate and transcription of the nitrate transporter operon (nrtA, B and C) were one of the most rapidly light induced transcripts in the whole genome (32-fold increase at ZT1 relative to ZT-0.25, Fig. 2.3D).

3.4. Heme and Chlorophyll

Cells halt transcription of pigment synthesis, reaction centers and light harvesting capacity when exposed to sudden high light stress (Muramatsu and Hihara 2012). Chlorophyll and heme biosynthesis share precursors until the formation of protoporphyrin IX. Transcript abundance of ferrochelatase (HemH), the enzyme that inserts iron into protoporphyrin IX and forms the branching point between heme and chl *a* synthesis, strongly decreased in abundance between ZT0.25 and ZT6 (Fig. 2.4A). Other components of heme synthesis increased in transcript abundance during the light period compared to the dark, except for porphobilinogen synthase (hemB) and porphobilinogen deaminase (hemC). This indicates that synthesis of heme was suppressed in favor of chl *a* during the light.

Transcript abundance of chlorophyll a synthase (chlG) and magnesium protoporphyrin IX chelatase subunit H (chlH) did not display a strong diurnal regulation (Fig.4B). The light independent reaction of chlorophyll synthesis, protochlorophyllide reduction, is catalyzed by a chlN and chlL duplex, and these two genes peaked in transcript abundance during the first hour after the light went off (around ZT12) but quickly decreased to a baseline abundance by ZT18. Other transcripts involved in the chlorophyll branch of protoporphyrin IX modulation increased in abundance during the light period compared to the dark (Fig. 2.4B). These results suggest dynamic regulation of heme and chlorophyll synthesis throughout the diel cycle.

3.5. The Light Harvesting Phycobilisome

The phycobilisome is the main light harvesting complex in cyanobacteria. The transcripts of components of the phycobilisome generally increased in abundance across the day (Fig. 2.5). Interestingly, one of the gene in the apcEABC operon encoding the core linker of the phycobilisome did not follow this trend (apcE; Fig. 2.5A). The ApcE gene encodes the core-to-membrane linker polypeptide that anchors the phycobilisome to the thylakoid membrane. The overall trend in transcript accumulation of the light harvesting phycocyanin rods and linker peptides (cpcA through G), which attache to the core and increase the absorption cross-section of the phycobilisome complex, was similar to that of allophycocyanin (Fig. 2.5B). Two genes involved in phycobilisome degradation (nblA1 and nbLA2; Fig. 2.5C) were suppressed throughout the light period indicating that the cells continued to assemble phycobilisomes to sustain growth during the day.

3.6. Photosystems I and II

Synechocystis needs to produce new PSII complexes throughout the day to maintain photosynthetic capacity during growth. Transcripts associated with the reaction center and peripheral protein coding genes of PSII increased in abundance throughout the day

(Fig. 2.6B and C). Interestingly, the D1 protein of PSII showed a different expression pattern (Fig. 2.6A). The D1 protein is the preliminary site of photodamage (Aro et al. 1993) and is encoded by three homologous genes in *Synechocystis* (psbA1, 2, and 3). psbA1 was transcribed at very low abundances (0.1% percent of total psbA transcripts) and it did not show a dynamic pattern of abundance across the day. There were however, dynamic patterns in the transcription of psbA2 and psbA3 (Fig. 2.6A). Relative PsbA2 transcript abundance was high at night, decreases upon illumination, and then showed a dynamic patter that resembled the changes in surface light intensity. However, the PsbA2 transcript abundance at ZT6 was only 50% higher than during the night. Transcription abundance of psbA3 declined from the start of the daytime throughout the day (ZT0 to ZT12) and then increased again at night. Most other components of the reaction center and peripheral proteins of PSII showed elevated transcript abundance during the day (Fig. 2.6B, C and D). The only components of the PSII complex that decreased in abundance during the day was isiA, which encodes a low iron and/or high light stress inducible proteins that can associated with both PSI and PSII, and psb28-2, which encodes and homolog to psba28 (Fig. 2.5D).

The transcription of both the reaction center and peripheral proteins associated with PSI changed in a similar way as PSII (Fig. 2.7A and B). The P700 apoprotein core, which consists of two subunits (psaA and psaB), showed an initial decline in relative abundance in the first hours of light and then trended towards higher abundance throughout the rest of the light period (Fig. 2.7C).

3.7. Other Components of Electron Transport

The components of the electron transport chain are largely shared between photosynthesis and respiration in cyanobacteria, as both processes are conducted in the thylakoid membrane. There was an elevated, and sustained, abundance of transcripts from the

cytochrome b_6/f complex across the light period, but two of the alternative Rieske iron-sulfur cluster proteins (petC2 and petC3) showed an opposite trend (Fig. 2.8A).

Synechocystis and other cyanobacteria have two soluble electron carriers operating between the cytochrome b_6/f complex and PSI or respiratory terminal oxidases: cytochrome c_6 and plastocyanin. PetE encodes plastocyanin, which contains a copper cofactor, whereas cytochrome c_6 has a iron containing heme cofactor and they are thought to be complementary but synthesized under different nutrient limiting conditions (Durán et al. 2004). I observed little dynamic transcription in plastocyanin (petE) but cytochrome c_6 (petJ) was highly upregulated during the light (Fig. 2.8B).

Ferredoxin, in conjunction with the ferredoxin-$NADP^+$ oxidoreductase, oxidizes PSI and generates NADPH. Ferredoxin is encoded by multiple genes in the *Synechocystis* genome, some of which are not involved in photosynthesis but other functions such as nitrogen assimilation, redox regulation and heterotrophic growth (Mustila et al. 2014). I observed highly variable expression patterns of the ferredoxin encoding genes (Fig. 2.8C). Ferredoxin 1 (petF, sll1382) is the only homolog known to be is essential for viability under autotrophic growth, but the transcription of ssl0020 is more responsive to light (Poncelet et al. 1998). I observed dynamic patterns in transcript abundance of these two genes were ssl0020 was upregulated in the light while sll1382 was down-regulated.

Adenosine triphosphate (ATP) synthase utilizes the proton motive force across the thylakoid membrane to generate energy. I observed a rapid increase in transcript abundance of all genes encoding the ATP synthase with a peak in abundance at ZT1 and a gradual decline over the course of the day (Fig. 2.8D).

3.8. Light Stress Responses

High light stress responses are well studied in *Synechocystis* and involve an orchestrated response of specific enzymes involved in photoprotection as well as catabolic

and anabolic processes. A meta-analysis by Muramatsu and Hihara (2012) identified numerous transcripts induced by a sudden shift from a sub-saturating acclimatization state to supra saturating light excess light. I explored if these high light stress responses in transcription were induced under my experimental conditions.

The high light inducible proteins (Hli) is encoded by a family of four genes in *Synechocystis.* They bind chl *a* and are involved in protecting PSII from photodamage, either through quenching of excess energy or through the stabilization of PSII complexes during their assembly (Chidgey et al. 2014). They are also essential for assembly of PSI under high light (Wang et al. 2008). One of the genes, HliD, was induced upon illumination but steadily decreased in abundance after ZT1 (Fig. 2.9A). The other three genes showed a steady decline in transcript abundance from ZT0 to ZT12. Interestingly, HlipB and HlipA, were two of only 30 genes that showed a more than one-fold change in abundance (positive or negative) between ZT-0.25 and ZT23 (Fig. 2.9A), indicating that they may be under circadian control and upregulated in anticipation of light.

Several enzymes are capable of detoxification of reactive oxygen species. A subset of these enzymes that were light stress responsive based on Muramatsu and Hihara (2012) is shown in Fig. 2.9B. These enzymes include glutathione peroxidase-like NADPH peroxidase (gpx2), thiophen and furan oxidation protein (trmE), glutathione synthetase (gshB), super oxide dismutase (sod), and catalase peroxidase (cpx). Some of these genes did show an initial increase in abundance upon first illumination (ZT0.25 to ZT1) but sod and cpx did not respond to any greater extent during the light treatment. By ZT3 transcription abundances of all these enzymes began declining and at maximum irradiance (ZT6) transcript abundance was equal to the that of the dark period, or slightly elevated (< one-fold increase). This transcription pattern did not follow my hypothesized patter of elevated transcript abundance as a function of increasing surface light intensity.

Transcription of proteases involved in repair of the damage PSII reaction centers and degradation of damaged proteins generally decreased in relative abundance across the light period, with the exception of DegT and one out of four ftsH genes (Fig. 2.9C). The same general pattern was seen in chaperones, or heat-shock proteins, (Fig. 2.9D). Many more members of these gene families did not change significantly and are consequently not shown in the figures (but see Table H2). One exception was transcripts of one out of three DnaK homologues (slr0086). DnaK proteins are molecular chaperones involved in protein folding and their transcription is upregulated under various stress conditions including high light (Rupprecht et al. 2008). The other two homologs did not follow this trend. DnaK1 was not changing significantly (Table H2) and dnaK2 decreased in abundance throughout the light period (Fig. 2.9D).

3.9. Photoprotective Responses

Transcription of genes involved in photoprotective mechanisms including NPQ and AET are also highly responsive to high light stress (Muramatsu and Hihara 2012). I observed some dynamics in the transcription of the orange carotenoid protein (OCP) with a one-fold increase between ZT0.25 and ZT1 (Fig. 2.10A). The fluorescence recovery protein, which relaxes NPQ, showed a modest increase in transcript abundance during the light period.

I also recorded high rates of alternative electron transport (AET) across the day (Fig. 1.10). Interestingly transcript abundance of flavodiiron proteins, which are thought to be the main player in AET (Ermakova et al. 2016), showed an inverted response to increases in light intensity across the day (Fig. 2.10B). The quinol oxidase, which is also capable of shuttling electrons from plastoquinone to water did not change significantly in abundance across the diel cycle. On the other hand, components of the cytomchrome *c* oxidase displayed the most dynamic transcription patterns of any complex known to be capable of alternative electron transport, increasing in abundance across the day and peaking at ZT9. However,

cytomchrome *c* oxidase is a component of respiration in *Synechocystis* and it may be upregulated in anticipation of the night.

4. Discussion

4.1 The Experimental Light Treatment and Growth Rates

I grew *Synechocystis* in a bench-top photobioreactor under a dynamic light environment that approximates conditions during mass cultivation. I have previously quantified how individual cells experience rapid fluctuations in light during the day using computational fluid dynamic (Chapter 1). Briefly cells were subjected to a time-integrated photon flux of about 15% that of the surface due to self-shading (300 μmol photons m^{-2} s^{-1} at ZT6). Importantly cells moved rapidly from full surface light (up to 2000 μmol photons m^{-2} s^{-1}) to almost complete darkness with an average frequency of 0.17 s^{-1}. Under static light condition growth of *Synechocystis* saturate around 100 μmol photons m^{-2} s^{-1} (Du et al. 2016) and I found that 300 μmol photons m^{-2} s^{-1} was also beyond the linear response of photosynthesis in cultures acclimatized to my growth conditions (Fig. 1.6A). These results indicate that the cells received a high enough photon load to saturate photosynthesis, at least under short periods of time (Fig. 1.7). These results are in agreement with predictions of how light environment in PBRs are perceived by individual cells during industrial scale cultivation (Barbosa et al. 2003; Huang et al. 2015; Perner-Nochta and Posten 2007). Light/dark oscillations in these PBR depend to a large extend on the geometrical shape of the PBR and the mixing rate and consequently range in frequency between 10 and 0.01 s^{-1}.

The photosynthetic capacity did not change across the day and there were no evidences of net-photodamage occurring (Fig. 1.6A and Fig. 1.8). Non-photochemical quenching (NPQ) was not an active photoprotective mechanism *in situ*, but significant amounts of photosynthetic reductant derived from PSII were diverted back to oxygen through light dependent oxygen consumption (Table 1.2, Fig. 1.10). These results did not support my

original hypothesis that subjection to short periods of supra-saturating light during growth under dynamic and rapidly fluctuating light either induces NPQ or causes photoinhibition in *Synechocystis*. However, I developed an alternative hypothesis that light driven oxygen consumption, or AET, was used used as an alternative electron sink, which I found evidence for (Chapter 1). This result suggests that AET diverted electron from linear electron transport and carbon fixation, possibly as a photoprotective mechanism.

4.2 Inorganic Carbon and Nitrogen Uptake

Given that the culture was continuously sparged with 1% CO_2 in air, at a flow rate of 0.5 L min^{-1} (see M&M Chapter 1), I did not expect to see transcriptional activation of *Synechocystis* low inorganic carbon (Ci) responses. The extra-cellular bicarbonate import system (cmp operon) is known to be induced up to a 1000 fold upon Ci depletion (Mcginn et al. 2003) and I did not see any upregulation in this operon during the daytime which suggested that the cultures were Ci replete during the light period (Fig. 2.3A). Some genes associated with the carboxysome were upregulated, but the carboxysome is an integrated component of photosynthesis in *Synechocystis* (Raven et al. 2014) and as such can be expected to respond to light. As the pH of the culture was maintained below 7.6 through the experiment and the formation of the carboxysome is an essential component of photosynthesis, these results did not indicate that the cells experience low Ci availability at any point throughout the treatment.

I observed a rapid light response in transcription of nitrate transporters. This response has been observed in other studies conducted under sub-saturating light (Beck et al. 2014; Saha et al. 2016). Nitrate transporters and other proteins involved in nitrogen assimilation processes are down regulated transcriptionally in response to light stress (Muramatsu and Hihara 2012). Since I established that the cultures were not nutrient limited

(Fig. F1A), this suggest that nitrogen assimilation processes behaved as expected without interference of light stress.

4.3 Light Harvesting Chlorophyll and Phycobilisome

The transcriptional dynamics of genes involved in heme and chl *a* synthesis indicated that chl *a* was preferentially synthesized during the day. Assuming that the transcriptional down in ferrochelatase (HemH; Fig. 2.4A) translated into a decline in protein abundance, this would have prevented protoporphyrin IX from being modified into heme. As a consequence, more chl *a* would have been synthesized as a result of upregulation in the genes involved in this synthesis pathway during the daytime (Fig. 2.4B).

Transcription of the phycobilisome related genes indicated *de-novo* synthesis during the day. I observed a large down of phycobilisome degradation proteins (nblA1 and 2; Fig. 2.5B) during the light period, which has been observed during growth under sub-saturating light (Labiosa et al. 2006; Saha et al. 2016). nblA1 and -2 are induced under stress conditions, such as nitrogen and sulfate starvation ,and recruits the clp proteases for degradation of the phycobilisome (Baier et al. 2014). This is presumably done to recycle amino acids from the phycobilisome into other proteins during nutrient limitation. This suggest that phycobilisomes were protected from degradation during the day or alternatively degraded during the night. The ApcE gene was not upregulated during the day, compared to night. ApcE encode the core to membrane linker polypeptide and has previously been shown to be transcribed as a monocistronic transcript in *Synechococcus* sp. PCC 6301 (Capuano et al. 1991). Since the core consists of 12 trimers of allophycocyanin, only two of which comprise ApcE, this uneven expression may simply mirror different molar ratios of Apc subunits needed for the assembly of functional phycobilisomes. Transcript abundance of other components of the phycobilisome generally increase 4-16 fold during the day (Fig. 2.5). This overall results indicate that the cells continue to synthesize light harvesting pigments and

phycobilisomes throughout the day. There were no indications of sudden light stress responses around the maximum intensity of light, which would result in reduced transcription of pigment and light harvesting complexes (Muramatsu and Hihara 2012).

4.5 Photosystem I and II

Transcript abundance of the two photosystems also increased during the light period. Notable exceptions were Psb28-2 and isiA (Fig. 2.6D). Disruption of Psb28-2 has no obvious phenotype in *Synechocystis* and the psb28 protein is the main component of functional PSII (Sakata et al. 2013), which explains the expression patterns of this gene. isiA is a chl *a* binding protein involved in protecting the two photosystems from light stress and is induced upon iron limitation (Havaux et al. 2005).

The psbA genes displayed interesting and dynamic patterns of transcript abundance (Fig. 2.6A). The psbA1 gene forms a protein product with poor functional properties and is only transcribed at very low levels (Mohamed et al. 1993). The psbA2 and psbA3 genes are highly transcribed and regulated through the redox state of the plastoquinone pool and small RNAs (El Bissati and Kirilovsky 2001), with psbA2 being up and psbA3 downregulated during light. My results followed the expected patterns of increasing psbA2 abundance following surface irradiances and decreasing psbA3 abundance throughout the daytime (Fig. 2.6A). However, psbA2 did not show a large amplitude in the variation between dark and light transcript abundance, would indicate light stress, since there was a dipped at the onset and offset of light.

4.6 Other Components of the Electron Transport Chain

Most components of the electron transport chain increased in abundance during the light period. This was true for the cytochrome b_6f complex, save for petC2 and petC1, which encodes alternative Riesk iron-sulfur subunit. PetC2 is thought not to be translated and petC3 has a lower midpoint potential than petC1, suggesting an alternative but unknown

function (Schneider et al. 2002), potentially during respiration or heterotrophic growth (Smart and Mcintosh 1991). Cytochrome c_6 was dynamically transcribed indicating that this is the main electron shuttle protein, which is expected under copper replete conditions (Durán et al. 2004). Out of the Ferredoxin homologues, I observed an expression pattern that followed other photosynthetic component in ssl0020, which together with sll1382 is known to be important during autotrophic growth (Poncelet et al. 1998). Components of the ATP-synthase were also upregulated during the light period, peaking early in the day. This is expected since *Synechocystis* slows down metabolic processes during the night (Angermayr et al. 2016), which is accompanied by a reduction in the rate of electron transport (only from NADPH dehydrogenase complexes). This likely leads to a greater amount of ATP synthesis during the day when it is needed for carbon fixation, compared to the dark when only respiration occurs.

4.7 Broad Responses in Photosynthetic Transcription

There were striking similarities between the diurnal changes in the transcriptome of my experiment and those conducted under sub-saturating light intensities. Both Beck et al. (2014) and Saha et al. (2016) have investigated diurnal changes in transcription across a 12h/12h square-wave light/dark cycle (80 and 50 µmol photons m^{-2} s^{-1}, respectively). These two studies were also conducted in shake flasks or tubes at high densities, which likely lowered the light exposure of individual cells further. Yet the major diel changes in transcriptional of photosynthetic genes under my experimental conditions, which include much higher light intensities, behaved very similarly with a constitutive up regulation of chlorophyll synthesis and phycobilisome genes, PSI and PSII across the light period (Fig. 2.5, 2.6 and 2.7). Similar observation have been made in *C. reinhardtii* (Zones et al. 2015). Genes involved in carbon fixation and ATP synthesis experienced more rapid light induced increases followed by a slow decline in transcript abundance across the day, and a rapid decline back to a baseline night level within an hour after dark (Fig. 2.3 and 8).

Despite the dynamic transcriptional responses from genes encoding the photosynthetic machinery I did not see any changes in changes in chl *a* content per cell bio-volume (Fig. 1.5A) or photosynthetic capacity (Fig. 1.6A) across the diel cycle. This suggest that the shifts in transcription observed either do not translated into more protein productions, or more likely increase synthesis in effort to sustain growth and cell division, which occurred throughout the day (Fig. 1.6E). Cell division and growth would dilute the effect of ramped up protein synthesis. Another possible explanation is that increases in transcription associated with the photosynthetic apparatus was done to support the replacement of photodamaged products. While I did not measure the rate of photodamage directly, I did measure the quantum yield of PSII (Fig. 1.8), which indicated that there was no net-photodamage. During photodamage, the D1 protein of PSII has to be replaced and if the oxidative stress has damaged surrounding proteins they may need to be degraded and synthesized anew. This would require an orchestrated response of the photorepair machinery, which I explore later in Section 4.7. The rate of photodamage could also be assessed through Western blots against the D1 and D2 protein in the presence of a protein synthesis inhibitor (Allakhverdiev and Murata 2004), or indirectly through staining for reactive oxygen species or assay of lipid peroxidation rates.

Paired observation of system level responses and physiology can yield important insight into how regulatory processes affects an organism. An upregulation in transcription can indicate different responses under different growth conditions. Without quantitative measurements of photosynthetic activity, I would likely have concluded that *Synechocystis* was increasing its photosynthetic capacity in response to dawn. However, my measurements showed that photosynthetic capacity was almost equal at ZT0.25 and ZT6 (Fig. 1.5A) suggesting that the radical shifts in transcription of photosynthetic genes observed between ZT-0.25 and ZT1 only maintained the status quo in terms of function. Transcription of the

photosynthetic machinery suggested that *Synechocystis* can acclimatize its cellular functions to perform photosynthesis under industrial light conditions, albeit with a slow growth rate as a consequence.

4.8 Few Indications of High Light Stress

I contrasted my transcriptomic results with microarray based responses to light stress (Muramatsu and Hihara 2012). Such experiments are done by bringing a low light acclimatized culture into supra-saturating light and do not capture dynamic changes in light or consider long-term acclimatization. As such, it is hard to estimate the ecological or industrial relevance of such treatments since organisms adapt to variable light under natural and industrial conditions. Yet results from such experiments have shaped the way photobioreactors (Posten 2009) and metabolic engineering strategies (Berteotti et al. 2016; Shigeoka et al. 2002) are designed.

Based on *in vivo* fluorescence measurements of the quantum yield of photosystem II (F_V/F_M; Fig. 1.8), I did not detect photoinhibition in response to diel changes in light intensity. As a whole my transcriptomic results show very few indications of light stress or gross-photodamage despite the dynamic changes in light intensity. If light became a stressor as it increased throughout the first part of the light period, I would have expected sudden induction of high light inducible proteins, the psbA2 gene encoding the D1 protein, molecular chaperons, and proteases to combat photodamage. Such responses to light were sparse and only evident in the first hour of light (Fig. 2.9) which is similar, but not as pronounced, as what Angermayr et al. (2016) observed under a square-wave high-light/dark cycle (1000 µmol photons m^{-2} s^{-1}). In my experiment the light intensitie at the surface was only 500 µmol photons m^{-2} s^{-1} at ZT1 which may explain the dampened effect. Transcription of the D1 protein of PSII did not respond strongly to increasing light either (Fig. 2.6A) and the the F_V/F_M did not decline significantly at any time during the day (Fig. 1.8). This suggests

that no net-photodamage occurred and together with few observation of other light stress responses there appeared to be little gross-photodamage either.

4.9 Photoprotective Responses

I could not detect any *in situ* induction of NPQ but high rates of light induced consumption of oxygen were observed throughout the day (Chapter 1). Transcriptional responses of OCP was seen during the first hour. In Chapter 1 OCP quenching was measured, both as maximum capacity and as *in vivo* activity, and I did observe a higher capacity for NPQ in the first 3 h of light (Table 1.2). This suggest that the initial transcription increase resulted in changes in maximum OCP quenching capacity, likely due to increased protein abundance.

Based on MIMS measurements I showed that AET was an active mechanism throughout the day (Fig. 1.10). Interestingly transcription of the flavodiiron genes were not upregulated in response to dynamics in surface light intensity (Fig. 2.10). However, there appeared to be a constant capacity for light induced consumption of oxygen across the day, as about 50% of the electrons were used in this pathway (Fig. 1.10) indicating that the genes involved in this process may be consecutive expressed. The cytochrome *c* oxidase did increase in transcript abundance across the day (Fig. 2.10). As this enzyme is involved in respiration, this response may be a consequence of circadian regulation (Layana and Diambra 2011). The transcription patterns of cytochrome *c* oxidase were very similar to that of the RNA polymerase sigma factor sigE (Table H2). sigE regulates respiration in *Synechocystis* (Summerfield and Sherman 2007) supporting a respiratory regulation dynamic. However, there is also evidence that the cytochrome *c* oxidase is involved in light-induced consumption of oxygen, but it has only been measured under continuous light (Ermakova et al. 2016). I measured high rates of oxygen consumption under fluctuating light (Fig. 1.10) and it is

possible that unknown regulatory function control electron flow differently if the plastoquinone pool is rapidly changing form reduced to oxidized. More research is needed to elucidate the complex interactions between various enzymes involved in alternative electron transport.

4.10 Conclusions

Many studies suggest that tuning NPQ and photoprotective mechanisms can improve growth under mass cultivation (Berteotti et al. 2016; Nakajima et al. 1998; Shigeoka et al. 2002; Yarnold et al. 2016). However, few of these studies have tested their engineered strains under dynamic and rapidly fluctuating light. In my treatment, photosynthesis in *Synechocystis* saturated at a fraction of the maximum light intensity cells experienced, at least temporarily. Yet *Synechocystis* could acclimatize to growth under such a rapidly fluctuating light environment without physiological (Chapter 1) or transcriptional indications of light stress or photoinhibition. To accomplish this, AET appeared to be used as a safety mechanism to prevent photodamage (Fig. 1.10). Given that we did not observe net-photodamage or dynamic transcription of proteins involved photorepair it is possible that AET could be downregulated without causing oxidative stress to the cells. This should divert more electron toward NADPH production which could increase carbon fixation and growth rates. The transcriptomic results suggest that the flavodiiron proteins may not be responsible for the light induced consumption and future studies should consider disrupting the cytochrome c oxidase in the light to modulate electron flow during autotrophic growth under dynamic and fluctuation light. In summary, my results reveal several new insights into our current understanding of photo-acclimatization to dynamic and fluctuating light. More research into photo-acclimatization to dynamic light environments in other species of algae and cyanobacteria is warranted to explore the interplay between AET, NPQ and photosynthetic efficiency in rapidly changing light.

5. Tables

Table 2.1. Sampling design. Surface irradiance and time points when samples for RNAseq were harvested. Numbers indicate quantity of biological replicates analyzed.

ZT time (h)	Surface PAR (μmol photons m^{-2} s^{-1})	Transcriptomic samples (#)
-0.25	0	3
0.25	130	4
1	500	4
3	1400	4
6	2000	4
9	1400	4
11	500	4
11.75	130	4
12.25	0	4
13	0	4
18	0	4
23	0	4

Table 2.2. Primers used in this study

Locus	Gen ID	Product length (bp)	Direction	Primer sequence
slr0342	petB	167	Forward primer	TGGGTGTAATGCTAGCCGTC
slr0342	petB	167	Reverse primer	AACGCTTTCACTACCTCGCA

Table 2.3. Summary of diurnal changes in transcription. Non transcribed genes were not detected at one or more time points. Statistical change is based on ANOVA with Bonferroni correction ($p < 0.05$). Fold change refers to comparison between the grand mean and the largest changing individual time point. Functional categories are a non-exhaustive, qualitative estimate of common genes that were not transcribed or did not change significantly across the diel cycle. n.s.= non significant.

	Open reading frames	Non-transcribed	No statistical change	Significantly change	1 < fold change	1 > fold change or n.s.
#of genes	3662	44	404	3214	2699	963
Common functional categories		Hypothetical (12) and transposase (32)				Hypothetical (300),Translation (42), Hik genes (44), DNA replication (20), transporters (52)

6. Figures

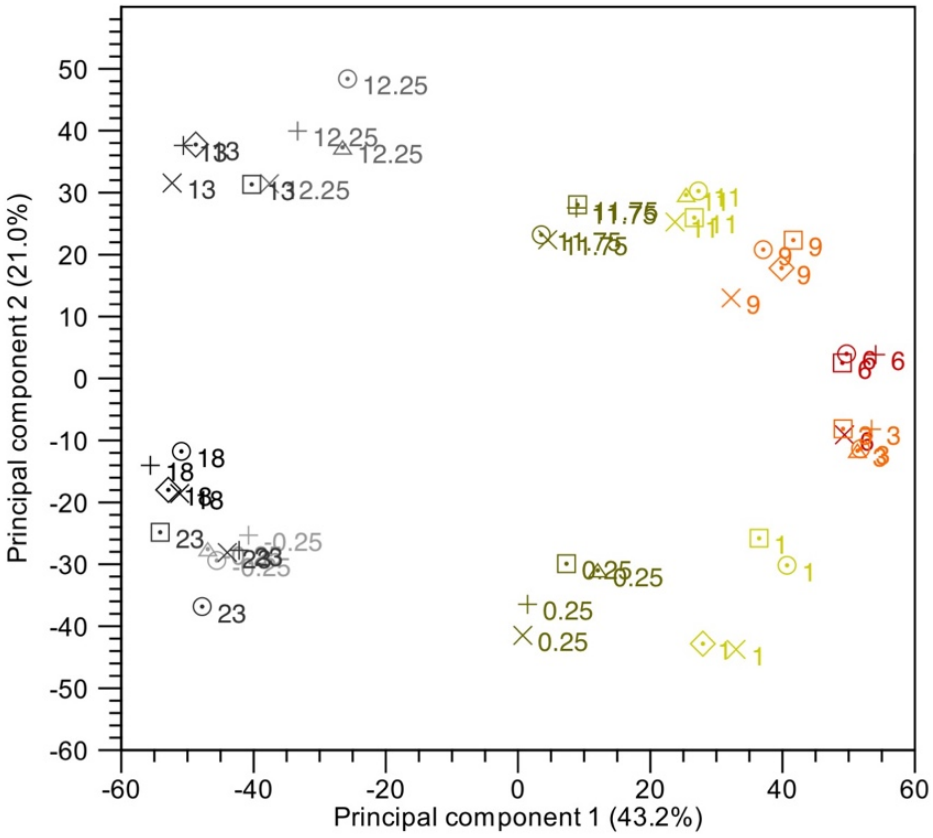

Figure 2.1. Principal component analysis of diel changes in global transcription. Shapes (cross, plus, square, circle, triangle, and diamond) indicate different biological replicate and the associated numbers indicates time points of sampling (in ZT). Color high-light the surface irradiance at individual time points (see Table 1 for irradiance information).

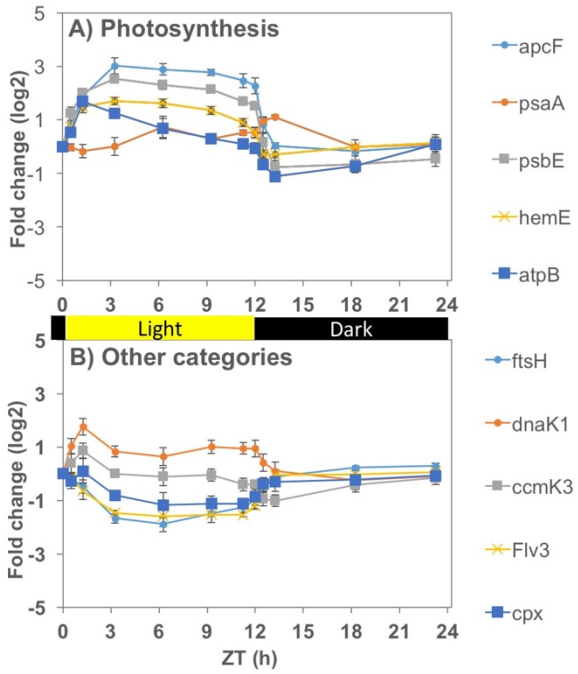

Figure 2.2. Example of variability between biological replicates of different genes from various functional groups and protein complexes. A) various components of photosynthesis, B) other metabolic functions. Shown are averages and standard deviation of four biological replicates per time point of randomly chosen genes in various functional categories. Legend show gene ID based on Cyanobase. Annotations to gene ID can be found in Table H2. RPKM data has been normalized to the expression level at ZT-0.25 and $\log_2$ transformed.

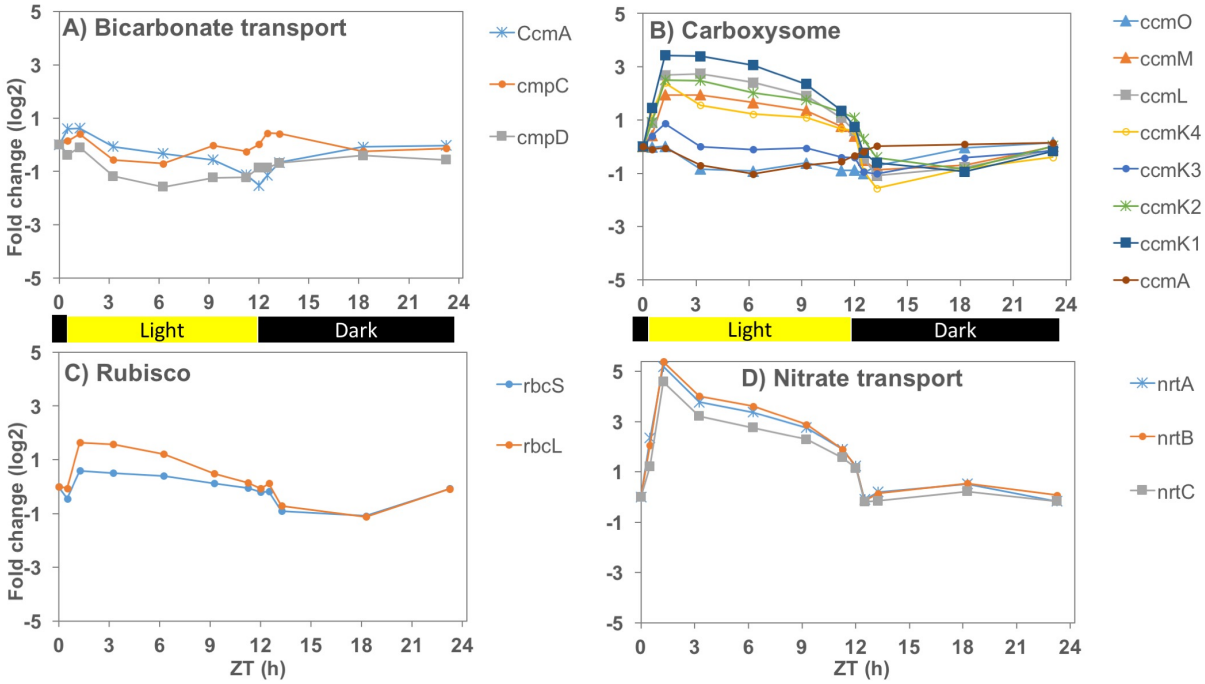

Figure 2.3. Diurnal changes in transcription of genes involved in inorganic carbon and nitrate transport as well as carbon concentrating and fixating mechanisms. A) extra-cellular and intra-cellular bicarbonate transporters, B) carboxysome components, C) small and large subunit of Ribulose-1,5-bisphosphate carboxylase/oxygenase (Rubisco), D) extra-cellular nitrate transport operon. Shown are averages of four biological replicates per time point of statistically changing genes only. Legend show gene ID based on Cyanobase. Annotations to gene ID can be found in Table H2. RPKM data has been normalized to the expression level at ZT-0.25 and $\log_2$ transformed.

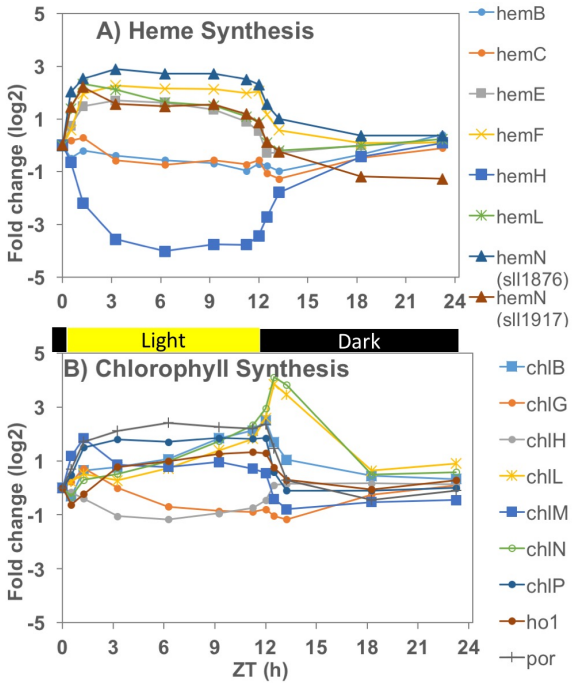

Figure 2.4. Diurnal changes in transcription genes encoding enzymes involved in synthesis of heme and chlorophyll. A) heme and chlorophyll precursors, B) chlorophyll. Shown are averages of four biological replicates per time point of statistically changing genes only. Legend show gene ID based on Cyanobase. Annotations to gene ID can be found in Table H2. RPKM data has been normalized to the expression level at ZT-0.25 and $\log_2$ transformed.

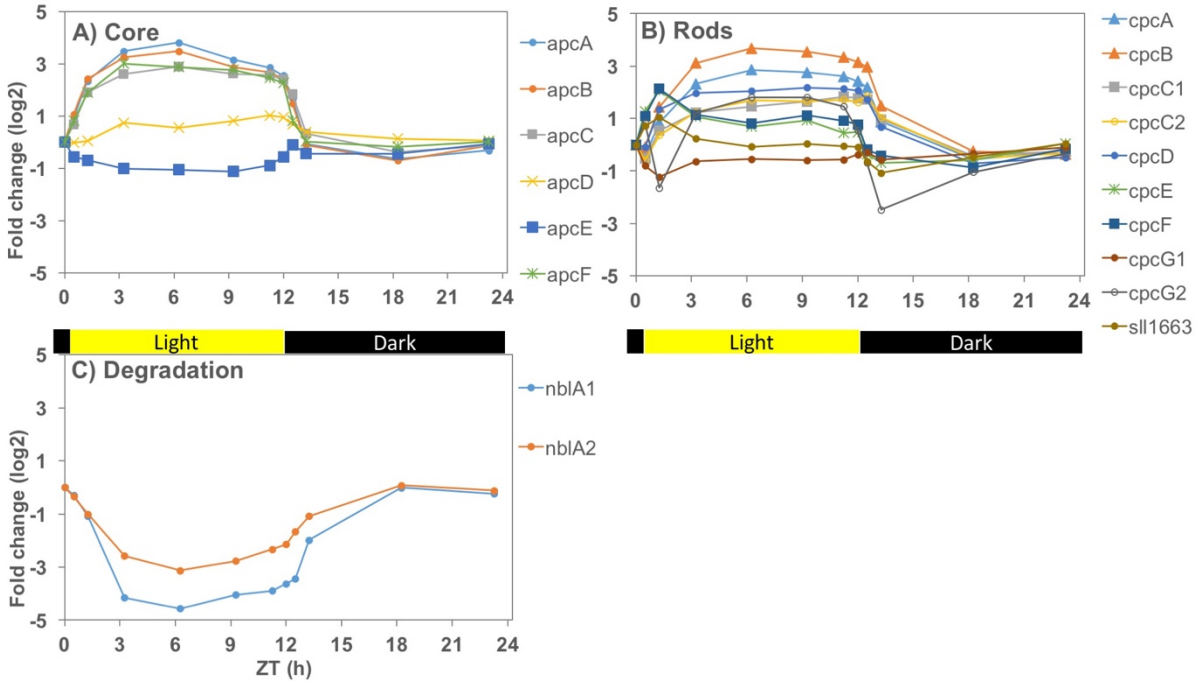

Figure 2.5. Diurnal changes in transcription of genes encoding the phycobilisome. A) the core structure, B) peripheral rod structure, C) degradation of phycobilisomes. Shown are averages of four biological replicates per time point of statistically changing genes only. Legend show gene ID based on Cyanobase. Annotations to gene ID can be found in Table H2. RPKM data has been normalized to the expression level at ZT-0.25 and $\log_2$ transformed.

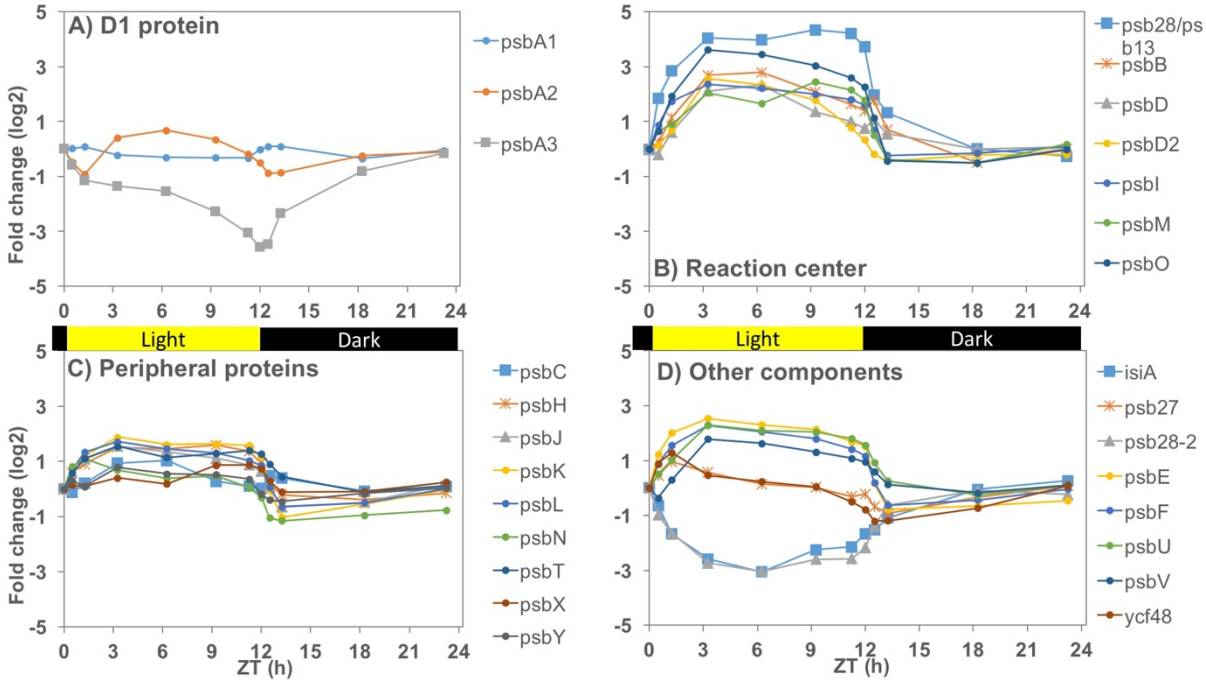

Figure 2.6. Diurnal changes in transcription of genes encoding photosystem II. A) transcript abundance of the three homologues of the D1 protein of photosystem II (note that PsbA1 transcripts were 1000-fold less abundant than PsbA2 and 3), B) other reaction center genes, C) peripheral proteins, D) other components including homologues, assembly proteins and electron carriers. Shown are averages of four biological replicates per time point of statistically changing genes only. Legend show gene ID based on Cyanobase. Annotations to gene ID can be found in Table H2.

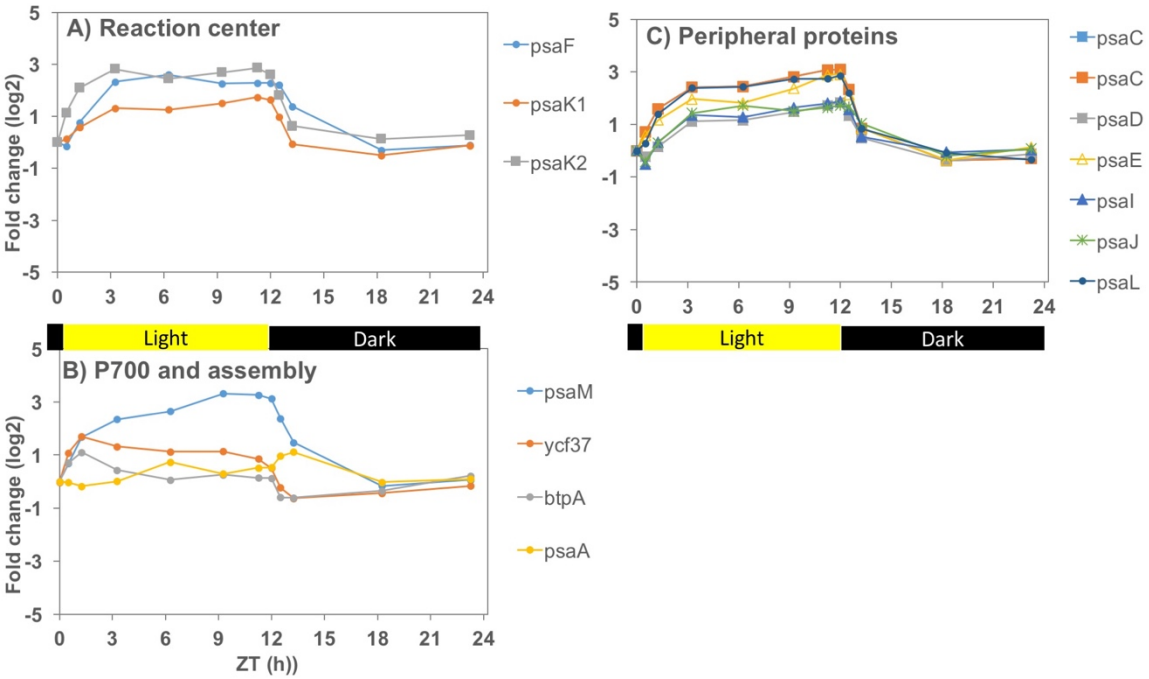

Figure 2.7. Diurnal changes in transcription of genes encoding Photosystem I. A) transcripts of the reaction center subunits, B) P700 core and assembly, C) the peripheral structure. Shown are averages of four biological replicates per time point of statistically changing genes only. Legend show gene ID based on Cyanobase. Annotations to gene ID can be found in Table H2. RPKM data has been normalized to the expression level at ZT-0.25 and $\log_2$ transformed.

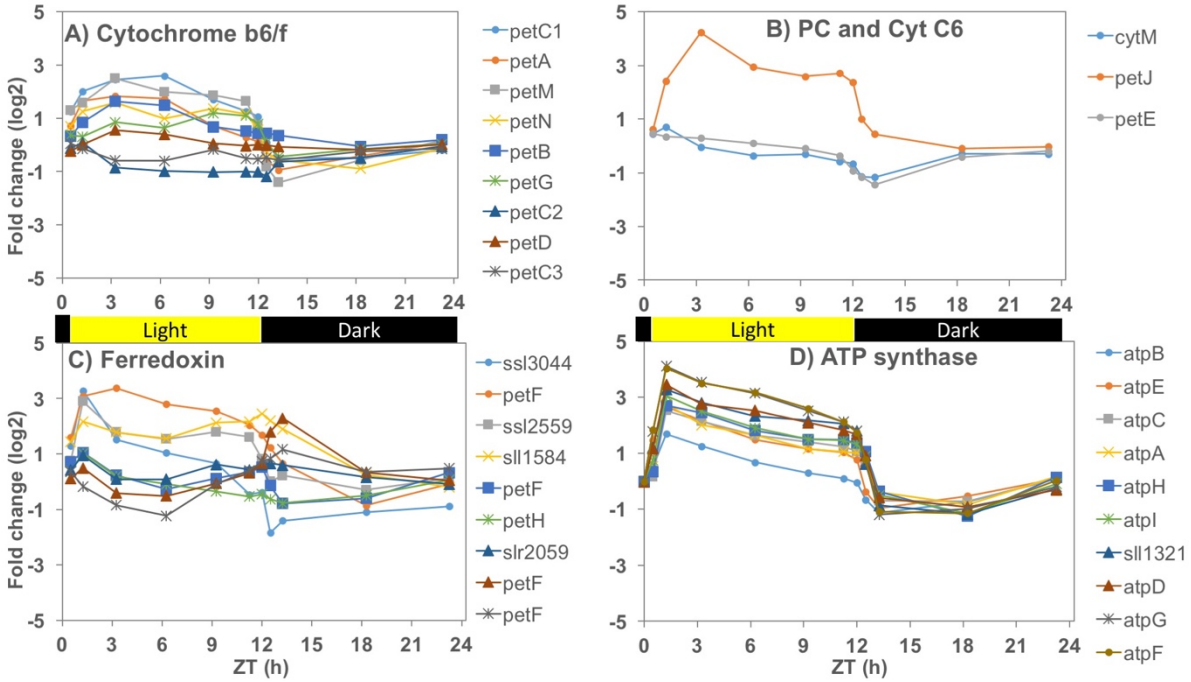

Figure 2.8. Diurnal changes in transcription of genes encoding electron transport components. A) cytochrome *b*$_6$*f*, B) plastocyanin (PC) and pre-coursors of cytochrome *c*$_6$, C) ferredoxin homologues, D) adenosine triphosphate (ATP) synthase. Note that all components except ferredoxin are shared by respiratory and photosynthetic electron transport and ATP generation. Shown are averages of four biological replicates per time point of statistically changing genes only. Legend show gene ID based on Cyanobase. Annotations to gene ID can be found in Table H2. RPKM data has been normalized to the expression level at ZT-0.25 and $\log_2$ transformed.

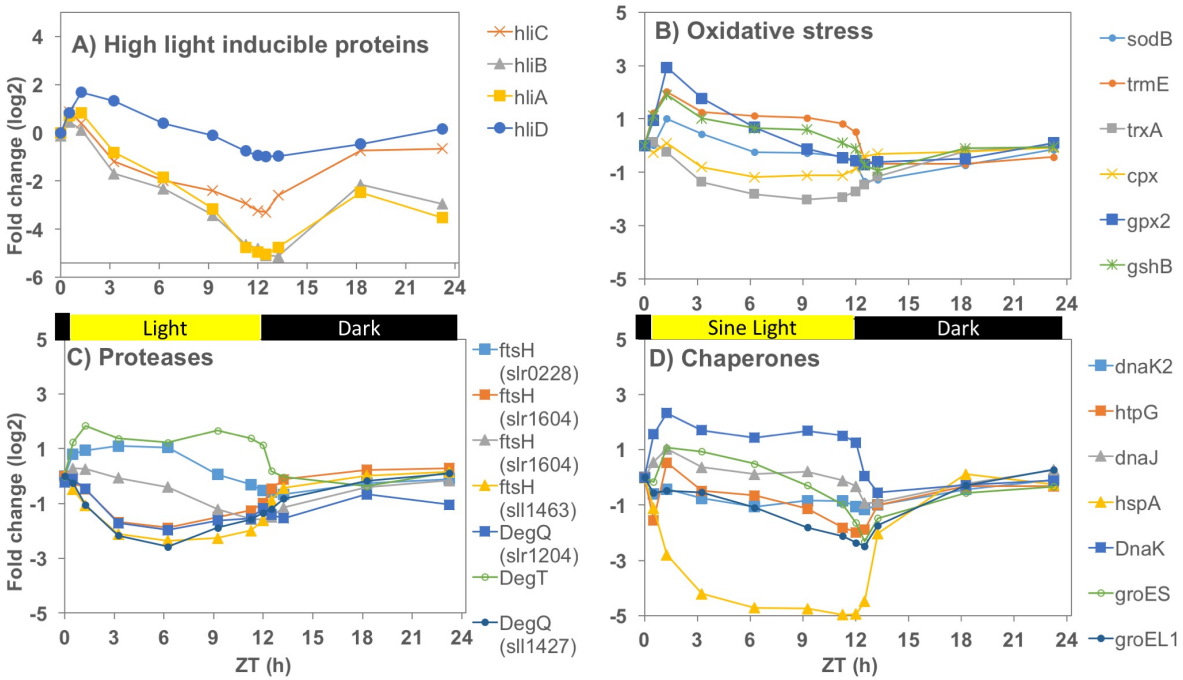

Figure 2.9. Diurnal changes in transcription of genes involved in mitigating photodamage. Genes encompass a sub-set of genes that were transcriptionally up-regulate under high light stress according to Muramatsu and Hihara (2012). A) high light inducible proteins involved in protection of photosystem II from photodamage, B) genes involved in detoxification of various reactive oxygen species, C) proteases involved in, among other things, repair of photodamaged, D) molecular chaperons. Shown are averages of four biological replicates per time point of statistically changing genes only. Legend show gene ID based on Cyanobase. Annotations to gene ID can be found in Table H2. RPKM data has been normalized to the expression level at ZT-0.25 and $\log_2$ transformed.

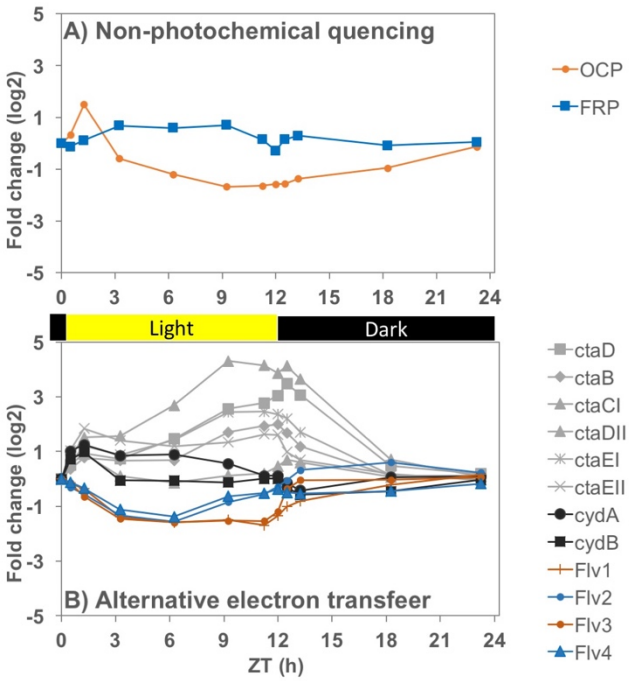

Figure 2.10. Diurnal changes in transcription of genes involved in photoprotection. Many of these genes were not annotated in Cyanobase necessitating manually annotated through primary literature. A) genes involved in induction (OCP) and relaxation (FRP) of non-photochemical quenching, B) genes involved in alternative electron transport, including flavodiiron (Flv), cytochrome bd quinol oxidase (cyd) and cytochrome c oxidase (cox). Shown are averages of four biological replicates per time point of statistically changing genes only. Legend show gene ID based on Cyanobase. Annotations to gene ID can be found in Table H2. RPKM data has been normalized to the expression level at ZT-0.25 and $\log_2$ transformed.

SUMMARIZING DISCUSSION

1. Experimental Approach

Light is constantly changing in natural environments. Photoautotrophs have evolved a suite of responses to acclimate to these changes in light (see General Introduction). To tease apart subtle changes within complex metabolic processes scientists need to reduce complexity. Consequently, photosynthetic processes are most often studied under conditions of constant sub-saturating light intensities. In addition, most of what is known about photo-acclimation in algae and cyanobacteria comes from experiments where cells are acclimatized to low light intensities and then suddenly subjected to high light (Förster et al. 2006; Hihara et al. 2001; Muramatsu and Hihara 2012). This may be an appropriate way to detect light stress responses, but at some point the environmental complexity needs to be reintroduced to test if hypotheses based on simplified conditions holds under more realistic conditions. The concept of dynamic light and its effect on photosynthesis is gaining recognition amongst some molecular biologists. However, the current golden standard is still to use highly artificial square-wave conditions lacking dynamic and stochastic changes in light intensities [e.g. (Allahverdiyeva et al. 2013; Ermakova et al. 2016)].

Biologists understand that observations in a controlled laboratory setting does not necessarily translate to more complex conditions. However, this understanding may get lost as it travels between disciplines. This is the case in terms of the understanding of light in the context of applied phycology and specifically development of cultivation systems, genetic engineering of production strains, and scaled-up field experiments. Among engineers, chemists and molecular biologists there is a widespread assumption that natural dynamics in light is a stressor to microbial autotrophs, causing photodamage, photoinhibition, and retardation of growth. This is largely based on two-step acclimatization experiments and has

little support from field experiments. As a consequence, design of photobioreactors (PBRs) and genetic engineering strategies focus largely on preventing photodamage and excessive induction of photoprotective mechanisms (Berteotti et al. 2016; Bitog et al. 2011; Kirst et al. 2012; Posten 2009; Shigeoka et al. 2002). Long-term acclimatization to dynamic light environments likely change how photosynthesis functions. In my thesis I wanted to explore how photosynthetic organisms acclimatize to complex and rapid changes in light intensities. I investigated the physiology of the model photosynthetic organism *Synechosystis* sp. PCC 6803 in a dynamic light environment. This mimicked a realistic environment during mass cultivation using a bench-top PBR.

2. Summary of Findings

During the treatment, individual cells of *Synechocystis* experienced rapid changes in light due to self-shading within the culture and rapid mixing. In addition, I changed the surface light intensity to mimic natural changes in light associated with a full day-cycle. To begin with, I wanted to understand how individual cells experienced the light treatment in a bench-top PBR. I accomplished this through collaboration with chemical engineers, and together we created a model of the mixing regime using computational fluid dynamics. The cell-specific light model illustrated how cells rapidly moved in and out of the light as they were mixed through the PBR. Individual cells experienced light intensities ranging from >0.1 to 2000 μmol photons m^{-2} s^{-1} as the surface light intensity changed across the day, but also continuously on the time scale of seconds due to self-shading within the culture. Cells were supplied with a time-integrated photon flux that saturated growth when it was supplied at a constant intensity in Erlenmeyer flasks. Still, the cells grew slowly in the PBR with a doubling time of 75 h compared to a maximum rate of 12 h. This suggested that light was used ineffectively for growth. I hypothesized that this was due to photodamage

causing a reduction in growth rate or induction of photoprotective mechanism causing dissipation of light energy.

Surprisingly the maximum photosynthetic capacity (P_{max}) was maintained at a near constant level across the day (470 to 530 μmol O_2 [mg chl *a*] h^{-1}). Photosynthetic parameters are commonly normalized to chlorophyll *a* since it mirrors the light harvesting capacity in eukaryotes with a chl *a/b* containing antenna complex. Since cyanobacteria have an antenna made up of phycobiliproteins, I argue that this normalization strategy is arbitrary and not suitable to compare different light acclimatization states. I therefore normalized photosynthesis on a biomass basis (organic carbon content) and compared the photosynthetic capacity of the PBR-grown culture with others grown under constant sub- and supra-saturating light (30 and 400 μmol photons m^{-2} s^{-1}). Interestingly the P_{max} was the same between the two constant light acclimatized states (10,500 μmol O_2 [g TOC]$^{-1}$ h^{-1}) but significantly higher in the PBR acclimatized cultures (19,100 μmol O_2 [g TOC]$^{-1}$). This discrepancy mirrors an interesting acclimatization to fluctuating light. This likely involves an elevated capacity to process electrons after they have been harvested by the phycobilisome or PSII. Whether this is achieved by elevating the rate of carbon fixation in the Calvin-Bassham-Benson cycle, increasing the rate of linear election transport, or some other mechanism, remains to be determined.

I observed no physiological indications of photoinhibition associated with diel changes in light intensity. The *in situ* quantum yield of photosystem II (F_v/F_m) was stable across the day and P_{max} did not change *ex situ*. The global transcriptional changes across the day also supported this physiological observation. There was little diel variation in transcriptional activity of molecular chaperones (dnaK, hsp. groE families), proteases (ftsH and Deg families), high light inducible proteins (hli), and reactive oxygen species scavengers (super-oxide dismutase and catalase peroxidase) that are known to be responsive to high light

stress (Muramatsu and Hihara 2012). If light was a stressor under my simulated PBR conditions, transcriptional activities of these genes would be anticipated to either co-vary with surface light intensity or be induced at a certain threshold of irradiance during the morning. This was not observed.

Collectively, my results suggest that *Synechocystis* did not experience light stress during the experimental light conditions and is capable of high levels of photosynthesis. How was this accomplished when the cell-specific light model indicated that cells were subjected to more photons than they could utilize? And why was the growth rate so slow? To investigate these questions, I explored the potential induction of photoprotective mechanisms that may be responsible for dissipating energy absorbed in excess of photosynthetic capacity. My first hypothesis was that non-photochemical quenching (NPQ) was activated during the brief exposures to high light when cells spent time near the surface. To measure NPQ *in situ* I had to design a new method since the standard method in the field is to quantify NPQ capacity *ex situ*. I found that even though the capacity for NPQ was high in the cells *ex situ* they did not actually utilize this photoprotective mechanism *in situ.* The transcriptomic data showed only a brief induction in transcription of the orange carotenoid protein (OCP) responsible for rapidly inducible NPQ in *Synechosystis* sp. PCC 6803. I also detected an elevated capacity for NPQ in the early morning suggesting that the transcriptional response resulted in an increased abundance of OCP protein. NPQ is often assumed to be an active photoprotective mechanism in large scale PBRs but my results challenge this assumption.

Another photoprotective mechanism is alternative electron transport (AET), also known as the water-to-water cycle. AET can only be measured as light-dependent oxygen consumption using stable isotope enrichment and a real-time membrane inlet mass spectrometer (MIMS). As a consequence, I could not set up measurements of AET *in situ* in the PBR. Instead I designed an *ex-situ* experiment where I used rapidly dimmable LED lights

to mimic the predicted cell-specific light environment of the PBR. Through this experiment I showed that AET was induced by light and that it consumed more than 50% of electrons derived from PSII or respiration across the diel cycle. The flavodiiron proteins are thought to be the main player in cyanobacterial AET (Ermakova et al. 2016). Interestingly, I did not see any induction in the transcription of the flavodiiron proteins during the light period, which either means that these genes are constituently expressed or that other enzymes may exist that are responsible for the AET. Previous light-dependent oxygen consumption measurements have only been done under constant light whereas I measured it under fluctuating light. This treatment may induce activity of other unknown enzymes. Further analysis of the transcriptomic data may uncover putative genes whose transcriptional pattern indicates that they may play a role in AET under fluctuating light.

3. Future Analyses

Despite being one of the least complex and most studies photosynthetic organism more than 50% of the putative protein coding genes of *Synechocystis* has no orthologue in other taxa. Many more have only been characterized based on *in silico* similarities with other organisms. By comparing the transcriptional response of these genes in my experiment to that of other studies under sub-saturating light [e.g. (Beck et al. 2014; Saha et al. 2016)] it may be possible to identify putative targets that respond differently to my light treatment. These genes may help explain how photosynthesis responds to dynamic light.

Further analysis into the dynamic regulation of gene expression is also needed. A wide array of two-component histidine-kinase and sigma factors regulates transcription in cyanobacteria. Through more rigorous statistical analysis in collaboration with a statistician (Wen Zhou) I aim to group genes by differential diurnal patterns, which will aid in this process. The preliminary analysis in Chapter 2 focused mainly on photosynthetic processes and needs to be expanded to cover central carbon metabolism and anabolic processes.

I also collected samples for proteomic analysis at ZT-1, -0.25, 3, 9, and 15 to confirm if transcriptional changes translated to changes in protein abundance. At the time of writing, these samples were still being analyzed. These results can be used to corroborate that transcriptional changes actually resulted in changes in protein abundances. Since cyanobacteria has complex translational regulation with small RNA making up 70-90% of the total RNA pool (Beck et al. 2014), post-translational regulation could cause changes in protein abundance without changes in transcript abundance. Another issue with RNAseq is that it only captures changes in relative abundance of RNA within a pool of total RNA. Consequently, it does not inform about total abundance of mRNA. The proteomic analysis will be normalized on a biomass basis and as such will control for mechanisms that are only used to sustain growth.

4. Future Outlook

My results challenge the current paradigm that microbial phototrophs are light stressed due to dynamic light conditions under mass cultivation and that they induce excessive NPQ to cope with this environment. Members of my lab have made similar observations in both diatom and green algae species (Cantrell and Peers in press; Jallet et al. 2016a). If these results extend to other species and scaled-up PBRs it would indicate that attempts at tuning NPQ through genetic engineering may have little effect on the productivity of PBRs contrary to previous observations (Berteotti et al. 2016; Peers 2015) and theoretical arguments (Melis 2009; Radakovits et al. 2010). Attempts at reducing photodamage through reactor design (Posten 2009), rapid fluctuations in light (Nedbal et al. 1996), or genetic engineering (Shigeoka et al. 2002) may also be misguided efforts. Instead my findings suggest that more focus should be devoted to exploring whether AET can be manipulated to increase the productivity of PBRs. However, further studies under natural sunlight in scaled

PBRs are needed to corroborate my findings. We also need a better understanding of how AET is regulated as a photoprotective mechanism under realistic light environments.

One way to simulate realistic light environments in a scaled-down and controlled laboratory setting would be to generate light models of industrial PBRs or raceway ponds, using computational fluid dynamics. These models could then be applied in the lab. This could be done by programming white LEDs to flash in accordance to the modelled light environment and grow thin cultures with a high degree of light penetration under such conditions. Individual cells would then experience similar light intensities as if they were moved around in a large scale cultivation system. Since all cells in the culture would be synchronized to one light treatment this would give researchers access to more biomass and enable studies with higher temporal resolution. This could, for example, be useful when investigating how a prolonged period of darkness (10 to 15 min sometimes) affects cells grown in raceway ponds, where cells may spend several min in darkness close to the bottom of the pond due to laminar flow (Prussi et al. 2014). This growth method could also be used to evaluate genetically modified production strains, screen for highly productive strains within ecological communities of algae and cyanobacteria, or screen for functionally important genes using a random mutagenesis approach.

This thesis highlights my research efforts to investigate dynamic changes in light associated with PBRs and its effect on photo-acclimation. I have isolated variable light as the sole treatment and shown that it does not cause photodamage or induce NPQ. However, photoautotrophs face a multitude of stressors under realistic growing conditions. This includes low concentrations of inorganic carbon, limitations in inorganic nutrients, viral and bacterial parasitism, and predation. Once a platform to mimic natural light has been established, future work should incorporate such additional stressors into experiments. This

will give insight into how dynamic changes in light intensities interact with other stressors to shape how photosynthesis and photoprotective mechanisms function in the real world.

REFERENCES

Abràmoff, M. D., P. J. Magalhães, and S. J. Ram. 2004. Image processing with ImageJ. Biophotonics International **11:** 36-42.

Allahverdiyeva, Y., H. Mustila, M. Ermakova, L. Bersanini, P. Richaud, G. Ajlani, N. Battchikova, L. Cournac, and E.-M. Aro. 2013. Flavodiiron proteins Flv1 and Flv3 enable cyanobacterial growth and photosynthesis under fluctuating light. Proceedings of the National Academy of Sciences **110:** 4111-4116.

Allakhverdiev, S. I., and N. Murata. 2004. Environmental stress inhibits the synthesis de novo of proteins involved in the photodamage–repair cycle of photosystem II in Synechocystis sp. PCC 6803. Biochimica et Biophysica Acta (BBA)-Bioenergetics **1657:** 23-32.

Anderson, S. L., and L. Mcintosh. 1991. Light-activated heterotrophic growth of the cyanobacterium Synechocystis sp. strain PCC 6803: a blue-light-requiring process. Journal of Bacteriology **173:** 2761-2767.

Angermayr, S. A., A. G. Rovira, and K. J. Hellingwerf. 2015. Metabolic engineering of cyanobacteria for the synthesis of commodity products. Trends in Biotechnology **33:** 352-361.

Angermayr, S. A., P. Van Alphen, D. Hasdemir, G. Kramer, M. Iqbal, W. Van Grondelle, H. C. Hoefsloot, Y. H. Choi, and K. J. Hellingwerf. 2016. Culturing of Synechocystis sp. PCC6803 with N2/CO2 in a diel regime shows multi-phase glycogen dynamics and low maintenance costs. Applied and Environmental Microbiology **82:** 4180-4189.

Aro, E.-M., I. Virgin, and B. Andersson. 1993. Photoinhibition of photosystem II. Inactivation, protein damage and turnover. Biochimica et Biophysica Acta (BBA)-Bioenergetics **1143:** 113-134.

Azadi, P., O. R. Inderwildi, R. Farnood, and D. A. King. 2013. Liquid fuels, hydrogen and chemicals from lignin: A critical review. Renewable and Sustainable Energy Reviews **21:** 506-523.

Baier, A., W. Winkler, T. Korte, W. Lockau, and A. Karradt. 2014. Degradation of Phycobilisomes in Synechocystis sp. PCC6803 Evidence for essential formation of an NblA1/NblA2 heterodimer and its codegradation by Clp protease complex Journal of Biological Chemistry **289:** 11755-11766.

Bailleul, B., J. Park, C. M. Brown, K. D. Bidle, S. H. Lee, and P. G. Falkowski. 2017. Direct measurements of the light dependence of gross photosynthesis and oxygen consumption in the ocean. Limnology and Oceanography.

Barbosa, M. J., M. Janssen, N. Ham, J. Tramper, and R. H. Wijffels. 2003. Microalgae cultivation in air‐lift reactors: modeling biomass yield and growth rate as a function of mixing frequency. Biotechnology and Bioengineering **82:** 170-179.

Battchikova, N., J. P. Vainonen, N. Vorontsova, M. Keranen, D. Carmel, and E. M. Aro. 2010. Dynamic changes in the proteome of Synechocystis 6803 in response to CO2 limitation revealed by quantitative proteomics. Journal of Proteome Research **9:** 5896-5912.

Beck, C., S. Hertel, A. Rediger, R. Lehmann, A. Wiegard, A. Kölsch, B. Heilmann, J. Georg, W. R. Hess, and I. M. Axmann. 2014. Daily expression pattern of protein-encoding genes and small noncoding RNAs in Synechocystis sp. strain PCC 6803. Applied and Environmental Microbiology **80:** 5195-5206.

Beckmann, K., J. Messinger, M. R. Badger, T. Wydrzynski, and W. Hillier. 2009. On-line mass spectrometry: membrane inlet sampling. Photosynthesis Research **102:** 511-522.

Behrenfeld, M. J., and Z. S. Kolber. 1999. Widespread iron limitation of phytoplankton in the South Pacific Ocean. Science **283:** 840-843.

Behrenfeld, M. J., O. Prasil, M. Babin, and F. Bruyant. 2004. In search of a physiological basis for covariations in light‐limited and light‐saturated photosynthesis. Journal of Phycology **40:** 4-25.

Bersanini, L., N. Battchikova, M. Jokel, A. Rehman, I. Vass, Y. Allahverdiyeva, and E.-M. Aro. 2014. Flavodiiron Protein Flv2/Flv4-Related Photoprotective Mechanism Dissipates Excitation Pressure of PSII in Cooperation with Phycobilisomes in Cyanobacteria. Plant Physiology **164:** 805-818.

Berteotti, S., M. Ballottari, and R. Bassi. 2016. Increased biomass productivity in green algae by tuning non-photochemical quenching. Scientific Reports **6:** 21339.

Bilgen, S. 2014. Structure and environmental impact of global energy consumption. Renewable and Sustainable Energy Reviews **38:** 890-902.

Bitog, J., I.-B. Lee, C.-G. Lee, K.-S. Kim, H.-S. Hwang, S.-W. Hong, I.-H. Seo, K.-S. Kwon, and E. Mostafa. 2011. Application of computational fluid dynamics for modeling and designing photobioreactors for microalgae production: a review. Computers and Electronics in Agriculture **76:** 131-147.

Boulay, C., A. Wilson, S. D'haene, and D. Kirilovsky. 2010. Identification of a protein required for recovery of full antenna capacity in OCP-related photoprotective mechanism in cyanobacteria. Proceedings of the National Academy of Sciences **107:** 11620-11625.

Brennan, L., and P. Owende. 2010. Biofuels from microalgae—a review of technologies for production, processing, and extractions of biofuels and co-products. Renewable and Sustainable Energy Reviews **14:** 557-577.

Caballero, M. A., D. Jallet, L. Shi, C. Rithner, Y. Zhang, and G. Peers. 2016. Quantification of chrysolaminarin from the model diatom Phaeodactylum tricornutum. Algal Research **20:** 180-188.

Campbell, D., V. Hurry, A. K. Clarke, P. Gustafsson, and G. Öquist. 1998. Chlorophyll fluorescence analysis of cyanobacterial photosynthesis and acclimation. Microbiology and Molecular Biology Reviews **62:** 667-683.

Cantrell, M., and G. Peers. in press. A mutant of Chlamydomonas without LHCSR maintains high rates of photosynthesis, but has reduced cell division rates in sinusoidal light conditions. PloS one.

Capuano, V., A.-S. Braux, N. T. De Marsac, and J. Houmard. 1991. The" anchor polypeptide" of cyanobacterial phycobilisomes. Molecular characterization of the Synechococcus sp. PCC 6301 apce gene. Journal of Biological Chemistry **266:** 7239-7247.

Carrieri, D., G. Ananyev, A. M. Garcia Costas, D. A. Bryant, and G. C. Dismukes. 2008. Renewable hydrogen production by cyanobacteria: Nickel requirements for optimal hydrogenase activity. International Journal of Hydrogen Energy **33:** 2014-2022.

Cazzaniga, S., L. Dall'osto, J. Szaub, L. Scibilia, M. Ballottari, S. Purton, and R. Bassi. 2014. Domestication of the green alga Chlorella sorokiniana: reduction of antenna size improves light-use efficiency in a photobioreactor. Biotechnology for Biofuels **7:** 157.

Challinor, A. J., J. Watson, D. Lobell, S. Howden, D. Smith, and N. Chhetri. 2014. A meta-analysis of crop yield under climate change and adaptation. Nature Climate Change **4:** 287-291.

Chaux, F., A. Burlacot, M. Mekhalfi, P. Auroy, S. Blangy, P. Richaud, and G. Peltier. 2017. Flavodiiron proteins promote fast and transient O2 photoreduction in Chlamydomonas. Plant Physiology**:** pp. 00421.02017.

Chidgey, J. W., M. Linhartová, J. Komenda, P. J. Jackson, M. J. Dickman, D. P. Canniffe, P. Koník, J. Pilný, C. N. Hunter, and R. Sobotka. 2014. A cyanobacterial chlorophyll synthase-HliD complex associates with the Ycf39 protein and the YidC/Alb3 insertase. The Plant Cell **26:** 1267-1279.

Chisti, Y. 2007. Biodiesel from microalgae. Biotechnology Advances **25:** 294-306.

---. 2016. Large-scale production of algal biomass: raceway ponds, p. 21-40. Algae Biotechnology. Springer.

Crutzen, P. J., A. R. Mosier, K. A. Smith, and W. Winiwarter. 2016. N2O release from agro-biofuel production negates global warming reduction by replacing fossil fuels, p. 227-238. Paul J. Crutzen: A Pioneer on Atmospheric Chemistry and Climate Change in the Anthropocene. Springer.

De La Cruz, J., and A. Vioque. 2001. Increased sensitivity to protein synthesis inhibitors in cells lacking tmRNA. Rna **7:** 1708-1716.

Derks, A., K. Schaven, and D. Bruce. 2015. Diverse mechanisms for photoprotection in photosynthesis. Dynamic regulation of photosystem II excitation in response to rapid environmental change. Biochimica et Biophysica Acta (BBA)-Bioenergetics **1847:** 468-485.

Devabhaktuni, V., M. Alam, S. S. S. R. Depuru, R. C. Green, D. Nims, and C. Near. 2013. Solar energy: Trends and enabling technologies. Renewable and Sustainable Energy Reviews **19:** 555-564.

Devarapalli, M., B. J. Lawrence, and S. V. Madihally. 2009. Modeling nutrient consumptions in large flow‐through bioreactors for tissue engineering. Biotechnology and Bioengineering **103:** 1003-1015.

Dhanasekharan, K. M., J. Sanyal, A. Jain, and A. Haidari. 2005. A generalized approach to model oxygen transfer in bioreactors using population balances and computational fluid dynamics. Chemical Engineering Science **60:** 213-218.

Du, W., J. A. Jongbloets, H. P. Hernández, F. J. Bruggeman, K. J. Hellingwerf, and F. B. Dos Santos. 2016. Photonfluxostat: A method for light-limited batch cultivation of cyanobacteria at different, yet constant, growth rates. Algal Research **20:** 118-125.

Durán, R. V., M. Hervás, A. Miguel, and J. A. Navarro. 2004. The efficient functioning of photosynthesis and respiration in Synechocystis sp. PCC 6803 strictly requires the presence of either cytochrome c6 or plastocyanin. Journal of Biological Chemistry **279:** 7229-7233.

Eilers, P., and J. Peeters. 1988. A model for the relationship between light intensity and the rate of photosynthesis in phytoplankton. Ecological Modelling **42:** 199-215.

El Bissati, K., and D. Kirilovsky. 2001. Regulation of psbA and psaE expression by light quality in Synechocystis species PCC 6803. A redox control mechanism. Plant Physiology **125:** 1988-2000.

Elanskaya, I., V. Grivennikova, V. Groshev, G. Kuznetsova, M. Semina, and K. Timofeev. 2004. Role of NAD (P) H: quinone oxidoreductase encoded by drgA gene in reduction of exogenous quinones in cyanobacterium Synechocystis sp. PCC 6803 cells. Biochemistry (Moscow) **69:** 137-142.

Elanskaya, I. V., E. A. Chesnavichene, C. Vernotte, and C. Astier. 1998. Resistance to nitrophenolic herbicides and metronidazole in the cyanobacterium Synechocystis sp. PCC 6803 as a result of the inactivation of a nitroreductase‐like protein encoded by drgA gene. FEBS letters **428:** 188-192.

Elanskaya, I. V., V. A. Toporova, V. G. Grivennikova, E. M. Muronets, E. P. Lukashev, and K. N. Timofeev. 2009. Reduction of photosystem I reaction center by recombinant DrgA protein in isolated thylakoid membranes of the cyanobacterium Synechocystis sp. PCC 6803. Biochemistry (Moscow) **74:** 1080-1087.

Elmorjani, K., J.-C. Thomas, and P. Sebban. 1986. Phycobilisomes of wild type and pigment mutants of the cyanobacterium Synechocystis PCC 6803. Archives of Microbiology **146:** 186-191.

Emlyn‐Jones, D., M. K. Ashby, and C. W. Mullineaux. 1999. A gene required for the regulation of photosynthetic light harvesting in the cyanobacterium Synechocystis 6803. Molecular Microbiology **33:** 1050-1058.

Ermakova, M., T. Huokko, P. Richaud, L. Bersanini, C. J. Howe, D. Lea-Smith, G. Peltier, and Y. Allahverdiyeva. 2016. Distinguishing the roles of thylakoid respiratory terminal oxidases in the cyanobacterium Synechocystis sp. PCC 6803. Plant Physiology **171:** 1307-1319.

Farquhar, G. V., S. V. Caemmerer, and J. Berry. 1980. A biochemical model of photosynthetic CO2 assimilation in leaves of C3 species. Planta **149:** 78-90.

Foyer, C. H., and G. Noctor. 2009. Redox regulation in photosynthetic organisms: signaling, acclimation, and practical implications. Antioxidants & Redox Signaling **11:** 861-905.

Fuszard, M. A., S. Y. Ow, C. S. Gan, J. Noirel, N. G. Ternan, G. Mcmullan, C. A. Biggs, K. F. Reardon, and P. C. Wright. 2013. The quantitative proteomic response of Synechocystis sp. PCC6803 to phosphate acclimation. Aquatic Biosystems **9:** 5.

Förster, B., U. Mathesius, and B. J. Pogson. 2006. Comparative proteomics of high light stress in the model alga Chlamydomonas reinhardtii. Proteomics **6:** 4309-4320.

Gill, R. T., E. Katsoulakis, W. Schmitt, G. Taroncher-Oldenburg, J. Misra, and G. Stephanopoulos. 2002. Genome-Wide Dynamic Transcriptional Profiling of the Light-to-Dark Transition in Synechocystis sp. Strain PCC 6803. Journal of Bacteriology **184:** 3671-3681.

Griffin, T. J., S. P. Gygi, T. Ideker, B. Rist, J. Eng, L. Hood, and R. Aebersold. 2002. Complementary profiling of gene expression at the transcriptome and proteome levels in Saccharomyces cerevisiae. Molecular & Cellular Proteomics **1:** 323-333.

Grobbelaar, J. U. 2012. Microalgae mass culture: the constraints of scaling-up. Journal of Applied Phycology **24:** 315-318.

Gründel, M., R. Scheunemann, W. Lockau, and Y. Zilliges. 2012. Impaired glycogen synthesis causes metabolic overflow reactions and affects stress responses in the cyanobacterium Synechocystis sp. PCC 6803. Microbiology **158:** 3032-3043.

Gwizdala, M., A. Wilson, A. Omairi-Nasser, and D. Kirilovsky. 2013. Characterization of the Synechocystis PCC 6803 Fluorescence Recovery Protein involved in photoprotection. Biochimica et Biophysica Acta **1827:** 348-354.

Han, J., S. M. Sen, D. M. Alonso, J. A. Dumesic, and C. T. Maravelias. 2014. A strategy for the simultaneous catalytic conversion of hemicellulose and cellulose from lignocellulosic biomass to liquid transportation fuels. Green Chemistry **16:** 653-661.

Havaux, M., G. Guedeney, M. Hagemann, N. Yeremenko, H. C. Matthijs, and R. Jeanjean. 2005. The chlorophyll‐binding protein IsiA is inducible by high light and protects the cyanobacterium Synechocystis PCC6803 from photooxidative stress. FEBS Letters **579:** 2289-2293.

Hihara, Y., A. Kamei, M. Kanehisa, A. Kaplan, and M. Ikeuchi. 2001. DNA microarray analysis of cyanobacterial gene expression during acclimation to high light. The Plant Cell **13:** 793-806.

Hihara, Y., K. Sonoike, M. Kanehisa, and M. Ikeuchi. 2003. DNA Microarray Analysis of Redox-Responsive Genes in the Genome of the Cyanobacterium Synechocystis sp. Strain PCC 6803. Journal of Bacteriology **185:** 1719-1725.

Hirose, Y., N. C. Rockwell, K. Nishiyama, R. Narikawa, Y. Ukaji, K. Inomata, J. C. Lagarias, and M. Ikeuchi. 2013. Green/red cyanobacteriochromes regulate complementary chromatic acclimation via a protochromic photocycle. Proceedings of the National Academy of Sciences **110:** 4974-4979.

Hong, S.-J., H. Kim, J. H. Jang, B.-K. Cho, H.-K. Choi, H. Lee, and C.-G. Lee. 2014. Proteomic analysis of Synechocystis sp. PCC6803 responses to low-temperature and high light conditions. Biotechnology and Bioprocess Engineering **19:** 629-640.

Houille-Vernes, L., F. Rappaport, F.-A. Wollman, J. Alric, and X. Johnson. 2011. Plastid terminal oxidase 2 (PTOX2) is the major oxidase involved in chlororespiration in Chlamydomonas. Proceedings of the National Academy of Sciences **108:** 20820-20825.

Hu, J.-Y., and T. Sato. 2017. A photobioreactor for microalgae cultivation with internal illumination considering flashing light effect and optimized light-source arrangement. Energy Conversion and Management **133:** 558-565.

Hu, Q., M. Sommerfeld, E. Jarvis, M. Ghirardi, M. Posewitz, M. Seibert, and A. Darzins. 2008. Microalgal triacylglycerols as feedstocks for biofuel production: perspectives and advances. The Plant Journal **54:** 621-639.

Huang, J., F. Feng, M. Wan, J. Ying, Y. Li, X. Qu, R. Pan, G. Shen, and W. Li. 2015. Improving performance of flat-plate photobioreactors by installation of novel internal mixers optimized with computational fluid dynamics. Bioresource Technology **182:** 151-159.

Hutmacher, D. W., and H. Singh. 2008. Computational fluid dynamics for improved bioreactor design and 3D culture. Trends in Biotechnology **26:** 166-172.

Hwang, H. J., A. Nagarajan, A. Mclain, and R. L. Burnap. 2008. Assembly and disassembly of the photosystem II manganese cluster reversibly alters the coupling of the reaction center with the light-harvesting phycobilisome. Biochemistry **47:** 9747-9755.

Iluz, D., and S. Abu-Ghosh. 2016. A novel photobioreactor creating fluctuating light from solar energy for a higher light-to-biomass conversion efficiency. Energy Conversion and Management **126:** 767-773.

Jallet, D., M. A. Caballero, A. A. Gallina, M. Youngblood, and G. Peers. 2016a. Photosynthetic physiology and biomass partitioning in the model diatom Phaeodactylum tricornutum grown in a sinusoidal light regime. Algal Research **18:** 51-60.

Jallet, D., M. Cantrell, and G. Peers. 2016b. New players for photoprotection and light acclimation. Chloroplasts: Current Research and Future Trends. Caister Academic Press.

Jameson, A. 1995. Optimum aerodynamic design using control theory. Computational Fluid Dynamics Review **3:** 495-528.

Kaneko, T., S. Sato, H. Kotani, A. Tanaka, E. Asamizu, Y. Nakamura, N. Miyajima, M. Hirosawa, M. Sugiura, and S. Sasamoto. 1996. Sequence analysis of the genome of the unicellular cyanobacterium Synechocystis sp. strain PCC6803. II. Sequence determination of the entire genome and assignment of potential protein-coding regions. DNA research **3:** 109-136.

Karandashova, I., M. Semina, E. Muronets, and I. Elanskaya. 2006. Expression of drgA gene encoding NAD (P) H: quinone-oxidoreductase in the cyanobacterium Synechocystis sp. PCC 6803. Russian Journal of Genetics **42:** 872-876.

Katsuda, T., K. Shimahara, H. Shiraishi, K. Yamagami, R. Ranjbar, and S. Katoh. 2006. Effect of flashing light from blue light emitting diodes on cell growth and astaxanthin production of Haematococcus pluvialis. Journal of Biosciences and Bioengineering **102:** 442-446.

Kim, H. W., R. Vannela, C. Zhou, and B. E. Rittmann. 2011. Nutrient acquisition and limitation for the photoautotrophic growth of Synechocystis sp. PCC6803 as a renewable biomass source. Biotechnology and Bioengineering **108:** 277-285.

Kirilovsky, D. 2007. Photoprotection in cyanobacteria: the orange carotenoid protein (OCP)-related non-photochemical-quenching mechanism. Photosynthesis Research **93:** 7-16.

Kirilovsky, D., R. Kaňa, and O. Prášil. 2014. Mechanisms modulating energy arriving at reaction centers in cyanobacteria, p. 471-501. Non-Photochemical Quenching and Energy Dissipation in Plants, Algae and Cyanobacteria. Springer.

Kirst, H., C. Formighieri, and A. Melis. 2014. Maximizing photosynthetic efficiency and culture productivity in cyanobacteria upon minimizing the phycobilisome light-harvesting antenna size. Biochimica et Biophysica Acta (BBA)-Bioenergetics **1837:** 1653-1664.

Kirst, H., J. G. Garcia-Cerdan, A. Zurbriggen, T. Ruehle, and A. Melis. 2012. Truncated photosystem chlorophyll antenna size in the green microalga Chlamydomonas reinhardtii upon deletion of the TLA3-CpSRP43 gene. Plant physiology **160:** 2251-2260.

Koksharova, C., and O. Wolk. 2002. Genetic tools for cyanobacteria. Applied Microbiology and Biotechnology **58:** 123-137.

Kolber, Z. S., O. Prášil, and P. G. Falkowski. 1998. Measurements of variable chlorophyll fluorescence using fast repetition rate techniques: defining methodology and experimental protocols. Biochimica et Biophysica Acta (BBA)-Bioenergetics **1367:** 88-106.

Kromdijk, J., K. Głowacka, L. Leonelli, S. T. Gabilly, M. Iwai, K. K. Niyogi, and S. P. Long. 2016. Improving photosynthesis and crop productivity by accelerating recovery from photoprotection. Science **354:** 857-861.

Kucho, K., K. Okamoto, Y. Tsuchiya, S. Nomura, M. Nango, M. Kanehisa, and M. Ishiura. 2005. Global analysis of circadian expression in the cyanobacterium Synechocystis sp. strain PCC 6803. Journal of Bacteriology **187:** 2190-2199.

Kudoh, K., Y. Kawano, S. Hotta, M. Sekine, T. Watanabe, and M. Ihara. 2014. Prerequisite for highly efficient isoprenoid production by cyanobacteria discovered through the over-expression of 1-deoxy-d-xylulose 5-phosphate synthase and carbon allocation analysis. Journal of Biosciences & Bioengineering **118:** 20-28.

Kurian, D., T. Jansèn, and P. Mäenpää. 2006. Proteomic analysis of heterotrophy in Synechocystis sp. PCC 6803. Proteomics **6:** 1483-1494.

Labiosa, R. G., K. R. Arrigo, C. J. Tu, D. Bhaya, S. Bay, A. R. Grossman, and J. Shrager. 2006. Examination of diel changes in global transcript accumulation in synechocystis (cyanobacteria) 1. Journal of Phycology **42:** 622-636.

Layana, C., and L. Diambra. 2011. Time-course analysis of Cyanobacterium transcriptome: detecting oscillatory genes. PloS One **6:** e26291.

Lea-Smith, D. J., P. Bombelli, R. Vasudevan, and C. J. Howe. 2016. Photosynthetic, respiratory and extracellular electron transport pathways in cyanobacteria. Biochimica et Biophysica Acta (BBA)-Bioenergetics **1857:** 247-255.

Lea-Smith, D. J., N. Ross, M. Zori, D. S. Bendall, J. S. Dennis, S. A. Scott, A. G. Smith, and C. J. Howe. 2013. Thylakoid terminal oxidases are essential for the cyanobacterium Synechocystis sp. PCC 6803 to survive rapidly changing light intensities. Plant Physiology **162:** 484-495.

Lee, C.-G. 1999. Calculation of light penetration depth in photobioreactors. Biotechnology and Bioprocess Engineering **4:** 78-81.

Li, W., H. Gao, C. Yin, and X. Xu. 2012. Identification of a novel thylakoid protein gene involved in cold acclimation in cyanobacteria. Microbiology **158:** 2440-2449.

Li, X.-P., O. Bjoèrkman, C. Shih, A. R. Grossman, M. Rosenquist, S. Jansson, and K. K. Niyogi. 2000. A pigment-binding protein essential for regulation of photosynthetic light harvesting. Nature **403:** 391-395.

Liffman, K., D. A. Paterson, P. Liovic, and P. Bandopadhayay. 2013. Comparing the energy efficiency of different high rate algal raceway pond designs using computational fluid dynamics. Chemical Engineering Research and Design **91:** 221-226.

Liu, S.-W., and B.-S. Qiu. 2012. Different responses of photosynthesis and flow cytometric signals to iron limitation and nitrogen source in coastal and oceanic Synechococcus strains (Cyanophyceae). Marine Biology **159:** 519-532.

Lucker, B. F., C. C. Hall, R. Zegarac, and D. M. Kramer. 2014. The environmental photobioreactor (ePBR): An algal culturing platform for simulating dynamic natural environments. Algal Research **6:** 242-249.

Ludwig, M., and D. A. Bryant. 2011. Transcription Profiling of the Model Cyanobacterium Synechococcus sp. Strain PCC 7002 by Next-Gen (SOLiD) Sequencing of cDNA. Front Microbiol **2:** 41.

Luo, H.-P., and M. H. Al-Dahhan. 2011. Verification and validation of CFD simulations for local flow dynamics in a draft tube airlift bioreactor. Chemical Engineering Science **66:** 907-923.

Macintyre, H. L., T. M. Kana, T. Anning, and R. J. Geider. 2002. Photoacclimation of Photosynthesis Irradiance Response Curves and Photosynthetic Pigments in Microalgae and Cyanobacteria. Journal of Phycology **38:** 17-38.

Masojidek, J., J. Kopecky, L. Giannelli, and G. Torzillo. 2011. Productivity correlated to photobiochemical performance of Chlorella mass cultures grown outdoors in thin-layer cascades. J Ind Microbiol Biotechnol **38:** 307-317.

Masojídek, J., Š. Papáček, M. Sergejevová, V. Jirka, J. Červený, J. Kunc, J. Korečko, O. Verbovikova, J. Kopecký, and D. Štys. 2003. A closed solar photobioreactor for cultivation of microalgae under supra-high irradiance: basic design and performance. Journal of Applied Phycology **15:** 239-248.

Masojidek, J., S. Papacek, M. Sergejevova, V. Jirka, J. Cerveny, J. Kunc, J. Korecko, O. Verbovikova, J. Kopecky, D. Stys, and G. Torzillo. 2003. A closed solar photobioreactor for cultivation of microalgae under supra-high irradiance: basic design and performance. Journal of Applied Phycology **15:** 239-248.

Matsuo, M., T. Endo, and K. Asada. 1998. Properties of the respiratory NAD (P) H dehydrogenase isolated from the cyanobacterium Synechocystis PCC6803. Plant and Cell Physiology **39:** 263-267.

Mcdonald, A. E., A. G. Ivanov, R. Bode, D. P. Maxwell, S. R. Rodermel, and N. P. Hüner. 2011. Flexibility in photosynthetic electron transport: the physiological role of plastoquinol terminal oxidase (PTOX). Biochimica et Biophysica Acta (BBA)-Bioenergetics **1807:** 954-967.

Mcginn, P. J., G. D. Price, R. Maleszka, and M. R. Badger. 2003. Inorganic carbon limitation and light control the expression of transcripts related to the CO2-concentrating mechanism in the cyanobacterium Synechocystis sp. strain PCC6803. Plant Physiology **132:** 218-229.

Mehrabadi, A., M. M. Farid, and R. Craggs. 2016. Variation of biomass energy yield in wastewater treatment high rate algal ponds. Algal Research **15:** 143-151.

Meier, R. 1955. Biological cycles in the transformation of solar energy into useful fuels. Solar Energy Research **23:** 179-183.

Melis, A. 2009. Solar energy conversion efficiencies in photosynthesis: minimizing the chlorophyll antennae to maximize efficiency. Plant Science **177:** 272-280.

Merchuk, J., and X. Wu. 2003. Modeling of photobioreactors: application to bubble column simulation. Journal of Applied Phycology **15:** 163-169.

Mettler, T., T. Mühlhaus, D. Hemme, M.-A. Schöttler, J. Rupprecht, A. Idoine, D. Veyel, S. K. Pal, L. Yaneva-Roder, and F. V. Winck. 2014. Systems analysis of the response of photosynthesis, metabolism, and growth to an increase in irradiance in the photosynthetic model organism Chlamydomonas reinhardtii. The Plant Cell **26:** 2310-2350.

Mi, H., T. Endo, U. Schreiber, T. Ogawa, and K. Asada. 1992. Electron donation from cyclic and respiratory flows to the photosynthetic intersystem chain is mediated by pyridine nucleotide dehydrogenase in the cyanobacterium Synechocystis PCC 6803. Plant and cell physiology **33:** 1233-1237.

Minagawa, J. 2011. State transitions—The molecular remodeling of photosynthetic supercomplexes that controls energy flow in the chloroplast. Biochimica et Biophysica Acta (BBA) - Bioenergetics **1807:** 897-905.

Moberg, A. K., G. K. Ellem, G. J. Jameson, and J. G. Herbertson. 2012. Simulated cell trajectories in a stratified gas–liquid flow tubular photobioreactor. Journal of Applied Phycology **24:** 357-363.

Mohamed, A., J. Eriksson, H. D. Osiewacz, and C. Jansson. 1993. Differential expression of the psbA genes in the cyanobacterium Synechocystis 6803. Molecular and General Genetics MGG **238:** 161-168.

Moody, J. W., C. M. Mcginty, and J. C. Quinn. 2014. Global evaluation of biofuel potential from microalgae. Proceedings of the National Academy of Sciences **111:** 8691-8696.

Morris, P. D., A. Narracott, H. Von Tengg-Kobligk, D. a. S. Soto, S. Hsiao, A. Lungu, P. Evans, N. W. Bressloff, P. V. Lawford, and D. R. Hose. 2016. Computational fluid dynamics modelling in cardiovascular medicine. Heart **102:** 18-28.

Mortazavi, A., B. A. Williams, K. Mccue, L. Schaeffer, and B. Wold. 2008. Mapping and quantifying mammalian transcriptomes by RNA-Seq. Nature methods **5:** 621-628.

Mu, D., R. Ruan, M. Addy, S. Mack, P. Chen, and Y. Zhou. 2017. Life cycle assessment and nutrient analysis of various processing pathways in algal biofuel production. Bioresource Technology **230:** 33-42.

Mullineaux, C. W., and J. F. Allen. 1990. State 1-state 2 transitions in the cyanobacterium Synechococcus 6301 are controlled by the redox state of electron carriers between photosystems I and II. Photosynthesis Research **23:** 297-311.

Mullineaux, C. W., and D. Emlyn-Jones. 2005. State transitions: an example of acclimation to low-light stress. Journal of Experimental Botany **56:** 389-393.

Murakami, A. 1997. Quantitative analysis of 77K fluorescence emission spectra in Synechocystis sp. PCC 6714 and Chlamydomonas reinhardtii with variable PS I/PS II stoichiometries. Photosynthesis Research **53:** 141-148.

Muramatsu, M., and Y. Hihara. 2012. Acclimation to high-light conditions in cyanobacteria: from gene expression to physiological responses. Journal of Plant Research **125:** 11-39.

Murchie, E. H., and K. K. Niyogi. 2011. Manipulation of photoprotection to improve plant photosynthesis. Plant Physiology **155:** 86-92.

Mustila, H., Y. Allahverdiyeva, J. Isojärvi, E. Aro, and M. Eisenhut. 2014. The bacterial-type [4Fe–4S] ferredoxin 7 has a regulatory function under photooxidative stress conditions in the cyanobacterium Synechocystis sp. PCC 6803. Biochimica et Biophysica Acta (BBA)-Bioenergetics **1837:** 1293-1304.

Mustila, H., P. Paananen, N. Battchikova, A. Santana-Sánchez, D. Muth-Pawlak, M. Hagemann, E.-M. Aro, and Y. Allahverdiyeva. 2016. The Flavodiiron Protein Flv3 Functions as a Homo-Oligomer During Stress Acclimation and is Distinct from the Flv1/Flv3 Hetero-Oligomer Specific to the O2 Photoreduction Pathway. Plant and Cell Physiology **57:** 1468-1483.

Mühlhaus, T., J. Weiss, D. Hemme, F. Sommer, and M. Schroda. 2011. Quantitative shotgun proteomics using a uniform 15N-labeled standard to monitor proteome dynamics in time course experiments reveals new insights into the heat stress response of Chlamydomonas reinhardtii. Molecular & Cellular Proteomics **10:** M110. 004739.

Nakajima, Y., and T. Itayama. 2003. Analysis of photosynthetic productivity of microalgal mass cultures. Journal of Applied Phycology **15:** 497-505.

Nakajima, Y., M. Tsuzuki, and R. Ueda. 1998. Reduced photoinhibition of a phycocyanin-deficient mutant of Synechocystis PCC 6714. Journal of Applied Phycology **10:** 447-452.

Nakajima, Y., and R. Ueda. 1997. Improvement of photosynthesis in dense microalgal suspension by reduction of light harvesting pigments. Journal of Applied Phycology **9:** 503-510.

Nedbal, L., V. Tichy, F. H. Xiong, and J. U. Grobbelaar. 1996. Microscopic green algae and cyanobacteria in high-frequency intermittent light. Journal of Applied Phycology **8:** 325-333.

Nigam, P. S., and A. Singh. 2011. Production of liquid biofuels from renewable resources. Progress in Energy and Combustion Science **37:** 52-68.

Niyogi, K. K. 2000. Safety valves for photosynthesis. Current Opinion in Plant Biology **3:** 455-460.

Norton, T., and D.-W. Sun. 2006. Computational fluid dynamics (CFD)–an effective and efficient design and analysis tool for the food industry: a review. Trends in Food Science & Technology **17:** 600-620.

Ooyabu, J., M. Ohtsuka, Y. Kashino, H. Koike, and K. Satoh. 2008. The expression pattern of NAD (P) H oxidases and the cyclic electron transport pathway around photosystem I

of Synechocystis sp. PCC6803 depend on growth conditions. Bioscience, Biotechnology, and Biochemistry **72:** 3180-3188.

Ort, D. R., S. S. Merchant, J. Alric, A. Barkan, R. E. Blankenship, R. Bock, R. Croce, M. R. Hanson, J. M. Hibberd, and S. P. Long. 2015. Redesigning photosynthesis to sustainably meet global food and bioenergy demand. Proceedings of the National Academy of Sciences **112:** 8529-8536.

Ort, D. R., X. Zhu, and A. Melis. 2011. Optimizing antenna size to maximize photosynthetic efficiency. Plant Physiology **155:** 79-85.

Oxborough, K., and P. Horton. 1988. A study of the regulation and function of energy-dependent quenching in pea chloroplasts. Biochimica et Biophysica Acta (BBA)-Bioenergetics **934:** 135-143.

Pachauri, R. K., M. R. Allen, V. R. Barros, J. Broome, W. Cramer, R. Christ, J. A. Church, L. Clarke, Q. Dahe, and P. Dasgupta. 2014. Climate change 2014: synthesis report. Contribution of Working Groups I, II and III to the fifth assessment report of the Intergovernmental Panel on Climate Change. IPCC.

Pandhal, J., P. C. Wright, and C. A. Biggs. 2007. A quantitative proteomic analysis of light adaptation in a globally significant marine cyanobacterium Prochlorococcus marinus MED4. Journal of Proteome Research **6:** 996-1005.

Park, K.-H., and C.-G. Lee. 2001. Effectiveness of flashing light for increasing photosynthetic efficiency of microalgal cultures over a critical cell density. Biotechnology and Bioprocess Engineering **6:** 189-193.

Parmesan, C., M. T. Burrows, C. M. Duarte, E. S. Poloczanska, A. J. Richardson, D. S. Schoeman, and M. C. Singer. 2013. Beyond climate change attribution in conservation and ecological research. Ecology Letters **16:** 58-71.

Patel, C. D., C. E. Bash, C. Belady, L. Stahl, and D. Sullivan. 2001. Computational fluid dynamics modeling of high compute density data centers to assure system inlet air specifications, p. 8-13. Proceedings of IPACK.

Peers, G. 2014. Increasing algal photosynthetic productivity by integrating ecophysiology with systems biology. Trends in Biotechnology **32:** 551-555.

---. 2015. Enhancement of biomass production by disruption of light energy dissipation pathways. United States of America Patent **8,940,508**.

Peers, G., T. B. Truong, E. Ostendorf, A. Busch, D. Elrad, A. R. Grossman, M. Hippler, and K. K. Niyogi. 2009. An ancient light-harvesting protein is critical for the regulation of algal photosynthesis. Nature **462:** 518-521.

Pérez-Collazo, C., D. Greaves, and G. Iglesias. 2015. A review of combined wave and offshore wind energy. Renewable and Sustainable Energy Reviews **42:** 141-153.

Perner-Nochta, I., and C. Posten. 2007. Simulations of light intensity variation in photobioreactors. Journal of Biotechnology **131:** 276-285.

Pienkos, P. T., and A. Darzins. 2009. The promise and challenges of microalgal-derived biofuels. Biofuels, Bioproducts and Biorefining **3:** 431-440.

Poloczanska, E. S., C. J. Brown, W. J. Sydeman, W. Kiessling, D. S. Schoeman, P. J. Moore, K. Brander, J. F. Bruno, L. B. Buckley, and M. T. Burrows. 2013. Global imprint of climate change on marine life. Nature Climate Change **3:** 919-925.

Poncelet, M., C. Cassier‐Chauvat, X. Leschelle, H. Bottin, and F. Chauvat. 1998. Targeted deletion and mutational analysis of the essential (2Fe‐2S) plant‐like ferredoxin in Synechocystis PCC6803 by plasmid shuffling. Molecular Microbiology **28:** 813-821.

Posten, C. 2009. Design principles of photo‐bioreactors for cultivation of microalgae. Engineering in Life Sciences **9:** 165-177.

Prussi, M., M. Buffi, D. Casini, D. Chiaramonti, F. Martelli, M. Carnevale, M. R. Tredici, and L. Rodolfi. 2014. Experimental and numerical investigations of mixing in raceway ponds for algae cultivation. Biomass and Bioenergy **67:** 390-400.

Radakovits, R., R. E. Jinkerson, A. Darzins, and M. C. Posewitz. 2010. Genetic engineering of algae for enhanced biofuel production. Eukaryot Cell **9:** 486-501.

Raven, J. A., J. Beardall, and M. Giordano. 2014. Energy costs of carbon dioxide concentrating mechanisms in aquatic organisms. Photosynthesis Research **121:** 111-124.

Richier, S., A. I. Macey, N. J. Pratt, D. J. Honey, C. M. Moore, and T. S. Bibby. 2012. Abundances of iron-binding photosynthetic and nitrogen-fixing proteins of Trichodesmium both in culture and in situ from the North Atlantic. PLoS one **7:** e35571.

Ritchie, R. J. 2006. Consistent Sets of Spectrophotometric Chlorophyll Equations for Acetone, Methanol and Ethanol Solvents. Photosynthesis Research **89:** 27-41.

Ritchie, R. J. 2008. Fitting light saturation curves measured using modulated fluorometry. Photosynthesis Research **96:** 201-215.

Rochaix, J.-D. 2011. Reprint of: Regulation of photosynthetic electron transport. Biochimica et Biophysica Acta (BBA)-Bioenergetics **1807:** 878-886.

Rupprecht, E., E. Fuhrmann, and D. Schneider. 2008. Stress regulated dnaK expression in Synechocystis sp. PCC 6803. Photosynthesis. Energy from the Sun**:** 1327-1330.

Saha, R., D. Liu, A. Hoynes-O'connor, M. Liberton, J. Yu, M. Bhattacharyya-Pakrasi, A. Balassy, F. Zhang, T. S. Moon, and C. D. Maranas. 2016. Diurnal Regulation of Cellular Processes in the Cyanobacterium Synechocystis sp. Strain PCC 6803: Insights from Transcriptomic, Fluxomic, and Physiological Analyses. mBio **7:** e00464-00416.

Sakata, S., N. Mizusawa, H. Kubota-Kawai, I. Sakurai, and H. Wada. 2013. Psb28 is involved in recovery of photosystem II at high temperature in Synechocystis sp. PCC 6803. Biochimica et Biophysica Acta (BBA)-Bioenergetics **1827:** 50-59.

Schluter, L., T. L. Lauridsen, G. Krogh, and T. Jorgensen. 2006. Identification and quantification of phytoplankton groups in lakes using new pigment ratios – a comparison between pigment analysis by HPLC and microscopy. Freshwater Biology **51:** 1474-1485.

Schneider, D., S. Skrzypczak, S. Anemüller, C. L. Schmidt, A. Seidler, and M. Rögner. 2002. Heterogeneous Rieske Proteins in the Cytochromeb 6 f Complex ofSynechocystis PCC6803? Journal of Biological Chemistry **277:** 10949-10954.

Schreiber, U., U. Schliwa, and W. Bilger. 1986. Continuous recording of photochemical and non-photochemical chlorophyll fluorescence quenching with a new type of modulation fluorometer. Photosynthesis Research **10:** 51-62.

Sforza, E., D. Simionato, G. M. Giacometti, A. Bertucco, and T. Morosinotto. 2012. Adjusted light and dark cycles can optimize photosynthetic efficiency in algae growing in photobioreactors. PLoS One **7:** e38975.

Shibata, M., H. Ohkawa, T. Kaneko, H. Fukuzawa, S. Tabata, A. Kaplan, and T. Ogawa. 2001. Distinct constitutive and low-CO2-induced CO2 uptake systems in cyanobacteria: genes involved and their phylogenetic relationship with homologous genes in other organisms. Proceedings of the National Academy of Sciences **98:** 11789-11794.

Shigeoka, S., T. Ishikawa, M. Tamoi, Y. Miyagawa, T. Takeda, Y. Yabuta, and K. Yoshimura. 2002. Regulation and function of ascorbate peroxidase isoenzymes. Journal of Experimental Botany **53:** 1305-1319.

Shimakawa, G., K. Shaku, A. Nishi, R. Hayashi, H. Yamamoto, K. Sakamoto, A. Makino, and C. Miyake. 2015. FLAVODIIRON2 and FLAVODIIRON4 proteins mediate an oxygen-dependent alternative electron flow in Synechocystis sp. PCC 6803 under CO2-limited conditions. Plant Physiology **167:** 472-480.

Sicora, C. I., S. E. Appleton, C. M. Brown, J. Chung, J. Chandler, A. M. Cockshutt, I. Vass, and D. A. Campbell. 2006. Cyanobacterial psbA families in Anabaena and Synechocystis encode trace, constitutive and UVB-induced D1 isoforms. Biochimica et Biophysica Acta **1757:** 47-56.

Smart, L. B., and L. Mcintosh. 1991. Expression of photosynthesis genes in the cyanobacteriumSynechocystis sp. PCC 6803: psaA-psaB andpsbA transcripts accumulate in dark-grown cells. Plant Molecular Biology **17:** 959-971.

Soo, R. M., J. Hemp, D. H. Parks, W. W. Fischer, and P. Hugenholtz. 2017. On the origins of oxygenic photosynthesis and aerobic respiration in Cyanobacteria. Science **355:** 1436-1440.

Stanier, R., R. Kunisawa, M. Mandel, and G. Cohen-Bazire. 1971. Purification and properties of unicellular blue-green algae (order Chroococcales). Bacteriological Reviews **35:** 171.

Steele, J. H. 1962. Environmental control of photosynthesis in the sea. Limnology and Oceanography **7:** 137-150.

Stephens, E., I. L. Ross, Z. King, J. H. Mussgnug, O. Kruse, C. Posten, M. A. Borowitzka, and B. Hankamer. 2010. An economic and technical evaluation of microalgal biofuels. Nature Biotechnology **28:** 126-128.

Summerfield, T. C., and L. A. Sherman. 2007. Role of sigma factors in controlling global gene expression in light/dark transitions in the cyanobacterium Synechocystis sp. strain PCC 6803. Journal of Bacteriology **189:** 7829-7840.

Takache, H., J. Pruvost, and H. Marec. 2015. Investigation of light/dark cycles effects on the photosynthetic growth of Chlamydomonas reinhardtii in conditions representative of photobioreactor cultivation. Algal Research **8:** 192-204.

Takeda, K., M. Iizuka, T. Watanabe, J. Nakagawa, S. Kawasaki, and Y. Niimura. 2007. Synechocystis DrgA protein functioning as nitroreductase and ferric reductase is capable of catalyzing the Fenton reaction. FEBS Journal **274:** 1318-1327.

Taniguchi, Y., P. J. Choi, G.-W. Li, H. Chen, M. Babu, J. Hearn, A. Emili, and X. S. Xie. 2010. Quantifying E. coli proteome and transcriptome with single-molecule sensitivity in single cells. Science **329:** 533-538.

Tcherkez, G. G., G. D. Farquhar, and T. J. Andrews. 2006. Despite slow catalysis and confused substrate specificity, all ribulose bisphosphate carboxylases may be nearly perfectly optimized. Proceedings of the National Academy of Sciences **103:** 7246-7251.

Tonon, T., D. Harvey, T. R. Larson, and I. A. Graham. 2002. Long chain polyunsaturated fatty acid production and partitioning to triacylglycerols in four microalgae. Phytochemistry **61:** 15-24.

Van Alphen, P., and K. J. Hellingwerf. 2015. Sustained circadian rhythms in continuous light in Synechocystis sp. PCC6803 growing in a well-controlled photobioreactor. PloS One **10:** e0127715.

Vernotte, C., M. Picaud, D. Kirilovsky, J. Olive, G. Ajlani, and C. Astier. 1992. Changes in the photosynthetic apparatus in the cyanobacterium Synechocystis sp. PCC 6714 following light-to-dark and dark-to-light transitions. Photosynthesis Research **32:** 45-57.

Waldbauer, J. R., S. Rodrigue, M. L. Coleman, and S. W. Chisholm. 2012. Transcriptome and proteome dynamics of a light-dark synchronized bacterial cell cycle. PloS One **7:** e43432.

Wang, J., L. Chen, Z. Chen, and W. Zhang. 2015. RNA-seq based transcriptomic analysis of single bacterial cells. Integrative Biology **7:** 1466-1476.

Wang, Q., S. Jantaro, B. Lu, W. Majeed, M. Bailey, and Q. He. 2008. The high light-inducible polypeptides stabilize trimeric photosystem I complex under high light conditions in Synechocystis PCC 6803. Plant Physiology **147:** 1239-1250.

Wellburn, A. R. 1994. The spectral determination of chlorophylls a and b, as well as total carotenoids, using various solvents with spectrophotometers of different resolution. Journal of Plant Physiology **144:** 307-313.

Wijffels, R. H., and M. J. Barbosa. 2010. An outlook on microalgal biofuels. Science **329:** 796-799.

Wilson, A., G. Ajlani, J. M. Verbavatz, I. Vass, C. A. Kerfeld, and D. Kirilovsky. 2006. A soluble carotenoid protein involved in phycobilisome-related energy dissipation in cyanobacteria. The Plant Cell **18:** 992-1007.

Wold, S., K. Esbensen, and P. Geladi. 1987. Principal component analysis. Chemometrics and Intelligent Laboratory Systems **2:** 37-52.

Woodson, J. D. 2016. Chloroplast quality control–balancing energy production and stress. New Phytologist **212:** 36-41.

Work, V. H., R. Radakovits, R. E. Jinkerson, J. E. Meuser, L. G. Elliott, D. J. Vinyard, L. M. Laurens, G. C. Dismukes, and M. C. Posewitz. 2010. Increased lipid accumulation in the Chlamydomonas reinhardtii sta7-10 starchless isoamylase mutant and increased carbohydrate synthesis in complemented strains. Eukaryotic Cell **9:** 1251-1261.

Wu, L., Z. Li, and Y. Song. 2009. Numerical investigation of flow characteristics and irradiance history in a novel photobioreactor. African Journal of Biotechnology **8:** 4672.

Xu, W., R. Yang, M. Li, Z. Xing, W. Yang, G. Chen, H. Guo, X. Gong, Z. Du, and Z. Zhang. 2011. Transcriptome phase distribution analysis reveals diurnal regulated biological processes and key pathways in rice flag leaves and seedling leaves. PLoS One **6:** e17613.

Yarnold, J., I. L. Ross, and B. Hankamer. 2016. Photoacclimation and productivity of Chlamydomonas reinhardtii grown in fluctuating light regimes which simulate outdoor algal culture conditions. Algal Research **13:** 182-194.

Young, J. D., A. A. Shastri, G. Stephanopoulos, and J. A. Morgan. 2011. Mapping photoautotrophic metabolism with isotopically nonstationary (13)C flux analysis. Metabolic Engineering **13:** 656-665.

Youngblood, M. T. 2015. Physiological Response of the Cyanobacterium Synechocystis sp. PCC 6803 to Fluctuating Light. Colorado State University. Libraries.

Zhang, P., M. Eisenhut, A. M. Brandt, D. Carmel, H. M. Silen, I. Vass, Y. Allahverdiyeva, T. A. Salminen, and E. M. Aro. 2012. Operon flv4-flv2 provides cyanobacterial photosystem II with flexibility of electron transfer. Plant Cell **24:** 1952-1971.

Zhu, X.-G., S. P. Long, and D. R. Ort. 2010a. Improving photosynthetic efficiency for greater yield. Annual Review of Plant Biology **61:** 235-261.

Zhu, X. G., S. P. Long, and D. R. Ort. 2010b. Improving photosynthetic efficiency for greater yield. Annu Rev Plant Biol **61:** 235-261.

Zones, J. M., I. K. Blaby, S. S. Merchant, and J. G. Umen. 2015. High-resolution profiling of a synchronized diurnal transcriptome from Chlamydomonas reinhardtii reveals continuous cell and metabolic differentiation. The Plant Cell **27:** 2743-2769.

A. Computational Fluid Dynamics Modeling

Supplemental information regarding the computational fluid dynamic model of the ePBR.

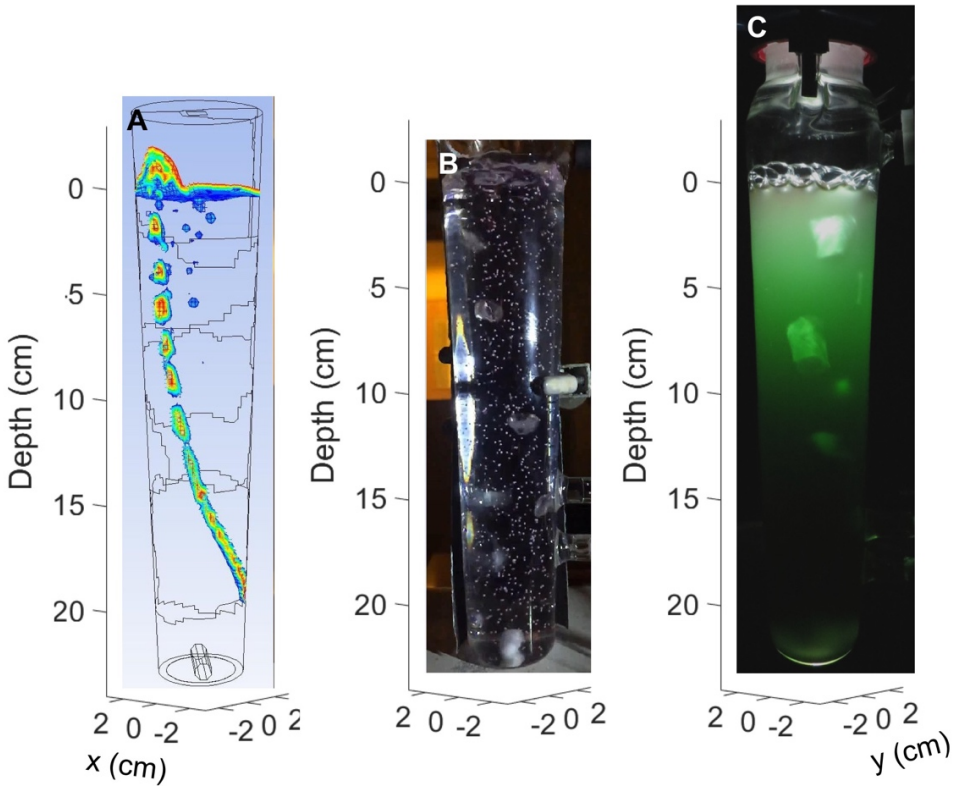

Figure A2. Detailed illustration of the velocity profiles of the four cross sections shown in Fig. 1.3. Sections 1, 2, 3, 4 are derived from depth 9, 14, 19, and 23 cm of the ePBR vessel, respectively. Vector arrows indicate direction and magnitude of fluid movement. *[Note from the author; figure credit Chen Shen as part of his dissertation]*

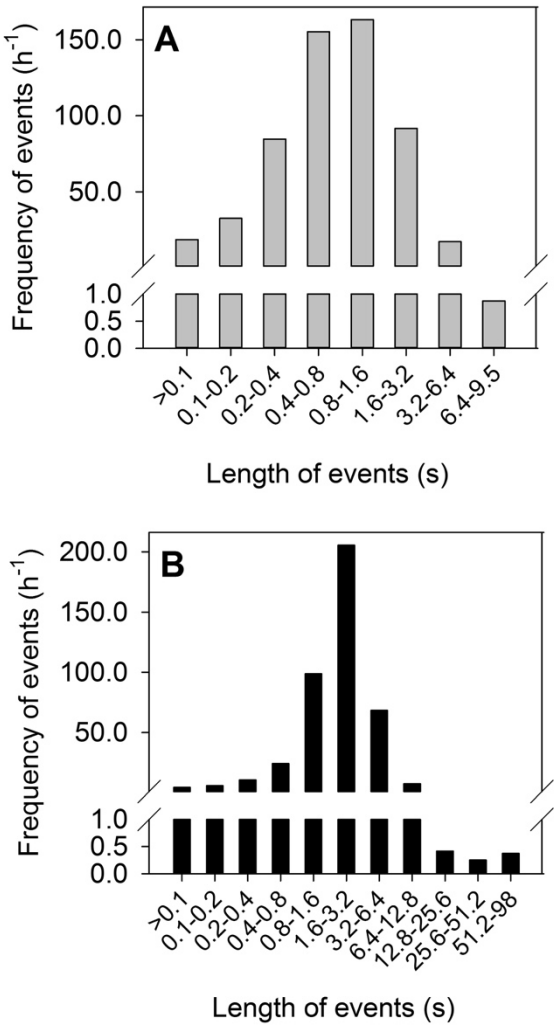

Figure A3. Frequency and length of events when a particle (cell) enters the surface and bottom zones. A) frequency and length of events when the particle enters the surface zone (>2 cm depth; >30% surface PAR), B) frequency and length of events where the particle enters the dark zone of the ePBR (<10 cm depth; <1% of surface PAR).

Supplemental Video 1:
Illustration of the computational fluid dynamic simulation of the ePBR with temporal resolution. A) slow-motion video of 1 mm in diameter neutrally buoyant beads in H_2O under ambient growth conditions, B) model of the air-stream with color indicating air-culture interface, C) fully developed model tracking simulated *Synechocystis* cells *in silico. [Note from the author; video credit Chen Shen as part of his dissertation]*

B. Non-photochemical Quenching Estimates

For method description, see section 2.3.4 and 2.3.5 of Chapter 1.

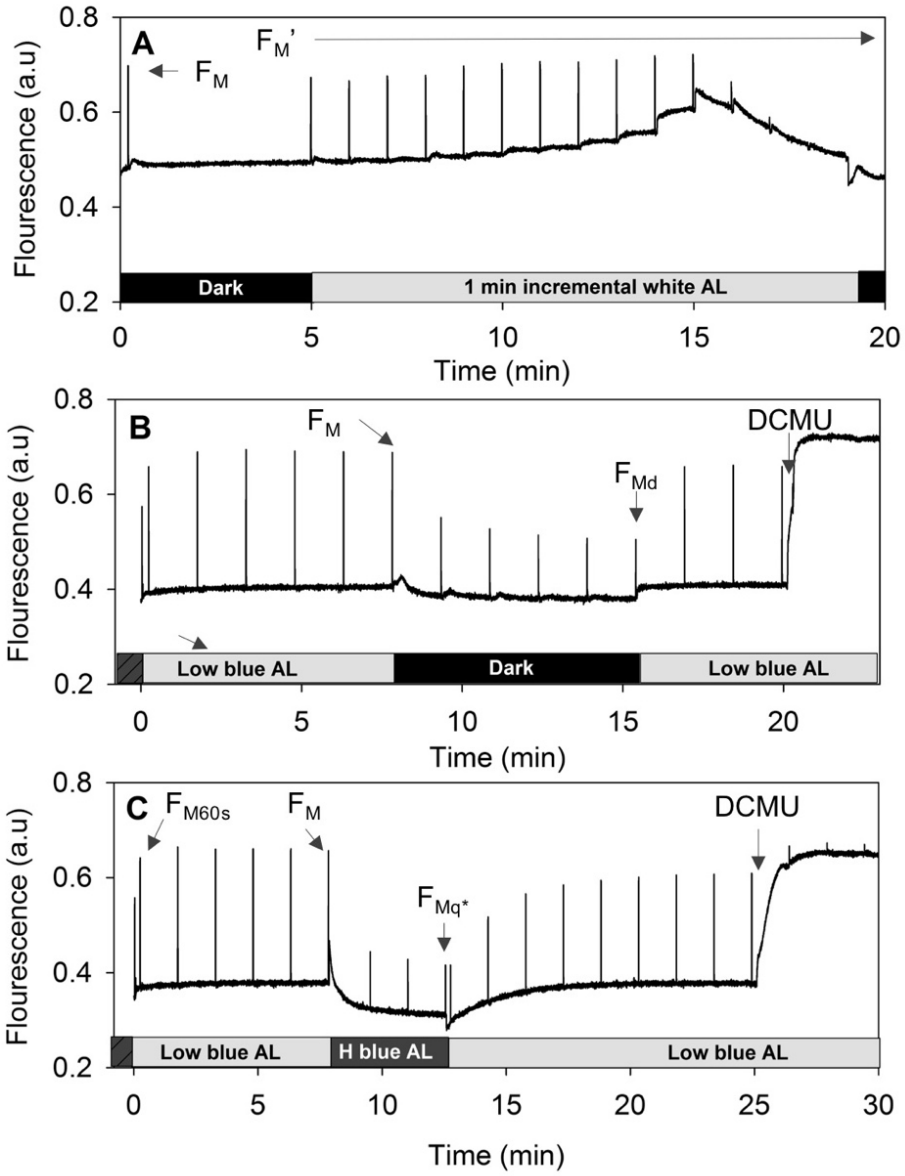

Figure B1. Fluorescence traces used to quantify non-photochemical quenching (NPQ). A) fluorescence trace used to calculate the NPQ parameter during the rapid photosynthesis versus irradiance curves (Fig. 1.6B), B) maximum NPQ amplitude of state transition was estimated based on the high fluorescence induced state (F_M) under low blue actin light (26 µmol photons m^{-2} s^{-1}; 430 nm) compared to the dark acclimatized state (F_{Md}), C) treatment used to quantify orange carotenoid protein dependent NPQ. Sample was removed from ePBR and subjected to 7 min of low blue actin light (26 µmol photons m^{-2} s^{-1}; 430 nm) followed by high blue light (880 µmol photons m^{-2} s^{-1}) for 7 min, and finally relaxation under low blue light for 15 min. See section 2.3.4 and 2.3.5 for full description of fluorescence parameters and calculations. After steady state florescence recovery was achieved, B and C were treated with 20 µM DCMU to induce maximal fluorescence. All samples shown were collected from ePBR cultures between ZT5 and ZT7. chl *a* concentration was 3±0.5 µg ml^{-1}.

C. Depth-dependent Changes in Spectral Composition of Light and Effects on Photosynthesis

The light intensity decreased rapidly as it penetrated the dense culture. Bear-lambert law (Eq. 2 Chapter 1) did not model the extinction accurately, as can be seen in the discrepancies between extinction coefficients at different densities in Table C1, and the non-exponential decline in measured irradiance in Fig. 1.3. The discrepancies in the extinction of light prompted us to investigate how the spectral composition of light changes through the ePBR vessel. We were specifically interested to find out if at some depth the composition of light was changed so it becomes less effective in driving photosynthesis.

Change in the spectral composition of light was measured at four discreet depths (surface, 2, 4 and 8 cm) of the ePBR, using a CHEMUSB4-UV-VIS spectrometer (Ocean Optics). The results indicated that blue light disappeared more rapidly than red, and that the proportion of green light was heavily enriched at >four cm depth (Fig. C1). To estimate the impact of this change in the quality of light, we generated rapid photosynthesis versus irradiance response curves with pre-filtered light. Two and 8 × concentrated cultures of *Synechocystis* (OD_{750} of 1.5 and 6, respectively) was placed in a one cm rectangular cuvette covering the actinic light path to the quartz cuvette. This caused the light to be filtered in a similar fashion as at two and 8 cm depths of the ePBR. The actinic light aimed at the initial cuvette was increased to a maximum level of 3000 µmol photons m^{-2} s^{-1} but due to the absorption of the culture within, only a fraction of this light reached the second cuvette from which oxygen and fluorescent measurements were taken. The filtrated light mimicking two cm depth did not change the α but at 8 cm depth there was a significant reduction (50%), suggesting that at this depth light had lost some of its ability to drive photosynthesis (Table C2). However, at 8 cm depth less than 5% of the surface PAR remains (Fig. 1.3A) and this reduction is unlikely to have an impact on the overall growth rate of the culture.

Table C1. Measured light intensities (PAR) at specific depths of the ePBR and with different culture densities. The absorption coefficients were calculated using Beer Lamberts law (see Chapter 1, Eq. 2).

OD750:	0.85	0.77	0.69	0.62	Mean (0.73)	
Depth (cm)	Light intensity (µmol photons m^{-2} s^{-1})					Absorption coefficient
0	1000	1000	1000	1000	1000	-
1	344	482	550	568	486	0.429
2	206	275	378	378	310	0.348
4	64	103	155	184	126	0.307
8	14	22	29	36	25	0.273
23	0.3	0.4	0.5	0.5	0.4	0.202

Table C2. Parameters derivate form the rapid photosynthesis versus irradiance curves at simulated depth. Differences between treatments were analyzed using 1 way-ANOVA (N=3) and letter denotes significance differences. n.d.: not detected.

P-I parameters on chl *a* basis			
Treatment	α (µmol O_2 [mg chl *a*] h^{-1})/ (µmol photons m^{-2} s^{-1})	P_{max} (µmol O_2 [mg chl *a*] h^{-1})	E_k (µmol photons m^{-2} s^{-1})
Surface	1.23 ± 0.05^a	527 ± 17^a	429 ± 31^a
2 cm depth	1.06 ± 0.13^a	400 ± 14^b	383 ± 65^b
8 cm depth	0.75 ± 0.07^b	n.d.	n.d.
$^1F_{2,6}$ $^2F_{1,5}$ *(p)*	*^{1}76 (<0.001)*	*^{2}228 (0.009)*	*^{2}21 (0.01)*

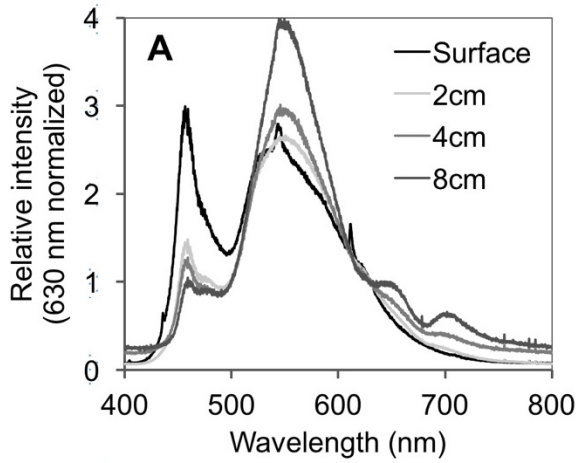

Figure C1. The spectrum of the ePBR LED light (surface) and changes as the light penetrates deeper into the culture (2, 4, and 8 cm depth). The spectrums are normalized to the peak *in vivo* phycobilisome absorption at 630 nm.

D. Selection and Evaluation of *ex situ* Fluctuating Light Treatment

An *ex situ* experiment was designed to investigate the real-time physiological impact of the CFD predicted cell-specific light environment. Membrane inlet mass spectrometry was used to quantify oxygen consumption and evolution (see Fig. 1 for the setup) To find a short but representative light treatment, we examining a three h portion of the CFD model, run under constant surface light (Fig. D2A). We searched for the shortest section that filled two criteria: 1) having the same integrated photon flux as the three h one, and 2) captured the variability in light intensities exhibited in the three h model. We found a five min part of the model were the average PAR stabilized at around 280 µmol photons m^{-2} s^{-1}, similar to the three h model (Fig. D2B). The five min section consisted of highly variable light intensities with about 25 brief flashes of surface light and three 20-30 s periods with almost complete darkness (Fig. D2C). Closer analysis of the temporal distribution of specific light intensities showed that the five min period mirrored the longer three h model (Fig. D2D).

The five min fluctuating light model was simplified to 1 s resolution and a script was created for the PAM were a mixture of one-part blue (430 nm) to two-parts red (635 nm) actinic light was applied in accordance to the model. The MIMS setup is described in detail in section 2.3.6 and an image of the setup can be seen in Fig. D1. The surface light intensity, which in Fig. D2A is shown as 2000 µmol photons m^{-2} s^{-1}, was modified according to the time of day ePBR samples were collected. The integrated light intensity across the five min period was 14% that of maximum surface intensity (Table D1). The fluctuating light model was looped four times to create a 20 min treatment during which change in oxygen concentrations could be monitored. We will refer to this treatment as the fluctuating light treatment throughout the text. We used an average of the oxygen fluxes during the two loops in the middle of the treatment to generate one estimate per experimental replicate. We should point out that because the actinic LED lights of the PAM specifically targets chl

a/phycobilisome peak absorption it drove photosynthesis three times as efficiently as the white LED of the ePBR (α of 3.72 compared with 1.23; Table 2). Hence the absolute rates of oxygen production and consumption should be interpreted cautiously.

The response of the ePBR culture to the fluctuating light treatment was contrasted to static light suppling the same integrated photon flux per unit time, but without the sharp fluctuations in light intensity (Fig. D4). The results show that the brief flashes of light during the fluctuating light treatment could not drive gross-photosynthesis as efficiently as static light (Fig. D4A). Meanwhile oxygen consumption did not change between the two treatments indicating that it was increasing proportionally to the total photon-flux (Fig. D4B). Combined, these two responses caused net-photosynthesis under fluctuating light to be reduced by more than 70 to 50% compare to static light (see ZT2 and ZT10, Fig. D4C). These results agree with the predictions based on P-I curves and the way cell are supplied with light *in situ* (Fig. 1.6).

Table D1. Surface (maximum under fluctuating light treatment) and time-integrated (corresponding to static treatment) PAR used at specific times of the *ex situ* fluctuating light experiment.

ZT (h past dawn)	Surface PAR (μmol photons m^{-2} s^{-1})	Time integrated, cells-specific light exposure (μmol photons m^{-2} s^{-1})
0.25	130	18
1	500	72
2	1000	141
3	1400	204
6	2000	283
9	1400	204
10	1000	141
11	500	72
11.75	130	18

Table D2. Photosynthesis versus irradiance parameters contrasting the PAM's actinic light with the ePBR's white LED light. A 1:2 ratio blue:red actinic light was used as the PAM's actinic light, corresponding to the *ex situ* fluctuating light treatment. Differences between treatments were analyzed using students *t*-test (N=3) and asterisks denote significance differences.

P-I parameters on chl *a* basis			
Treatment	α (μmol O_2 [mg chl *a*] h^{-1})/ (μmol photons m^{-2} s^{-1})	P_{max} (μmol O_2 [mg chl *a*] h^{-1})	E_k (μmol photons m^{-2} s^{-1})
ePBR light	1.23±0.05	527±17	429±31
PAM dichromatic light	3.72±0.27*	497±18	134±5*
t-statistic *(p)*	*15 (<0.001)*	*2.1 (0.1)*	*16 (<0.001)*

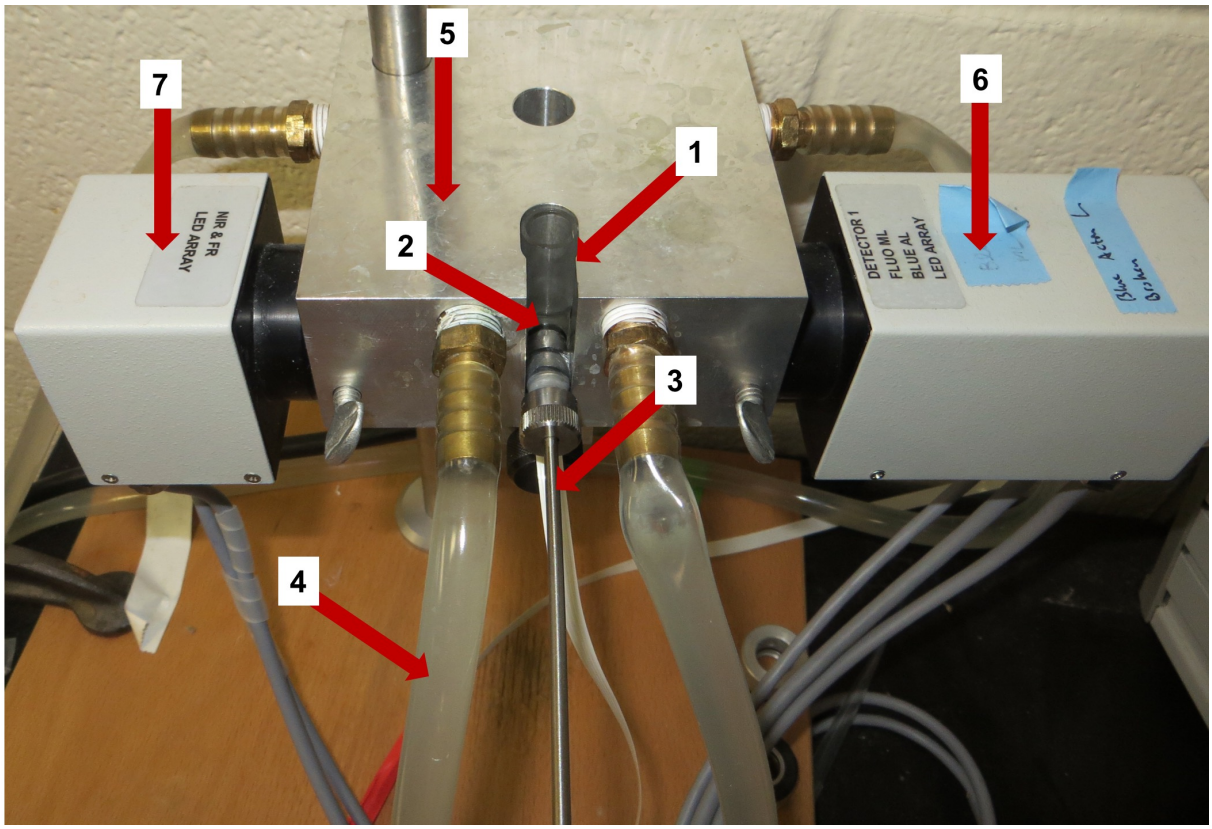

Figure D1. Set-up of the Membrane-inlet Mass Spectrometer (MIMS) and the Dual Pulse-Amplitude Modulation (PAM) fluorometer. Arrows point out: 1) 1.5 mL quartz cuvette, 2) MIMS membrane/sample interface, 3) vacuum column connected to MIMS, 4) water from the isothermal water bath, 5) thermally regulated aluminum holder with internal water circulation. 6) LED array from PAM that apply red (654 nm) and blue (430 nm) actinic light, as well as red (620 nm) measuring light, 7) secondary LED array that apply red (654 nm) actinic light.

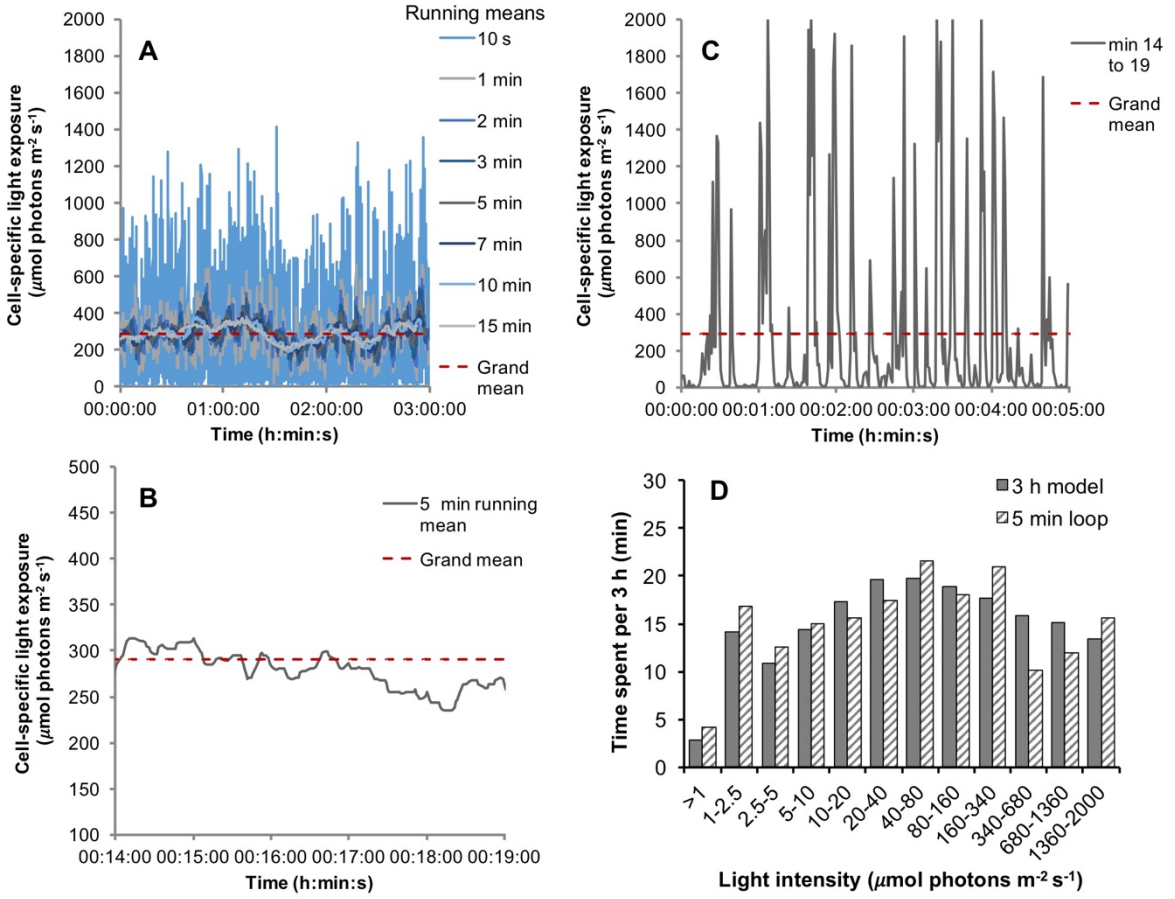

Figure D2. Selection of the *ex situ* fluctuating light treatment. A) a 3-h cell-specific light exposure model run under constant surface light (2000 µmol photons m^{-2} s^{-1}) with the temporal variability smoothed out through incremental running means, B) A zoom at region between the 14th to 19th min showing five min running means, C) cell-specific light exposure in the five min range (14th to 19th min). This corresponds to the light treatment used in the *ex situ* fluctuating light treatment, D) comparison of the variability in cell-specific light intensities between the five min fluctuating light treatment and the three h model.

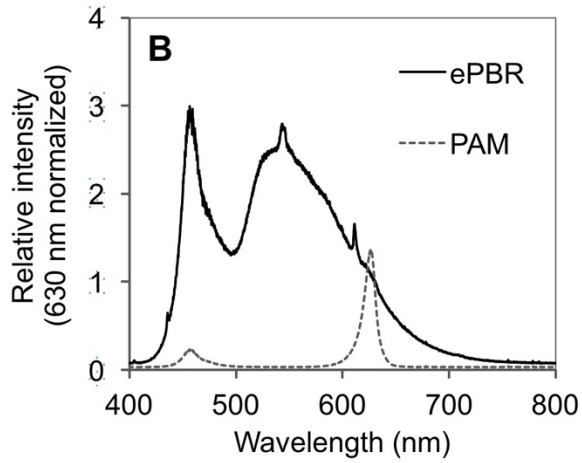

Figure D3. Spectral composition of light used in the *ex situ* experiments. B) Comparison of the ePBRs white LED light with the blue and red PAM light used in the fluctuating light treatment. The spectra are normalized to the peak *in vivo* phycobilisome absorption at 630 nm. Note, ratios between blue and red light of the PAM does not show relative photon abundance to the two lights. This was quantified independently for each light using a light meter. The spectrum recorder has a very narrow inlet to the detector, which skews how much of each light was let in depending on the angel of the detector in relation to the two actinic light sources.

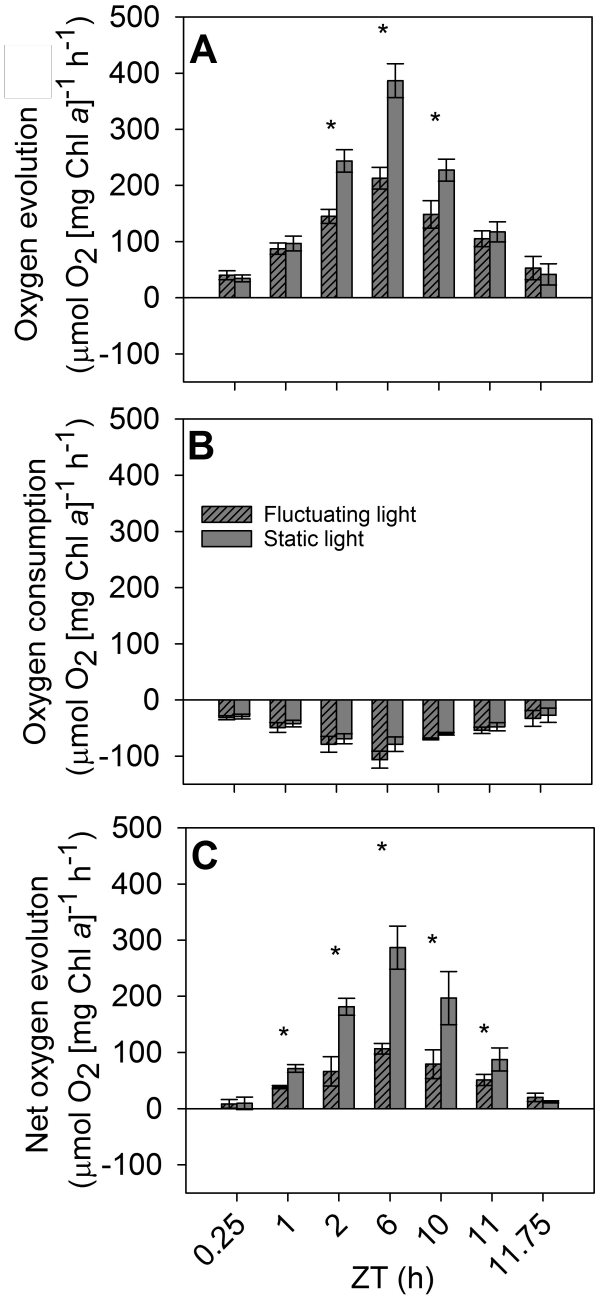

Figure D4. Illuminated rates of oxygen evolution and consumption during the *ex situ* fluctuating light experiment. Static and fluctuating light refers to ePBR acclimatized cultures subjected to the same time integrated photon flux (see Table 1) and measurements were collected using membrane inlet mass spectrometry. A) oxygen evolution corresponding to gross photosynthesis, B) light-dependent oxygen consumption, corresponding to respiration and alternative electron transport, and C) net oxygen evolution (evolution + consumption). Treatment differences (fluctuating versus static light) of oxygen evolution, consumption and net-photosynthesis were analyzed using 2-way RM-ANOVA with $F_{2,12}$ = 810, 16.0, and 330, respectively, and $p<0.001$, $p=0.056$, and $p<0.001$. Asterisks indicate significant differences between fluctuating light and static light. Chl *a* concentration was 15 μg mL^{-1}.

E. Statistical Information for Fig. 1.4 and 1.8 of Chapter 1.

See section 2.3.1, 2.3.2, and 2.3.5 of Chapter 1 for method description

Table E1. Diurnal changes in physiological parameters of *Synechocystis* growing in the ePBR. Data corresponds to that presented in Fig. 1.5 and 1.8 and includes the results of one-way RM-ANOVA (N=4-6). Letters denote significantly differences between time points.

Time (ZT)	Bio-volume (μm^3 $cell^{-1}$)	Chl a (fg [μm^3 bio-volume]$^{-1}$)	Carotenoid:chl a ratio (g g^{-1})	Total organic carbon (pg $cell^{-1}$)	Carbon accumulation (mg TOC L^{-1} h^{-1})	F_V/F_M
-0.25	1.548 ± 0.0144^{e}	12.903 ± 2.210	0.434 ± 0.0125^{cd}	0.499 ± 0.0541^{c}		0.472 ± 0.0145^{d}
0.25	1.539 ± 0.0144^{e}	12.805 ± 1.125	0.433 ± 0.00840^{cde}	0.489 ± 0.100^{bc}		0.527 ± 0.0121^{a}
1	1.535 ± 0.0125^{e}	12.430 ± 0.673	0.442 ± 0.00848^{bc}	0.531 ± 0.0719^{bc}	3.477 ± 1.10^{a}	0.529 ± 0.0128^{a}
3	1.570 ± 0.00787^{de}	12.603 ± 0.577	0.452 ± 0.00786^{a}	0.523 ± 0.0683^{ab}		0.518 ± 0.0131^{a}
6	1.671 ± 0.00882^{a}	13.247 ± 1.462	0.447 ± 0.00699^{ab}	0.653 ± 0.0757^{ab}		0.498 ± 0.0141^{ce}
9	1.702 ± 0.0168^{a}	12.116 ± 0.788	0.435 ± 0.00726^{cd}	0.611 ± 0.0736^{ab}		0.500 ± 0.0112^{bc}
11	1.677 ± 0.0247^{ab}	11.908 ± 0.589	0.425 ± 0.00761^{def}	0.615 ± 0.0847^{ab}		0.515 ± 0.00638^{abe}
11.75	1.663 ± 0.0158^{b}	12.525 ± 0.559	0.421 ± 0.00851^{f}	0.579 ± 0.0594^{ab}	-3.769 ± 2.46^{b}	0.524 ± 0.00705^{ae}
12.25	1.616 ± 0.0278^{c}	12.798 ± 0.261	0.423 ± 0.00624^{def}	0.590 ± 0.0298^{bc}		0.488 ± 0.0132^{cd}
13	1.588 ± 0.0278^{cd}	13.191 ± 1.211	0.425 ± 0.00954^{def}	0.580 ± 0.0634^{bc}		0.475 ± 0.0106^{d}
18	1.524 ± 0.0230^{e}	11.765 ± 1.358	0.426 ± 0.00748^{def}	0.529 ± 0.0592^{bc}	-0.465 ± 0.66^{c}	0.463 ± 0.00462^{d}
23	1.493 ± 0.0272^{f}	12.558 ± 0.607	0.429 ± 0.00682^{de}	0.513 ± 0.0553^{bc}		0.452 ± 0.000500^{d}
23.75	1.489 ± 0.0247^{f}	12.215 ± 1.107	0.430 ± 0.00692^{dce}	0.490 ± 0.0647^{c}		0.448 ± 0.00424^{d}
F statistic	*$F_{12,60}=116$ ($p<0.001$)*	*$F_{12,59}=1.11$ ($p=0.366$)*	*$F_{12,59}=38.5$ ($p<0.001$)*	*$F_{12,60}=4.521$ ($p<0.001$)*	*$F_{2,10}=26.6$ ($p<0.001$)*	*$F_{12,47}=45.5$ ($p<0.001$)*

F. Contrasts Between ePBR, High-, and Low Light Acclimatized Cultures

As a contrast to the ePBR we grew cultures in common laboratory conditions (Allahverdiyeva et al. 2013; Hihara et al. 2001; Wilson et al. 2006) of constant low (30 µmol photons m^{-2} s^{-1}) or high (400 µmol photons m^{-2} s^{-1}) light and exponential growth. We also grew cultures under a 12/12h light/dark cycle (180 µmol photons m^{-2} s^{-1}), which corresponded to the same diurnal photon flux as individual cells experienced in the ePBR, based on the cell-specific light model. Cultures were grown in a volume of 50 mL BG11 in 500 mL Erlenmeyer flasks (~1 cm culture depth) under a 1% CO_2 atmosphere on a rotating board (100 rpm) in a

Percival incubator. Cultures were acclimatized to the light regime for >5 days, diluted, and sampled in late exponential phase (OD_{750} of 0.2–0.4, pH<8).

Exponentially growing cells under high light were three-times larger than under low light and in the ePBR and contained 2.5 times more TOC (Table F1). High light caused an increase in the total carotenoid:chl a ratio from 0.3 to 0.6, compared to low light, and appeared to be driven by a 70% reduction in chl *a* (5.37 and 16.1 fg [μm^3 bio-volume]$^{-1}$, respectively). The F_V/F_M was also significantly lower under high than low light (0.519 and 0.615 respectively). Generally, the ePBR culture displayed an intermediate phenotype between high and low light, with the exception that the F_V/F_M, which more closely resembled that of the high light acclimatized state (Table F1).

We choose to present chl *a* normalized P-I parameters in the main body of the manuscript since it is standard in the field of algal research. In eukaryotes this normalizes the P-I parameters to the size of the light harvesting antenna, which means that α is often constant across light acclimatized states (Behrenfeld et al. 2004). However, chl *a* is not a component of the antenna complex in cyanobacteria and 80% of the chl *a* resides in PSI. Hence modifications to the PSI:PSII ratio and reactor center abundance, not the antenna size, affects chl *a* concentration making this an arbitrary normalization strategy. Since we observed large changes in the chl *a* concentration per biomass between acclimatization states we chose to normalize the P-I curves using total organic carbon (TOC) rather than chl *a*. Arguably this is also a more relevant strategy to compare the maximum capacity of photosynthesis (P_{max}) between acclimatization states since TOC mirror biomass rather than light harvesting capacity.

On a TOC basis, the α was three-times higher in the low light acclimatized culture than the ePBR, and half that of the high light acclimatized culture (Table F2) This changes likely steams from modifications to the phycobilisome antenna size, and suggest that

the antenna is relatively small in the ePBR culture. The P_{max} of the ePBR culture was almost twice as high as both low and high light acclimatized cultures (19,100±600 versus 10,500±1,800 μmol O_2 [g TOC]$^{-1}$ h^{-1} (Table F2), which suggest a highly efficient metabolic capacity to process reduced metabolites downstream of PSI. Finally, the dark respiration rate was three-times lower in the ePBR culture then both light acclimatized states (-570±312 versus -1,940 and -1,640 μmol O_2 [g TOC]$^{-1}$ h^{-1}, potentially as a consequence of the large reduction in growth rate (see doubling time, Table F2).

Collectively these results show that the major modification between high and low light acclimatized cells resides in the size of the light harvesting antenna and not in metabolic processes downstream of PSI. More importantly the elevated P_{max} in the ePBR culture suggests that the it has maximized the capacity to process electrons rapidly downstream of PSI, potentially in an effort to utilize as much light as possible during the brief flashes of light it depended on for growth. Yet the growth rate was severely reduced in the dense ePBR culture compared to exponentially growing cells, both in the ePBR light regime and constant low or high light (Table F1). Compared to the dens ePBR cultures grown under a 12 h 180 μmol photons m^{-2} s^{-1}/12 h dark cycle the doubling time was increased 10-fold (Fig. F1B).

Table F1. Comparison between physiological parameters of cultures grown in the ePBR and Erlenmeyer flask under continuous low light (30 μmol photons m^{-2} s^{-1}) and high light (400 μmol photons m^{-2} s^{-1}). ePBR parameters per biological replicates were calculates as a 5-point avarage based on ZT0.25, 3, 6, 9, and 11.75 (see Chapter 1, Fig. 1.5). Differences between treatments were analyzed using 1-way ANOVA (N=3-6) and letters denote significant differences.

Physiological parameters of cultures grown under different light treatments

	Bio-volume (μm^3)	Chlorophyll *a* (fg [μm^3 bio-volume]$^{-1}$)	Total carotanoid:chl *a* ratio (g g^{-1})	TOC (pg cell^{-1})	F_V/F_M	Doubling time (h)
ePBR	1.63±0.01^a	12.7±0.28^a	0.438±0.007^a	0.571±0.040^a	0.513±0.008^a	75±22^a
Low light	1.43±0.05^a	16.1±3.36^b	0.298±0.006^b	0.573±0.111^a	0.615±0.016^b	16±2.5^b
High light	4.79±0.27^b	5.37±0.35^c	0.601±0.047^c	2.06±0.08^b	0.519±0.033^a	4.2±0.37^b
$F_{2,9}$	*706*	*35.7*	*135*	*501*	*32.7*	*23.8*
(p)	*(<0.001)*	*(<0.001)*	*(<0.001)*	*(<0.001)*	*(<0.001)*	*(<0.001)*

Table F2. Parameters derivate form the rapid photosynthesis versus irradiance curves. Oxygen evolution rates were normalized to total organic carbon due to the large difference in chl *a* content between acclimatization states. The ZT6 time point of the semi-continuously grown ePBR was compared to low (30 µmol photons m^{-2} s^{-1}) and high (400 µmol photons m^{-2} s^{-1}) light acclimatized cultures growing exponentially. Letters denote significant differences based on 1-way ANOVA (N=3). Samples were Chl *a* normalized to a concentration of 3 µg mL^{-1} for the measurements.

P-I parameters on a carbon basis

Culture conditions	Dark respiration (µmol O_2 [g TOC]$^{-1}$ h^{-1})	Compensation point (µmol photons m^{-2} s^{-1})	α (µmol O_2 [g TOC]$^{-1}$ h^{-1}) [µmol photons m^{-2} s^{-1}]$^{-1}$	P_{max} (µmol O_2 [g TOC]$^{-1}$ h^{-1})	E_k (µmol photons m^{-2} s^{-1})
ePBR (ZT6)	-570±312 [a]	9.33±6.03[a]	44.7±1.8[a]	19,100±600[a]	429±31[a]
Low light	-1,940±796 [b]	22.6±6.5[a]	103 ±20[b]	10,500±1,300[b]	103±11[b]
High light	-1,640±108 [b]	86.7±6.1[b]	20.5 ±0.4[c]	10,500±1,800[b]	512±86[a]
$F_{2,6}$ *(p)*	7.57 *(0.023)*	133 *(<0.001)*	41.0 *(<0.001)*	42.0 *(<0.001)*	49.9 *(<0.001)*

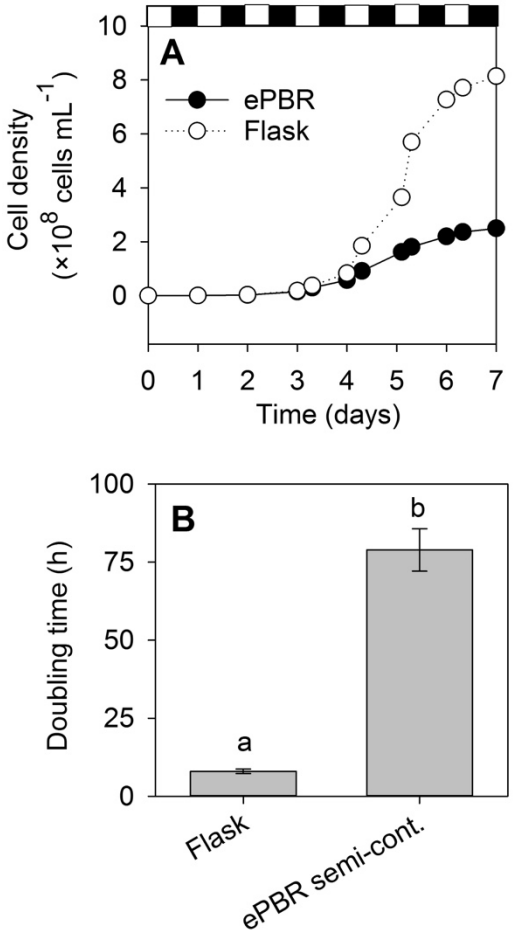

Figure F1. Comparison of growth rates in the ePBR versus Erlenmeyer flasks commonly used in laboratory experiments. Based on the cell specific-light model both cultures experienced the same integrated photon flux on a diurnal basis, but in the Erlenmeyer flasks light was supplied as static 12 h 180 µmol photons m^{-2} s^{-1}/ 12 h darkness. A) two representative growth curves of Erlenmeyer flasks and ePBR cultures grown in batch mode, B) doubling times of the Erlenmeyer culture at a density between 0.1 and 2×10^8 cells mL^{-1} compared to the dens semi-continuous ePBR culture at 1.5×10^8 cells mL^{-1}. Letters denotes significant differences based on students *t*-teste (t=17.5. df=7, $p<0.001$).

G. A putative NAD(P)H:quinone oxidoreductase protein (DrgA) serves a vital function during heterotrophic growth in the cyanobacterium *Synechocystis sp* PCC 6803

Summary

The DrgA protein, encoded by slr1719 in *Synechocystis* sp. PCC 6803, catalyzes various redox-reactions, including nitro-reduction, NAD(P)H:quinone reduction, and the fenton reaction *ex situ*. The *in vivo* function is poorly understood but it has been suggested that DrgA is involved in regulating NAD(P)H homeostasis or in cyclic electron transfer. This appendix describes growth and physiological characterizations of a strain of *Synechocystis* sp. PCC 6803 with a disrupted slr1719 locus (BA13). Under sub-saturating light BA13 has a 30-40% reduction in its maximal growth rate, an elevated carotenoid content, and reduced phycobilisome and/or chlorophyll content. The growth rate of BA13 is not impeded further by stressors known to induce cyclic electron transfer, such as high light or high salinity. Under CO_2 limitation the growth phenotype disappears indicating that the DrgA protein is not essential for cyclic electron transfer. The growth phenotype is exacerbated under heterotrophic growth (77% reduction compared to WT) showing that the DrgA protein is not exclusively involved in a photosynthetic process. Heterotrophic growth also causes enlargement of BA13 cells (200% of WT) and 50% reduction in respiration suggesting a reduced capacity to metabolize external glucose. I suggest that further studies should aim to identify links between the DrgA protein and respiration of glucose through the oxidative pentose phosphate pathway.

1. Background

The DrgA protein (slr1719) in *Synechocystis* sp. PCC6803 is a strong redox enzyme. It was first described as causing elevated toxicity of Dinoseb, a nitro-aromatic

herbicide. It was speculated, and later confirmed (Takeda et al. 2007), that the DrgA protein had nitro-reductase active and that the disruption of the slr1719 locus inferred resistance to Dinoseb through reduced formation of superoxide as a result of this activity (Elanskaya et al. 1998). The protein fractionates with the soluble part of the proteome suggesting mobility in the cytoplasm or weak interactions with membrane bound proteins (Elanskaya et al. 2009). The DrgA protein has been shown to perform several other redox reactions *in vitro*, including NAD(P)H:quinone (Elanskaya et al. 2009; Matsuo et al. 1998) and ferric reductase activities (Takeda et al. 2007). Transcription of the slr1719 locus is enhanced under both light and the addition of glucose (Karandashova et al. 2006) suggesting a role in either autotrophic or heterotrophic growth. Elanskaya et al. (2004) suggested that disruption of the DrgA gene does not impair glucose metabolism based on short-term $P700^{+}$ reduction kinetics but that it alters kinetics under illumination, suggesting a role in cyclic electron transfer. Abundance, or activity, of the DrgA protein increased during low CO_2 and high salinity stress based on *in vitro* assays (Ooyabu et al. 2008), conditions that induce cyclic electron transfer.

The Peers lab became interested in the DrgA protein as it showed increased abundance under fluctuating light in a non-targeted proteomic experiment (Youngblood 2015). There has been no rigorous characterization of growth phenotypes or fundamental photophysiological phenotypes of slr1719 disrupted mutants based on the published literature. In this appendices I disrupt the slr1719 gene and assay fundamental phenotypic characteristics of the mutant using PAM fluorometery, oxygen evolution measurements, and growth kinetics.

2. Materials and Method

2.1. Disruption of the slr1719 Locus

The slr1719 locus in a glucose tolerant strain of the cyanobacterium *Synechocystis* sp. PCC6803 (*Synechocystis* from here onwards) was disrupted using homologous recombination (Koksharova and Wolk 2002). A plasmid containing an 1147 bp

long kanamycin (kan) resistance cassette, flanked by regions of the slr1719 gene was used to disrupt the native gene (Fig. G1A). Youngblood (2015) cloned the disruption plasmid and it was re-amplified in *Escherichia coli*, purified, and novel transformants of *Synechocystis* were created for this study. Transformation was conducted in liquid BG-11 media (see Chapter 1 for media details) using an un-digested plasmid and exponentially growing WT *Synechocystis* cells at 30°C, 30 μmol photons m^{-2} s^{-1}. After 5 h incubation selection for successful transformation was carried out on 1% agar plates of BG11 + 50 μg L^{-1} Kan + 10 mM glucose. For unknown reasons selection could not be accomplished without added glucose. Disruption of the slr1719 locus was confirmed through a PCR screen across the insertion site of the Kan resistance cassette (Fig. G1B) using primers shown in Table 1.

2.2. Growth Conditions and Medias

Slr1719 disruption mutants were allowed to rapidly grow dense in 200 mL BG11 + 50 μg L^{-1} Kan media which was concentrated and divided into aliquots which were cryo-preserved. Cryo-samples were thawed in BG11 + 50 μg L^{-1} Kan for > 24h and switched to BG11 without Kan one week prior to experiments. Growth experiments were conducted in Percival incubator at atmospheric CO_2 and 30°C. Cultures were maintained in either Roux flasks sparged with 0.5 L min^{-1} air, or 125 mL Erlenmeyer flasks rotated at 100 rpm to encourage diffusion of gases. Illumination was either below photosynthetic and growth saturation or under excess light (Allahverdiyeva et al. 2013; Hihara et al. 2001; Wilson et al. 2006), corresponding to 50 or 400 μmol photons m^{-2} s^{-1} light supplied by Phillips cool white F17T8/TL841/ALTO light tubes. To test the effect of diurnal rhythms on the mutant, experiments were conducted either under continuous illumination or 12h/12h light/dark regimes. Cultures were also grown exponentially in photometric environmental PBR [ePBR; (Lucker et al. 2014)] under a sinusoidal 12h light regime as described in Jallet et al. (2016a). When referring to diurnal time points we use Zeitgeber Time (ZT) based on circadian rhythm

as described in (Van Alphen and Hellingwerf 2015), with ZT0 corresponding to dawn/light on.

Stress conditions were induced through modification of the BG11 media. Since *Synechocystis* is a limnic species, salt stress induces cyclic electron transfer (CET) to generate ATP to actively pump ions out of the cell (Mi et al. 1992; Ooyabu et al. 2008). High salt media was made by amending BG11 with 3.5 % NaCl mimicking oceanic osmolality. Low availability of inorganic carbon also induces CET in Synechocystis in order to supply ATP for carbon concentrating transporters (Shibata et al. 2001). CO_2 limitation was induced by re-inoculating cultures at high density in BG11 without $NaCO_3$. These cultures were grown in Erlenmeyer flasks until pH >8.5 and cells started dividing in a linear fashion, utilizing the constant supply of inorganic carbon that diffused into the culture from the atmosphere. Experiments were terminated when the cells came within 50% of the density of inorganic macro-nutrient limited stationary phase (8×10^8 cells mL^{-1}, see Appendix F).

Heterotrophic growth was achieved by amending BG11 with 10 mM glucose and wrapping the Erlenmeyer flasks in aluminum foil with sampling occurring under low illumination to minimize the exposure to light. Cultures were exposed to 5 min of low light once per day to maintain active glucose respiration in the cells (Anderson and Mcintosh 1991).

2.3. Growth Rate and Flow Cytometry

Cell densities, cell-specific bio-volumes and fluorescence were measured using Flow Cytometry as described in Chapter 1. Additionally, the phycobilisome and chlorophyll *a* (chl *a*) fluorescence was recorded using the FLV4 laser and detector (640 nm excitation and 675±25 detection) and used as a proxy for cell-specific pigmentation. FLV4 was normalized to forward scatter (FSCA), to account for variation in cell size so that 'pigmentation' = FLV4/FSCA.

The specific (Exponential) growth rate was calculated using linear regression across natural logarithmic transformed cell densities. Linear growth (CO_2 limitation only) was calculated using linear regression across non-transformed cell densities.

2.4. Pigment Extraction and *in vivo* Absorption Spectrum

Pigments were extracted in 100% methanol and quantified as described in Chapter 1. *In vivo* absorption spectra across the photosynthetically active radiation range (400 to 800 nm) of intact cells was recorded using a Cary 60 UV-Vis spectrometer (Agilent Technologies). To account for differences in cell densities, spectrums were normalized to absorption at 750 nm (OD_{750}). In addition to the two soret bands of chlorophyll *a*, *Synechocystis* has a peak phycobilisome absorption at 630 nm and carotenoid species that absorb in the lower spectral range (Elmorjani et al. 1986; Wellburn 1994).

2.5. PAM Fluorometery and Oxygen Evolution Under CO_2 Limitation and Heterotrophic Growth.

Pulse amplitude modulated (PAM) florescence and oxygen concentration was used to measure heterotrophic respiration and autotrophic oxygen evolution. Measurements were done in a custom made quartz cuvette using a A Walz DUAL-PAM 100 fluorometer and FiresSting Optical Oxygen Meter as described in Chapter 1 section 2.3.3.

During a short-term CO_2 limitation experiment a red measuring light (620 nm) was used to monitor chl *a*/phycobilisome fluorescence. Cultures were collected at mid-linear, CO_2 limited growth and concentrated to 1 ug chl *a* mL^{-1} in their growth medium without addition of $NaCO_3$. Samples were dark incubated for 10 min after which low red actinic light (77 μmol photons m^{-2} s^{-1}; 620 nm) was applied until the CO_2 released during dark respiration was consumed. This event was characterized through a rapid rise in F_0 coinciding with a sharp decrease in oxygen evolution as PSII reaction centers closed (Fig. S1).

Heterotrophic rates of respiration were measured under ambient glucose concentrations in early-exponential and late exponentially growth phase.

2.6. Statistics

Full factorial designs were applied to test for interactions between the two strains and various treatments. Significant interactions indicate different responses between WT and the slr1719 disruption strain to the treatment. Statistical analysis included *t*-test 1, 2, and 3-way analysis of variance (ANOVA) and were run using Sigma Plot (v 1.3, Systat Software Inc.). Repeated measurement- (RM) ANOVA, with time as the fixed variable, was used to analyze time series measurements. Temporal and treatment differences were further analyzed using Tukey's post-hoc test. Samples with $p<0.05$ were considered statistically different and data are presented as averages ± 1 standard deviation (SD) unless noted otherwise. The degrees of confidence is indicated with one, two or three asterisks, indicating $p < 0.05$, 0.01, and 0.001, respectively. F-statistics are presented with the degree of freedoms between groups (time points or treatments) followed by the total degrees of freedoms (between measuring-points) as $F_{df(\text{time points}, df(\text{measuring-points})}$.

3. Results and discussion

3.1. Cloning and Initial Phenotypic Observations

Successful disruption of the slr1719 locus was confirmed in three separate strains (Fig. G1B). Under sub-saturating light (50 µmol photons m^{-2} s^{-1}) and 12h:12h L/D cycle, the three slr1719 disrupted strains (named BA12, BA13 and BA26) showed growth reduction of 58 to 62% compared to WT (Fig. G1C). *In vivo* absorption spectra indicated that the pigmentation of all three slr1719 disrupted strains were different form WT, with relatively less absorption in the phycobilisome and chl *a* range and more in the carotenoid range (Fig. G1D). It should be stressed at this point that both growth and pigment phenotypes were transient and disappeared after 1-2 months of continuous cultivation with Kan selection pressure. This was

not due to re-occurrence of the native slr1719 gene (PCR data not shown). This necessitated a stock of cryo-preserved samples to be used and slr1719 disrupted strains to maintained in continuous cultivation for up to one month before being discarded.

3.2. Changes in Pigmentation

The pigmentation phenotype observed in the *in vivo* spectrums was confirmed in the three slr1719 disrupted strains through an elevated carotenoid: chl *a* ratio (Fig. G2A). Individually, the chl *a* and carotenoid content per cell showed large variability, likely as a consequence of variation in cell size, and it was never established whether carotenoids, chl *a,* or both were consistently altered in the slr1719 disrupted strains. Regardless, the carotenoid: chl *a* ratio, which is insensitive to variations in cell size, was consistently elevated in BA13 under both constant high light (HL = 400 μmol photons m^{-2} s^{-1}) and low light (LL = 50 μmol photons m^{-2} s^{-1}) as shown in Fig. G2B. Under a sinusoidal light regime, the carotenoid: chl *a* ratio increased diurnally following the surface irradiance in both WT and BA13, although it was consistently higher in BA13 across the day and the discrepancy appeared larger in the afternoon (Fig. G2C). The *in vivo* absorption spectra indicated that phycobilisome and/or chl *a* content oscillated across the day under sinusoidal light in WT (Fig. G2D) but that it declined throughout the entire day in BA13 (Fig. G2E). Together these results indicate that disruption of the slr1719 locus causes reduction of phycobilisome and chl *a* content and elevation of carotenoid species in *Synechocystis*.

The pigmentation phenotype was observed to be lost in tandem with the growth phenotype under prolonged cultivation of slr1719 disrupted strains. Early warning signs of the reversion of a culture could be seen as the formation of two distinct populations in the flow cytometer using the FLV4:FSCA ratio (data not shown). This ‘pigmentation’ proxy generates a stable characterization of the slr1719 disruption strain throughout exponential and early linear growth (Fig. G3B), and is insensitive to variations in cell size and other metabolic

changes that occurs between these different growth stages and light intensities (Fig. G3A). The FLV4:FSCA ratio does change with density, likely in response to self-shading within the culture, but the change is seen both in WT and BA13 (Fig. G3B). The pigmentation phenotype does appear to be more pronounced under LL and this condition can be used as a control to show that the slr1719 disrupted strain has not reversed its phenotype before elaborate experiments or measurements are conducted.

3.3. Autotrophic Growth Under High Light and Different Light Regimes

High light treatment increased the growth rate of WT and BA13 by a small fraction showing that the culture was light limited at under the LL treatment (Fig. G4). Under a 12h/12h light:dark regime WT growth rate was reduced by 43% at HL and 57% at LL, compared to constant light. This deviation from an expected ratio of 50%, assuming equal growth under illumination and no net-respiration during darkness, indicates that some beneficial cellular functions are performed in the 12h dark period under HL. There were no major changes in the growth rate phenotype of BA13 between HL and LL or diurnal and continuous light regimes, and was between 60 to 72% that of WT (Fig. G4). However, the 3-way ANOVA did show a statistically significant interaction between strain and light regime (Table 2), indicating that WT and BA13 responded differently to diurnal versus continuous light. No significant interaction between strain and light intensity was found suggesting that light stress did not affect the slr1719 disruption strain differently than WT.

3.4. Autotrophic Growth Under Stress Conditions

Cultures were grown under cyclic electron inducing conditions of high salinity (3.5% by weight) and CO_2 limitation to test if the slr1719 disruption strain responded differently to these conditions. High salinity did not affect the growth rate of either WT or BA13 (Fig. G5; Table 3), indicating that both strains could adjust to the elevated osmolality of the medium or that the treatment. It is therefore possible that the treatment did not induce the intended stress-

and CET response. However, studies have shown that CET is induced under these same conditions (Ooyabu et al. 2008; Shibata et al. 2001) so the lack of response in the slr1719 disruption strain may also be due non-involvement of the DrgA protein in CET.

Long-term CO_2 limitation maintained cultures in linear growth for 3-4 days under continuous LL (data not shown) and was characterized by an increase in pH to between 8.5 and 11 and a reduction in average cell bio-volume (Fig. G6A). Under CO_2 limitation the exponential growth phenotype of BA13 disappeared, and the mutant strain grew slightly faster than WT (Fig. G5). Additionally, while WT decreased its pigmentation in response to CO_2 limitation, BA13 increased it, causing the two to acquire almost the same final pigmentation (Fig. G6B). Furthermore, there were no differences in the rate of dark respiration, sub saturated net-photosynthesis, or CO_2 limited net-photosynthesis between WT and BA13 acclimated to CO_2 limitation (Fig. G6C; Table 3). In conclusion these results suggest that the slr1719 disrupted strain was in-sensitive to CET inducing conditions in terms of it capacity to grow exponentially and it maintained its photosynthetic capacity.

3.5. Heterotrophic Growth

To test if the DrgA protein is exclusively involved in photosynthesis, WT and BA13 were grown under heterotrophic conditions. Interestingly, BA13 responded to the switch from autotrophic to heterotrophic growth by doubling its cell size from 2 to 4 μm $cell^{-1}$. This response was not observed in WT (Fig. G7A). The heterotrophic growth rate was reduced 5-fold in WT compared to autotrophic growth under constant LL (0.58±0.01 day^{-1} versus 2.6±0.1 day^{-1}). Heterotrophic growth was even more restricting in BA13 at 0.14±0.03 day^{-1}, only 23% the rate of WT (Fig.7B). Respiration was reduced by 50% in BA13 indicating that the strain lacking the slr1719 gene could not metabolize glucose as efficiently as WT. These observations suggest that the role of the DrgA protein is not restricted to CET or photosynthesis.

4. Conclusion

- The DrgA protein has a distinct photosynthetic growth phenotype, with reduced light harvesting pigmentation and/or elevated carotenoid content.
- Disruption of the DrgA strain caused a growth reduction under sub-saturating light, which was not enhanced during low CO_2, high light, or high salinity. This suggests that the protein is not essential for cyclic electron transfer around PSI.
- Disruption of the DrgA strain caused a reduction in the capacity to respire glucose, causing enlarged cells, and enhanced the growth phenotype observed under autotrophic growth. This indicated that loss of the DrgA protein may cause a bottleneck in the capacity to respire glucose. It also suggests that the DrgA protein forms a link between NAD(P)H production from the oxidative pentos phosphate pathway and the plastoquinone pool in the electron transport chain.

5. Future direction

Investigation into the role of DrgA in heterotrophic respiration may be a way to elucidate its function. I suggest that further studies should aim to identify links between the DrgA protein and respiration of glucose through the oxidative pentose phosphate pathway.

6. Tables

Table G1. Primers used in this study.

Target gene	Name	Direction	Expected product (WT/disrupted slr1719)	Sequence
inside slr1719	BA5	Forward	259/1406	AACATCCAACATTGGCGATTC
inside slr1719	BA6	Reverse	259/1406	TGGACCGTTGGGCTTCATC
psbA2	MBC14	Forward	1048	TCCAATCTGAACATCGACAAA
psbA2	MBC15	Reverse	1048	TTGCGTTCGTGCATTACTTC

Table G2. Statistical results from 3-way ANOVA analysis (full factorial design, N=3 per treatment) on growth rate response to changes in light intensity (400 vs 40 μmol photons m^{-2} s^{-1}) and light regime (constant light vs 12h/12h light/dark) as shown in Fig. G4.

Source of Variation	Degrees of freedom	Sum of squares	Mean squares	F-statistic	*p*-value
Strain (WT vs BA13)	1	3.18	3.18	453	<0.001
Treatment (Light intensity)	1	1.12	1.12	160	<0.001
Treatment (Light regime)	1	8.25	8.25	1180	<0.001
Interaction (Strain x Light intensity)	1	0.00817	0.00817	1.17	0.296
Interaction (Strain x Light regime)	1	0.293	0.293	41.7	<0.001
Interaction Light intensity x Light regime	1	0.0109	0.0109	1.55	0.231
2-way interaction (Strain x Light intensity x Light regime)	1	0.127	0.127	18.0	<0.001
Residual	16	0.112	0.00701		
Total	23	13.1	0.570		

Table G3. Statistical results from 2-way ANOVA analysis (N=3 per treatment) on the responses to elevated (3.5% by weight) versus ambient salinity of wild type and an slr1719 disruption strain (Fig. G5).

Source of Variation	Degrees of freedom	Sum of squares	Mean squares	F-statistic	*p*-value
Strain	1	5.85	5.85	125	<0.001
Salt Treatment	1	0.0675	0.0675	1.44	0.264
Strain x Salt Treatment	1	0.000	0.000	0.000	1.000
Residual	8	0.375	0.0469		
Total	11	6.294	0.572		

Table 4. Statistical results from 2-way RM ANOVA analysis (N=3 per treatment) on oxygen evolution response to short-term CO_2 depletion of wild type and an slr1719 disrupted strain (Fig. G6C).

Source of Variation	Degrees of freedom	Sum of squares	Mean squares	F-statistic	*p*-value
Strain (WT vs BA13)	1	0.00130	0.00130	0.140	0.744
Light treatment (actinic light)	2	5.93	2.96	553	<0.001
Strain x Light treatment	2	0.00684	0.00342	0.315	0.746
Residual	4	0.0434	0.0108		
Total	17	6.027	0.355		

7. Figures

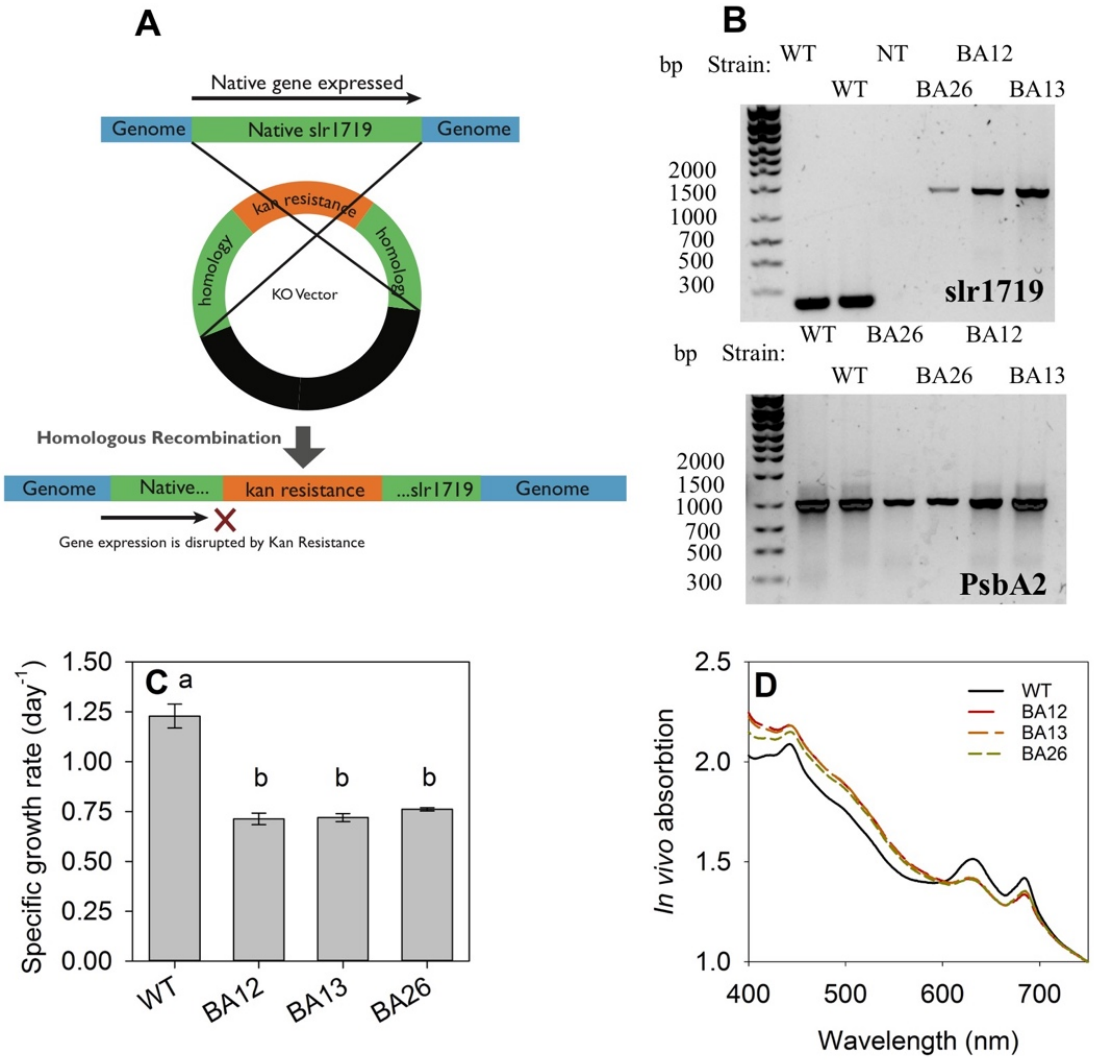

Figure G1. Disruption of slr1719 loci and phenotype observation. A) cloning vector and transformation strategy, B) PCR confirmation of disruption of slr1719 in three strains with PsbA as negative control, C) mid-exponential growth under 12h/12h 50 µmol photons m^{-2} s^{-1}/darkness, D) OD_{750} normalized *in vivo* absorption spectra at ZT6. Differences in A was analyzed using 1-way ANOVA ($F_{3,8} = 153$, $p < 0.001$) and letters denote significant differences.

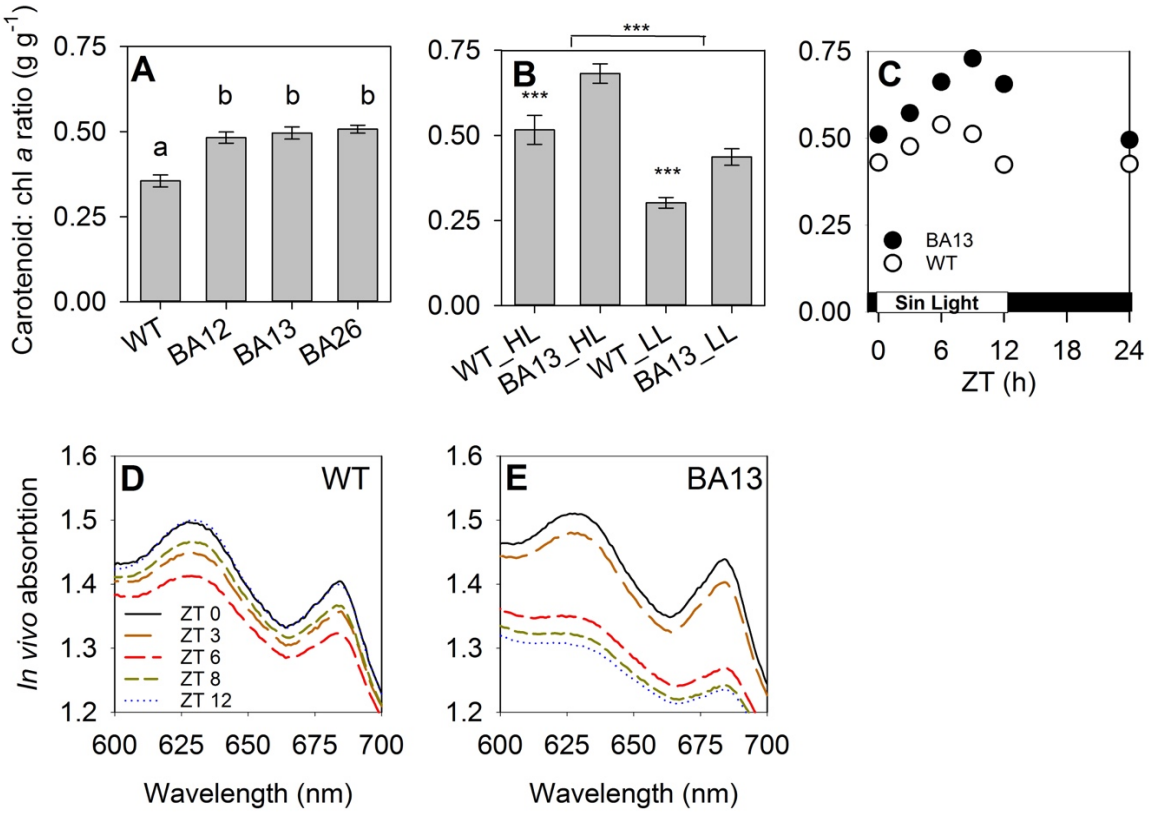

Figure G2. Changes in pigmentation across different light regimes. A) carotenoid: chlorophyll *a* ratio at ZT6 under 12h/12h 50 µmol photons m^{-2} s^{-1}/darkness, B) carotenoid: chlorophyll *a* ratio at mid exponential growth under constant high light (HL) of 400 µmol photons m^{-2} s^{-1} and low light (LL) of 50 µmol photons m^{-2} s^{-1}, C) diurnal changes in carotenoid: chlorophyll *a* ratio under sinusoidal light reaching 50 at zenith, D) diurnal changes in Wild Type's *in vivo* absorption spectra (OD_{750} normalized) under sinusoidal light, diurnal changes in slr1719 disrupted strain BA13's *in vivo* absorption spectra (OD_{750} normalized) under sinusoidal light. Differences in A was analyzed using 1-way ANOVA ($F_{3,8} = 57$, $p < 0.001$) and letters denote significant differences. In B, 2-way ANOVA was used with light treatment and strain having significant effects ($F_{1,8} = 183$, $p < 0.001$ and $F_{1,8} = 78$, $p < 0.001$, respectively). Three asterisk (***) signifies $p<0.001$ differences between strains.

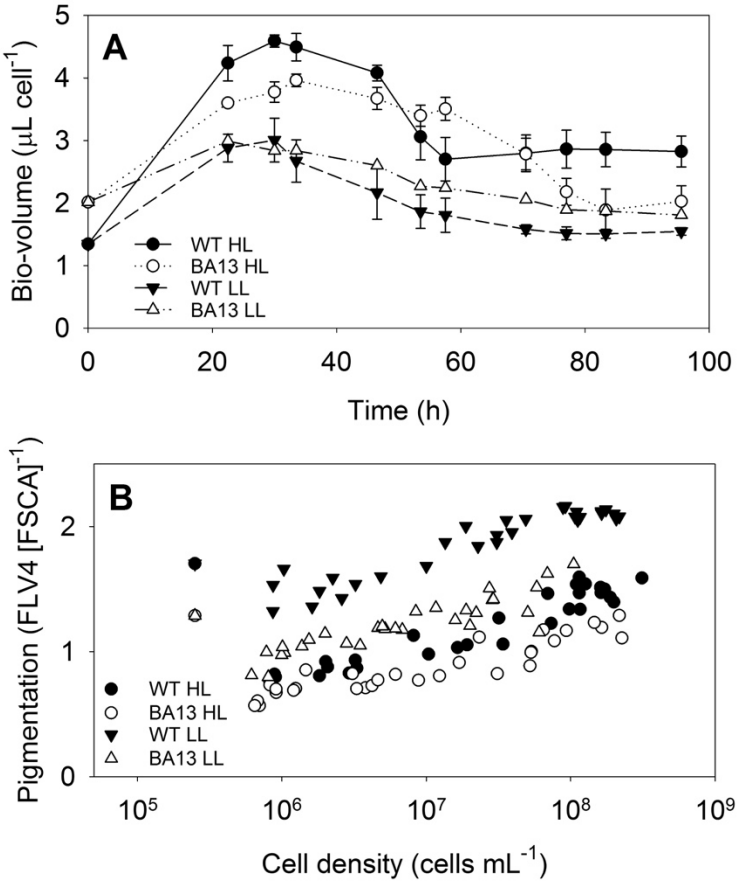

Figure G3. Changes in bio-volume and pigmentation in batch grown cultures under constant light. HL: High light (400 µmol photons m^{-2} s^{-1}), LL: 50 µmol photons m^{-2} s^{-1}. A) Changes in bio-volume per cell, B, change in cell specific pigmentation estimated using forward scatter (FSCA) and fluorescence (FLV4) measured with flow cytometry.

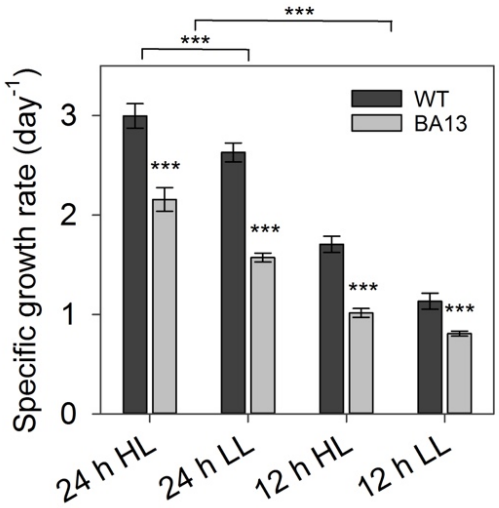

Figure G4. Changes in growth rates under diurnal versus constant light (12 vs 24) and high (400 µmol photons m^{-2} s^{-1}) versus low (50 µmol photons m^{-2} s^{-1}) light. Growth rates were measured using a full factorial design and analyzed using 3-way ANOVA. Three asterisk (***) signifies $p<0.001$. See table 2 for full statistical results. Error bars show S.D. of N=3.

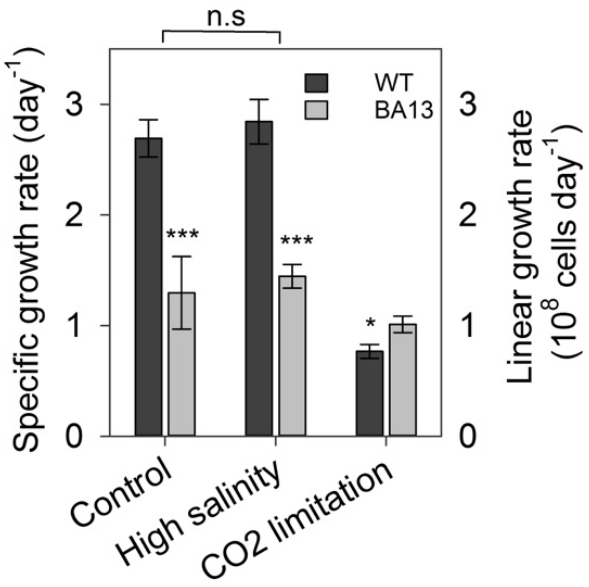

Figure G5. Changes in growth rate under stress conditions. Control: exponential growth under constant (50 µmol photons m^{-2} s^{-1}) light in normal BG11, High salt: exponential growth in BG11 + 3.5% NaCl, CO_2 limitation: linear growth under CO_2 limitation induced by high density of cells. Differences between Wild Type and the slr1719 disrupted strain (BA13) with respect to high salinity was analyzed using 2-way ANOVA (see statistical results in Table 2). Students *t*-test was used for the CO_2 limited growth ($t = 4.322$, N = 3, $p = 0.006$).

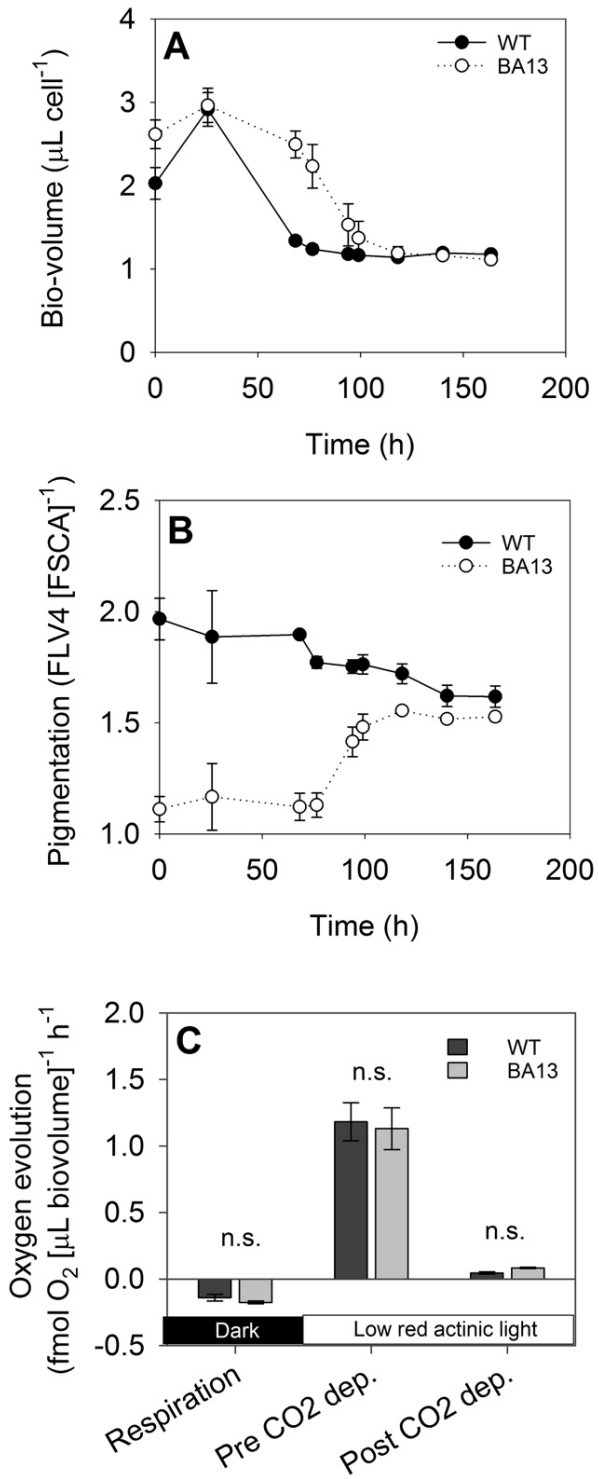

Figure G6. Long and short term responses to CO_2 limited growth under constant 50 µmol photons m^{-2} s^{-1} light. A) long-term changes in cell bio-volume in response to the onset of CO_2 limitation (pH increases >8.5 between 24 to 72 h), B) change in cell specific pigmentation estimated using forward scatter (FSCA) and fluorescence (FLV4) measured with flow cytometry, C) changes in short-term oxygen evolution capacity at 124 h. For C, cells where incubated in the dark for 10 min after which 77 µmol photons m^{-2} s^{-1} red actinic light was applied until the cells had consumed the CO_2 in the cuvette. Chl *a* concentration was 3 ug mL^{-1}. Data was analyzed using 2-way RM ANOVA with statistical parameters shown in table 3. n.s. indicates non-significant differences between wild type and BA13 (p >0.05).

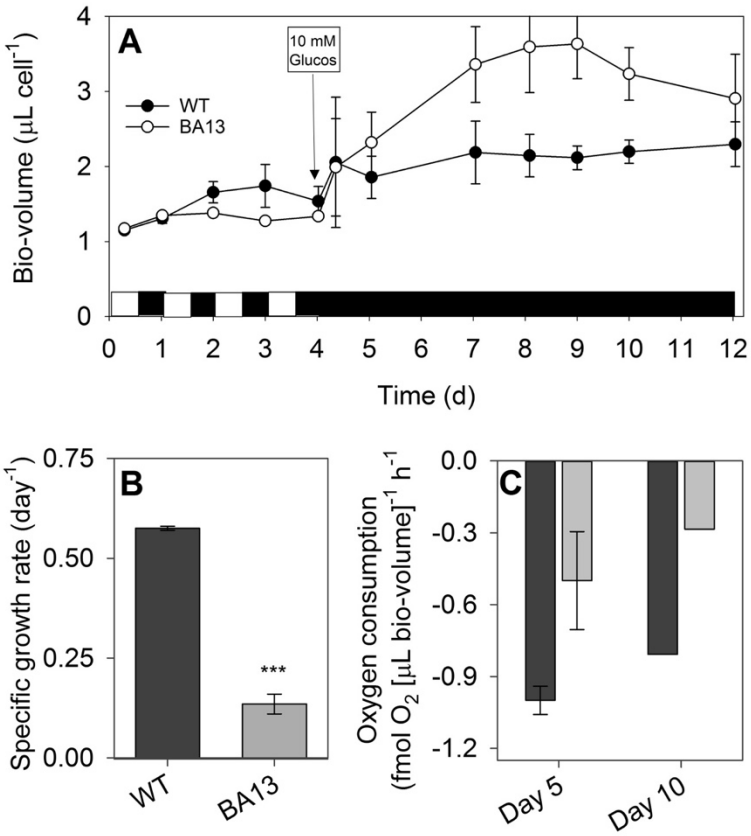

Figure G7. Responses to heterotrophic growth. A) response in cell bio-volume to switch from autotrophy (12h/12h, 50 µmol photons m^{-2} s^{-1}/dark) to heterotrophy (addition of 10 mM glucose and constant dark), B) specific growth rates under heterotrophic conditions (day 5 to 10), C) respiration under heterotrophic growth. Differences in growth rates were analyzed using students *t*-test ($t = 29.8$, N = 3, $p < 0.001$). Averages ± 1 standard deviation is shown for A and B, while C shows averages ± range for day 5 (N=2) and results from one single replicate at day 10.

H. Supplemental information to Chapter 2

Table H1: RNA sequencing results

Biological metadata			Sequencing metadata				
ZT time (h)	Time-point (MST)	Biological replicate	Sample alias	Lane	Number of reads (x 10^6)	Q30%	Average Quality Score
-0.25	745am	R31	BA-S37	5	12.6	97.12	39.40
-0.25	745am	L29	BA-S47	5	16.7	97.20	39.42
-0.25	745am	R29	BA-S30	5	14.5	97.19	39.42
0.25	815am	L29	BA-S34	5	14.9	97.24	39.43
0.25	815am	L31	BA-S43	5	16.4	97.16	39.41
0.25	8.15am	L28	BA-S6	4	15.2	97.31	39.46
0.25	8.15am	R31	BA-S1	4	11.5	97.23	39.43
1	9am	R28	BA-S11	4	14.7	97.32	39.46
1	9am	L31	BA-S13	4	14.7	97.24	39.44
1	9am	L28	BA-S24	4	17.5	97.30	39.46
1	9am	R29	BA-S44	5	13.0	97.14	39.40
3	11am	R31	BA-S17	4	18.6	97.31	39.46
3	11am	L29	BA-S19	4	21.2	97.33	39.46
3	11am	R29	BA-S20	4	16.0	97.29	39.45
3	11am	L31	BA-S36	5	27.4	97.18	39.41
6	14pm	L31	BA-S26	5	16.7	97.19	39.42
6	14pm	R29	BA-S29	5	15.5	97.13	39.40
6	14pm	L28	BA-S54	5	15.3	97.16	39.41
6	14pm	L29	BA-S55	5	18.2	97.16	39.41
9	17pm	R29	BA-S12	4	17.1	97.33	39.46
9	17pm	L28	BA-S31	5	16.2	97.21	39.43
9	17pm	R28	BA-S35	5	16.1	97.20	39.42
9	17pm	L31	BA-S5	4	14.6	97.29	39.45
11	19pm	L28	BA-S21	4	18.5	97.28	39.45
11	19pm	L31	BA-S22	4	17.5	97.32	39.46
11	19pm	R31	BA-S28	5	16.1	97.19	39.42
11	19pm	R29	BA-S46	5	16.4	97.19	39.42
11.75	19.45pm	L29	BA-S14	4	17.4	97.30	39.46
11.75	19.45pm	L28	BA-S18	4	16.1	97.25	39.44
11.75	19.45pm	R29	BA-S25	5	12.9	97.11	39.39
11.75	19.45pm	L31	BA-S42	5	13.6	97.12	39.39
12.25	20.15pm	R29	BA-S27	5	14.5	97.17	39.41
12.25	20.15pm	R31	BA-S3	4	14.1	97.30	39.45
12.25	20.15pm	L28	BA-S45	5	15.6	97.12	39.39
12.25	20.15pm	L29	BA-S53	5	17.5	97.17	39.41
13	21pm	L31	BA-S23	4	19.1	97.33	39.47
13	21pm	R28	BA-S39	5	15.6	97.14	39.40
13	21pm	L28	BA-S4	4	14.5	97.31	39.46
13	21pm	L29	BA-S40	5	15.1	97.12	39.39
18	02am	R29	BA-S15	4	15.1	97.27	39.45
18	02am	R28	BA-S41	5	14.2	97.18	39.41
18	02am	L28	BA-S7	4	15.5	97.32	39.46
18	02am	L29	BA-S9	4	11.3	97.27	39.45
23	07am	L29	BA-S10	4	15.6	97.36	39.47
23	07am	R29	BA-S16	4	14.9	97.26	39.44
23	07am	L31	BA-S50	4	13.7	97.34	39.47
23	07am	L28	BA-S8	4	14.2	97.26	39.44

Table H2: Statistically changing gene based on transcriptomic analysis

GeneID	Gene Symbol	Protein annotation (Cyanobase)	Max time-point mean (RPKM)	Max $\log_2$ fold chang	Largest fold change (ZT)	*p*-value (Bonferroni corrected)
sll0869	aat	Leu/Phe-tRNA-protein transferase	42	1.2	6 vs. 23	0
slr0435	accB	biotin carboxyl carrier protein of acetyl-CoA carboxylase	231	1.3	1 vs. 13	0
ssl2084	acpP	acyl carrier protein	971	4.6	3 vs. 13	0
sll1900	act	acetyltransferase	44	1.2	9 vs. 23	0
sll1815	adk	adenylate kinase	99	1.0	3 vs. 23	2.435E-10
sll0108	amt1	ammonium/methylammonium permease	7544	2.7	1 vs. 13	0
sll1017	amt2	ammonium/methylammonium permease	318	1.6	1 vs. -0.25	0
sll0537	amt3	ammonium/methylammonium permease	19	1.9	1 vs. 18	0
slr2067	apcA	allophycocyanin alpha subunit	16823	3.9	6 vs. 18	0
slr1986	apcB	allophycocyanin beta subunit	16430	3.6	6 vs. 18	0
ssr3383	apcC	phycobilisome small core linker polypeptide	7241	2.7	6 vs. 18	0
sll0928	apcD	allophycocyanin-B	6168	-1.5	1 vs. 12.25	0
slr0335	apcE	phycobilisome core-membrane linker polypeptide	1513	-1.9	1 vs. -0.25	0
slr1459	apcF	phycobilisome core component	3653	-2.5	-0.25 vs. 6	0
slr1898	argB	N-acetylglutamate kinase	88	2.3	1 vs. 18	0
sll0080	argC	N-acetyl-gamma-glutamyl-phosphate reductase	1310	-3.1	6 vs. 13	0
slr1022	argD	N-acetylornithine aminotransferase	177	-2.5	3 vs. 13	0
slr1133	argH	L-argininosuccinate lyase	69	1.0	1 vs. 12.25	0
sll1883	argJ	arginine biosynthesis bifunctional protein ArgJ	254	-1.8	6 vs. 18	0
sll0502	argS	arginyl-tRNA-synthetase	94	-1.8	9 vs. 23	0
slr0444	aroA	3-phosphoshikimate 1-carboxyvinyltransferase	84	1.1	11.75 vs. 13	0
slr2130	aroB	3-dehydroquinate synthase	75	1.8	1 vs. 12.25	0
slr1559	aroE	shikimate 5-dehydrogenase	155	-2.1	6 vs. 23	0
sll0109	aroH	chorismate mutase	355	-1.4	6 vs. 12.25	0
sll1112	aroQ	3-dehydroquinate dehydratase	383	-1.2	0.25 vs. 13	0
slr0946	arsC	arsenate reductase	15	-1.1	1 vs. 13	6.889E-10
slr0549	asd	aspartate beta-semialdehyde dehydrogenese	311	-2.3	9 vs. 23	0
sll0495	asnS	asparaginyl-tRNA synthetase	55	1.8	6 vs. 13	0
sll0402	aspC	aspartate aminotransferase	135	-1.3	3 vs. 11.75	0
slr0036	aspC	aspartate aminotransferase	16	-1.2	9 vs. 23	0
slr1720	aspS	aspartyl-tRNA synthetase	158	1.7	1 vs. -0.25	0
sll1326	atpA	ATP synthase alpha chain	734	2.3	1 vs. 18	0
slr1329	atpB	ATP synthase beta subunit	1539	1.8	3 vs. 13	0
sll1327	atpC	ATP synthase gamma chain	1598	2.1	3 vs. 13	0

sll1325	atpD	ATP synthase delta chain of CF(1)	420	3.0	1 vs. 18	0
slr1330	atpE	ATP synthase epsilon chain of CF(1)	1517	2.5	1 vs. 13	0
sll1324	atpF	ATP synthase B chain (subunit I) of CF(0)	520	4.0	1 vs. 13	0
sll1323	atpG	ATP synthase subunit b' of CF(0)	1003	4.1	1 vs. 13	0
ssl2615	atpH	ATP synthase C chain of CF(0)	7660	2.8	3 vs. 18	0
sll1322	atpI	ATP synthase A chain of CF(0)	7156	2.9	1 vs. 18	0
slr0905	bchE	Mg-protoporphyrin IX monomethyl ester oxidative cyclase	29	1.8	3 vs. 23	0
slr1735	bgtA	ATP-binding subunit of the ABC-type Bgt permease for basic amino acids and glutamine	318	-1.8	6 vs. 23	0
sll1270	bgtB	periplasmic substrate-binding and integral membrane protein of the ABC-type Bgt permease for basic amino acids and glutamine BgtB	1338	1.1	11.75 vs. 18	0.0001399
slr1364	bioB	biotin synthetase	241	1.1	0.25 vs. 13	0
slr0917	bioF	7-keto-8-aminopelargonic acid synthetase	8584	-1.3	1 vs. 13	0
sll0634	btpA	photosystem I biogenesis protein BtpA	159	-1.1	12.25 vs. 23	1.016E-11
slr1784	bvdR	biliverdin reductase	45	2.4	1 vs. 18	0
sll0099	cbiE cobL	precorrin-6y C5. 15-methyltransferase (decarboxylating)	15	-1.0	1 vs. 12.25	0.0000178 6
sll0621	ccdA	putative c-type cytochrome biogenesis protein CcdA	333	-2.9	6 vs. 23	0
sll0934	ccmA	carboxysome formation protein CcmA	879	-1.7	6 vs. 18	0
sll1029	ccmK1	carbon dioxide concentrating mechanism protein CcmK	589	3.6	3 vs. 18	0
sll1028	ccmK2	carbon dioxide concentrating mechanism protein CcmK	2592	2.5	3 vs. 18	0
slr1838	ccmK3	carbon dioxide concentrating mechanism protein CcmK homolog 3. putative carboxysome assembly protein	309	1.2	-0.25 vs. 12.25	0
slr1839	ccmK4	carbon dioxide concentrating mechanism protein CcmK homolog 4. putative carboxysome assembly protein	650	2.9	1 vs. 13	0
sll1030	ccmL	carbon dioxide concentrating mechanism protein CcmL. putative carboxysome assembly protein	704	3.2	3 vs. 13	0
sll1031	ccmM	carbon dioxide concentrating mechanism protein CcmM. putative carboxysome structural protein	337	2.2	3 vs. 13	0
sll1032	ccmN	carbon dioxide concentrating mechanism protein CcmN. putative carboxysome assembly protein	192	2.2	3 vs. 13	0
slr0436	ccmO	carbon dioxide concentrating mechanism protein CcmO	85	-1.7	11 vs. 23	0
slr2087	ccs1	c-type cytochrome biogenesis protein Ccs1	130	1.1	3 vs. 13	0
sll1513	ccsA	c-type cytochrome synthesis protein	375	-2.2	9 vs. 13	0
slr1369	cdsA	phosphatidate cytidylyltransferase	483	-1.8	1 vs. 13	0
slr1043	cheW	similar to chemotaxis protein CheW	324	-1.7	6 vs. 18	0
slr0772	chlB	light-independent protochlorophyllide reductase subunit ChlB	271	-3.1	0.25 vs. 11.75	0
slr0056	chlG	chlorophyll a synthase	587	-1.6	9 vs. 23	0
slr1055	chlH	magnesium protoporphyrin IX chelatase subunit H	164	-2.0	3 vs. 18	0

slr0749	chlL	light-independent protochlorophyllide reductase iron protein subunit ChlL	483	-4.4	1 vs. 12.25	0
slr0525	chlM	Mg-protoporphyrin IX methyl transferase	108	1.5	1 vs. 13	0
slr0750	chlN	light-independent protochlorophyllide reductase subunit ChlN	312	-5.1	0.25 vs. 12.25	0
sll1091	chlP	geranylgeranyl hydrogenase	1787	-1.6	0.25 vs. 11.75	0
slr1641	clpB1	ClpB protein	42	1.5	-0.25 vs. 6	0
slr0156	clpB2	ClpB protein	91	2.1	6 vs. 13	0
sll0534	clpP2	ATP-dependent Clp protease proteolytic subunit 2	294	-1.3	9 vs. 23	0
slr0165	clpP3	ATP-dependent Clp protease proteolytic subunit	1356	-2.2	9 vs. 23	0
slr0164	clpP4	ATP-dependent Clp protease proteolytic subunit	925	2.9	-0.25 vs. 9	0
slr0043	cmpC	bicarbonate transport system ATP-binding protein	9	-1.5	3 vs. 13	0
slr0044	cmpD	bicarbonate transport system ATP-binding protein	12	1.9	-0.25 vs. 6	0
sll0030	cmpR	cmp operon transcriptional regulator. LysR family protein	5	-1.2	1 vs. 12.25	0.000003006
ssl2667	cnfU	an assembly factor for iron-sulfur culsters	1116	-1.8	1 vs. 13	0
slr0797	coaT	cobalt-transporting P-type ATPase (cobalt efflux pump) involved in cobalt tolerance	17	1.3	-0.25 vs. 11	3.46E-09
sll0378	cobA	uroporphyrin-III C-methyltransferase	34	2.7	1 vs. 13	0
sll0166	cobA/hemD	a fusion protein between uroporphyrinogen-III C-methyltransferase (CobA/CorA) and uroporphyrinogen-III synthase (HemD)	65	-1.4	9 vs. 23	0
sll1501	cobB	cobyrinic acid a.c-diamide synthase	53	-1.4	6 vs. 23	0
slr1925	cobD	cobalamin biosynthesis protein CobD	69	1.4	6 vs. 13	0
sll0916	cobH	precorrin isomerase. precorrin-8X methylmutase	28	2.0	1 vs. 13	0
slr0969	cobJ	precorrin methylase	28	-1.0	3 vs. 12.25	0
slr0239	cobM	precorrin-4 C11-methyltransferase	25	-1.7	-0.25 vs. 6	0
slr1211	cobN	cobalt-chelatase subunit CobN	39	2.3	6 vs. 13	0
slr0618	cobQ	cobyric acid synthase	71	-2.4	3 vs. 13	0
slr0502	cobW	cobalamin synthesis protein cobW homolog	19	-1.0	-0.25 vs. 13	0.00007321
sll1929	comE	competence protein ComE	41	-1.1	6 vs. 12.25	0
slr0904	comM	competence protein ComM homolog	96	-1.3	11 vs. 23	0
sll0794	corR	cobalt-dependent transcriptional regulator	50	-1.0	1 vs. 12.25	1.626E-12
sll1578	cpcA	phycocyanin alpha subunit	76674	3.6	6 vs. 0.25	0
sll1577	cpcB	phycocyanin beta subunit	60026	4.0	6 vs. 0.25	0
sll1580	cpcC1	phycobilisome rod linker polypeptide	11739	-2.8	0.25 vs. 12.25	0
sll1579	cpcC2	phycobilisome rod linker polypeptide	6809	-3.0	0.25 vs. 12.25	0
ssl3093	cpcD	phycobilisome small rod linker polypeptide	3766	2.5	6 vs. 0.25	0
slr1878	cpcE	phycocyanin alpha-subunit phycocyanobilin lyase	48	1.7	1 vs. 13	0
sll1051	cpcF	phycocyanin alpha-subunit phycocyanobilin lyase	46	1.7	1 vs. 18	0
slr2051	cpcG1	phycobilisome rod-core linker polypeptide	18225	-2.4	1 vs. -0.25	0

sll1471	cpcG2	phycobilisome rod-core linker polypeptide	1141	-4.2	1 vs. 6	0
slr0473	cph1	cyanobacterial phytochrome 1. two-component sensor histidine kinase	1257	-6.0	1 vs. 13	0
sll0821	cph2	phytochrome-like protein	57	-1.6	11 vs. 23	0
slr2002	cphA	cyanophycin synthetase	241	1.8	1 vs. 13	0
sll1489	cpmA	circadian phase modifier CpmA homolog	45	-1.3	3 vs. 12.25	0
sll1987	cpx	catalase peroxidase	76	1.9	-0.25 vs. 9	0
slr0083	crhR	RNA helicase Light	1057	1.9	1 vs. 12.25	0
slr0088	crtO	beta-carotene ketolase	14	1.4	6 vs. 13	0
slr0940	crtQ-2	zeta-carotene desaturase	42	2.8	0.25 vs. 12.25	0
sll1468	crtR	beta-carotene hydroxylase	301	1.7	6 vs. 13	0
sll1899	ctaB	cytochrome c oxidase folding protein	469	-1.9	0.25 vs. 11.75	0
slr1136	ctaCI	cytochrome c oxidase subunit II	355	-4.0	-0.25 vs. 12.25	0
slr1137	ctaDI	cytochrome c oxidase subunit I	322	-3.5	0.25 vs. 12.25	0
slr2082	ctaDII	cytochrome c oxidase subunit I	71	-1.1	9 vs. 13	0
slr1138	ctaEI	cytochrome c oxidase subunit III	125	-2.2	0.25 vs. 12.25	0
slr2083	ctaEII	cytochrome c oxidase subunit III	94	1.1	11.75 vs. 23	0
slr0008	ctpA	carboxyl-terminal processing protease	167	-2.1	11 vs. 23	0
slr0257	ctpB	periplasmic carboxyl-terminal protease	249	-2.5	6 vs. 18	0
slr1044	ctr1	methyl-accepting chemotaxis protein. required for the biogenesis of thick pilli	194	-1.2	6 vs. 13	0
slr1991	cya1	adenylate cyclase	102	-2.5	6 vs. 13	0
sll0646	cya2	guanylyl cyclase	57	-1.1	6 vs. 23	0
slr0899	cynS	cyanate lyase	221	4.9	1 vs. 13	0
slr0676	cysC	adenylylsulfate kinase	191	3.0	3 vs. 12.25	0
slr1842	cysK	cysteine synthase	58	1.7	1 vs. 18	0
slr0958	cysS	cysteinyl-tRNA synthetase	100	-1.4	11 vs. 23	0
slr1453	cysT	sulfate transport system permease protein	20	1.3	-0.25 vs. 9	1.626E-12
sll1245	cytM	cytochrome cM	288	1.4	-0.25 vs. 12.25	0
slr0550	dapA	dihydrodipicolinate synthase	340	-1.8	9 vs. 23	0
slr1665	dapF	diaminopimelate epimerase	191	-1.5	9 vs. 23	0
slr1350	desA	acyl-lipid desaturase (delta 12)	233	1.9	6 vs. 18	0
sll1441	desB	acyl-lipid desaturase (omega-3)	309	-1.7	6 vs. 23	0
sll0541	desC	acyl-lipid desaturase (delta 9)	4451	1.5	9 vs. 0.25	0
sll0262	desD	acyl-lipid desaturase (delta 6)	215	2.5	3 vs. 18	0
sll0848	dnaA	chromosomal replication initiator protein DnaA	17	1.5	12.25 vs. 23	0
slr0833	dnaB	replicative DNA helicase [Contains: Ssp dnaB intein]	104	-2.1	-0.25 vs. 6	0
sll1572	dnaE	DNA polymerase III alpha subunit [Contains: Ssp dnaE intein]	61	-1.6	-0.25 vs. 12.25	0
sll0897	dnaJ	DnaJ protein. heat shock protein 40. molecular chaperone	108	-1.4	12.25 vs. 23	0
slr0093	dnaJ	DnaJ protein. heat shock protein 40.	17	-1.1	6 vs. 23	1.748E-11

		molecular chaperone				
sll0170	dnaK2	DnaK protein 2. heat shock protein 70. molecular chaperone	4125	1.5	-0.25 vs. 11.75	0
slr0965	dnaN	DNA polymerase III beta subunit	38	-1.2	-0.25 vs. 6	0
sll1360	dnaX	DNA polymerase III subunit gamma/tau [Contains: Ssp dnaX intein]	27	-1.1	1 vs. 13	0
slr1719	DrgA	DrgA protein homolog	526	-2.7	-0.25 vs. 11	0
slr0051	ecaB	periplasmic beta-type carbonic anhydrase	92	-1.3	3 vs. 13	0
slr0434	efp	elongation factor P	475	1.3	1 vs. 13	0
slr2023	fabD	malonyl coenzyme A-acyl carrier protein transacylase	49	2.5	6 vs. 13	0
sll0018	fbaA	fructose-bisphosphate aldolase. class II	7556	3.5	-0.25 vs. 11.75	0
slr2094	fbpI	fructose-1.6-/sedoheptulose-1.7-bisphosphatase	1492	2.7	1 vs. 13	0
slr0943	fda	fructose-bisphosphate aldolase. class I	146	1.6	-0.25 vs. 9	0
slr1392	feoB	ferrous iron transport protein B	131	-3.4	9 vs. 23	0
sll1521	Flv1	flavoprotein	50	-2.5	11 vs. 23	0
sll0219	Flv2	flavoprotein	32	-2.7	6 vs. 18	0
sll0550	Flv3	flavoprotein	196	-2.4	9 vs. 18	0
sll0217	Flv4	flavoprotein	53	1.8	-0.25 vs. 6	0
slr0070	fmt	methionyl-tRNA formyltransferase	38	-1.1	-0.25 vs. 6	0
sll1612	folC	folylpolyglutamate synthase	35	1.3	18 vs. 13	0
sll0753	folD	FolD bifunctional protein	34	-1.6	-0.25 vs. 11.75	2.032E-12
slr0426	folE	GTP cyclohydrolase I	297	1.6	3 vs. 18	0
slr1093	folK	2-amino-4-hydroxy-6-hydroxymethyldihydropteridine pyrophosphokinase	130	1.1	-0.25 vs. 6	0
slr2026	folP	dihydropteroate synthase	51	-1.7	6 vs. 13	0
slr1689	fpg	formamidopyrimidine-DNA glycosylase	4410	-2.8	0.25 vs. 11.75	0
slr1964	FRP	hypothetical protein	352	-1.3	1 vs. 13	0
sll0145	frr	ribosome releasing factor	326	2.8	3 vs. 13	0
ssr0330	ftrV	ferredoxin-thioredoxin reductase. variable chain	279	1.6	3 vs. 13	0
sll1463	ftsH	cell division protein FtsH	294	-3.2	9 vs. 23	0
slr0228	ftsH	cell division protein FtsH	471	1.7	6 vs. 11.75	0
slr1390	ftsH	cell division protein FtsH	232	-2.7	6 vs. 18	0
slr1604	ftsH	cell division protein FtsH	897	2.2	-0.25 vs. 11	0
sll1633	ftsZ	cell division protein FtsZ	447	1.0	1 vs. 13	0
sll0567	fur	ferric uptake regulation protein	65	1.4	6 vs. 12.25	0
sll0830	fus	elongation factor EF-G	114	-3.7	1 vs. 12.25	0
sll1098	fus	elongation factor EF-G	1888	-1.7	1 vs. 23	0
slr1463	fus	elongation factor EF-G	673	-1.9	9 vs. 23	0
slr1295	futA1	iron transport system substrate-binding protein	189	-1.7	9 vs. 23	0
slr0884	gap1	glyceraldehyde 3-phosphate dehydrogenase 1 (NAD+)	314	-4.2	1 vs. 12.25	0

sll1342	gap2	NAD(P)-dependent glyceraldehyde-3-phosphate dehydrogenase	2277	1.8	3 vs. 13	0
slr0710	gdhA	glutamate dehydrogenase (NADP+)	54	-1.7	9 vs. 23	0
sll1566	ggpS	glucosylglycerolphosphate synthase	32	-2.2	3 vs. 18	0
slr0747	ggtA	glucosylglycerol transport system ATP-binding protein	38	1.5	1 vs. -0.25	0
slr0530	ggtC	glucosylglycerol transport system permease protein	22	1.6	6 vs. 13	0
slr0072	gidB	glucose inhibited division protein B	128	1.4	1 vs. 18	0
ssl1911	gifA	glutamine synthetase inactivating factor IF7	16111	-3.9	1 vs. 13	0
sll1515	gifB	glutamine synthetase inactivating factor IF17	6367	-4.3	1 vs. 13	0
sll1189	glcE	glycolate oxidase subunit GlcE	90	-1.9	6 vs. 13	0
sll0771	glcP	glucose transport protein	923	-2.7	1 vs. 11.75	0
slr1167	gldA	glycerol dehydrogenase	188	-1.7	3 vs. 18	0
sll0945	glgA	glycogen synthase	124	1.3	1 vs. 13	0
slr1756	glnA	glutamate--ammonia ligase	1032	1.8	1 vs. 9	0
slr0288	glnN	glutamate--ammonia ligase	530	2.8	1 vs. 12.25	0
slr1672	glpK	glycerol kinase	17	-1.4	3 vs. 12.25	0
sll1499	glsF	ferredoxin-dependent glutamate synthase	134	-2.0	9 vs. 23	0
sll1502	gltB	NADH-dependent glutamate synthase large subunit	140	-2.6	3 vs. 13	0
sll1027	gltD	NADH-dependent glutamate synthase small subunit	271	-2.2	3 vs. 13	0
sll1931	glyA	serine hydroxymethyltransferase	1404	-3.3	9 vs. 23	0
slr0220	glyS	glycyl-tRNA synthetase beta chain	102	1.3	1 vs. 13	0
slr1992	gpx2	glutathione peroxidase-like NADPH peroxidase	2142	2.9	1 vs. 11.75	0
sll0416	groEL-2	60 kDa chaperonin 2. GroEL2. molecular chaperone	667	-2.1	11.75 vs. 23	0
slr2076	groEL1	60kD chaperonin	1729	-3.2	11.75 vs. 23	0
slr2075	groES	10kD chaperonin	1191	2.9	3 vs. 12.25	0
slr1238	gshB	glutathione synthetase	238	1.7	1 vs. 13	0
sll1102	gtrA	integral membrane protein (small) of a TRAP-type permease that mediates sodium-dependent glutamate transport GtrA	113	-1.5	-0.25 vs. 9	0
sll1103	gtrB	integral membrane protein (large) of a TRAP-type permease that mediates sodium-dependent glutamate transport GtrB	107	-1.5	1 vs. 18	0
sll1104	gtrC	periplasmic substrate-binding protein of a TRAP-type permease that mediates sodium-dependent glutamate transport GtrC	35	-1.0	0.25 vs. 13	5.261E-09
sll1941	gyrA	DNA gyrase A subunit	26	1.6	1 vs. 13	0
slr0417	gyrA	DNA gyrase subunit A	190	-2.5	9 vs. 23	0
sll2005	gyrB	DNA gyrase B subunit [Contains: Ssp gyrB intein]	426	2.1	6 vs. 13	0
slr0143	hat	WD-repeat protein. Hat protein. involved in the control of a high-affinity transport system for inorganic carbon	66	-2.3	6 vs. 23	0
slr1808	hemA	transfer RNA-Gln reductase	136	2.3	6 vs. 18	0
sll1994	hemB	porphobilinogen synthase (5-aminolevulinate dehydratase)	164	-2.0	11 vs. 23	0

slr1887	hemC	porphobilinogen deaminase (hydroxymethylbilane synthase. preuroporphyrinogen synthase)	251	1.3	-0.25 vs. 13	0
slr0536	hemE	uroporphyrinogen decarboxylase	151	1.7	6 vs. 12.25	0
sll1185	hemF	coproporphyrinogen III oxidase. aerobic (oxygen-dependent)	99	2.0	6 vs. 0.25	0
slr0839	hemH	ferrochelatase	2953	-4.6	6 vs. 23	0
sll0017	hemL	glutamate-1-semialdehyde aminomutase	237	1.7	3 vs. 13	0
sll1876	hemN	coproporphyrinogen III oxidase. anaerobic (oxygen-independent)	20	-2.4	-0.25 vs. 6	0
sll1917	hemN	coproporphyrinogen III oxidase. anaerobic (oxygen-independent)	16	2.2	1 vs. 23	0
slr1393	hik1	phytochrome-like protein. two-component sensor histidine kinase	34	-1.5	6 vs. 23	0
slr0533	hik10	two-component sensor histidine kinase	60	-3.4	6 vs. 18	0
sll1003	hik13	two-component sensor histidine kinase	100	-2.0	1 vs. 12.25	0
sll1353	hik15	two-component sensor histidine kinase	49	-1.0	-0.25 vs. 11	0
slr1805	hik16	two-component sensor histidine kinase	62	-3.9	1 vs. 18	0
sll1687	hik17	unknown protein	44	-1.6	3 vs. 18	0
sll1905	hik19	two-component hybrid sensor and regulator	118	-2.6	6 vs. 18	0
slr1147	hik2	two-component sensor histidine kinase	64	-2.1	6 vs. 23	0
sll1590	hik20	two-component sensor histidine kinase	52	-2.1	6 vs. 13	0
slr2098	hik21	two-component hybrid sensor and regulator	27	-1.6	3 vs. 18	0
slr2104	hik22	two-component hybrid sensor and regulator	42	-1.2	1 vs. -0.25	0
slr1324	hik23	two-component hybrid sensor and regulator	68	-2.5	3 vs. 13	0
slr1969	hik24	two-component sensor histidine kinase	74	2.0	9 vs. 23	0
slr0484	hik26	two-component sensor histidine kinase	149	-1.2	11 vs. 23	0
sll0790	hik31	two-component sensor histidine kinase	57	-2.4	6 vs. 18	0
sll1475	hik32	a part of phytochrome-like sensor histidine kinase gene (disrupted by insertion of IS)	72	2.2	6 vs. 12.25	0
slr1285	hik34	two-component sensor histidine kinase	46	-2.6	3 vs. 18	0
slr0073	hik36	two-component sensor histidine kinase	462	-1.7	23 vs. 13	0
sll0094	hik37	two-component sensor histidine kinase	825	-3.9	6 vs. 23	0
sll1296	hik39	two-component hybrid sensor and regulator	111	1.4	1 vs. 13	0
sll1229	hik41	two-component hybrid sensor and regulator	193	-3.0	6 vs. 18	0
slr0322	hik43	two-component hybrid sensor and regulator	99	-1.1	6 vs. 13	0
sll1888	hik5	two-component sensor histidine kinase	78	-1.2	11 vs. 23	0
sll1871	hik6	two-component system sensory histidine kinase	81	-1.3	1 vs. 18	0
sll0750	hik8	two-component sensor histidine kinase. KaiC-interacting protein. involved in circadian rhythm	141	-1.2	11.75 vs. 23	0
slr0210	hik9	two-component sensor histidine kinase	36	-1.2	3 vs. 13	0
slr0500	hisB	imidazoleglycerol-phosphate dehydratase	172	-2.2	3 vs. -0.25	0
sll1713	hisC	histidinol-phosphate aminotransferase	397	1.3	11.75 vs. 23	0
sll1958	hisC	histidinol phosphate aminotransferase	73	1.5	1 vs. 13	0
slr0682	hisD	histidinol dehydrogenase	119	-2.2	1 vs. 18	0

slr1848	hisD	histidinol dehydrogenase	1250	-2.5	6 vs. 18	0
sll0900	hisG	ATP phosphoribosyltransferase	165	1.9	3 vs. 18	0
slr0084	hisH	amidotransferase HisH	164	-1.8	6 vs. 23	0
slr1560	hisS	histidyl tRNA synthetase	121	-1.4	6 vs. 23	0
ssl2542	hliA	high light-inducible polypeptide HliA. CAB/ELIP/HLIP superfamily	874	5.5	0.25 vs. 11	0
ssr2595	hliB	high light-inducible polypeptide HliB. CAB/ELIP/HLIP superfamily	1232	5.3	-0.25 vs. 13	0
ssl1633	hliC	high light-inducible polypeptide HliC. CAB/ELIP/HLIP superfamily	12914	3.9	0.25 vs. 11.75	0
ssr1789	hliD	CAB/ELIP/HLIP-related protein HliD	341	2.1	3 vs. 11.75	0
sll1184	ho1	heme oxygenase	6640	-2.1	0.25 vs. 11	0
sll1220	hoxE	putative diaphorase subunit of the bidirectional hydrogenase	143	-3.4	3 vs. 12.25	0
sll1221	hoxF	diaphorase subunit of the bidirectional hydrogenase	32	-1.8	6 vs. 12.25	0
sll1226	hoxH	hydrogenase subunit of the bidirectional hydrogenase	55	-2.1	-0.25 vs. 12.25	0
sll1223	hoxU	diaphorase subunit of the bidirectional hydrogenase	86	-2.0	1 vs. 12.25	0
sll1224	hoxY	hydrogenase subunit of the bidirectional hydrogenase	50	2.2	12.25 vs. 23	0
sll1988	hsp33	33 kDa chaperonin	331	-2.8	9 vs. 13	0
sll1514	hspA	16.6 kDa small heat shock protein. molecular chaperone	9460	-5.9	11.75 vs. 18	0
sll0430	htpG	HtpG. heat shock protein 90. molecular chaperone	159	2.6	-0.25 vs. 11.75	0
slr2135	hupE	hydrogenase accessory protein HupE	164	1.9	1 vs. 13	0
slr1675	hypA1	putative hydrogenase expression/formation protein HypA1	77	-1.6	11.75 vs. 18	1.626E-12
sll1432	hypB	putative hydrogenase expression/formation protein HypB	339	-3.3	3 vs. 13	0
ssl3580	hypC	putative hydrogenase expression/formation protein HypC	139	-1.5	3 vs. 11.75	0
slr1498	hypD	putative hydrogenase expression/formation protein HypD	36	-2.1	6 vs. 13	0
sll0322	hypF	putative hydrogenase expression/formation protein HypF	22	1.9	6 vs. 23	0
slr1860	icfG	carbon metabolisms regulatory protein IcfG	493	3.2	11 vs. 13	0
slr1515	ictB	putative membrane protein required for bicarbonate uptake	169	-1.9	6 vs. 23	0
sll1362	ileS	isoleucyl-tRNA synthetase	78	1.4	6 vs. 13	0
sll1981	ilvB	acetolactate synthase	287	-3.0	3 vs. 23	0
slr2088	ilvG	acetohydroxy acid synthase	1151	-3.4	3 vs. 18	0
sll0065	ilvN	acetolactate synthase small subunit	516	1.1	-0.25 vs. 13	0
ssl3441	infA	initiation factor IF-1	126	1.3	3 vs. 0.25	3.126E-07
slr0744	infB	translation initiation factor IF-2	358	-2.4	6 vs. 18	0
sll0247	isiA	iron-stress chlorophyll-binding protein. homologous to psbC (CP43)	118	-3.8	6 vs. 23	0
slr0756	kaiA	circadian clock protein KaiA homolog	256	3.9	1 vs. 12.25	0
slr0757	kaiB1	circadian clock protein KaiB homolog	95	4.5	3 vs. 12.25	0
sll1596	kaiB2	circadian clock protein KaiB homolog	509	1.5	6 vs. 13	0

sll0486	kaiB3	circadian clock protein KaiB homolog	106	-1.7	-0.25 vs. 11.75	0
slr0758	kaiC1	circadian clock protein KaiC homolog	108	2.1	3 vs. 18	0
sll1595	kaiC2	circadian clock protein KaiC homolog	90	2.0	6 vs. 13	0
slr1942	kaiC3	circadian clock protein KaiC homolog	86	1.7	1 vs. 13	0
slr1728	kdpA	potassium-transporting P-type ATPase A chain	44	-1.8	3 vs. 13	0
slr1729	kdpB	potassium-transporting P-type ATPase B chain	35	-2.0	9 vs. 23	0
slr1509	ktrB	membrane subunit of a Ktr-like ion transport system	71	1.7	1 vs. 13	0
slr0186	leuA	2-isopropylmalate synthase	779	-2.5	3 vs. 18	0
slr1517	leuB	3-isopropylmalate dehydrogenase	107	1.7	1 vs. 13	0
sll1470	leuC	3-isopropylmalate dehydratase large subunit	69	-1.1	6 vs. 23	0
sll1074	leuS	leucyl-tRNA synthetase	107	1.2	1 vs. 13	0
sll1209	lig	DNA ligase	23	1.3	3 vs. 18	0
sll0947	lrtA	light repressed protein A homolog	6608	-4.6	0.25 vs. 12.25	0
sll0504	lysA	diaminopimelate decarboxylase	83	-1.8	9 vs. 23	0
slr1550	lysS	lysyl-tRNA synthetase	62	1.2	1 vs. 12.25	0
slr0492	menE	O-succinylbenzoic acid-CoA ligase	18	1.2	0.25 vs. 13	4.11E-09
slr0817	menF	salicylate biosynthesis isochorismate synthase	202	2.0	1 vs. 13	0
sll0784	merR	nitrilase	16	3.7	1 vs. 18	0
sll0288	minC	septum site-determining protein MinC	58	1.0	1 vs. 13	0
sll0289	minD	septum site-determining protein MinD	149	1.5	3 vs. 13	0
ssl0546	minE	septum site-determining protein MinE	110	2.5	1 vs. 12.25	0
sll1599	mntA	manganese transport system ATP-binding protein MntA	13	-2.6	1 vs. 18	0
sll1598	mntC	Mn transporter MntC	6	-2.1	1 vs. 13	0
slr0901	moaA	molybdopterin biosynthesis protein A	316	4.0	1 vs. 13	0
slr0902	moaC	molybdenum cofactor biosynthesis protein C. fused to molybdopterin-guanine dinucleotide biosynthesis protein MobA	231	3.1	1 vs. 23	0
slr0903	moaE	molybdopterin (MPT) converting factor. subunit 2	239	3.7	1 vs. 18	0
slr0900	moeA	molybdopterin biosynthesis MoeA protein	405	2.8	1 vs. 13	0
sll1536	moeB	molybdopterin biosynthesis MoeB protein	461	-1.7	1 vs. 18	0
slr0017	murA	UDP-N-acetylglucosamine 1-carboxyvinyltransferase	508	-1.1	0.25 vs. 13	0
sll2010	murD	UDP-N-acetylmuramoylalanine--D-glutamate ligase	46	2.1	3 vs. 12.25	0
slr1351	murF	UDP-N-acetylmuramoylalanyl-D-glutamyl-2 6-diaminopimelate--D-alanyl-D-alanine ligase	67	1.8	3 vs. 13	0
slr1656	murG	UDP-N-acetylglucosamine--N-acetylmuramyl-(pentapeptide) pyrophosphoryl -undecaprenol N-acetylglucosamine transferase	43	-1.0	0.25 vs. 12.25	1.301E-09
sll1772	mutS	DNA mismatch repair protein MutS	45	2.9	3 vs. 13	0
slr0936	nadC	nicotinate-nucleotide pyrophosphorylase	18	-1.3	3 vs. 13	0
sll1454	narB	ferredoxin-nitrate reductase	345	5.6	1 vs. 23	0

slr0467	natA	conserved component of ABC transporter for natural amino acids	35	1.7	3 vs. 13	0
slr0559	natB	periplasmic binding protein of ABC transporter for natural amino acids	590	1.6	3 vs. 13	0
sll0146	natC	Integral membrane protein of the ABC-type. Nat permease for neutral amino acids	278	1.6	1 vs. 13	0
slr0949	natD	Integral membrane protein of the ABC-type Nat permease for neutral amino acids NatD	173	1.0	1 vs. 13	0
slr1881	natE	ATP-binding subunit of the ABC-type Nat permease for neutral amino acids	76	1.7	1 vs. 11	0
ssl0452	nblA1	phycobilisome degradation protein NblA	2135	-5.2	6 vs. 18	0
ssl0453	nblA2	phycobilisome degradation protein NblA	1970	-3.9	6 vs. 18	0
slr0851	ndbA	type 2 NADH dehydrogenase	63	-1.3	6 vs. 0.25	0
slr1743	ndbB	type 2 NADH dehydrogenase NdbB	77	1.3	-0.25 vs. 12.25	0
sll1484	ndbC	type 2 NADH dehydrogenase	45	-1.3	0.25 vs. 12.25	0
sll0519	ndhA	NADH dehydrogenase subunit 1	323	1.2	1 vs. 13	0
sll0223	ndhB	NADH dehydrogenase subunit 2	1879	-2.1	0.25 vs. 13	0
slr1279	ndhC	NADH dehydrogenase subunit 3	299	1.0	1 vs. 11	0
slr0331	ndhD1	NADH dehydrogenase subunit 4 (involved in photosystem-1 cyclic electron flow)	3280	-3.5	1 vs. 13	0
slr1291	ndhD2	NADH dehydrogenase subunit 4	361	3.3	1 vs. 11	0
sll1733	ndhD3	NADH dehydrogenase subunit 4 (involved in low CO2-inducible. high affinity CO2 uptake)	72	-2.2	3 vs. 18	0
sll0027	ndhD4	NADH dehydrogenase subunit 4 (involved in constitutive. low affinity CO2 uptake)	167	1.7	3 vs. 13	0
slr2009	ndhD6	NADH dehydrogenase subunit 4	47	-1.2	9 vs. 23	0
sll0522	ndhE	NADH dehydrogenase subunit 4L	367	2.4	3 vs. 13	0
slr0844	ndhF1	NADH dehydrogenase subunit 5	733	-1.7	9 vs. 13	0
sll1732	ndhF3	NADH dehydrogenase subunit 5 (involved in low CO2-inducible. high affinity CO2 uptake)	39	1.6	6 vs. 23	0
sll0026	ndhF4	NADH dehydrogenase subunit 5 (involved in constitutive. low affinity CO2 uptake)	303	1.4	1 vs. 13	0
sll0521	ndhG	NADH dehydrogenase subunit 6	744	1.9	1 vs. 13	0
slr0261	ndhH	NADH dehydrogenase subunit 7	252	1.5	1 vs. 13	0
sll0520	ndhI	NADH dehydrogenase subunit NdhI	257	1.1	6 vs. 13	0
slr1280	ndhK	NADH dehydrogenase subunit NdhK	196	1.2	1 vs. 11	0
sll1594	ndhR	ndhF3 operon transcriptional regulator. LysR family protein	46	1.3	1 vs. 12.25	0
sll0273	nhaS2	Na+/H+ antiporter	133	1.5	1 vs. 13	0
sll0689	nhaS3	Na+/H+ antiporter	253	1.4	1 vs. 12.25	0
slr1595	nhaS4	Na+/H+ antiporter	111	1.6	1 vs. 13	0
sll0704	nifS	cysteine desulfurase	157	-2.4	6 vs. 23	0
slr0077	nifS	cysteine desulfurase	105	1.7	6 vs. 23	4.296E-07
slr0387	nifS	cysteine desulfurase NifS	17	-1.0	3 vs. 13	0
slr0898	nirA	ferredoxin--nitrite reductase	389	3.0	1 vs. 23	0
sll0450	norB	cytochrome b subunit of nitric oxide reductase	261	-5.1	1 vs. 12.25	0
slr0794	nrsA	cation efflux system protein involved in	16	-2.0	6 vs. 18	0

		nickel and cobalt tolerance				
slr0793	nrsB	cation efflux system protein involved in nickel and cobalt tolerance	5	-2.1	3 vs. -0.25	0.0006197
slr0796	nrsD	nickel permease involved in nickel and cobalt tolerance	26	-1.5	6 vs. 13	0
sll0797	nrsR	redox-responsive and/or Ni(II)-responsive regulator. two-component response regulator OmpR subfamily	8	1.4	6 vs. 18	0.001498
sll0798	nrsShik 30	Ni(II)-sensor and/or redox sensor. two-component sensor histidine kinase	8	1.4	3 vs. 13	5.955E-10
sll1450	nrtA	nitrate/nitrite transport system substrate-binding protein	647	4.3	1 vs. 12.25	0
sll1451	nrtB	nitrate/nitrite transport system permease protein	491	4.5	1 vs. 12.25	0
sll1452	nrtC	nitrate/nitrite transport system ATP-binding protein	492	3.8	1 vs. 12.25	0
sll1453	nrtD	nitrate/nitrite transport system ATP-binding protein	458	4.7	1 vs. 12.25	0
slr0395	ntcB	nitrate assimilation transcriptional activator. LysR family protein	37	3.1	1 vs. 13	0
slr1963	OCP	water-soluble carotenoid protein	2056	2.7	1 vs. 9	0
slr1734	opcA	glucose 6-phosphate dehydrogenase assembly protein	173	-3.7	3 vs. 13	0
sll0672	pacL	cation-transporting p-type ATPase PacL	35	1.4	1 vs. 13	0
sll1920	pacS	copper-transporting P-type ATPase PacS	51	-1.4	9 vs. 23	0
slr0526	panB	3-methyl-2-oxobutanoate hydroxymethyltransferase	70	2.0	1 vs. 13	0
sll1249	panC	pantothenate synthetase/cytidylate kinase	63	1.4	3 vs. 13	0
sll0892	panD	aspartate 1-decarboxylase	123	-1.1	6 vs. 18	0
slr0116	pcyA	phycocyanobilin:ferredoxin oxidoreductase	79	1.8	3 vs. 12.25	0
slr1254	pds crtP	phytoene dehydrogenase (phytoene desaturase)	185	2.0	-0.25 vs. 11	0
sll1440	pdxH	pyridoxamine 5'-phosphate oxidase	133	1.4	1 vs. 18	0
slr1779	pdxJ	pyridoxal phosphate biosynthetic protein PdxJ	114	1.3	3 vs. 12.25	0
sll1317	petA	apocytochrome f. component of cytochrome b6/f complex	662	2.4	6 vs. 13	0
slr0342	petB	cytochrome b6	3469	1.5	6 vs. 0.25	0
sll1316	petC1	cytochrome b6-f complex iron-sulfur subunit (Rieske iron sulfur protein)	519	2.8	6 vs. 13	0
slr1185	petC2	cytochrome b6-f complex alternative iron-sulfur subunit (Rieske iron sulfur protein)	22	1.8	-0.25 vs. 9	0
sll1182	petC3	cytochrome b6-f complex alternative iron-sulfur subunit (Rieske iron sulfur protein)	123	-1.4	1 vs. -0.25	0
slr0343	petD	cytochrome b6-f complex subunit 4	7184	-1.1	1 vs. 18	0
sll0199	petE	plastocyanin	11765	1.4	-0.25 vs. 11.75	1.694E-07
sll1382	petF	ferredoxin. petF-like protein	4809	-2.8	6 vs. 13	0
slr0150	petF	ferredoxin. petF-like protein	623	-3.2	3 vs. 13	0
slr1828	petF	ferredoxin. petF-like protein	618	1.1	23 vs. 13	8.129E-13
ssl0020	petF	ferredoxin I. essential for growth	31170	3.3	3 vs. 18	0
smr0010	petG	cytochrome b6-f complex subunit 5	5579	-1.3	1 vs. 9	1.626E-12
slr1643	petH	ferredoxin-NADP oxidoreductase	768	-1.2	11 vs. 23	0
sll1796	petJ	cytochrome c553	1731	3.6	3 vs. 0.25	0

smr0003	petM	cytochrome b6-f complex subunit PetM	2390	3.0	3 vs. 13	0
sml0004	petN	cytochrome b6-f complex subunit VIII	231	1.6	3 vs. 18	0
slr0394	pgk	phosphoglycerate kinase	2110	2.6	-0.25 vs. 11	0
slr1993	phaA	PHA-specific beta-ketothiolase	96	-2.8	6 vs. 13	0
slr1994	phaB	PHA-specific acetoacetyl-CoA reductase	339	-3.3	6 vs. 13	0
slr1830	phaC	poly(3-hydroxyalkanoate) synthase	122	-2.9	6 vs. 13	0
slr1829	phaE	putative poly(3-hydroxyalkanoate) synthase component	186	-2.0	23 vs. 13	0
sll0454	pheS	phenylalanyl-tRNA synthetase alpha chain	110	1.4	1 vs. 13	0
slr0854	phrA	DNA photolyase	52	-1.1	3 vs. 18	0
sll1694	pilA1	pilin polypeptide PilA1	30136	-3.2	1 vs. 18	0
slr2016	pilA10	type 4 pilin-like protein. essential for motility	113	-1.2	1 vs. 18	5.284E-12
slr2017	pilA11	type 4 pilin-like protein. essential for motility	94	-1.1	11.75 vs. 18	0.0000018 1
sll1695	pilA2	pilin polypeptide PilA2	355	-1.5	1 vs. 13	0
slr1456	pilA4	type 4 pilin-like protein. or general secretion pathway protein G	46	-2.4	1 vs. 18	0
slr1928	pilA5	type 4 pilin-like protein	329	-2.1	1 vs. 23	0
slr1929	pilA6	type 4 pilin-like protein	513	-1.4	1 vs. -0.25	0
slr1930	pilA7	type 4 pilin-like protein	338	-1.5	1 vs. -0.25	0
slr2015	pilA9	type 4 pilin-like protein. essential for motility	38	-1.6	1 vs. 18	0
slr0063	pilB1	pilus biogenesis protein homologous to general secretion pathway protein E	85	-1.5	3 vs. 13	0
slr0162	pilC	a part of pilC. pilin biogenesis protein. required for twitching motility	144	-2.1	9 vs. 13	0
slr0163	pilC'	a part of pilC. pilin biogenesis protein. required for twitching motility	201	-2.0	3 vs. 13	0
slr0161	pilT1	twitching motility protein PilT	213	-1.6	3 vs. 13	0
sll1533	pilT2	twitching mobility protein	255	-3.3	3 vs. 13	0
sll0038	pixG taxP1 rer1	positive phototaxis protein. two-component response regulator PatA subfamily	281	-2.6	3 vs. 23	0
sll0040	pixI	positive phototaxis protein. homologous to chemotaxis protein CheW	3104	-2.8	6 vs. 18	0
sll0041	pixJ1 taxD1	phytochrome-like photoreceptor protein for positive phototaxis; homologous to methyl-accepting chemotaxis protein	133	-2.6	3 vs. 13	0
sll0042	pixJ2	methyl-accepting chemotaxis protein for positive phototaxis	55	-1.6	6 vs. 23	0
sll0043	pixL hik18	positive phototaxis protein. homologous to chemotaxis protein CheA. two-component hybrid histidine kinase	34	-1.1	6 vs. 18	0
sll1124	plpA	two-component sensor histidine kinase. phytochrome-like protein	68	-1.1	6 vs. 23	0
slr1510	plsX	fatty acid/phospholipid synthesis protein PlsX	110	1.9	3 vs. 13	0
sll1968	pmgA	photomixotrophic growth related protein. PmgA	110	-1.8	3 vs. 18	0
slr1239	pntA	pyridine nucleotide transhydrogenase alpha subunit	289	-3.8	0.25 vs. 13	0
slr1434	pntB	pyridine nucleotide transhydrogenase beta subunit	158	-2.5	0.25 vs. 13	0

slr0707	polA	DNA polymerase I	37	-1.6	-0.25 vs. 6	0
slr0506	por	light-dependent NADPH-protochlorophyllide oxidoreductase	109	2.3	6 vs. 18	0
slr1622	ppa	soluble inorganic pyrophosphatase	788	4.2	3 vs. 12.25	0
sll0227	ppiB	peptidyl-prolyl cis-trans isomerase B. periplasmic protein	183	1.0	3 vs. 11.75	0
sll0290	ppk	polyphosphate kinase	24	-1.2	6 vs. 18	0
sll1387	pppA	serine/threonine protein phosphatase PppA	570	-3.4	6 vs. 18	0
sll1110	prfA	peptide chain release factor 1	77	1.0	6 vs. 12.25	0
sll1865	prfB	peptide chain release factor 2	87	1.2	6 vs. 23	0
sll1525	prk	phosphoribulokinase	1741	1.4	1 vs. 13	0
sll0373	proA	gamma-glutamyl phosphate reductase	60	1.2	1 vs. 9	0
sll0461	proA	gamma-glutamyl phosphate reductase	235	-2.0	6 vs. 23	0
slr1834	psaA	P700 apoprotein subunit Ia	30764	-2.4	1 vs. 13	0
slr1835	psaB	P700 apoprotein subunit Ib	37972	-2.8	1 vs. 13	0
ssl0563	psaC	photosystem I subunit VII	28975	2.8	11.75 vs. 23	0
slr0737	psaD	photosystem I subunit II	23074	-2.2	0.25 vs. 11.75	0
ssr2831	psaE	photosystem I subunit IV	20978	-2.6	0.25 vs. 11.75	0
sll0819	psaF	photosystem I reaction center subunit III precursor (PSI-F). plastocyanin (cyt c553) docking protein	22903	3.0	6 vs. 0.25	0
smr0004	psaI	photosystem I subunit VIII	14870	-2.6	0.25 vs. 12.25	0
sml0008	psaJ	photosystem I subunit IX	53748	-2.6	0.25 vs. 12.25	0
ssr0390	psaK1	photosystem I reaction center subunit X	6669	-1.7	0.25 vs. 11	0
sll0629	psaK2	alternative photosystem I reaction center subunit X	1425	-2.3	-0.25 vs. 11	0
slr1655	psaL	photosystem I subunit XI	14822	-2.8	0.25 vs. 11.75	0
smr0005	psaM	photosystem I subunit XII	88361	-2.7	-0.25 vs. 11	0
slr1645	psb27	photosystem II 11 kD protein	770	1.1	23 vs. 13	0
sll1398	psb28 psb13 ycf79	photosystem II reaction center 13 kDa protein	430	3.9	9 vs. 23	0
slr1739	psb28-2	photosystem II 13 kDa protein homolog	217	3.6	-0.25 vs. 6	0
slr1181	psbA1	photosystem II D1 protein	44	-1.1	1 vs. 13	0
slr1311	psbA2	photosystem II D1 protein	122077	-2.3	1 vs. 6	0
sll1867	psbA3	photosystem II D1 protein	51390	4.0	-0.25 vs. 11.75	0
slr0906	psbB	photosystem II core light harvesting protein	7058	2.8	6 vs. 0.25	0
sll0851	psbC	photosystem II CP43 protein	8709	-1.6	1 vs. 6	0
sll0849	psbD	photosystem II reaction center D2 protein	6087	2.9	6 vs. 0.25	0
slr0927	psbD2	photosystem II reaction center D2 protein	18066	2.5	6 vs. 0.25	0
ssr3451	psbE	cytochrome b559 alpha subunit	2527	2.7	6 vs. 13	0
smr0006	psbF	cytochrome b559 b subunit	2593	2.2	6 vs. 13	0
ssl2598	psbH	photosystem II PsbH protein	14175	1.2	6 vs. 13	0

sml0001	psbI	photosystem II reaction center PsbI protein	12288	2.0	6 vs. 13	0
smr0008	psbJ	photosystem II PsbJ protein	7163	1.5	6 vs. 13	0
sml0005	psbK	photosystem II PsbK protein	7842	2.2	6 vs. 13	0
smr0007	psbL	photosystem II PsbL protein	4492	1.7	3 vs. 13	0
sml0003	psbM	photosystem II reaction center M protein	5292	2.2	9 vs. 13	0
smr0009	psbN	photosystem II PsbN protein	1182	1.3	0.25 vs. 12.25	0
sll0427	psbO	photosystem II manganese-stabilizing polypeptide	10312	3.4	6 vs. 13	0
smr0001	psbT	photosystem II PsbT protein	5232	1.0	3 vs. 0.25	0
sll1194	psbU	photosystem II 12 kDa extrinsic protein	9952	1.9	6 vs. 0.25	0
sll0258	psbV	cytochrome c550	5718	2.3	6 vs. 0.25	0
sml0002	psbX	photosystem II PsbX protein	10232	-1.3	1 vs. 23	8.129E-13
sml0007	psbY	photosystem II protein Y	4873	-1.1	1 vs. 6	0
sll1281	psbZ	photosystem II PsbZ protein	1534	2.6	6 vs. 13	0
sll0421	purB	adenylosuccinate lyase	137	1.6	1 vs. 13	0
slr1226	purC	phosphoribosyl aminoidazole succinocarboxamide synthetase	154	1.3	1 vs. 12.25	0
slr1159	purD	glycinamide ribonucleotide synthetase	45	1.2	6 vs. 18	0
sll0757	purF	amidophosphoribosyltransferase	1004	-2.6	6 vs. 23	0
slr0597	purH	phosphoribosyl aminoimidazole carboxy formyl formyltransferase/inosinemonophosphate cyclohydrolase (PUR-H(J))	54	1.3	-0.25 vs. 11	0
sll0578	purK	phosphoribosylaminoimidazole carboxylase ATPase subunit	50	1.7	1 vs. 13	0
slr0520	purL	phosphoribosyl formylglycinamidine synthase	161	-1.1	9 vs. 18	0
slr0477	purN	phosphoribosylglycinamide formyltransferase	50	-2.0	6 vs. 23	0
slr0861	purT	glycinamide ribonucleotide transformylase	122	-1.0	6 vs. 23	0
sll1561	putA	proline oxidase	57	-1.5	9 vs. 23	0
sll1685	pxcA ycf10	protein involved in light-induced Na+-dependent proton extrusion	28	-2.2	-0.25 vs. 12.25	0
sll0370	pyrA	carbamoyl-phosphate synthase. pyrimidine-specific. large chain	78	-1.6	-0.25 vs. 11.75	0
slr1476	pyrB	aspartate carbamoyltransferase	93	1.7	3 vs. 13	0
slr1418	pyrD	dihydroorotate dehydrogenase	26	-1.3	3 vs. 13	0
sll0838	pyrF	orotidine 5' monophosphate decarboxylase	121	-1.1	6 vs. 23	0
sll0144	pyrH	uridine monophosphate kinase	264	2.9	1 vs. 13	0
slr1255	pys	phytoene synthase	199	1.9	1 vs. 13	0
slr0448	radA	DNA repair protein RadA	33	1.7	1 vs. 13	0
sll0766	radC	DNA repair protein RadC	100	-1.5	6 vs. 18	0
slr0009	rbcL	ribulose bisphosphate carboxylase large subunit	2329	2.0	3 vs. 18	0
slr0012	rbcS	ribulose bisphosphate carboxylase small subunit	3576	1.2	-0.25 vs. 0.25	0
slr0011	rbcX	possible Rubisco chaperonin	3641	1.5	3 vs. 18	0
sll0517	rbp1	putative RNA binding protein	6546	1.6	11.75 vs. 23	3.252E-12
ssr1480	rbp2	putative RNA-binding protein	32987	1.4	3 vs. 13	0

slr0193	rbp3	RNA-binding protein	1019	1.8	1 vs. 12.25	0
slr0474	rcp1	two-component response regulator CheY subfamily. regulator for phytochrome 1 (Cph1)	1685	-5.5	3 vs. 13	0
sll1277	recF	RecF protein	24	2.2	1 vs. 13	0
slr0020	recG	DNA recombinase	18	-1.1	3 vs. 12.25	0
sll1354	recJ	single-strand-DNA-specific exonuclease RecJ	83	-2.1	6 vs. 18	0
sll1520	recN	DNA repair protein RecN	8	1.7	3 vs. -0.25	0
slr1536	recQ	ATP-dependent DNA helicase RecQ	77	1.1	11.75 vs. 18	0
slr0809	rfbB	dTDP-glucose 4.6-dehydratase	107	1.2	23 vs. 13	0
slr0836	rfbB	dTDP-glucose 4.6-dehydratase	44	1.3	1 vs. 12.25	0
slr0985	rfbC	dTDP-4-dehydrorhamnose 3.5-epimerase	151	1.8	1 vs. 13	0
slr1933	rfbC	dTDP-4-dehydrorhamnose 3.5-epimerase	32	2.5	1 vs. 12.25	0
slr0983	rfbF	glucose-1-phosphate cytidylyltransferase	184	1.9	3 vs. 13	0
slr0984	rfbG	CDP-glucose 4.6-dehydratase	136	1.4	1 vs. 13	0
sll1370	rfbM	mannose-1-phosphate guanylyltransferase	49	1.3	3 vs. 13	0
slr1130	rhnB	ribonuclease HII	109	1.2	-0.25 vs. 6	0
sll1894	ribA	riboflavin biosynthesis protein RibA	85	-2.5	11 vs. 23	0
slr0066	ribD	riboflavin biosynthesis protein RibD	25	-1.0	6 vs. 23	4.667E-09
slr1882	ribF	riboflavin biosynthesis protein RibF	22	2.1	1 vs. 13	0
sll1282	ribH	riboflavin synthase beta subunit	486	2.5	3 vs. 13	0
slr0346	rnc	ribonuclease III	157	1.6	1 vs. 13	0
slr1646	rnc	ribonuclease III	330	1.8	3 vs. 13	0
slr1129	rne	ribonuclease E	120	1.8	-0.25 vs. 6	0
slr0080	rnhA	ribonuclease H	344	1.0	1 vs. 13	0
slr0115	rpaA	response regulator for energy transfer from phycobilisomes to photosystems	198	-1.1	1 vs. 23	0
slr0947	rpaB	response regulator for energy transfer from phycobilisomes to photosystems	484	-1.2	23 vs. 13	0
sll0807	rpe	pentose-5-phosphate-3-epimerase	1469	2.2	1 vs. 13	0
slr0194	rpiA	ribose 5-phosphate isomerase	249	2.6	3 vs. 12.25	0
sll1745	rpl10	50S ribosomal protein L10	4880	1.5	3 vs. 0.25	0
sll1743	rpl11	50S ribosomal protein L11	982	1.3	3 vs. 23	0
sll1746	rpl12	50S ribosomal protein L12	6161	1.5	3 vs. 0.25	0
sll1806	rpl14	50S ribosomal protein L14	141	1.6	6 vs. 0.25	0
sll1813	rpl15	50S ribosomal protein L15	480	1.6	3 vs. 0.25	0
sll1805	rpl16	50S ribosomal protein L16	56	-2.2	-0.25 vs. 6	0
sll1811	rpl18	50S ribosomal protein L18	207	-1.1	0.25 vs. 18	0
sll1740	rpl19	50S ribosomal protein L19	1475	1.4	3 vs. 13	0
sll1802	rpl2	50S ribosomal protein L2	187	1.7	6 vs. 13	0
sll0767	rpl20	50S ribosomal protein L20	4492	1.7	3 vs. 13	0
slr1678	rpl21	50S ribosomal protein L21	4367	-2.0	6 vs. 18	0
sll1803	rpl22	50S ribosomal protein L22	142	1.7	6 vs. 13	0
sll1801	rpl23	50S ribosomal protein L23	217	1.3	6 vs. 13	0

sll1807	rpl24	50S ribosomal protein L24	135	1.5	6 vs. 0.25	0
ssr2799	rpl27	50S ribosomal protein L27	13743	-2.3	6 vs. 18	0
ssr1604	rpl28	50S ribosomal protein L28	6690	1.0	11 vs. 13	8.129E-13
ssl3436	rpl29	50S ribosomal protein L29	87	1.2	6 vs. 13	1.707E-10
sll1799	rpl3	50S ribosomal protein L3	347	1.7	3 vs. -0.25	0
ssr1736	rpl32	50S ribosomal protein L32	1531	2.0	0.25 vs. 12.25	0
ssr1398	rpl33	50S ribosomal protein L33	1025	2.0	0.25 vs. 13	0
smr0011	rpl34	50S ribosomal protein L34	532	1.0	9 vs. 13	0
ssl1426	rpl35	50S ribosomal protein L35	5232	2.1	6 vs. 23	0
sll1800	rpl4	50S ribosomal protein L4	342	1.1	18 vs. 13	0
sll1808	rpl5	50S ribosomal protein L5	140	-1.4	0.25 vs. 18	4.065E-13
sll1810	rpl6	50S ribosomal protein L6	408	-2.3	9 vs. 18	0
sll1244	rpl9	50S ribosomal protein L9	2681	1.3	3 vs. 13	0
sll1787	rpoB	RNA polymerase beta subunit	312	1.4	23 vs. 13	0
slr1265	rpoC1	RNA polymerase gamma-subunit	1660	-2.8	6 vs. 18	0
sll1789	rpoC2	RNA polymerase beta prime subunit	413	1.2	23 vs. 13	0
sll1101	rps10	30S ribosomal protein S10	889	2.2	1 vs. 12.25	0
sll1096	rps12	30S ribosomal protein S12	1160	1.3	6 vs. 12.25	0
slr0628	rps14	30S ribosomal protein S14	8584	1.8	0.25 vs. 12.25	0
ssl1784	rps15	30S ribosomal protein S15	1295	1.5	0.25 vs. 13	0
ssr0482	rps16	30S ribosomal protein S16	1263	2.4	0.25 vs. 12.25	0
ssl3437	rps17	30S ribosomal protein S17	82	1.7	6 vs. 13	0
ssr1399	rps18	30S ribosomal protein S18	1658	2.1	0.25 vs. 13	0
ssl3432	rps19	30S ribosomal protein S19	102	-2.0	-0.25 vs. 6	0
ssl0601	rps21	30S ribosomal protein S21	22996	2.7	3 vs. 12.25	0
sll1804	rps3	30S ribosomal protein S3	115	1.7	6 vs. 13	0
slr0469	rps4	30S ribosomal protein S4	4876	1.2	3 vs. 12.25	0
sll1812	rps5	30S ribosomal protein S5	233	1.3	6 vs. 0.25	0
sll1767	rps6	30S ribosomal protein S6	2461	2.1	3 vs. 13	0
sll1097	rps7	30S ribosomal protein S7	660	1.5	6 vs. 12.25	0
sll1809	rps8	30S ribosomal protein S8	334	-1.7	9 vs. 18	0
slr2033	rubA	membrane-associated rubredoxin. essential for photosystem I assembly	800	2.4	-0.25 vs. 12.25	0
sll0876	ruvA	Holliday junction DNA helicase RuvA	25	1.2	6 vs. 13	2.032E-12
slr0593	samp	cAMP binding membrane protein	44	-1.8	6 vs. 23	0
slr1512	sbtA	sodium-dependent bicarbonate transporter	76	-2.0	0.25 vs. 13	0
slr0611	sds	solanesyl diphosphate synthase	105	-1.0	12.25 vs. 23	0.0004904
sll0616	secA	preprotein translocase SecA subunit	85	1.3	1 vs. 12.25	0
slr0774	secD	protein-export membrane protein SecD	86	1.4	6 vs. 13	0
ssr3307	secG	preprotein translocase SecG subunit	1888	1.5	0.25 vs. 12.25	0
sll1814	secY	preprotein translocase SecY subunit	1028	-1.3	0.25 vs. 18	0
slr1703	serS	seryl-tRNA synthetase	92	2.0	3 vs. 13	0

slr2089	shc	squalene-hopene-cyclase	172	-2.1	6 vs. 23	0
slr0653	sigA	principal RNA polymerase sigma factor SigA	526	-2.3	9 vs. 18	0
sll0306	sigB	RNA polymerase group 2 sigma factor	967	-3.3	6 vs. 18	0
sll0184	sigC	group2 RNA polymerase sigma factor SigC	79	2.3	-0.25 vs. 11	0
sll2012	sigD	group2 RNA polymerase sigma factor SigD	109	1.9	1 vs. 11	0
sll1689	sigE	group2 RNA polymerase sigma factor SigE	200	4.2	9 vs. 23	0
slr1564	sigF	group 3 RNA polymerase sigma factor	171	-1.8	3 vs. -0.25	0
slr1545	sigG	RNA polymerase ECF-type (group 3) sigma-E factor	6422	-2.6	6 vs. 18	0
sll0856	sigH	RNA polymerase ECF-type (group 3) sigma-E factor	119	-2.3	1 vs. 18	0
sll0687	sigI	RNA polymerase ECF-type (group 3) sigma factor	27	-4.4	3 vs. 18	0
slr0963	sir	ferredoxin-sulfite reductase	61	-1.1	11 vs. 23	0
slr1516	sodB	superoxide dismutase	9622	1.4	-0.25 vs. 12.25	0
sll0228	speB1	arginase	141	1.4	1 vs. 13	0
sll1077	speB2	agmatinase	40	1.3	1 vs. 18	0
sll1574	spkA'	a part of spkA: serine/threonine protein kinase. regulates cellular motility (disrupted by frameshift mutation)	277	-2.1	6 vs. 23	0
sll0776	spkD	serine/threonine kinase	225	-3.2	1 vs. 13	0
slr0384	sqdX	sulfoquinovosyldiacylglycerol biosynthesis protein SqdX	87	1.7	1 vs. 12.25	0
sll1924	sycrp2	cAMP receptor protein sycrp1 homolog	101	-1.9	-0.25 vs. 6	0
sll1786	tatD	putative deoxyribonuclease. tatD homolog	749	-1.1	12.25 vs. 23	0
slr0713	tgt	tRNA-guanine transglycosylase	450	3.1	3 vs. 13	0
slr0633	thiG	thiamine biosynthesis protein ThiG	110	-2.3	6 vs. 13	0
sll1172	thrC	threonine synthase	171	1.3	1 vs. 13	0
sll1688	thrC	threonine synthase	2032	3.1	0.25 vs. 12.25	0
sll0078	thrS	threonyl-tRNA synthetase	70	-1.1	11 vs. 23	0
slr1322	tldD	putative modulator of DNA gyrase; TldD	90	1.9	-0.25 vs. 11.75	0
slr2058	topA	DNA topoisomerase I	53	-1.5	3 vs. 13	0
slr0966	trpA	tryptophan synthase alpha chain	329	1.8	3 vs. 13	0
slr0543	trpB	tryptophan synthase beta subunit	176	-1.9	6 vs. 23	0
slr0546	trpC	indole-3-glycerol phosphate synthase	35	1.3	1 vs. -0.25	3.315E-09
slr1867	trpD	anthranilate phosphoribosyltransferase	202	-2.6	9 vs. 23	0
slr0738	trpE	anthranilate synthetase alpha-subunit	124	1.8	11.75 vs. 18	0
slr1979	trpE	anthranilate synthase component I	47	-2.0	-0.25 vs. 6	0
sll0356	trpF	N-(5'-phosphoribosyl)anthranilate isomerase	18	-1.1	11.75 vs. 23	0.0000715
slr0055	trpG	anthranilate synthase component II	99	1.3	1 vs. 12.25	0
slr1884	trpS	tryptophanyl-tRNA synthetase	57	1.7	1 vs. 18	0
sll1980	trxA	thiol:disulfide interchange protein TrxA	698	-2.7	9 vs. 18	0
slr0623	trxA	thioredoxin	4576	-1.3	6 vs. 12.25	0

slr1139	trxA	thioredoxin	222	1.1	9 vs. 18	0
slr0233	trxM1	thioredoxin M	761	2.5	-0.25 vs. 6	0
sll1057	trxM2	thioredoxin M	361	-2.0	6 vs. 13	0
slr2081	tyrA	prephenate dehydrogenase	178	-2.4	6 vs. 18	0
slr1031	tyrS	tyrosyl tRNA synthetase	59	-2.0	-0.25 vs. 6	0
slr0926	ubiA	4-hydroxybenzoate-octaprenyl transferase	272	-1.4	9 vs. 23	0
sll0420	ureB	urease beta subunit	147	1.5	11.75 vs. 23	0
sll1750	ureC	urease alpha subunit	235	-2.2	6 vs. 23	0
sll1639	ureD	urease accessory protein D	1108	2.2	3 vs. 13	0
slr0447	urtA	periplasmic protein. ABC-type urea transport system substrate-binding protein	2694	1.5	1 vs. 18	0
sll0764	urtD	urea transport system ATP-binding protein	85	1.9	1 vs. 13	0
sll0374	urtE	urea transport system ATP-binding protein	127	2.1	1 vs. 23	0
slr1844	uvrA	excinuclease ABC subunit A	100	1.4	1 vs. 13	0
sll0459	uvrB	excinuclease ABC subunit B	24	-1.5	6 vs. 13	0
slr0557	valS	valyl-tRNA synthetase	98	1.2	1 vs. -0.25	0
ssl2922	vapB	similar to virulence-associated protein VapB	285	3.1	3 vs. 23	0
ssl2923	vapC	similar to virulence-associated protein VapC	249	3.0	6 vs. 23	0
sll0617	vipp1	plasma membrane protein essential for thylakoid formation	913	1.4	3 vs. 12.25	0
sll0047	ycf12	hypothetical protein YCF12	3269	-1.8	-0.25 vs. 9	0
ssr2142	ycf19	hypothetical protein YCF19	3232	-1.8	3 vs. 13	0
sll1797	ycf21	hypothetical protein YCF21	89	2.9	0.25 vs. 11	0
sll0751	ycf22	hypothetical protein YCF22	133	-1.1	1 vs. 23	0
slr0074	ycf24	ABC transporter subunit	186	-2.2	11 vs. 13	0
ssr1425	ycf34	hypothetical protein YCF34	265	-2.2	9 vs. 18	0
sll0661	ycf35	hypothetical protein YCF35	1052	2.4	6 vs. 23	0
sll0584	ycf36	hypothetical protein YCF36	205	-2.7	3 vs. 18	0
slr0171	ycf37	photosystem I assembly related protein Ycf37	265	1.4	6 vs. 13	0
sll0760	ycf38	hypothetical protein YCF38	297	-1.7	9 vs. 0.25	0
sll1218	ycf39	hypothetical protein YCF39	79	1.9	6 vs. 23	0
slr0399	ycf39	chaperon-like protein for quinone binding in photosystem II	160	3.4	1 vs. 12.25	0
slr1218	ycf39	hypothetical protein YCF39	150	2.3	11.75 vs. 23	0
slr1034	ycf41	hypothetical protein YCF41	602	1.6	-0.25 vs. 6	0
sll0194	ycf43	putative sec-independent protein translocase	161	-1.5	6 vs. 23	0
slr0692	ycf45	hypothetical protein YCF45	93	-1.5	6 vs. 18	0
slr0480	ycf46	hypothetical protein YCF46	27	1.2	1 vs. -0.25	1.219E-12
slr2034	ycf48	putative homolog of plant HCF136. which is essential for stability or assembly of photosystem II	184	1.6	0.25 vs. 12.25	0
slr2073	ycf50	hypothetical protein YCF50	3899	1.3	1 vs. 23	0
sll1702	ycf51	hypothetical protein YCF51	241	-1.3	12.25 vs. 23	0
slr1780	ycf54	hypothetical protein YCF54	131	3.3	3 vs. 13	0

slr0050	ycf56	hypothetical protein YCF56	83	1.3	-0.25 vs. 9	0
slr1417	ycf57	hypothetical protein YCF57	1844	-2.2	9 vs. 18	0
slr2049	ycf58	hypothetical protein YCF58	227	1.2	1 vs. 13	0
sll1214	ycf59	hypothetical protein YCF59	1245	1.6	6 vs. 13	0
sll1737	ycf60	hypothetical protein YCF60	340	1.3	6 vs. 23	0
ssl2982	ycf61	probable DNA-directed RNA polymerase omega subunit	427	1.6	3 vs. 18	0
slr1045	ycf63	hypothetical protein YCF63	128	1.2	-0.25 vs. 6	0
slr1846	ycf64	hypothetical protein YCF64	718	2.0	6 vs. 23	0
slr0923	ycf65	hypothetical protein YCF65	1342	1.7	3 vs. 13	0
slr0503	ycf66	hypothetical protein YCF66	417	-3.0	6 vs. 23	0
slr1972	ycf81	hypothetical protein YCF81	238	-2.7	3 vs. -0.25	0
slr0882	ycf84	hypothetical protein YCF84	136	-1.4	9 vs. 23	0
slr0251	ycf85	ATP-binding protein of ABC transporter	70	1.1	3 vs. 11	0
sll1910	zam	protein conferring resistance to acetazolamide Zam	65	1.2	23 vs. 13	0
slr0798	ziaA	zinc-transporting P-type ATPase (zinc efflux pump) involved in zinc tolerance	38	-1.4	3 vs. 13	0.0001349
slr1843	zwf	glucose 6-phosphate dehydrogenase	106	-1.5	23 vs. 13	0
sgl0001		hypothetical protein	51	-1.7	0.25 vs. 11	7.141E-10
sll0002		penicillin-binding protein	162	-2.7	6 vs. 23	0
sll0005		hypothetical protein	79	1.1	1 vs. 12.25	0
sll0006		putative aminotransferase	147	-1.2	12.25 vs. 23	0
sll0008		unknown protein	268	1.5	6 vs. 12.25	0
sll0012		putative transposase [ISY523f: 2482725 - 2483595]	36	-1.3	6 vs. 13	6.097E-12
sll0016		probable membrane-bound lytic transglycosylase A	71	-1.6	0.25 vs. 12.25	0
sll0019		1-deoxy-d-xylulose 5-phosphate reductoisomerase	64	1.7	6 vs. 13	0
sll0020		ATP-dependent Clp protease ATPase subunit	3929	-3.6	6 vs. 18	0
sll0021		probable exonuclease	34	-1.7	3 vs. 13	0
sll0022		unknown protein	152	-3.0	3 vs. 12.25	0
sll0023		hypothetical protein	85	-1.9	1 vs. 12.25	0
sll0024		unknown protein	256	-2.2	1 vs. 12.25	0
sll0031		hypothetical protein	130	1.1	-0.25 vs. 6	0
sll0036		hypothetical protein	30	-1.2	3 vs. 13	0
sll0037		hypothetical protein	95	-1.6	9 vs. 23	0
sll0048		unknown protein	262	-2.5	6 vs. 13	0
sll0051		hypothetical protein	1292	-3.2	1 vs. 13	0
sll0055		processing protease	34	-2.0	6 vs. 23	0
sll0060		hypothetical protein	44	1.5	1 vs. 18	0
sll0062		hypothetical protein	279	-1.1	3 vs. 13	0
sll0063		hypothetical protein	102	-1.5	6 vs. 23	0
sll0064		periplasmic protein. putative polar amino acid transport system substrate-binding protein	113	-2.8	-0.25 vs. 6	0

sll0066	unknown protein	331	-3.7	3 vs. 18	0
sll0067	glutathione S-transferase	87	-1.2	6 vs. 18	0
sll0068	unknown protein	112	-1.5	6 vs. 23	0
sll0071	hypothetical protein	50	1.6	3 vs. 18	0
sll0072	hypothetical protein	57	2.2	6 vs. 13	0
sll0083	phosphoheptose isomerase	588	1.1	0.25 vs. 13	0
sll0084	putative phosphatase	101	1.8	1 vs. 13	0
sll0085	unknown protein	36	1.2	1 vs. 13	0
sll0086	putative arsenical pump-driving ATPase	110	1.9	-0.25 vs. 11.75	0
sll0088	hypothetical protein	282	-3.0	3 vs. 18	0
sll0092	putative transposase [ISY391c: 2997600 - 2998989]	113	-1.5	1 vs. 23	0
sll0095	hypothetical protein	114	1.2	1 vs. 13	0
sll0098	hypothetical protein	276	-3.6	3 vs. 13	0
sll0100	N-acyl-L-amino acid amidohydrolase	84	-2.7	3 vs. 18	0
sll0101	unknown protein	206	-1.3	-0.25 vs. 9	0
sll0103	hypothetical protein	307	-3.6	3 vs. 18	0
sll0107	KHG/KDPG aldolase	52	1.8	1 vs. 13	0
sll0135	putative 5'-methylthioadenosine phosphorylase	130	1.9	0.25 vs. 12.25	0
sll0141	hypothetical protein	73	2.3	0.25 vs. 12.25	0
sll0142	probable cation efflux system protein	53	-2.0	11 vs. 23	0
sll0148	hypothetical protein	169	-1.6	9 vs. 23	0
sll0149	hypothetical protein	187	-2.4	6 vs. 23	0
sll0154	hypothetical protein	503	-1.8	9 vs. 23	0
sll0156	unknown protein	251	-2.9	6 vs. 23	0
sll0157	hypothetical protein	95	2.8	-0.25 vs. 9	0
sll0160	hypothetical protein	123	1.3	1 vs. 13	0
sll0162	hypothetical protein	29	-1.2	1 vs. 13	3.401E-09
sll0163	WD-repeat protein	77	-2.5	6 vs. 18	0
sll0169	cell division protein Ftn2 homolog	509	-2.7	3 vs. 18	0
sll0172	periplasmic protein. function unknown	177	1.3	-0.25 vs. 11	0
sll0175	hypothetical protein	31	1.5	6 vs. 18	0
sll0176	hypothetical protein	45	1.4	3 vs. -0.25	0.0000037 18
sll0177	hypothetical protein	23	2.0	1 vs. 13	0
sll0178	hypothetical protein	249	1.9	6 vs. 12.25	0
sll0180	hypothetical protein	407	-2.5	1 vs. 12.25	0
sll0181	unknown protein	478	-2.4	-0.25 vs. 11	0
sll0182	ABC transporter ATP-binding protein	86	-1.3	0.25 vs. 11	0
sll0183	hypothetical protein	902	-1.9	6 vs. 18	0
sll0185	hypothetical protein	464	-1.9	3 vs. 18	0
sll0188	unknown protein	301	-3.8	6 vs. 23	0

sll0189	hypothetical protein	72	-1.5	6 vs. 23	0
sll0191	unknown protein	139	-1.1	1 vs. -0.25	0.0000037 79
sll0192	hypothetical protein	15	1.7	1 vs. 13	0
sll0195	probable ATP-dependent protease	94	2.8	1 vs. 13	0
sll0198	hypothetical protein	40	1.6	-0.25 vs. 9	0
sll0202	glucose inhibited division protein	36	-1.4	6 vs. 23	0
sll0205	hypothetical protein	364	-1.2	1 vs. -0.25	3.252E-12
sll0208	hypothetical protein	2195	-2.2	11 vs. 23	0
sll0209	hypothetical protein	358	1.8	1 vs. 13	0
sll0210	bacitracin resistance protein	88	-1.0	9 vs. 23	0
sll0216	hypothetical protein	27	1.4	1 vs. 12.25	8.251E-09
sll0218	hypothetical protein	9	-2.1	3 vs. 23	0
sll0221	bacterioferritin comigratory protein	82	-1.5	9 vs. 13	0
sll0222	putative purple acid phosphatase	186	2.1	3 vs. 13	0
sll0224	amino-acid ABC transporter binding protein	56	2.1	6 vs. 23	0
sll0225	unknown protein	46	2.0	9 vs. 23	0
sll0230	hypothetical protein	311	1.4	1 vs. 12.25	0
sll0240	ABC transporter ATP-binding protein	36	2.5	-0.25 vs. 6	0
sll0241	unknown protein	339	-3.7	1 vs. 12.25	0
sll0242	unknown protein	143	-3.0	1 vs. 13	0
sll0243	unknown protein	317	-2.7	0.25 vs. 13	0
sll0244	UDP-glucose 4-epimerase	46	2.0	1 vs. 13	0
sll0245	probable GTP binding protein	84	2.0	1 vs. 13	0
sll0249	hypothetical protein	11	-1.4	3 vs. 13	0.0200721 87
sll0250	pantothenate metabolism flavoprotein	105	1.5	1 vs. 18	0
sll0252	unknown protein	124	1.2	1 vs. 13	0
sll0253	hypothetical protein	756	-4.0	0.25 vs. 12.25	0
sll0254	probable phytoene dehydrogenase Rieske iron-sulfur component	121	-1.7	1 vs. 12.25	0
sll0257	hypothetical protein	30	1.2	18 vs. 11	0.0000894 4
sll0261	hypothetical protein	23	-2.1	3 vs. 13	0
sll0263	unknown protein	88	1.1	3 vs. 13	0.0000207
sll0264	probable dioxygenase Rieske iron-sulfur component	87	-1.7	1 vs. 13	0
sll0265	unknown protein	29	-1.1	11.75 vs. 13	3.414E-11
sll0267	unknown protein	45	-1.9	6 vs. 18	0
sll0269	hypothetical protein	62	1.3	1 vs. -0.25	7.581E-09
sll0270	primosomal protein N'	39	1.4	1 vs. 13	0
sll0272	hypothetical protein	300	2.3	1 vs. 13	0
sll0274	hypothetical protein	68	-1.7	3 vs. 23	0
sll0280	unknown protein	8	1.7	9 vs. 18	2.975E-09
sll0283	hypothetical protein	276	-3.5	1 vs. 12.25	0

sll0284	hypothetical protein	37	-1.0	-0.25 vs. 11	0
sll0293	unknown protein	152	-1.7	3 vs. 18	0
sll0294	hypothetical protein	82	-1.9	3 vs. 13	0
sll0296	hypothetical protein	139	1.3	9 vs. 23	0
sll0297	hypothetical protein	218	-2.1	11 vs. 23	0
sll0298	hypothetical protein	299	-2.1	9 vs. 23	0
sll0309	unknown protein	31	1.4	1 vs. 23	0.019764178
sll0312	probable oligopeptides ABC transporter permease protein	34	-1.3	9 vs. 23	0
sll0314	periplasmic protein. function unknown	205	1.9	-0.25 vs. 9	0
sll0315	putative transposase [ISY203i: 2443391 - 2443924. join 2444874 - 2445513]	32	-2.2	-0.25 vs. 9	0
sll0317	putative transposase [ISY203i: 2443391 - 2443924. join 2444874 - 2445513]	16	8.0	6 vs. 12.25	1.138E-11
sll0320	probable ribonuclease D	132	-1.0	-0.25 vs. 9	8.942E-11
sll0321	unknown protein	55	-1.0	1 vs. 13	0
sll0327	unknown protein	120	-1.7	1 vs. 0.25	0
sll0328	unknown protein	57	1.9	11 vs. 13	0
sll0329	6-phosphogluconate dehydrogenase	642	-3.2	3 vs. 13	0
sll0330	sepiapterine reductase	69	-5.3	9 vs. 23	0
sll0335	hypothetical protein	56	2.1	1 vs. 12.25	0
sll0354	hypothetical protein	117	1.4	3 vs. 18	0
sll0355	hypothetical protein	93	1.3	0.25 vs. 12.25	0
sll0361	hypothetical protein	30	-1.7	-0.25 vs. 6	0
sll0364	hypothetical protein	24	-1.6	18 vs. 11	0
sll0369	unknown protein	44	1.3	3 vs. 13	1.626E-11
sll0371	unknown protein	400	-3.6	-0.25 vs. 9	0
sll0375	unknown protein	392	-2.5	0.25 vs. 12.25	0
sll0376	unknown protein	913	-3.6	1 vs. 13	0
sll0379	acyl-[acyl-carrier-protein]--UDP-N-acetylglucosamine o-acyltransferase	157	2.1	1 vs. 13	0
sll0380	probable glycosyltransferase	75	2.5	1 vs. 18	0
sll0382	hypothetical protein	145	2.2	23 vs. 13	0
sll0383	cobalamin biosynthesis protein M	94	2.1	0.25 vs. 13	0
sll0384	unknown protein	39	2.3	1 vs. 13	0
sll0385	ATP-binding protein of ABC transporter	30	1.5	1 vs. 23	5.025E-07
sll0394	unknown protein	85	-1.9	9 vs. 18	0
sll0398	deoxyguanosinetriphosphate triphosphohydrolase	22	-1.4	6 vs. 13	0
sll0400	hypothetical protein	155	1.5	-0.25 vs. 6	0
sll0401	citrate synthase	105	-1.9	6 vs. 23	0
sll0403	unknown protein	239	-1.7	-0.25 vs. 9	0
sll0405	unknown protein	167	-1.0	-0.25 vs. 9	0
sll0406	unknown protein	76	1.4	6 vs. 23	0

sll0408	peptidyl-prolyl cis-trans isomerase	699	1.3	3 vs. 11.75	0
sll0409	similar to O-succinylbenzoate-CoA synthase	9	1.1	1 vs. -0.25	0.003682
sll0410	hypothetical protein	41	1.5	18 vs. 11	0
sll0412	hypothetical protein	38	-2.4	9 vs. 23	0
sll0415	ATP-binding protein of ABC transporter	110	-1.6	1 vs. 23	0
sll0418	2-methyl-6-phytylbenzoquinone methyltransferase	211	-2.0	6 vs. 23	0
sll0422	asparaginase	100	3.3	1 vs. 13	0
sll0423	hypothetical protein	87	-2.5	9 vs. 18	0
sll0426	unknown protein	2471	-3.6	3 vs. 13	0
sll0428	unknown protein	71	1.3	9 vs. 12.25	0
sll0436	hypothetical protein	63	1.1	6 vs. 13	1.097E-11
sll0441	unknown protein	250	-1.6	-0.25 vs. 11	0
sll0442	hypothetical protein	150	-1.7	0.25 vs. 11	0
sll0443	unknown protein	98	1.5	11.75 vs. 23	0
sll0444	unknown protein	72	-1.3	0.25 vs. 12.25	0
sll0445	unknown protein	36	-1.2	0.25 vs. 13	0
sll0446	unknown protein	229	-1.7	-0.25 vs. 11	0
sll0447	unknown protein	842	-2.9	-0.25 vs. 11	0
sll0448	unknown protein	159	-3.6	-0.25 vs. 9	0
sll0449	unknown protein	47	-2.9	-0.25 vs. 9	0
sll0451	hypothetical protein	56	1.6	9 vs. 18	0
sll0456	hypothetical protein	39	-1.4	3 vs. 13	0
sll0462	hypothetical protein	72	-1.6	9 vs. 23	0
sll0467	S-adenosylmethionine:tRNA ribosyltransferase-isomerase	21	2.0	1 vs. 12.25	0
sll0469	ribose-phosphate pyrophosphokinase	489	-2.0	6 vs. 13	0
sll0470	hypothetical protein	395	-1.5	11 vs. 13	0
sll0473	unknown protein	51	-3.1	6 vs. 18	0
sll0477	putative biopolymer transport ExbB-like protein	67	-1.8	3 vs. -0.25	0
sll0479	unknown protein	30	1.5	1 vs. 23	1.498E-07
sll0480	probable aminotransferase	267	-2.2	9 vs. 23	0
sll0482	unknown protein	184	-2.7	6 vs. 23	0
sll0484	ATP-binding protein of ABC transporter	24	-1.1	1 vs. 13	4.688E-09
sll0488	hypothetical protein	52	-1.2	3 vs. -0.25	0
sll0493	hypothetical protein	95	1.5	1 vs. 12.25	0
sll0494	unknown protein	246	1.8	3 vs. 0.25	0
sll0496	hypothetical protein	88	2.6	3 vs. -0.25	0
sll0498	hypothetical protein	598	-3.1	3 vs. 13	0
sll0501	probable glycosyltransferase	110	2.4	3 vs. 12.25	0
sll0503	hypothetical protein	44	1.7	3 vs. 13	0
sll0505	hypothetical protein	99	-1.4	9 vs. 23	0

sll0506	undecaprenyl pyrophosphate synthetase	147	-1.6	6 vs. 23	0
sll0507	probable cation transporter	78	2.3	3 vs. 13	0
sll0513	hypothetical protein	110	1.5	11.75 vs. 23	0
sll0518	unknown protein	181	2.4	1 vs. 13	0
sll0524	hypothetical protein	67	-1.6	6 vs. 18	0
sll0525	hypothetical protein	337	-1.1	1 vs. 18	1.256E-10
sll0528	hypothetical protein	215	2.0	1 vs. 9	0
sll0529	hypothetical protein	116	1.6	1 vs. 13	0
sll0533	trigger factor	109	2.4	3 vs. 13	0
sll0536	probable potassium channel protein	110	2.2	0.25 vs. 12.25	0
sll0539	unknown protein	132	-1.4	3 vs. 13	0
sll0542	acetyl-coenzyme A synthetase	73	-1.2	0.25 vs. 12.25	0
sll0543	hypothetical protein	3617	-5.0	0.25 vs. 12.25	0
sll0545	hypothetical protein	63	1.5	1 vs. 18	0
sll0547	unknown protein	586	-2.3	6 vs. 23	0
sll0549	hypothetical protein	100	-2.9	11 vs. 23	0
sll0552	unknown protein	25	-1.7	-0.25 vs. 12.25	0
sll0553	hypothetical protein	45	-1.4	6 vs. 13	0
sll0555	methionine aminopeptidase	356	1.6	3 vs. 12.25	0
sll0563	unknown protein	64	-1.1	1 vs. 13	1.408E-07
sll0564	hypothetical protein	74	1.4	6 vs. 13	0
sll0565	hypothetical protein	69	1.5	6 vs. 13	0
sll0572	hypothetical protein	254	-4.0	3 vs. 13	0
sll0573	carbamate kinase	298	-4.6	3 vs. 18	0
sll0574	probable permease protein of lipopolysaccharide ABC transporter	160	2.6	6 vs. 13	0
sll0575	probable lipopolysaccharide ABC transporter ATP binding subunit	94	2.5	6 vs. 13	0
sll0576	putative sugar-nucleotide epimerase/dehydratease	173	3.7	3 vs. 13	0
sll0577	hypothetical protein	582	2.0	1 vs. 13	0
sll0585	hypothetical protein	32	1.5	18 vs. 11	0
sll0586	hypothetical protein	20	-2.1	6 vs. 23	0
sll0587	pyruvate kinase	32	-1.9	23 vs. 13	0
sll0588	unknown protein	3255	-2.4	-0.25 vs. 11.75	0
sll0590	unknown protein	114	1.2	6 vs. 23	0
sll0601	nitrilase homolog	68	1.1	23 vs. 13	5.3E-10
sll0602	hypothetical protein	61	1.2	-0.25 vs. 9	0
sll0609	hypothetical protein	52	-1.1	9 vs. 23	0.0000016 91
sll0611	hypothetical protein	446	-4.2	3 vs. 13	0
sll0614	unknown protein	34	-1.4	-0.25 vs. 9	8.734E-09
sll0615	hypothetical protein	96	3.5	1 vs. 13	0

sll0623	unknown protein	240	-2.5	3 vs. 18	0
sll0624	unknown protein	364	1.3	6 vs. 23	0
sll0625	unknown protein	142	-1.1	11.75 vs. 13	0.0002023
sll0630	unknown protein	2387	-2.2	0.25 vs. 11	0
sll0638	periplasmic protein. function unknown	71	-1.0	11 vs. 23	0
sll0639	hypothetical protein	88	-1.9	3 vs. -0.25	0
sll0640	probable sodium/sulfate symporter	78	1.1	1 vs. 13	2.845E-12
sll0641	unknown protein	64	2.0	3 vs. 13	0
sll0645	unknown protein	103	1.5	-0.25 vs. 9	0
sll0647	unknown protein	86	-1.1	9 vs. 23	0
sll0648	probable glycosyltransferase	162	1.0	-0.25 vs. 11	0
sll0650	putative transposase [ISY100j: 421739 - 422684]	12	4.6	3 vs. 18	0
sll0654	alkaline phosphatase	39	-2.8	6 vs. 18	0
sll0656	unknown protein	81	-2.6	3 vs. 18	0
sll0657	phospho-N-acetylmuramoyl-pentapeptide-transferase	135	1.6	3 vs. 12.25	0
sll0659	hypothetical protein	60	2.4	3 vs. 13	0
sll0662	4Fe-4S type iron-sulfur protein	579	1.7	9 vs. 0.25	0
sll0664	unknown protein	380	-2.3	-0.25 vs. 9	0
sll0665	putative transposase [ISY523r: 3109761 - 3110626]	56	-2.4	-0.25 vs. 11	0
sll0666	putative transposase [ISY523r: 3109761 - 3110626]	54	-1.3	3 vs. 18	1.479E-10
sll0668	putative transposase [ISY352e: 2921301 - 2921595. join 3108631 - 3109754]	227	1.4	9 vs. 18	0
sll0670	hypothetical protein	37	-2.0	1 vs. 13	0
sll0671	probable cation transporter	30	1.7	11 vs. 23	0
sll0677	putative transposase [ISY523h: 3093889 - 3094759]	35	-1.3	6 vs. 13	4.065E-13
sll0678	hypothetical protein	32	-1.3	-0.25 vs. 9	0.0000019 04
sll0681	phosphate transport system permease protein PstC homolog	150	-1.2	6 vs. 23	0
sll0682	phosphate transport system permease protein PstA homolog	43	-1.9	9 vs. 23	0
sll0684	phosphate transport ATP-binding protein PstB homolog	41	1.1	1 vs. 18	0.0000136 4
sll0685	hypothetical protein	45	-4.5	9 vs. 18	0
sll0686	probable cytochrome c-type biogenesis protein	191	-4.5	6 vs. 18	0
sll0688	unknown protein	12	-1.6	12.25 vs. 18	0.003206
sll0696	hypothetical protein	29	-1.0	6 vs. 23	0.0000019 58
sll0702	unknown protein	26	-1.4	9 vs. 0.25	0.002004
sll0703	unknown protein	18	1.4	1 vs. 13	8.129E-13
sll0708	dimethyladenosine transferase	21	1.1	9 vs. 12.25	0.0000012 72
sll0709	putative endonuclease	904	-1.3	-0.25 vs. 6	0

sll0710	unknown protein	686	-2.1	-0.25 vs. 6	0
sll0716	leader peptidase I (signal peptidase I)	124	-3.1	9 vs. 18	0
sll0720	RTX toxin activating protein homolog	24	3.8	6 vs. 23	0
sll0721	unknown protein	44	1.5	9 vs. 23	0
sll0722	unknown protein	80	2.0	3 vs. -0.25	0
sll0723	unknown protein	56	-2.8	-0.25 vs. 11	0
sll0726	phosphoglucomutase	162	-2.0	9 vs. 23	0
sll0727	hypothetical protein	50	1.1	3 vs. -0.25	0
sll0729	probable DNA methyltransferase	76	-1.9	-0.25 vs. 6	0
sll0732	hypothetical protein	11	2.0	11.75 vs. 23	0.005835
sll0733	unknown protein	144	1.9	0.25 vs. 18	0
sll0735	hypothetical protein	126	2.9	6 vs. 13	0
sll0736	hypothetical protein	128	3.0	1 vs. 13	0
sll0740	hypothetical protein	43	-1.7	11.75 vs. 18	0
sll0741	pyruvate flavodoxin oxidoreductase	88	-4.8	6 vs. 13	0
sll0742	hypothetical protein	174	-3.5	1 vs. 13	0
sll0743	hypothetical protein	347	-3.7	1 vs. 12.25	0
sll0744	hypothetical protein	72	-3.2	1 vs. 13	0
sll0745	phosphofructokinase	45	-1.4	3 vs. 13	0
sll0749	hypothetical protein	36	2.8	18 vs. 11	0
sll0754	ribosome binding factor A	479	1.1	-0.25 vs. 9	0
sll0756	unknown protein	141	-1.6	12.25 vs. 23	0
sll0759	ABC transporter ATP-binding protein	155	-2.1	11.75 vs. 18	0
sll0761	unknown protein	293	-1.5	9 vs. 13	0
sll0762	unknown protein	667	-2.1	6 vs. 13	0
sll0772	probable porin; major outer membrane protein	62	-1.2	0.25 vs. 11.75	0
sll0775	unknown protein	139	-4.1	1 vs. 13	0
sll0777	putative carboxypeptidase	81	-1.9	1 vs. 13	0
sll0778	ABC transporter. ATP-binding protein	27	-1.3	1 vs. 13	0
sll0780	unknown protein	79	1.1	9 vs. 13	0
sll0781	hypothetical protein	101	2.1	6 vs. 23	0
sll0783	unknown protein	405	4.9	1 vs. 12.25	0
sll0785	unknown protein	13	2.3	1 vs. 13	0
sll0786	unknown protein	10	3.0	1 vs. 23	8.576E-11
sll0787	hypothetical protein	14	2.0	1 vs. 13	0
sll0788	hypothetical protein	300	3.6	-0.25 vs. 11	0
sll0793	hypothetical protein	44	1.9	1 vs. -0.25	0.0001392
sll0800	hypothetical protein	78	-1.9	1 vs. 13	0
sll0808	putative transposase [ISY508a: 1710788 - 1711753]	259	-2.1	-0.25 vs. 6	0
sll0809	hypothetical protein	12	-1.3	3 vs. 13	0.0000013

sll0811	unknown protein	98	2.7	1 vs. 23	1.626E-12
sll0812	hypothetical protein	59	2.0	1 vs. 12.25	0
sll0814	hypothetical protein	667	-2.7	9 vs. 23	0
sll0816	probable oxidoreductase	59	1.2	3 vs. -0.25	0
sll0817	tRNA delta-2-isopentenylpyrophosphate (IPP) transferase	32	1.5	1 vs. 23	0
sll0818	tetrapyrrole methylase family protein	74	-1.9	0.25 vs. 13	0
sll0822	hypothetical protein	6284	4.4	1 vs. 13	0
sll0823	probable succinate dehydrogenase iron-sulfur protein	405	3.0	1 vs. 12.25	0
sll0825	polyA polymerase	32	-2.1	-0.25 vs. 11	0
sll0834	low affinity sulfate transporter	35	1.1	3 vs. 0.25	0
sll0837	periplasmic protein. function unknown	199	-1.2	6 vs. 23	0
sll0842	neopullulanase	22	2.4	-0.25 vs. 6	0
sll0843	unknown protein	394	-3.0	3 vs. 13	0
sll0844	tRNA (5-methylaminomethyl-2-thiouridylate)-methyltransferase	95	-2.4	6 vs. 23	0
sll0846	hypothetical protein	843	3.4	18 vs. 11	0
sll0853	hypothetical protein	101	2.2	3 vs. 13	0
sll0855	putative channel transporter	56	1.5	1 vs. -0.25	0
sll0857	unknown protein	133	-2.7	6 vs. 18	0
sll0858	hypothetical protein	31	-1.7	9 vs. 18	0
sll0860	hypothetical protein	54	1.2	1 vs. 18	9.918E-07
sll0861	hypothetical protein	22	1.3	6 vs. 18	0
sll0863	hypothetical protein	52	1.4	3 vs. 12.25	0
sll0864	hypothetical protein	13	2.1	1 vs. 23	0.0001796
sll0867	hypothetical protein	41	-1.6	3 vs. 12.25	0
sll0871	hypothetical protein	129	-1.7	3 vs. 13	0
sll0872	unknown protein	1086	-2.1	0.25 vs. 12.25	0
sll0873	carboxynorspermidine decarboxylase	39	1.2	1 vs. 9	4.065E-13
sll0875	hypothetical protein	72	1.5	1 vs. 13	0
sll0877	hypothetical protein	96	-1.6	1 vs. 13	0
sll0891	malate dehydrogenase	669	-2.7	9 vs. 18	0
sll0898	hypothetical protein	58	1.8	1 vs. 13	0
sll0899	UDP-N-acetylglucosamine pyrophosphorylase	123	1.3	9 vs. 13	0
sll0905	hypothetical protein	63	-2.8	11 vs. 23	0
sll0909	unknown protein	94	-1.9	-0.25 vs. 9	0
sll0910	unknown protein	353	-1.8	-0.25 vs. 6	0
sll0911	unknown protein	289	-1.9	-0.25 vs. 6	0
sll0914	unknown protein	32	2.6	3 vs. 13	0
sll0915	periplasmic protease	38	1.1	1 vs. 13	0
sll0923	unknown protein	2524	3.1	-0.25 vs. 6	0
sll0924	hypothetical protein	89	-1.5	6 vs. 23	0

sll0925	hypothetical protein	88	-1.9	3 vs. 13	0
sll0927	S-adenosylmethionine synthetase	460	2.4	3 vs. 13	0
sll0930	unknown protein	191	2.1	6 vs. 23	0
sll0931	hypothetical protein	100	1.7	1 vs. 12.25	0
sll0932	hypothetical protein	107	1.5	23 vs. 13	0
sll0933	hypothetical protein	1210	1.8	0.25 vs. 12.25	0
sll0939	hypothetical protein	19	1.7	3 vs. 23	7.723E-12
sll0944	hypothetical protein	207	3.1	0.25 vs. 12.25	0
sll0980	unknown protein	127	-3.4	3 vs. 23	0
sll0981	unknown protein	39	1.1	-0.25 vs. 11.75	1.054E-09
sll0982	unknown protein	780	2.6	-0.25 vs. 11.75	0
sll0983	hypothetical protein	128	2.5	-0.25 vs. 9	0
sll0985	unknown protein	75	1.2	3 vs. 13	0
sll0986	putative transposase [ISY120f(partial copy): 664387 - 664775]	48	1.0	12.25 vs. 18	0.00213
sll0992	putative esterase	56	-1.7	9 vs. 23	0
sll0993	potassium channel	107	-2.0	6 vs. 13	0
sll0995	hypothetical protein	91	-1.2	6 vs. 18	0
sll0996	hypothetical protein	50	1.1	1 vs. 13	1.829E-11
sll0997	hypothetical protein	182	-2.7	1 vs. 13	0
sll1009	unknown protein	6040	-5.0	1 vs. 13	0
sll1011	hypothetical protein	16	-1.3	11.75 vs. 23	3.199E-07
sll1019	hydroxyacylglutathione hydrolase	27	1.8	1 vs. 12.25	0
sll1020	probable glycosyltransferase	61	1.2	11 vs. 23	0
sll1021	hypothetical protein	122	-2.4	6 vs. 13	0
sll1023	succinyl-CoA synthetase beta chain	42	1.4	1 vs. 13	0
sll1024	hypothetical protein	27	1.9	1 vs. 12.25	0
sll1033	probable protein phosphatase	106	-1.1	6 vs. 23	0
sll1037	unknown protein	29	-1.1	-0.25 vs. 12.25	0
sll1043	polyribonucleotide nucleotidyltransferase	429	-1.0	9 vs. 23	0
sll1045	mutator MutT protein	26	1.9	1 vs. 12.25	0
sll1049	hypothetical protein	194	2.9	-0.25 vs. 6	0
sll1052	hypothetical protein	58	-1.7	18 vs. 11	0
sll1053	hypothetical protein	137	-3.1	9 vs. 23	0
sll1054	hypothetical protein	32	-1.1	11.75 vs. 23	0.0000284
sll1060	hypothetical protein	59	-2.2	9 vs. 23	0
sll1061	unknown protein	170	-1.0	1 vs. 23	1.748E-10
sll1063	hypothetical protein	125	-1.2	1 vs. 23	1.666E-11
sll1068	unknown protein	43	2.5	3 vs. 13	0
sll1069	3-oxoacyl-[acyl-carrier-protein] synthase II	237	1.6	1 vs. 13	0
sll1070	transketolase	1777	-2.0	9 vs. 23	0

sll1071	hypothetical protein	87	1.9	0.25 vs. 11.75	0
sll1072	hypothetical protein	70	1.4	0.25 vs. 11.75	0
sll1080	ABC transport system substrate-binding protein	56	1.7	1 vs. 18	0
sll1082	ABC transport system ATP-binding protein	8	-1.9	-0.25 vs. 9	0.0000011 84
sll1086	unknown protein	856	-3.5	1 vs. 13	0
sll1087	similar to sodium/glucose cotransporter	144	-1.7	0.25 vs. 13	0
sll1092	hypothetical protein	221	-2.2	-0.25 vs. 6	0
sll1094	putative transposase	73	-1.1	0.25 vs. 11	0.0000035 43
sll1108	stationary-phase survival protein SurE homolog	185	1.3	1 vs. 9	0
sll1109	hypothetical protein	846	3.0	6 vs. 18	0
sll1118	hypothetical protein	122	1.2	11 vs. 23	0
sll1119	hypothetical protein	117	2.6	0.25 vs. 12.25	0
sll1121	hypothetical protein	12	-1.1	6 vs. 18	0
sll1123	hypothetical protein	78	-2.5	3 vs. 13	0
sll1129	2-hydroxy-6-oxohepta-2.4-dienoate hydrolase	38	-2.4	9 vs. 18	0
sll1130	unknown protein	2472	2.7	1 vs. 13	0
sll1131	unknown protein	188	1.5	0.25 vs. 13	0
sll1132	unknown protein	65	1.7	6 vs. 13	0
sll1135	unknown protein	32	-1.9	1 vs. 13	0
sll1138	hypothetical protein	63	-1.9	3 vs. -0.25	0
sll1147	glutathione S-transferase	163	1.3	-0.25 vs. 11	0
sll1151	unknown protein	69	-1.1	11 vs. 23	0
sll1154	putative antibiotic efflux protein	239	-3.5	9 vs. 23	0
sll1155	hypothetical protein	295	-1.6	1 vs. -0.25	0
sll1156	putative transposase [ISY120b: 1385747 - 1386548]	117	-1.3	0.25 vs. 23	0
sll1158	hypothetical protein	47	3.2	1 vs. 13	0
sll1160	hypothetical protein	46	1.1	1 vs. 13	7.396E-09
sll1162	hypothetical protein	24	1.7	3 vs. 18	0
sll1163	unknown protein	29	1.8	3 vs. 23	2.439E-12
sll1164	hypothetical protein	94	1.8	9 vs. 23	0
sll1165	DNA mismatch repair protein	36	1.8	1 vs. -0.25	0
sll1166	hypothetical protein	92	1.1	3 vs. -0.25	1.475E-10
sll1169	hypothetical protein	7	-1.3	1 vs. 13	0.0275199 03
sll1170	unknown protein	49	-1.1	1 vs. 13	6.483E-10
sll1173	hypothetical protein	51	2.2	3 vs. 13	0
sll1174	unknown protein	63	2.2	3 vs. 13	0
sll1178	probable carbamoyl transferase	132	1.7	1 vs. 13	0
sll1181	similar to hemolysin secretion protein	299	-1.2	9 vs. 18	0

sll1186	hypothetical protein	126	-1.7	1 vs. 13	0
sll1187	prolipoprotein diacylglyceryl transferase	139	1.7	6 vs. 23	0
sll1188	hypothetical protein	182	1.7	6 vs. 0.25	0
sll1191	hypothetical protein	209	-1.5	3 vs. 11.75	0.017686491
sll1193	hypothetical protein	276	-1.8	3 vs. 18	0
sll1196	phosphofructokinase	177	-3.9	0.25 vs. 12.25	0
sll1198	tRNA (guanine-N1)-methyltransferase	304	-2.0	0.25 vs. 11.75	0
sll1200	hypothetical protein	50	1.1	1 vs. 13	0
sll1201	hypothetical protein	301	1.0	-0.25 vs. 11.75	0
sll1202	iron(III) dicitrate-binding protein of ABC transporter. FecB homolog	55	1.5	6 vs. 23	0
sll1203	hypothetical protein	33	2.0	6 vs. 23	0
sll1204	similar to macrolide efflux protein	18	-2.2	-0.25 vs. 9	0
sll1212	GDP-mannose 4.6-dehydratase	168	2.9	1 vs. 13	0
sll1213	GDP-fucose synthetase	148	1.8	1 vs. 13	0
sll1217	unknown protein	43	-1.1	0.25 vs. 13	5.218E-09
sll1219	hypothetical protein	664	2.6	1 vs. 13	0
sll1222	hypothetical protein	143	-2.4	1 vs. 12.25	0
sll1225	unknown protein	373	2.1	12.25 vs. 23	0
sll1231	mannosyltransferase	55	-2.3	-0.25 vs. 6	0
sll1232	hypothetical protein	67	2.1	3 vs. 18	0
sll1233	hypothetical protein	54	1.5	1 vs. 13	0
sll1234	adenosylhomocysteinase	2549	2.5	-0.25 vs. 12.25	0
sll1239	unknown protein	1573	-2.9	0.25 vs. 11	0
sll1240	unknown protein	876	3.4	11 vs. 23	0
sll1241	unknown protein	458	-3.8	-0.25 vs. 11	0
sll1247	hypothetical protein	443	-2.7	1 vs. -0.25	0
sll1250	hypothetical protein	56	1.2	9 vs. 23	2.569E-10
sll1251	hypothetical protein	56	-2.7	1 vs. 13	0
sll1252	hypothetical protein	23	1.7	6 vs. 13	0
sll1254	hypothetical protein	137	1.2	-0.25 vs. 11.75	0
sll1255	putative transposase [ISY203c: 1728942 - 1730115]	22	1.7	6 vs. 13	0
sll1258	dCTP deaminase	81	2.3	3 vs. 23	0
sll1263	cation efflux system protein	185	2.2	1 vs. 13	0
sll1265	unknown protein	39	-1.3	1 vs. 13	0
sll1267	unknown protein	842	1.9	6 vs. 23	0
sll1268	unknown protein	557	-3.3	3 vs. 18	0
sll1271	probable porin; major outer membrane protein	101	2.4	1 vs. 18	0
sll1272	unknown protein	337	-1.4	-0.25 vs. 9	0

sll1273	unknown protein	543	1.6	6 vs. 23	0
sll1274	hypothetical protein	111	-1.8	6 vs. 18	0
sll1283	similar to stage II sporulation protein D	125	1.5	6 vs. 13	0
sll1284	esterase	135	1.2	1 vs. 13	0
sll1285	hypothetical protein	77	3.4	6 vs. 13	0
sll1289	hypothetical protein	80	1.4	1 vs. 12.25	0
sll1293	unknown protein	402	1.0	1 vs. 9	0
sll1294	methyl-accepting chemotaxis protein	123	1.7	1 vs. 12.25	0
sll1297	probable dioxygenase. Rieske iron-sulfur component	123	1.7	6 vs. 12.25	0
sll1298	putative carboxymethylenebutenolidase	58	-1.0	-0.25 vs. 11.75	0
sll1299	acetate kinase	31	1.2	6 vs. 18	0
sll1304	unknown protein	136	1.7	11 vs. 23	0
sll1305	probable hydrolase	144	-2.1	-0.25 vs. 11	0
sll1306	periplasmic protein. function unknown	124	1.7	11 vs. 23	0
sll1307	periplasmic protein. function unknown	264	-1.6	0.25 vs. 12.25	0
sll1308	probable oxidoreductase	31	1.6	11.75 vs. 18	0
sll1314	putative C4-dicarboxylase binding protein. periplasmic protein	257	-1.4	-0.25 vs. 11	0
sll1315	unknown protein	235	1.8	11 vs. 23	0
sll1318	hypothetical protein	45	1.5	6 vs. 13	0
sll1319	hypothetical protein	27	2.1	3 vs. -0.25	0
sll1321	hypothetical protein	17383	3.1	3 vs. 18	0
sll1333	unknown protein	56	-1.2	0.25 vs. 12.25	0
sll1338	unknown protein	38818	-3.7	3 vs. 13	0
sll1340	hypothetical protein	76	-1.1	6 vs. 0.25	4.307E-09
sll1344	unknown protein	83	1.2	6 vs. 18	0
sll1348	hypothetical protein	27	2.1	6 vs. 13	0
sll1349	phosphoglycolate phosphatase	92	-1.0	-0.25 vs. 6	3.563E-07
sll1355	hypothetical protein	1560	-4.0	6 vs. 23	0
sll1356	glycogen phosphorylase	53	-2.7	1 vs. 12.25	0
sll1358	putative oxalate decarboxylase. periplasmic protein	273	-3.4	0.25 vs. 12.25	0
sll1359	unknown protein	47	-2.3	0.25 vs. 12.25	0
sll1367	hypothetical protein	84	-1.2	1 vs. 23	0
sll1373	unknown protein	53	1.5	9 vs. 18	0
sll1376	hypothetical protein	175	1.3	0.25 vs. 11	0
sll1377	probable glycosyltransferase	154	-1.4	9 vs. 18	0
sll1378	periplasmic protein. function unknown	45	1.6	1 vs. 12.25	0
sll1381	hypothetical protein	75	-1.1	-0.25 vs. 6	6.503E-12
sll1386	hypothetical protein	36	2.9	-0.25 vs. 9	0
sll1388	hypothetical protein	80	-1.7	3 vs. -0.25	0

sll1389	hypothetical protein	31	1.8	18 vs. 11	0
sll1396	unknown protein	241	2.1	-0.25 vs. 11.75	0
sll1399	hypothetical protein	177	-2.5	-0.25 vs. 11	0
sll1400	hypothetical protein	298	1.8	11 vs. 23	0
sll1401	unknown protein	338	1.4	11 vs. 23	0
sll1404	biopolymer transport ExbB protein homolog	28	-3.3	9 vs. 18	0
sll1405	biopolymer transport ExbD protein homolog	15	-2.9	9 vs. 23	0
sll1406	ferrichrome-iron receptor	27	-1.4	1 vs. 18	0
sll1407	probable methyltransferase	30	1.3	3 vs. -0.25	0
sll1411	hypothetical protein	58	-1.9	-0.25 vs. 9	0
sll1414	hypothetical protein	112	1.2	6 vs. 13	0
sll1426	unknown protein	217	1.2	-0.25 vs. 6	0
sll1427	protease	552	-3.1	6 vs. 23	0
sll1429	unknown protein	237	-1.9	1 vs. 9	0
sll1430	adenine phosphoribosyltransferase	143	2.4	1 vs. 23	0
sll1433	hypothetical protein	76	-3.1	3 vs. 13	0
sll1434	penicillin-binding protein	495	-2.6	6 vs. 23	0
sll1439	unknown protein	155	2.0	6 vs. 23	0
sll1442	hypothetical protein	116	1.0	9 vs. 12.25	1.056E-07
sll1444	3-isopropylmalate dehydratase small subunit	283	-1.5	11 vs. 23	0
sll1447	hypothetical protein	147	1.1	0.25 vs. 23	0
sll1455	hypothetical protein	231	2.4	6 vs. 23	0
sll1456	unknown protein	49	2.6	3 vs. 13	0
sll1457	probable glycosyltransferase	143	2.3	6 vs. 13	0
sll1461	hypothetical protein	137	1.1	-0.25 vs. 6	0
sll1464	hypothetical protein	29	1.0	1 vs. 23	0
sll1466	probable glycosyltransferase	97	1.8	0.25 vs. 13	0
sll1469	hypothetical protein	46	-1.2	12.25 vs. 11	0
sll1472	unknown protein	277	1.9	9 vs. 13	0
sll1473	a part of phytochrome-like sensor histidine kinase gene (disrupted by insertion of IS)	68	-1.9	1 vs. 6	0
sll1479	6-phosphogluconolactonase	122	-3.0	3 vs. 12.25	0
sll1481	ABC-transporter membrane fusion protein	116	-1.8	3 vs. 18	0
sll1482	ABC transporter permease protein	67	-2.4	12.25 vs. 23	0
sll1483	periplasmic protein. similar to transforming growth factor induced protein	472	2.8	1 vs. 12.25	0
sll1485	hypothetical protein	81	-1.7	3 vs. 13	0
sll1486	hypothetical protein	152	-1.9	6 vs. 12.25	0
sll1488	hypothetical protein	332	-2.0	6 vs. 23	0
sll1491	periplasmic WD-repeat protein	76	-2.4	1 vs. 12.25	0
sll1496	mannose-1-phosphate guanyltransferase	52	-1.7	6 vs. 23	0
sll1498	carbamoyl-phosphate synthase small chain	236	-1.8	6 vs. 18	0
sll1503	unknown protein	1285	2.4	9 vs. 23	0

sll1504	hypothetical protein	849	-3.5	-0.25 vs. 9	0
sll1505	hypothetical protein	448	-3.7	-0.25 vs. 6	0
sll1508	UDP-3-0-acyl N-acetylglcosamine deacetylase	42	2.2	1 vs. 13	0
sll1510	unknown protein	81	-1.4	-0.25 vs. 9	0
sll1511	unknown protein	48	1.0	0.25 vs. 23	0.0000229 2
sll1512	hypothetical protein	75	-1.3	1 vs. 18	0
sll1516	hypothetical protein	18	1.1	1 vs. 11	0
sll1524	hypothetical protein	123	1.3	1 vs. 12.25	0
sll1526	hypothetical protein	344	2.8	3 vs. 13	0
sll1527	unknown protein	176	4.4	3 vs. 23	0
sll1528	unknown protein	114	2.5	3 vs. 18	0
sll1530	unknown protein	200	2.8	3 vs. 18	0
sll1531	unknown protein	241	3.7	3 vs. 13	0
sll1534	probable glycosyltransferase	95	-1.2	1 vs. 13	0
sll1537	similar to mutator MutT protein	80	3.0	3 vs. 13	0
sll1538	similar to beta-hexosaminidase a precursor	61	1.6	1 vs. 13	0
sll1541	hypothetical protein	47	2.9	0.25 vs. 11.75	0
sll1542	hypothetical protein	37	-1.1	1 vs. 13	1.624E-07
sll1545	glutathione S-transferase	85	1.1	-0.25 vs. 11	0
sll1547	hypothetical protein	38	-1.3	-0.25 vs. 6	8.129E-13
sll1549	salt-enhanced periplasmic protein	6	-1.2	1 vs. 6	0.006236
sll1550	probable porin; major outer membrane protein	120	-1.0	1 vs. 23	0.0064
sll1552	unknown protein	10	1.6	12.25 vs. 23	0.0291426 19
sll1556	isopentenyl-dephosphate delta-isomerase	55	-1.6	-0.25 vs. 12.25	0
sll1558	mannose-1-phosphate guanyltransferase	121	-1.2	-0.25 vs. 9	0
sll1560	putative transposase [ISY203d: 1970882 - 1972055]	17	4.4	6 vs. 18	0
sll1562	unknown protein	360	1.9	6 vs. 13	0
sll1563	unknown protein	344	2.4	6 vs. 13	0
sll1564	putative lyase	142	-2.7	6 vs. 18	0
sll1568	fibrillin	157	1.2	6 vs. 13	0
sll1570	unknown protein	46	-1.5	9 vs. 18	0
sll1571	hypothetical protein	567	-2.3	6 vs. 13	0
sll1573	hypothetical protein	146	-1.3	1 vs. 12.25	0
sll1582	unknown protein	272	2.8	6 vs. 23	0
sll1583	unknown protein	129	-1.7	0.25 vs. 11.75	0
sll1584	ferredoxin like protein	54	2.1	12.25 vs. 23	0
sll1586	unknown protein	44	-1.3	1 vs. 13	0
sll1601	hypothetical protein	71	2.7	-0.25 vs. 6	0
sll1605	(3R)-hydroxymyristol acyl carrier protein	149	2.1	3 vs. 13	0

	dehydrase				
sll1606	hypothetical protein	155	1.4	1 vs. 18	0
sll1611	unknown protein	52	-1.5	-0.25 vs. 9	0
sll1615	thiophen and furan oxidation protein	24	1.6	1 vs. 12.25	0
sll1618	hypothetical protein	208	-1.8	9 vs. 0.25	0
sll1620	hypothetical protein	248	1.9	1 vs. 13	0
sll1621	AhpC/TSA family protein	5267	2.0	3 vs. 11	4.065E-12
sll1623	ABC transporter ATP-binding protein	46	-1.7	3 vs. 18	0
sll1629	bacterial cryptochrome	47	3.1	6 vs. 13	0
sll1630	unknown protein	69	-1.3	-0.25 vs. 6	0
sll1631	putative cytidine and deoxycytidylate deaminase	57	1.5	1 vs. 12.25	0
sll1632	hypothetical protein	120	-1.1	0.25 vs. 12.25	0
sll1634	hypothetical protein	35	1.7	1 vs. 13	0
sll1635	Thy1 protein homolog	42	3.4	3 vs. 13	0
sll1636	ferripyochelin binding protein	98	1.3	1 vs. 13	0
sll1638	hypothetical protein	5502	3.0	3 vs. 13	0
sll1640	hypothetical protein	39	2.1	1 vs. 13	0
sll1641	glutamate decarboxylase	101	-2.0	0.25 vs. 12.25	0
sll1642	hypothetical protein	94	-2.2	-0.25 vs. 6	0
sll1643	hypothetical protein	243	-2.7	3 vs. 13	0
sll1647	probable phosphinothricin N-acetyltransferase	93	-1.1	6 vs. 12.25	0
sll1651	hypothetical protein	363	-1.2	1 vs. 6	0
sll1652	hypothetical protein	261	1.3	6 vs. 11.75	0.000009604
sll1654	hypothetical protein	429	-1.9	6 vs. 13	0
sll1655	similar to biotin [acetyl-CoA-carboxylase] ligase	389	-2.5	6 vs. 13	0
sll1656	hypothetical protein	747	-3.0	9 vs. 23	0
sll1658	hypothetical protein	41	-2.6	3 vs. 13	0
sll1659	hypothetical protein	66	-1.6	3 vs. 18	0
sll1662	probable prephenate dehydratase	223	-2.3	6 vs. 23	0
sll1663	phycocyanin alpha phycocyanobilin lyase related protein	261	1.2	23 vs. 13	0
sll1665	unknown protein	613	-1.7	3 vs. 12.25	0
sll1666	DnaJ-like protein	150	-2.7	3 vs. 18	0
sll1667	periplasmic protein. similar to mitochondrial outer membrane 72K protein	56	-1.2	11 vs. 23	0
sll1675	hypothetical protein	187	-1.6	6 vs. 18	0
sll1676	4-alpha-glucanotransferase	68	-1.7	3 vs. 23	0
sll1677	similar to spore maturation protein B	105	1.5	3 vs. 23	0
sll1678	similar to spore maturation protein A	72	1.7	9 vs. 23	0
sll1682	alanine dehydrogenase	29	1.1	0.25 vs. 13	3.386E-10
sll1683	lysine decarboxylase	22	1.9	1 vs. 13	0
sll1686	hypothetical protein	49	1.4	3 vs. 13	0

sll1691	hypothetical protein	35	-1.2	11.75 vs. 23	0.0000957
sll1696	hypothetical protein	353	-1.3	1 vs. 11	0
sll1697	hypothetical protein	207	-2.6	9 vs. 23	0
sll1698	hypothetical protein	34	1.8	9 vs. 23	1.565E-09
sll1699	oligopeptide-binding protein of oligopeptide ABC transporter	46	2.0	6 vs. 13	0
sll1703	protease IV	39	2.1	1 vs. 13	0
sll1704	probable short chain dehydrogenase	28	1.6	3 vs. 12.25	0
sll1709	3-ketoacyl-acyl carrier protein reductase	102	1.5	1 vs. 13	0
sll1710	putative transposase [ISY523b: 1275354 - 1276224]	73	1.3	1 vs. 23	0
sll1712	DNA binding protein HU	4952	-1.3	0.25 vs. 13	0
sll1714	unknown protein	133	-1.2	3 vs. 13	0
sll1715	hypothetical protein	134	-1.1	1 vs. 13	0
sll1716	putative transposase [ISY523a: 967549 - 968419]	29	-1.2	23 vs. 13	0.000001869
sll1717	unknown protein	101	1.3	9 vs. 23	0
sll1721	pyruvate dehydrogenase E1 component. beta subunit	162	1.7	3 vs. 13	0
sll1722	hypothetical protein	13	-1.4	1 vs. 18	0
sll1724	probable glycosyltransferase	9	-1.5	1 vs. 12.25	0.000001519
sll1730	unknown protein	230	2.4	-0.25 vs. 6	0
sll1738	hypothetical protein	102	-3.0	-0.25 vs. 6	0
sll1751	hypothetical protein	215	1.6	3 vs. 23	0
sll1752	hypothetical protein	136	-2.6	3 vs. 13	0
sll1757	hypothetical protein	208	1.3	6 vs. 13	0
sll1758	MrsA protein homolog	344	-2.0	6 vs. 13	0
sll1762	periplasmic protein. putative polar amino acid transport system substrate-binding protein	196	1.3	11.75 vs. 23	0
sll1763	unknown protein	115	-1.3	3 vs. -0.25	0
sll1764	unknown protein	51	-1.2	3 vs. 18	5.487E-11
sll1765	unknown protein	115	-1.0	1 vs. 18	0
sll1768	probable oligopeptides ABC transporter permease protein	67	1.7	-0.25 vs. 9	0
sll1769	hypothetical protein	387	2.2	0.25 vs. 12.25	0
sll1770	hypothetical protein	93	1.3	1 vs. 12.25	0
sll1773	hypothetical protein	95	-2.6	9 vs. 18	0
sll1774	hypothetical protein	189	-2.1	1 vs. 13	0
sll1776	deoxyribose-phosphate aldolase	48	1.8	1 vs. 12.25	0
sll1783	hypothetical protein	1114	-1.9	1 vs. 11	0
sll1784	periplasmic protein. function unknown	449	-1.5	1 vs. 12.25	0
sll1785	periplasmic protein. function unknown	238	-1.3	-0.25 vs. 12.25	0
sll1791	putative transposase [ISY802a: 852462 - 853369]	33	-2.1	1 vs. 13	0
sll1825	hypothetical protein	251	-1.6	1 vs. 18	0

sll1830	unknown protein	92	-2.8	-0.25 vs. 11.75	0
sll1832	hypothetical protein	475	-2.2	9 vs. 18	0
sll1833	penicillin-binding protein	111	-2.0	9 vs. 23	0
sll1835	periplasmic protein. function unknown	150	3.0	6 vs. 18	0
sll1841	pyruvate dehydrogenase dihydrolipoamide acetyltransferase component (E2)	655	-2.2	9 vs. 23	0
sll1852	nucleoside diphosphate kinase	653	3.2	1 vs. 12.25	0
sll1853	unknown protein	167	3.7	1 vs. 12.25	0
sll1854	exodeoxyribonuclease III	25	2.3	1 vs. 13	0
sll1858	unknown protein	67	-1.0	3 vs. 23	0
sll1860	putative transposase [ISY523d: 2226601 - 2227471]	37	-1.3	6 vs. 12.25	0
sll1861	putative transposase [ISY523o(partial copy): 2225804 - 2226597]	78	-1.2	1 vs. 13	7.194E-11
sll1862	unknown protein	1453	2.4	-0.25 vs. 23	0.0000482 4
sll1863	unknown protein	211	-1.8	6 vs. 23	0
sll1864	probable chloride channel protein	15	-1.4	6 vs. 18	0
sll1866	hypothetical protein	84	2.1	0.25 vs. 13	0
sll1870	ATP-binding protein of ABC transporter	57	-2.7	-0.25 vs. 6	0
sll0485	two-component response regulator NarL subfamily	78	-1.7	1 vs. 12.25	0
sll0594	transcriptional regulator	32	-1.0	3 vs. 23	0.0000030 77
sll1873	unknown protein	2770	2.4	6 vs. 23	0
sll1874	hypothetical protein	6	-1.7	-0.25 vs. 6	0.006961
sll1878	iron(III)-transport ATP-binding protein	434	-2.7	3 vs. 23	0
sll1882	unknown protein	165	-3.7	1 vs. 13	0
sll1886	hypothetical protein	230	-2.0	3 vs. 23	0
sll0649	two-component response regulator OmpR subfamily	36	1.6	6 vs. 12.25	0
sll1890	cobalt-chelatase subunit CobN-like protein	161	-1.2	-0.25 vs. 9	0
sll1892	unknown protein	154	2.7	-0.25 vs. 11	0
sll1898	hypothetical protein	676	-3.8	0.25 vs. 12.25	0
sll0782	transcriptional regulator	20	1.5	0.25 vs. 12.25	8.292E-11
sll1911	hypothetical protein	262	3.6	3 vs. 18	0
sll1913	hypothetical protein	17	-1.4	-0.25 vs. 6	0
sll1915	hypothetical protein	282	-2.2	6 vs. 23	0
sll1921	hypothetical protein	376	-2.3	6 vs. 23	0
sll0789	two-component response regulator OmpR subfamily	131	-2.7	11 vs. 23	0
sll1926	hypothetical protein	1514	-2.9	1 vs. 12.25	0
sll1927	ABC transporter ATP-binding protein	123	-1.5	6 vs. 12.25	0
sll1934	hypothetical protein	127	-2.8	9 vs. 18	0
sll1005	MazG protein homolog	13	1.7	1 vs. -0.25	3.926E-08
sll1938	hypothetical protein	80	-1.3	1 vs. 13	0

sll1939	unknown protein	115	-1.1	-0.25 vs. 9	0
sll1942	unknown protein	171	-1.5	9 vs. 18	0
sll1945	1-deoxyxylulose-5-phosphate synthase	1785	-2.0	6 vs. 23	0
sll1949	unknown protein	337	-1.7	1 vs. 23	0
sll1950	unknown protein	102	-1.8	6 vs. 13	0
sll1951	unknown protein	1702	1.0	-0.25 vs. 0.25	0
sll1959	probable inositol monophosphatase	32	2.9	1 vs. 13	0
sll1960	hypothetical protein	90	1.7	1 vs. 13	0
sll1965	hypothetical protein	51	-1.9	-0.25 vs. 9	0
sll1973	hypothetical protein	288	-1.1	9 vs. 23	0
sll1979	hypothetical protein	277	1.1	1 vs. 13	0
sll1982	putative transposase [ISY352c: 1553414 - 1553903. join 1554854 - 1555790]	356	-1.9	1 vs. 23	0
sll1985	putative transposase [ISY352c: 1553414 - 1553903. join 1554854 - 1555790]	66	2.0	1 vs. 23	0
sll1999	putative transposase [ISY203h: 1623060 - 1623693. join 1624643 - 1625182]	21	9.0	3 vs. 0.25	1.179E-11
sll2002	hypothetical protein	50	1.5	3 vs. 12.25	0
sll2003	hypothetical protein	111	1.4	23 vs. 13	0
sll2006	hypothetical protein	83	1.6	1 vs. 12.25	0
sll2008	processing protease	227	-3.0	3 vs. 13	0
sll2009	processing protease	75	-1.9	3 vs. 18	0
sll2011	hypothetical protein	54	1.6	1 vs. 12.25	0
sll2013	hypothetical protein	171	2.8	6 vs. 18	0
sll1161	probable adenylate cyclase	35	1.2	11 vs. 23	0
slr0001	hypothetical protein	544	1.0	0.25 vs. 11.75	0
slr0006	unknown protein	330	-2.7	1 vs. 12.25	0
slr0013	hypothetical protein	329	2.0	3 vs. 13	0
slr0018	fumarase	33	1.5	-0.25 vs. 12.25	0
slr0023	unknown protein	70	1.5	6 vs. 12.25	0
slr0038	hypothetical protein	208	1.6	-0.25 vs. 9	0
slr0042	probable porin; major outer membrane protein	24	-1.8	6 vs. 18	0
slr0053	hypothetical protein	221	-2.1	3 vs. 23	0
slr0054	diacylglycerol kinase	412	-2.3	3 vs. 23	0
slr0060	unknown protein	49	1.2	6 vs. 23	0
slr0064	hypothetical protein	55	1.1	-0.25 vs. 11	0
slr0067	MRP protein homolog	118	-1.7	9 vs. 23	0
slr0069	unknown protein	41	1.2	9 vs. 23	2.306E-09
sll1286	transcriptional regulator	159	-3.0	0.25 vs. 12.25	0
slr0078	putative 6-pyruvoyl tetrahydrobiopterin synthase	108	-1.1	9 vs. 18	0
slr0079	probable general secretion pathway protein E	79	-2.0	6 vs. 18	0

sll1291	two-component response regulator PatA subfamily	225	1.3	0.25 vs. 18	0
slr0082	hypothetical protein	677	2.0	-0.25 vs. 11	0
slr0086	similar to DnaK protein	45	1.7	1 vs. 13	0
slr0089	gamma-tocopherol methyltransferase	50	-1.6	3 vs. 13	0
slr0090	probable 4-hydroxyphenylpyruvate dioxygenase	23	1.6	9 vs. 23	0
slr0091	aldehyde dehydrogenase	19	1.9	9 vs. 23	0
slr0092	hypothetical protein	12	2.5	6 vs. 18	0
slr0096	low affinity sulfate transporter	68	-4.2	3 vs. 13	0
slr0103	unknown protein	92	-2.0	3 vs. 18	0
slr0108	unknown protein	119	1.4	-0.25 vs. 23	0
slr0109	unknown protein	18	1.4	0.25 vs. 23	0
slr0110	hypothetical protein	158	2.0	1 vs. 13	0
slr0111	unknown protein	85	2.5	6 vs. 13	0
slr0112	unknown protein	85	-1.5	3 vs. 18	0
sll1292	two-component response regulator CheY subfamily	375	1.8	1 vs. 18	0
slr0119	hypothetical protein	101	1.6	1 vs. 23	0
slr0120	probable tRNA/rRNA methyltransferase	18	1.4	1 vs. -0.25	0.009747
slr0142	hypothetical protein	14	-1.8	-0.25 vs. 9	0.0000489
slr0144	hypothetical protein	1315	-4.0	1 vs. 12.25	0
slr0145	unknown protein	314	-3.7	3 vs. 13	0
slr0146	hypothetical protein	535	-4.1	3 vs. 13	0
slr0147	hypothetical protein	1472	-4.3	3 vs. 13	0
slr0148	hypothetical protein	491	-2.7	0.25 vs. 13	0
slr0149	hypothetical protein	392	-2.7	0.25 vs. 13	0
slr0151	unknown protein	1732	-4.2	3 vs. 13	0
sll1329	inositol monophosphate family protein	140	-2.1	3 vs. 23	0
slr0157	unknown protein	353	3.0	6 vs. 13	0
slr0168	unknown protein	109	2.2	3 vs. 23	0
slr0169	hypothetical protein	197	1.1	1 vs. 13	0
slr0172	hypothetical protein	174	1.2	6 vs. 13	0
slr0179	hypothetical protein	312	-3.6	1 vs. 12.25	0
slr0180	putative transposase [ISY203f: 2326926 - 2328099]	23	-2.7	-0.25 vs. 11.75	0
slr0181	hypothetical protein	195	-1.3	0.25 vs. 12.25	0
slr0184	unknown protein	91	-2.5	3 vs. 18	0
slr0191	amidase enhancer. periplasmic protein	47	-1.6	9 vs. 23	0
slr0195	hypothetical protein	73	1.1	3 vs. 13	0
slr0196	unknown protein	40	-1.4	3 vs. 12.25	0
slr0201	heterodisulfide reductase subunit B	85	-2.5	3 vs. 13	0
slr0207	hypothetical protein	44	-1.5	3 vs. 13	0
slr0209	unknown protein	452	2.4	6 vs. 12.25	0

sll1330	two-component system response regulator OmpR subfamily	228	2.5	11.75 vs. 23	0
slr0211	hypothetical protein	445	-1.7	6 vs. 23	0
slr0214	cytosine-specific methyltransferase(5'-CGATCG-3')	27	1.3	9 vs. 18	0
slr0217	hypothetical protein	210	-2.3	3 vs. 12.25	0
slr0226	unknown protein	319	-3.6	1 vs. 23	0
slr0229	3-hydroxyisobutyrate dehydrogenase	43	-1.4	-0.25 vs. 6	0
slr0231	probable DNA-3-methyladenine glycosylase	18	3.8	3 vs. 23	0
slr0232	hypothetical protein	67	1.4	-0.25 vs. 6	0
slr0236	similar to glutathione S-transferase	306	-1.5	6 vs. 18	0
slr0237	glycogen operon protein GlgX homolog	49	-2.4	0.25 vs. 13	0
slr0238	hypothetical protein	142	-1.5	-0.25 vs. 11	0
sll1334	two-component sensor histidine kinase	181	-1.1	3 vs. 23	0
slr0241	hypothetical protein	198	-1.4	6 vs. 13	0
slr0242	bacterioferritin comigratory protein homolog	154	-1.0	0.25 vs. 18	0
slr0243	hypothetical protein	59	1.9	6 vs. 23	0
slr0244	hypothetical protein	333	-3.1	0.25 vs. 12.25	0
slr0245	Histone deacetylase family protein	47	-2.3	6 vs. 13	0
slr0249	hypothetical protein	54	-2.3	6 vs. 13	0
slr0250	hypothetical protein	488	-2.6	6 vs. 18	0
slr0252	probable precorrin-6x reductase	34	2.6	3 vs. 13	0
slr0254	hypothetical protein	47	-2.4	9 vs. 23	0
slr0262	unknown protein	1604	-2.1	-0.25 vs. 12.25	0
slr0264	hypothetical protein	150	-3.5	6 vs. 23	0
slr0265	putative transposase [ISY523c: 1513158 - 1514023]	49	-1.2	3 vs. 13	3.402E-09
slr0267	hypothetical protein	23	1.1	1 vs. -0.25	0.009048
slr0269	hypothetical protein	51	-2.7	6 vs. 23	0
slr0270	hypothetical protein	329	1.6	-0.25 vs. 11	0
slr0271	unknown protein	67	-2.9	1 vs. 13	0
slr0272	unknown protein	15	-2.7	1 vs. 23	0
slr0280	hypothetical protein	51	-1.3	3 vs. 18	0
slr0285	hypothetical protein	75	1.4	6 vs. 23	0
slr0286	protein involved in functional assembly of photosystem II	172	2.0	6 vs. 12.25	0
slr0287	hypothetical protein	2188	2.5	0.25 vs. 12.25	0
slr0291	hypothetical protein	167	-1.5	-0.25 vs. 9	0
slr0292	hypothetical protein	172	3.0	-0.25 vs. 11.75	0
slr0293	glycine dehydrogenase	97	-1.7	11 vs. 23	0
slr0294	unknown protein	419	2.2	6 vs. 18	0
slr0298	FraH protein homolog	227	-3.7	3 vs. 13	0
slr0299	hypothetical protein	59	-2.0	3 vs. 13	0

slr0301	phosphoenolpyruvate synthase	426	-6.3	1 vs. 13	0
slr0303	hypothetical protein	27	1.5	6 vs. 23	0
slr0304	hypothetical protein	43	1.4	6 vs. 23	0
slr0305	hypothetical protein	37	-1.3	-0.25 vs. 11	0
slr0309	probable methyltransferase	69	-1.9	3 vs. 12.25	0
slr0315	probable oxidoreductase	15	-1.2	1 vs. 18	1.504E-11
slr0318	unknown protein	49	1.7	1 vs. 13	0
slr0319	beta-lactamase	26	1.4	6 vs. 13	0
slr0320	hypothetical protein	55	1.6	0.25 vs. 11	0
sll1383	probable myo-inositol-1(or 4)-monophosphatase	50	-1.1	11 vs. 13	0
slr0323	putative alpha-mannosidase	208	1.7	6 vs. 23	0
slr0324	probable oligopeptides ABC transporter permease protein	89	1.7	1 vs. -0.25	0
slr0325	hypothetical protein	31	3.3	3 vs. 23	0
slr0328	low molecular weight phosphotyrosine protein phosphatase	54	2.0	3 vs. 13	0
slr0329	glucokinase	46	1.9	1 vs. 23	0
slr0333	unknown protein	9238	6.2	9 vs. 0.25	0
slr0334	unknown protein	5258	6.1	9 vs. 0.25	0
slr0337	hypothetical protein	76	-2.7	3 vs. 12.25	0
slr0338	probable oxidoreductase	260	-1.7	12.25 vs. 23	0
slr0344	probable glycosyltransferase	46	-2.8	-0.25 vs. 9	0
slr0345	unknown protein	411	1.1	1 vs. 13	0
slr0350	putative transposase [ISY523e: 2441031 - 2441901]	28	-9.8	-0.25 vs. 11.75	0.002348
slr0352	putative transposase [ISY100e: 2443927 - 2444873]	9	5.3	3 vs. -0.25	1.219E-12
slr0353	unknown protein	97	2.9	6 vs. 18	0
slr0354	ATP-binding protein of ABC transporter	92	1.4	3 vs. 18	0
slr0355	hypothetical protein	95	-2.1	9 vs. 23	0
slr0356	hypothetical protein	161	-1.3	1 vs. 23	0
slr0358	unknown protein	148	-1.7	0.25 vs. 13	0
slr0359	hypothetical protein	85	-1.8	1 vs. 12.25	0
slr0362	hypothetical protein	113	1.6	1 vs. 13	0
slr0363	hypothetical protein	76	-2.2	6 vs. 13	0
slr0364	hypothetical protein	11	-1.2	1 vs. 18	0
slr0366	unknown protein	18	-1.7	1 vs. 18	0
slr0368	unknown protein	638	-2.4	3 vs. 12.25	0
slr0369	RND multidrug efflux transporter	219	-2.0	1 vs. 13	0
slr0370	succinate-semialdehyde dehydrogenase (NADP+)	240	-2.4	6 vs. 18	0
slr0373	hypothetical protein	94964	-4.7	6 vs. 18	0
slr0374	hypothetical protein	91985	-5.0	6 vs. 18	0
slr0376	hypothetical protein	60376	-3.4	1 vs. 12.25	0
slr0377	unknown protein	113	-1.3	3 vs. 13	0

slr0381	lactoylglutathione lyase	140	1.5	1 vs. 12.25	0
slr0383	hypothetical protein	31	1.5	1 vs. 13	0
slr0388	hypothetical protein	20	-1.1	3 vs. 13	0.0004151
slr0392	unknown protein	857	2.7	6 vs. 23	0
slr0393	unknown protein	453	3.5	6 vs. 23	0
slr0397	hypothetical protein	55	-1.8	3 vs. 13	0
slr0400	hypothetical protein	108	-1.2	9 vs. 0.25	0
slr0401	periplasmic polyamine-binding protein of ABC transporter	187	-1.0	12.25 vs. 23	4.959E-11
slr0402	hypothetical protein	43	1.3	1 vs. -0.25	6.528E-10
slr0404	hypothetical protein	1264	-2.3	9 vs. 13	0
sll1392	transcriptional regulator	14	-1.9	0.25 vs. 18	8.129E-13
slr0420	hypothetical protein	440	1.8	3 vs. 18	0
slr0423	hypothetical protein	148	3.4	1 vs. -0.25	0
slr0427	putative competence-damage protein	56	1.6	3 vs. 13	0
slr0431	hypothetical protein	93	-1.2	9 vs. 13	0
slr0439	unknown protein	37	-1.2	3 vs. 18	0
slr0440	hypothetical protein	74	-1.1	1 vs. 13	0
slr0442	unknown protein	238	-2.3	1 vs. 18	0
slr0443	hypothetical protein	243	4.4	3 vs. 18	0
slr0445	hypothetical protein	238	-2.0	1 vs. 13	0
sll1408	transcriptional regulator	83	2.0	9 vs. 23	0
slr0451	putative helicase	110	-2.7	3 vs. 13	0
slr0453	hypothetical protein	98	-1.2	6 vs. 12.25	0
slr0458	unknown protein	18	1.5	3 vs. 12.25	5.69E-12
slr0460	putative transposase [ISY352g: 3511668 - 3512290. join 3513238 - 3514051]	28	-3.1	11.75 vs. 13	0.003697
slr0462	putative transposase [ISY352g: 3511668 - 3512290. join 3513238 - 3514051]	27	-1.5	-0.25 vs. 9	0.0000011 7
slr0468	unknown protein	425	-1.9	-0.25 vs. 6	0
sll1544	two-component response regulator NarL subfamily	11	-2.0	-0.25 vs. 13	0
sll1592	two-component response regulator NarL subfamily	35	-1.6	9 vs. 23	0
slr0476	unknown protein	3082	1.5	-0.25 vs. 11	0
slr0482	unknown protein	31	-1.3	9 vs. 12.25	8.942E-12
slr0483	hypothetical protein	7740	1.2	11.75 vs. 18	0
sll1624	two-component response regulator	146	-2.3	3 vs. 23	0
slr0489	unknown protein	61	-1.7	3 vs. 23	0
slr0493	similar to mannose-1-phosphate guanylyltransferase	88	1.7	0.25 vs. 13	0
slr0498	unknown protein	45	1.0	3 vs. 23	3.013E-09
slr0505	hypothetical protein	39	-1.1	9 vs. 18	6.636E-08
slr0509	hypothetical protein	201	-1.2	1 vs. 11	0
slr0510	hypothetical protein	27	1.5	1 vs. 13	0
slr0513	iron transport system substrate-binding	568	-3.6	9 vs. 23	0

	protein. periplasmic protein				
slr0514	unknown protein	16	1.3	0.25 vs. 13	0.000003424
slr0516	hypothetical protein	13	1.8	1 vs. 12.25	0.000003278
slr0517	hypothetical protein	119	-2.7	6 vs. 13	0
slr0518	similar to alpha-L-arabinofuranosidase B	726	-2.5	1 vs. -0.25	0
slr0519	hypothetical protein	159	1.2	-0.25 vs. 9	0
slr0521	unknown protein	92	2.0	1 vs. 13	0
slr0522	unknown protein	72	1.8	3 vs. 23	0
slr0523	similar to dethiobiotin synthetase	112	1.1	1 vs. 12.25	7.316E-12
sll1626	LexA repressor	14543	-4.4	1 vs. 13	0
sll1670	heat-inducible transcription repressor HrcA homolog	74	1.2	6 vs. 13	0
slr0534	probable transglycosylase	81	-1.3	12.25 vs. 23	0
slr0535	protease	108	-1.6	3 vs. 18	0
slr0537	putative sugar kinase	299	1.6	23 vs. 13	0
slr0541	probable amidotransferase	30	-1.5	11 vs. 23	0
slr0544	ATP-binding protein of ABC transporter	36	2.0	-0.25 vs. 6	0
slr0545	hypothetical protein	40	-1.9	1 vs. 13	0
slr0551	hypothetical protein	812	2.9	18 vs. 11	0
slr0552	hypothetical protein	436	1.4	3 vs. 11.75	0
slr0553	hypothetical protein	195	1.3	1 vs. 12.25	0
slr0554	hypothetical protein	38	-2.0	1 vs. 13	0
slr0556	hypothetical protein	127	2.7	-0.25 vs. 6	0
slr0565	hypothetical protein	488	-1.7	6 vs. 13	0
slr0573	unknown protein	537	-2.3	0.25 vs. 11	0
slr0574	cytochrome P450	33	-1.5	1 vs. 13	0
slr0575	hypothetical protein	233	1.1	-0.25 vs. 6	0
slr0579	unknown protein	148	-2.3	3 vs. 13	0
slr0581	unknown protein	426	-3.1	3 vs. 18	0
slr0582	unknown protein	887	-3.6	1 vs. 18	0
slr0583	similar to GDP-fucose synthetase	90	-1.4	3 vs. 23	0
slr0586	hypothetical protein	212	1.6	1 vs. 13	0
slr0587	unknown protein	261	-2.4	3 vs. 18	0
slr0589	hypothetical protein	154	1.5	3 vs. 13	0
slr0590	hypothetical protein	58	1.6	3 vs. -0.25	0
slr0591	ribonucleoside-diphosphate reductase beta chain	249	-1.8	1 vs. 18	0
slr0592	hypothetical protein	24	-1.1	9 vs. 0.25	0.0007671
slr0594	hypothetical protein	145	-2.9	3 vs. 18	0
slr0598	hypothetical protein	428	1.1	-0.25 vs. 6	4.101E-08
sll1673	two-component response regulator	163	1.1	11 vs. 23	0
slr0600	NADP-thioredoxin reductase	67	-1.8	1 vs. 13	0
slr0601	unknown protein	498	-2.1	0.25 vs. 13	8.906E-08

slr0602	unknown protein	329	-2.1	9 vs. 13	0
slr0604	GTP-binding protein	877	-2.9	6 vs. 18	0
slr0606	hypothetical protein	422	-1.9	9 vs. 23	0
slr0607	hypothetical protein	68	3.8	3 vs. 18	0
slr0609	hypothetical protein	161	-1.3	1 vs. 23	0
slr0610	hypothetical protein	57	1.3	1 vs. 12.25	0
slr0615	ATP-binding protein of ABC transporter	96	-1.6	3 vs. 18	0
slr0617	unknown protein	193	-2.2	6 vs. 23	0
slr0619	hypothetical protein	95	1.1	3 vs. 23	0
slr0625	hypothetical protein	76	-1.7	-0.25 vs. 11	0
slr0626	probable glycosyltransferase	60	1.2	1 vs. 13	0
slr0630	hypothetical protein	51	-1.2	9 vs. 13	0
slr0635	hypothetical protein	38	-1.2	-0.25 vs. 13	0
slr0639	mechanosensitive ion channel homolog	116	-1.4	-0.25 vs. 6	0
slr0642	hypothetical protein	53	1.9	0.25 vs. 11	0
slr0643	hypothetical protein	41	-2.1	9 vs. 18	0
slr0644	nitrogen regulation protein NifR3 homolog	17	-1.1	12.25 vs. 18	0.0000675
slr0645	hypothetical protein	86	-2.2	-0.25 vs. 12.25	0
slr0646	probable D-alanyl-D-alanine carboxypeptidase	42	-2.1	-0.25 vs. 11.75	0
slr0657	aspartate kinase	106	1.1	1 vs. 13	0
slr0662	arginine decarboxylase	39	-1.1	3 vs. 13	0
slr0664	hypothetical protein	104	-1.1	11.75 vs. 18	0.000002202
slr0665	aconitate hydratase	144	-2.2	6 vs. 18	0
slr0667	unknown protein	1194	1.8	6 vs. 18	0
slr0668	unknown protein	461	2.9	6 vs. 23	0
slr0670	hypothetical protein	124	1.1	-0.25 vs. 11	0
slr0677	biopolymer transport ExbB like protein	537	-1.9	9 vs. 18	0
slr0678	biopolymer transport ExbD like protein	426	-3.2	9 vs. 23	0
slr0679	sun protein	555	-3.5	6 vs. 18	0
slr0680	hypothetical protein	132	-1.6	0.25 vs. 13	0
slr0681	probable sodium/calcium exchanger protein	51	-1.3	0.25 vs. 13	0
slr0686	hypothetical protein	864	1.7	12.25 vs. 23	0
sll1708	two-component response regulator NarL subfamily	35	-1.4	3 vs. 18	0
slr0689	hypothetical protein	276	-1.2	3 vs. 11.75	0
slr0695	hypothetical protein	363	1.1	-0.25 vs. 9	9.755E-12
slr0700	probable amino acid permease	32	1.5	3 vs. 23	0
sll1872	transcriptional regulator	88	1.4	1 vs. 23	0
slr0702	unknown protein	104	-3.3	6 vs. 18	0
slr0708	periplasmic protein. function unknown	300	2.7	3 vs. -0.25	0

slr0709	hypothetical protein	83	2.1	1 vs. 13	0
slr0719	unknown protein	108	-1.3	0.25 vs. 13	0
slr0722	hypothetical protein	58	-1.3	1 vs. 11	1.943E-10
sll1937	ferric uptake regulation protein	199	1.5	-0.25 vs. 9	0
slr0725	hypothetical protein	48	2.8	1 vs. 13	0
slr0727	unknown protein	676	2.1	6 vs. 23	0
slr0728	hypothetical protein	95	-1.5	11 vs. 23	0
slr0729	hypothetical protein	329	1.5	-0.25 vs. 6	0
slr0730	hypothetical protein	79	-1.3	3 vs. 23	0
slr0731	hypothetical protein	106	1.4	1 vs. 18	0
slr0732	hypothetical protein	229	1.6	6 vs. 13	0
slr0733	integrase-recombinase protein	93	1.6	1 vs. 13	0
slr0734	hypothetical protein	11	-2.2	3 vs. 13	0
slr0740	hypothetical protein	220	-1.3	12.25 vs. 23	0
sll2014	sugar fermentation stimulation protein	104	2.0	6 vs. 13	0
slr0742	hypothetical protein	173	2.0	1 vs. 23	0
slr0743	similar to N utilization substance protein	34	1.9	3 vs. 23	0
slr0751	hypothetical protein	276	1.3	0.25 vs. 13	1.552E-08
slr0752	enolase	317	1.1	1 vs. 18	0
slr0753	probable transport protein	23	-1.2	6 vs. 18	0
slr0755	hypothetical protein	1224	3.0	1 vs. 23	0
slr0765	hypothetical protein	109	1.7	6 vs. 13	0
slr0769	hypothetical protein	194	1.4	3 vs. 23	0
slr0771	hypothetical protein	293	1.3	11 vs. 23	0
slr0776	UDP-3-o-[3-hydroxymyristoyl] glucosamine n-acyltransferase	269	-1.3	9 vs. 23	0
slr0779	hypothetical protein	77	-1.0	0.25 vs. 11.75	0
slr0780	hypothetical protein	270	1.4	0.25 vs. 13	0
slr0784	hypothetical protein	395	-1.4	0.25 vs. 12.25	0
slr0787	hypothetical protein	35	-2.2	1 vs. -0.25	0
slr0788	similar to pre-B cell enhancing factor	6	-1.2	1 vs. 23	1.64E-08
slr0789	hypothetical protein	416	-1.7	9 vs. 13	0
slr0790	similar to ultraviolet light resistance protein B	90	1.4	3 vs. 23	0
slr0799	putative transposase [ISY802c: 3066278 - 3067184]	46	-1.9	0.25 vs. 13	0
slr0800	putative transposase [ISY802c: 3066278 - 3067184]	41	1.8	9 vs. 23	0.0006996
slr0804	probable D-alanyl-D-alanine carboxypeptidase	407	1.7	1 vs. 13	0
slr0806	hypothetical protein	180	3.4	3 vs. 13	0
slr0807	probable o-sialoglycoprotein endopeptidase	50	-1.5	3 vs. 23	0
slr0808	16S rRNA processing protein RimM homolog	23	-1.7	-0.25 vs. 9	5.995E-10
slr0810	hypothetical protein	136	-1.5	23 vs. 13	0

slr0812	hypothetical protein	35	1.0	1 vs. -0.25	4.155E-08
slr0813	hypothetical protein	17	2.0	1 vs. -0.25	0
slr0818	hypothetical protein	34	-2.0	1 vs. 13	0
slr0820	probable glycosyltransferase	28	-1.2	9 vs. 23	0
slr0821	hypothetical protein	857	1.4	3 vs. 12.25	0
slr0822	cation-transporting P-type ATPase PacL	109	-2.7	3 vs. 18	0
slr0827	alanine racemase	244	-1.1	1 vs. 13	0
slr0829	unknown protein	125	-1.3	1 vs. 18	0
slr0081	two-component response regulator OmpR subfamily	382	-2.3	1 vs. 13	0
slr0842	hypothetical protein	130	-1.7	1 vs. 13	0
slr0845	hypothetical protein	50	1.4	-0.25 vs. 11	0
slr0847	phosphopantetheine adenylyltransferase	69	1.0	1 vs. 18	2.301E-09
slr0848	hypothetical protein	127	1.5	1 vs. 13	0
slr0853	ribosomal-protein-alanine acetyltransferase	45	1.1	1 vs. 0.25	0.0000214 6
slr0856	putative transposase [ISY100l: 1346125 - 1347070]	70	1.8	6 vs. 18	0
slr0857	putative transposase [ISY100l: 1346125 - 1347070]	25	3.5	3 vs. -0.25	0
slr0862	probable sugar kinase	133	1.9	1 vs. 13	0
slr0865	hypothetical protein	58	1.1	1 vs. 12.25	0
slr0868	unknown protein	27	-3.0	0.25 vs. 12.25	0
slr0869	hypothetical protein	111	-3.6	-0.25 vs. 12.25	0
slr0870	hypothetical protein	402	3.4	12.25 vs. 23	0
slr0871	unknown protein	244	3.5	11 vs. 23	0
slr0875	large-conductance mechanosensitive channel	708	2.0	3 vs. 13	0
slr0876	hypothetical protein	75	-2.2	0.25 vs. 13	0
slr0877	glutamyl-tRNA(Gln) amidotransferase subunit A	136	1.3	1 vs. 13	0
slr0878	hypothetical protein	57	1.1	1 vs. 23	3.354E-09
slr0879	glycine decarboxylase complex H-protein	200	2.4	3 vs. 13	0
slr0880	similar to fibronectin binding protein	49	1.8	3 vs. 13	0
slr0883	hypothetical protein	117	1.0	3 vs. 23	0
slr0885	hypothetical protein	133	-1.5	1 vs. 13	0
slr0886	3-oxoacyl-[acyl-carrier protein] reductase	60	1.6	3 vs. 23	0
slr0887	hypothetical protein	105	2.3	1 vs. 13	0
slr0888	hypothetical protein	4075	-5.9	1 vs. 12.25	0
slr0889	hypothetical protein	1182	-3.5	1 vs. 12.25	0
slr0890	unknown protein	60	-2.1	1 vs. 13	0
slr0891	N-acetylmuramoyl-L-alanine amidase	32	-1.2	9 vs. 23	0
slr0152	serine/threonine protein kinase	64	-1.1	6 vs. 23	0
slr0897	probable endoglucanase	40	-2.3	6 vs. 23	0
slr0907	unknown protein	132	1.6	3 vs. 13	0

slr0909	unknown protein	575	3.0	6 vs. 13	0
slr0912	unknown protein	486	1.2	3 vs. 13	0
slr0913	unknown protein	971	3.1	3 vs. 13	0
slr0914	unknown protein	424	3.5	3 vs. -0.25	0
slr0915	putative endonuclease [encoded in trnfM-intron: 2791054 - 2791708]	78692	-1.0	1 vs. -0.25	0
slr0918	methionine aminopeptidase	61	-1.3	1 vs. 23	0
slr0919	hypothetical protein	44	-1.5	-0.25 vs. 9	2.764E-11
slr0924	periplasmic protein. function unknown	334	1.0	3 vs. 23	0
slr0929	chromosome partitioning protein. ParA family	175	-1.2	3 vs. 11.75	0
slr0935	hypothetical protein	434	-3.1	3 vs. 13	0
slr0937	unknown protein	100	-1.4	1 vs. 18	0
slr0941	hypothetical protein	138	1.9	1 vs. 12.25	0
slr0942	alcohol dehydrogenase [NADP+]	269	2.7	-0.25 vs. 6	0
slr0945	arsenical resistance protein ArsH homolog	21	-1.7	6 vs. 12.25	0
slr0240	transcriptional regulator	234	-2.4	3 vs. 13	0
slr0950	hemolysin-like protein	35	2.7	1 vs. 18	0
slr0951	4-diphosphocytidyl-2C-methyl-D-erythritol synthase	11	1.3	6 vs. 13	0.000006962
slr0955	probable tRNA/rRNA methyltransferase	72	1.6	1 vs. 23	0
slr0957	hypothetical protein	717	2.0	0.25 vs. 12.25	0
slr0959	hypothetical protein	126	1.7	1 vs. 11	0
slr0960	unknown protein	178	-1.6	3 vs. 13	0
slr0967	hypothetical protein	1798	-4.7	1 vs. 13	0
slr0971	hypothetical protein	247	-3.0	6 vs. 23	0
slr0975	hypothetical protein	573	-3.0	6 vs. 13	0
slr0977	ABC transporter. permease component	162	1.3	3 vs. 13	0
slr0978	hypothetical protein	473	1.2	-0.25 vs. 6	0
slr0980	hypothetical protein	198	-1.1	0.25 vs. 13	0
slr0982	probable polysaccharide ABC transporter ATP binding subunit	136	1.4	1 vs. 13	0
slr0990	hypothetical protein	88	-2.2	3 vs. 23	0
slr0992	probable tRNA/rRNA methyltransferase	51	1.8	1 vs. 13	0
slr0994	lipoate-protein ligase B	44	1.8	1 vs. 23	0
slr1023	unknown protein	31	-2.0	-0.25 vs. 12.25	4.065E-12
slr1025	hypothetical protein	28	1.6	9 vs. 18	2.301E-07
slr1028	unknown protein	99	-2.9	1 vs. 12.25	0
slr1033	unknown protein	558	1.1	6 vs. 0.25	0
slr1035	hypothetical protein	226	1.5	-0.25 vs. 6	0
slr0418	putative transcripton factor DevT homolog	122	-1.7	6 vs. 23	0
slr0449	probable transcriptional regulator	10	-1.4	1 vs. 12.25	1.317E-07
slr0527	transcription regulator ExsB homolog	27	-2.1	-0.25 vs. 13	0
slr1046	putative TatA protein	177	2.3	3 vs. 13	0

slr1048	hypothetical protein	98	-1.5	-0.25 vs. 9	0
slr1050	hypothetical protein	286	1.3	0.25 vs. 13	0
slr1051	enoyl-[acyl-carrier-protein] reductase	56	1.9	1 vs. 13	0
slr1052	hypothetical protein	90	1.4	1 vs. 13	0
slr1053	unknown protein	115	2.4	1 vs. 13	0
slr1056	unknown protein	713	-2.1	-0.25 vs. 11	0
slr1062	unknown protein	1189	1.2	3 vs. 0.25	0
slr1063	probable glycosyltransferase	2883	2.5	3 vs. 13	0
slr1064	probable glycosyltransferase	878	2.2	3 vs. 18	0
slr1065	probable glycosyltransferase	1932	2.2	3 vs. 18	0
slr1066	unknown protein	1545	2.2	3 vs. 13	0
slr1067	UDP-glucose 4-epimerase	807	2.2	3 vs. 18	0
slr1068	hypothetical protein	2502	2.2	3 vs. 0.25	0
slr1069	hypothetical protein	1257	2.1	3 vs. 0.25	0
slr1070	unknown protein	900	2.2	3 vs. 0.25	0
slr1071	unknown protein	1780	2.2	3 vs. 0.25	0
slr1072	GDP-D-mannose dehydratase	304	2.2	3 vs. 18	0
slr1073	unknown protein	943	2.1	3 vs. 18	0
slr1074	unknown protein	1668	2.1	3 vs. 18	0
slr1075	putative transposase [ISY100b: 378993 - 379939]	162	2.5	3 vs. 18	0
slr1076	probable glycosyltransferase	482	1.6	3 vs. 1	0
slr1077	probable glycosyltransferase	91	-1.3	1 vs. 13	0
slr1078	similar to UDP-glucose 4-epimerase	64	1.3	-0.25 vs. 9	0
slr1079	unknown protein	174	-2.2	1 vs. -0.25	0
slr1082	unknown protein	85	2.2	-0.25 vs. 11.75	0
slr1083	hypothetical protein	52	1.2	-0.25 vs. 11	9.283E-07
slr1084	unknown protein	159	-1.1	1 vs. -0.25	0
slr1085	probable glycosyltransferase	82	-1.1	1 vs. -0.25	0
slr1087	hypothetical protein	39	-1.2	1 vs. 23	0
slr1094	hypothetical protein	65	2.3	-0.25 vs. 9	0
slr1095	hypothetical protein	29	-1.5	12.25 vs. 23	0
slr1096	dihydrolipoamide dehydrogenase	128	1.5	1 vs. 13	0
slr1097	hypothetical protein	189	1.1	-0.25 vs. 13	0
slr1098	hypothetical protein	270	1.7	3 vs. 13	0
slr1100	hypothetical protein	308	-3.0	3 vs. 12.25	0
slr1101	hypothetical protein	82	1.5	-0.25 vs. 6	0
slr1102	hypothetical protein	48	-1.1	3 vs. 13	0
slr1103	hypothetical protein	111	-1.1	1 vs. 13	0
slr1105	GTP-binding protein TypA/BipA homolog	243	2.1	1 vs. 11.75	0
slr1106	prohibitin	60	1.2	1 vs. 18	0
slr1107	unknown protein	33	-1.4	9 vs. 18	0

slr1109	similar to ankyrin	51	-1.3	6 vs. 23	0
slr1110	hypothetical protein	48	-2.0	11 vs. 23	0
slr1113	ATP-binding protein of ABC transporter	80	-2.0	1 vs. 13	0
slr1114	hypothetical protein	144	-3.2	6 vs. 18	0
slr1115	probable methyltransferase	60	-2.4	9 vs. 23	0
slr1118	probable UDP-N-acetyl-D-mannosaminuronic acid transferase	26	1.4	3 vs. 13	0
slr1119	hypothetical protein	176	2.7	-0.25 vs. 11.75	0
slr1120	type 4 prepilin-like proteins leader peptide processing enzyme	127	-2.3	3 vs. 13	0
slr1122	hypothetical protein	107	-1.2	6 vs. 12.25	0
slr1123	guanylate kinase	39	-1.7	12.25 vs. 18	0
slr1124	phosphoglycerate mutase	126	2.4	1 vs. 13	0
slr1125	probable glucosyl transferase	50	2.0	1 vs. 12.25	0
slr1127	unknown protein	929	2.7	-0.25 vs. 6	0
slr1128	hypothetical protein	147	-1.4	9 vs. 13	0
slr1134	mutator MutT homolog	84	-1.7	0.25 vs. 11.75	0
slr1135	unknown protein	404	2.5	6 vs. 13	0
slr1140	DegT/DnrJ/EryC1/StrS family protein	99	1.2	9 vs. 18	0
slr1142	hypothetical protein	286	1.7	9 vs. 13	0
slr1143	hypothetical protein	37	1.3	1 vs. -0.25	0
slr0599	serine/threonine kinase	104	-2.6	6 vs. 23	0
slr1148	unknown protein	17	-1.8	-0.25 vs. 9	0.0000031 12
slr1149	ATP-binding protein of ABC transporter	25	-1.4	1 vs. 13	0
slr1152	hypothetical protein	497	-4.3	6 vs. 18	0
slr1160	periplasmic protein. function unknown	306	3.6	1 vs. 13	0
slr1161	hypothetical protein	976	2.4	11 vs. 23	0
slr1162	unknown protein	545	-2.3	-0.25 vs. 9	0
slr1163	unknown protein	141	-1.6	0.25 vs. 11.75	0
slr1164	ribonucleotide reductase subunit alpha	86	-1.2	-0.25 vs. 13	0
slr1165	sulfate adenylyltransferase	98	2.7	1 vs. 13	0
slr1166	UDP-glucose:tetrahydrobiopterin glucosyltransferase	80	3.1	1 vs. 13	0
slr1168	unknown protein	328	-1.2	1 vs. 18	2.398E-11
slr1169	unknown protein	148	-1.0	3 vs. 18	0
slr1170	hypothetical protein	73	-1.1	9 vs. 13	0
slr1173	hypothetical protein	338	-1.5	1 vs. 11	0
slr1174	hypothetical protein	198	-1.0	6 vs. 18	0
slr1176	glucose-1-phosphate adenylyltransferase	460	2.8	1 vs. 13	0
slr1177	hypothetical protein	435	-1.6	9 vs. 23	0
slr1178	hypothetical protein	185	-1.0	0.25 vs. 12.25	0
slr1183	hypothetical protein	30	-1.2	-0.25 vs.	0.001745

slr1187	unknown protein	307	-1.9	9 vs. 23	0
slr1192	probable alcohol dehydrogenase	116	-2.3	3 vs. 23	0
slr1194	hypothetical protein	157	-1.3	0.25 vs. 13	0
slr1195	hypothetical protein	66	-1.1	-0.25 vs. 6	1.26E-11
slr1198	antioxidant protein	3198	-1.8	1 vs. 18	0
slr1200	urea transport system permease protein	550	3.3	1 vs. 13	0
slr1201	urea transport system permease protein	187	3.0	1 vs. 13	0
slr1202	permease protein of sugar ABC transporter	86	-1.7	6 vs. 23	0
slr1204	protease	239	2.5	-0.25 vs. 6	0
slr1207	hypothetical protein	113	-1.6	6 vs. 18	0
slr1209	hypothetical protein	198	1.1	6 vs. 12.25	0
slr1210	unknown protein	371	1.4	6 vs. 13	0
slr0687	probable two-component response regulator	43	-1.7	1 vs. -0.25	0
slr0701	transcriptional regulator	47	-3.0	0.25 vs. 13	0
slr0724	HtaR suppressor protein homolog	51	1.3	9 vs. 12.25	0
slr1215	hypothetical protein	141	-1.5	6 vs. 23	0
slr1216	Mg2+ transport protein	45	1.1	1 vs. 18	0
slr1220	hypothetical protein	370	-1.7	11.75 vs. 23	0
slr1222	unknown protein	116	1.6	1 vs. 13	0
slr1224	ATP-binding protein of sugar ABC transporter	60	1.5	1 vs. 13	0
slr0741	transcriptional regulator	52	2.2	-0.25 vs. 11	0
slr1229	sulfate permease	36	2.7	3 vs. -0.25	0
slr1230	hypothetical protein	25	1.9	3 vs. 12.25	0
slr1232	unknown protein	259	-2.8	1 vs. 13	0
slr1233	succinate dehydrogenase flavoprotein subunit	62	-1.8	0.25 vs. 13	0
slr0835	MoxR protein homolog	105	1.6	1 vs. 13	0
slr1236	hypothetical protein	5111	4.3	-0.25 vs. 6	0
slr1240	unknown protein	758	-4.5	1 vs. 12.25	0
slr1241	hypothetical protein	1207	-3.8	1 vs. 12.25	0
slr1243	unknown protein	543	-1.9	-0.25 vs. 6	0
slr0895	transcriptional regulator	44	1.9	1 vs. 23	4.489E-08
slr1247	phosphate-binding periplasmic protein precursor (PBP)	24	-1.2	0.25 vs. 13	0
slr1248	phosphate transport system permease protein PstC homolog	18	-2.2	6 vs. 18	0
slr1249	phosphate transport system permease protein PstA homolog	16	-2.0	6 vs. 13	0
slr1250	phosphate transport ATP-binding protein PstB homolog	13	1.9	3 vs. -0.25	0.0000867
slr1251	peptidyl-prolyl cis-trans isomerase	1695	4.0	3 vs. 13	0
slr1253	unknown protein	924	-2.9	3 vs. 13	0
slr1258	unknown protein	59	-1.5	3 vs. 13	0
slr1259	hypothetical protein	87	-1.3	3 vs. 13	0

slr1260	hypothetical protein	79	-1.6	3 vs. 13	0
slr1261	hypothetical protein	48	-1.8	9 vs. 13	0
slr1262	hypothetical protein	48	-1.7	9 vs. 18	0
slr1263	hypothetical protein	42	-1.0	1 vs. 13	0
slr1270	periplasmic protein. function unknown	185	1.1	1 vs. 18	0
slr1272	probable porin; major outer membrane protein	1491	-2.3	1 vs. 13	0
slr1273	hypothetical protein	588	-1.5	1 vs. 13	0
slr1277	pilus assembly protein homologous to general secretion pathway protein D	541	-1.5	-0.25 vs. 6	0
slr1282	putative transposase [ISY508b: 1877114 - 1878081]	394	1.8	6 vs. 23	0
slr1283	putative transposase [ISY508b: 1877114 - 1878081]	127	1.9	6 vs. 18	0
slr1037	two-component response regulator CheY subfamily	43	1.7	6 vs. 13	0
slr1287	hypothetical protein	29	1.7	1 vs. 13	0
slr1288	hypothetical protein	143	-1.4	6 vs. 23	0
slr1290	hypothetical protein	126	-1.7	9 vs. 18	0
slr1293	similar to phytoene dehydrogenase	11	2.3	0.25 vs. 11	0
slr1299	UDP-glucose dehydrogenase	79	1.8	3 vs. 13	0
slr1300	similar to 2-octaprenyl-6-methoxyphenol hydroxylase	225	-3.0	11 vs. 23	0
slr1303	hypothetical protein	45	2.0	1 vs. 12.25	0
slr1306	hypothetical protein	719	-2.8	9 vs. 23	0
slr1315	hypothetical protein	570	-2.6	3 vs. 13	0
slr1316	ABC-type iron(III) dicitrate transport system permease protein	28	-1.7	6 vs. 23	0
slr1317	ABC-type iron(III) dicitrate transport system permease protein	99	-3.6	6 vs. 23	0
slr1318	iron(III) dicitrate transport system ATP-binding protein	23	-1.1	11 vs. 23	6.881E-10
slr1319	iron(III) dicitrate transport system substrate-binding protein	37	-1.0	3 vs. 18	0
slr1041	two-component response regulator PatA subfamily	86	-1.4	1 vs. -0.25	0
slr1042	two-component response regulator CheY subfamily	965	-1.4	1 vs. 13	0
slr1327	hypothetical protein	558	-1.0	1 vs. 18	0.0000426 4
slr1331	periplasmic processing protease	92	1.9	1 vs. 13	0
slr1332	beta ketoacyl-acyl carrier protein synthase	21	1.2	18 vs. 11	1.119E-08
slr1334	phosphoglucomutase/phosphomannomutase	51	1.7	9 vs. 13	0
slr1336	H+/Ca2+ exchanger	330	-2.1	6 vs. 18	0
slr1338	hypothetical protein	370	1.1	6 vs. 11.75	2.17E-08
slr1340	unknown protein	345	1.1	6 vs. 13	0
slr1342	hypothetical protein	132	1.4	1 vs. 18	0
slr1343	hypothetical protein	45	2.4	1 vs. 13	0
slr1347	beta-type carbonic anhydrase localized in the carboxysome	78	-1.3	11 vs. 23	0
slr1353	hypothetical protein	88	-1.4	3 vs. 18	0

slr1363	hypothetical protein	80	-2.3	-0.25 vs. 11.75	0
slr1365	hypothetical protein	367	-1.3	6 vs. 23	0
slr1366	lipoprotein signal peptidase (signal peptidase II)	124	1.0	1 vs. 13	0
slr1367	glycogen phosphorylase	161	-2.0	3 vs. 12.25	0
slr1376	hypothetical protein	241	2.1	-0.25 vs. 9	0
slr1377	leader peptidase I (signal peptidase I)	111	-1.2	11 vs. 23	0
slr1383	unknown protein	274	-2.3	6 vs. 18	0
slr1391	unknown protein	267	-2.5	6 vs. 23	0
slr1212	similar to two-component sensor histidine kinase	79	1.2	3 vs. -0.25	0
slr1394	hypothetical protein	564	-1.1	6 vs. 23	5.284E-12
slr1396	unknown protein	2634	3.1	9 vs. 13	0
slr1397	unknown protein	1205	-1.4	1 vs. 23	0
slr1398	unknown protein	326	1.1	9 vs. 23	0
slr1406	periplasmic protein. function unknown	260	1.1	12.25 vs. 18	0
slr1407	unknown protein	136	1.2	3 vs. -0.25	0
slr1409	periplasmic WD-repeat protein	77	1.7	3 vs. 18	0
slr1410	periplasmic WD-repeat protein	34	2.7	3 vs. 23	0
slr1411	hypothetical protein	45	-1.2	6 vs. 13	0
slr1413	hypothetical protein	90	-3.3	3 vs. 18	0
slr1419	hypothetical protein	77	-1.1	3 vs. -0.25	0
slr1420	probable sugar kinase	19	1.2	0.25 vs. 13	4.032E-10
slr1421	unknown protein	123	-1.1	1 vs. 13	0.0000728 4
slr1424	UDP-N-acetylenolpyruvoylglucosamine reductase	81	1.7	1 vs. -0.25	0
slr1425	hypothetical protein	207	1.1	3 vs. 13	4.059E-07
slr1428	hypothetical protein	80	1.6	1 vs. 13	0
slr1429	hypothetical protein	52	1.3	3 vs. 23	0
slr1431	hypothetical protein	169	-1.5	9 vs. 23	0
slr1435	PmbA protein homolog	26	1.1	6 vs. 23	0
slr1436	unknown protein	74	1.9	6 vs. 23	0
slr1437	unknown protein	243	-3.3	0.25 vs. 13	0
slr1438	hypothetical protein	525	-2.5	6 vs. 13	0
slr1440	hypothetical protein	19	-1.5	1 vs. 12.25	6.425E-08
slr1441	hypothetical protein	7	-1.6	3 vs. 23	0.005354
slr1442	hypothetical protein	514	-2.8	6 vs. 18	0
slr1213	two-component response regulator AraC subfamily	27	2.0	3 vs. 18	0
slr1444	hypothetical protein	19	-2.0	1 vs. 13	0
slr1448	fructokinase	89	2.3	-0.25 vs. 6	0
slr1450	unknown protein	148	-1.0	11.75 vs. 23	0
slr1451	hypothetical protein	241	-1.8	3 vs. 18	0
slr1461	hypothetical protein	186	-2.4	6 vs. 18	0

slr1462	hypothetical protein	53	-1.5	3 vs. 18	0
slr1464	hypothetical protein	56	-1.3	3 vs. 18	0
slr1467	precorrin isomerase	33	-1.2	3 vs. 23	0
slr1468	hypothetical protein	31	1.9	3 vs. 18	0
slr1472	hypothetical protein	299	2.3	6 vs. 23	0
slr1474	hypothetical protein	58	2.1	6 vs. 23	0
slr1478	hypothetical protein	35	1.1	11 vs. 13	0.0003789
slr1484	unknown protein	40	-4.6	3 vs. 23	0
slr1485	putative phosphatidylinositol phosphate kinase. salt-induced periplasmic protein	8	-2.0	6 vs. 23	0
slr1488	multidrug resistance family ABC transporter	18	-2.3	6 vs. 23	0
slr1214	two-component response regulator PatA subfamily	67	-2.6	1 vs. 18	0
slr1490	ferrichrome-iron receptor	15	1.3	9 vs. 23	4.065E-12
slr1493	hypothetical protein	21	2.0	9 vs. 13	4.471E-12
slr1495	hypothetical protein	21	-1.9	3 vs. 18	0
slr1496	putative transposase	412	-1.8	1 vs. 23	0
slr1501	probable acetyltransferase	29	-1.5	3 vs. 13	2.578E-09
slr1503	hypothetical protein	104	-1.6	1 vs. 12.25	0
slr1505	unknown protein	186	2.4	-0.25 vs. 9	0
slr1508	probable glycosyltransferase	713	-2.9	6 vs. 23	0
slr1513	periplasmic protein. function unknown	917	-2.1	-0.25 vs. 6	0
slr1520	oxidoreductase. aldo/keto reductase family	16	1.6	1 vs. 13	2.54E-10
slr1522	putative transposase [ISY352d: 1614422 - 1615835]	113	-1.8	1 vs. 23	0
slr1524	putative transposase [ISY100u(partial copy): 1616832 - 1617509]	470	-1.8	-0.25 vs. 6	0
slr1530	hypothetical protein	192	-1.1	1 vs. 18	0
slr1534	hypothetical protein	30	-1.1	11 vs. 13	1.219E-12
slr1535	hypothetical protein	146	-1.5	0.25 vs. 11.75	0
slr1538	cobalamin biosynthesis protein D	40	1.5	9 vs. 18	0
slr1540	mRNA-binding protein	60	1.1	1 vs. 11	0
slr1541	hypothetical protein	44	1.2	3 vs. 18	0
slr1542	2-C-methyl-D-erythritol 2.4-cyclodiphosphate synthase	53	1.4	1 vs. 13	5.166E-10
slr1544	unknown protein	677	3.4	0.25 vs. 11.75	0
slr1546	hypothetical protein	594	-2.1	0.25 vs. 13	0
slr1547	hypothetical protein	148	1.3	12.25 vs. 23	0
slr1549	polypeptide deformylase	168	-1.1	12.25 vs. 18	0
slr1552	unknown protein	152	3.6	3 vs. 13	0
slr1556	2-hydroxyacid dehydrogenase homolog	106	-1.7	1 vs. 13	0
slr1557	hypothetical protein	113	-1.9	9 vs. 23	0
slr1562	glutaredoxin	160	-2.3	3 vs. 18	0
slr1563	hypothetical protein	96	-1.5	6 vs. 18	0

slr1567	unknown protein	19	-1.0	-0.25 vs. 9	1.219E-12
slr1568	hypothetical protein	39	-1.4	-0.25 vs. 9	3.487E-10
slr1570	hypothetical protein	293	-2.4	6 vs. 13	0
slr1571	unknown protein	49	-1.6	6 vs. 13	0
slr1573	hypothetical protein	84	1.3	6 vs. 13	0
slr1575	probable potassium efflux system	14	-1.4	-0.25 vs. 11.75	0
slr1576	unknown protein	316	1.1	11.75 vs. 23	0
slr1579	hypothetical protein	116	-1.2	9 vs. 23	0
slr1583	hypothetical protein	1054	-2.3	6 vs. 0.25	0
slr1585	putative transposase [ISY508c(partial copy): 3405449 - 3406337]	29	-2.2	-0.25 vs. 9	0
slr1586	putative transposase [ISY508c(partial copy): 3405449 - 3406337]	16	2.0	3 vs. 18	2.189E-08
slr1590	hypothetical protein	279	1.9	-0.25 vs. 9	0
slr1592	probable pseudouridine synthase	5	-1.9	11 vs. 23	0.00016
slr1593	hypothetical protein	275	-4.0	9 vs. 0.25	0
slr1225	serine/threonine kinase	76	-1.7	6 vs. 23	0
slr1597	chromosome partitioning ATPase. ParA family	42	1.8	3 vs. 18	0
slr1598	lipoic acid synthetase	64	-1.0	12.25 vs. 18	0
slr1599	hypothetical protein	227	-1.1	6 vs. 12.25	0
slr1600	hypothetical protein	613	2.7	1 vs. 13	0
slr1601	hypothetical protein	180	1.3	6 vs. 23	0
slr1603	hypothetical protein	90	-2.1	3 vs. 18	0
slr1608	putative glucose dehydrogenase-B. periplasmic protein	49	-2.7	3 vs. 13	0
slr1610	putative C-3 methyl transferase	70	1.7	1 vs. 13	0
slr1611	hypothetical protein	287	-1.2	11.75 vs. 18	6.255E-10
slr1613	hypothetical protein	647	1.1	3 vs. 11.75	4.853E-10
slr1614	hypothetical protein	1005	1.0	6 vs. 13	0
slr1616	unknown protein	713	1.5	3 vs. 23	0
slr1617	similar to UDP-glucose 4-epimerase	1378	1.9	3 vs. 18	0
slr1618	unknown protein	909	2.1	3 vs. 23	0
slr1619	hypothetical protein	417	2.6	3 vs. 13	0
slr1623	hypothetical protein	254	2.4	1 vs. -0.25	0
slr1626	dihydroneopterin aldolase	240	-1.2	-0.25 vs. 12.25	0
slr1634	hypothetical protein	92913	-5.0	1 vs. 18	0
slr1636	unknown protein	59	-1.1	-0.25 vs. 6	0
slr1639	SsrA-binding protein	111	-1.5	-0.25 vs. 6	0
slr1647	hypothetical protein	36	1.3	1 vs. 23	0
slr1648	hypothetical protein	95	-2.2	6 vs. 23	0
slr1649	hypothetical protein	164	1.2	6 vs. 13	0
slr1651	ABC transporter ATP-binding protein	40	-1.5	18 vs. 11	0

slr1653	N-acyl-L-amino acid amidohydrolase	83	-2.5	3 vs. -0.25	0
slr1658	unknown protein	113	2.0	0.25 vs. 13	0
slr1659	hypothetical protein	91	1.3	9 vs. 12.25	0
slr1660	hypothetical protein	79	-1.3	9 vs. 0.25	0
slr1661	hypothetical protein	101	1.5	0.25 vs. 13	0
slr1234	protein kinase C inhibitor	270	-1.1	-0.25 vs. 12.25	0
slr1667	hypothetical protein (target gene of sycrp1)	285	-2.9	1 vs. 23	0
slr1670	unknown protein	15	-1.6	-0.25 vs. 11.75	0
slr1673	probable tRNA/rRNA methyltransferase	39	-1.9	9 vs. 23	0
slr1674	hypothetical protein	401	2.3	-0.25 vs. 12.25	0
slr1676	hypothetical protein	497	2.9	3 vs. 12.25	0
slr1677	hypothetical protein	137	2.8	1 vs. 12.25	0
slr1679	hypothetical protein	28	2.0	6 vs. 23	0
slr1681	unknown protein	236	2.2	0.25 vs. 12.25	0
slr1682	putative transposase [ISY391b: 1970517 - 1970880. join 1972064 - 1973077]	323	-1.3	-0.25 vs. 11	0
slr1683	putative transposase [ISY391b: 1970517 - 1970880. join 1972064 - 1973077]	92	2.3	6 vs. 18	0
slr1684	putative transposase [ISY391b: 1970517 - 1970880. join 1972064 - 1973077]	21	-1.8	18 vs. 11	0.0000019 54
slr1686	hypothetical protein	243	-1.9	6 vs. 18	0
slr1687	hypothetical protein	118	2.9	0.25 vs. 11.75	0
slr1690	hypothetical protein	83	1.2	6 vs. 11.75	0
slr1691	glutamine-dependent NAD(+) synthetase	45	1.9	3 vs. 12.25	0
slr1692	hypothetical protein	129	1.1	6 vs. 23	0
slr1245	transcriptional regulator	23	1.1	6 vs. 18	1.912E-09
slr1325	GTP pyrophosphokinase	95	-2.0	1 vs. 13	0
slr1702	hypothetical protein	111	1.5	1 vs. 13	0
slr1704	hypothetical protein	1173	-2.6	6 vs. 18	0
slr1705	aspartoacylase	104	-2.0	1 vs. 13	0
slr1706	dihydroflavonol 4-reductase	70	-1.7	3 vs. 18	0
slr1708	probable peptidase	506	-1.6	9 vs. 23	0
slr1712	hypothetical protein	124	-1.5	0.25 vs. 13	0
slr1718	hypothetical protein	372	2.6	1 vs. 13	0
slr1723	permease protein of sugar ABC transporter	66	1.8	0.25 vs. 13	0
slr1726	unknown protein	46	1.7	18 vs. 11	0
slr1727	Na+/H+ antiporter	75	1.1	3 vs. -0.25	0
slr1732	hypothetical protein	219	-2.8	3 vs. 13	0
slr1736	homogentisate phytyltransferase	48	-1.8	1 vs. 12.25	0
slr1737	hypothetical protein	15	-1.6	-0.25 vs. 12.25	0
slr1740	oligopeptide binding protein of ABC transporter	74	-2.4	11 vs. 23	0
slr1744	N-acetylmuramoyl-L-alanine amidase.	372	-1.7	9 vs. 13	0

	periplasmic protein				
slr1746	glutamate racemase	821	1.2	3 vs. 23	0
slr1747	cell death suppressor protein Lls1 homolog	44	1.9	0.25 vs. 11.75	0
slr1748	probable phosphoglycerate mutase	77	-2.6	6 vs. 23	0
slr1751	periplasmic carboxyl-terminal protease	268	-1.9	3 vs. 13	0
slr1752	hypothetical protein	159	-1.6	3 vs. 13	0
slr1753	hypothetical protein	140	-1.7	6 vs. 18	0
slr1755	NAD+ dependent glycerol-3-phosphate dehydrogenase	92	-1.3	6 vs. 23	0
slr1443	serine/threonine kinase	27	1.0	23 vs. 13	0
slr1761	FKBP-type peptidyl-prolyl cis-trans isomerase. periplasmic protein	1422	4.7	3 vs. 18	0
slr1762	hypothetical protein	41	1.3	1 vs. 0.25	0
slr1763	probable methyltransferase	225	3.2	6 vs. 13	0
slr1764	similar to tellurium resistance protein TerE	219	-1.7	-0.25 vs. 9	0
slr1767	hypothetical protein	67	2.1	12.25 vs. 23	0
slr1768	unknown protein	134	-2.1	3 vs. 13	0
slr1770	hypothetical protein	1803	-3.8	3 vs. 12.25	0
slr1771	unknown protein	469	-3.5	6 vs. 18	0
slr1772	probable hydrolase. periplasmic protein	47	1.1	3 vs. 23	0
slr1773	unknown protein	15	-1.2	3 vs. 13	2.656E-09
slr1778	unknown protein	257	-2.3	-0.25 vs. 6	0
slr1787	thiamine-monophosphate kinase	57	-1.2	6 vs. 23	0
slr1788	unknown protein	76	-1.4	1 vs. 13	0
slr1789	unknown protein	57	-1.2	1 vs. 11	0
slr1793	transaldolase	401	-3.5	3 vs. 12.25	0
slr1794	probable anion transporting ATPase	109	1.2	3 vs. 18	0
slr1795	peptide methionine sulfoxide reductase	169	1.5	1 vs. 23	0
slr1796	hypothetical protein	199	2.8	3 vs. 12.25	0
slr1798	unknown protein	253	1.2	6 vs. 23	0
slr1799	hypothetical protein	98	1.3	0.25 vs. 12.25	0
slr1800	hypothetical protein	46	2.3	1 vs. 13	0
slr1803	adenine-specific DNA methylase	311	2.3	6 vs. 13	0
slr1804	unknown protein	168	-4.3	1 vs. 13	0
slr1489	transcriptional regulator	24	1.3	0.25 vs. 13	2.601E-11
slr1807	hypothetical protein	72	-2.3	6 vs. 18	0
slr1809	unknown protein	324	-3.4	6 vs. 18	0
slr1811	hypothetical protein	173	-1.7	1 vs. 18	0
slr1812	hypothetical protein	168	-1.8	1 vs. 13	0
slr1813	hypothetical protein	785	-1.7	1 vs. 13	0
slr1814	hypothetical protein	428	-2.1	1 vs. 13	0
slr1815	hypothetical protein	1021	-2.8	1 vs. 12.25	0
slr1816	hypothetical protein	484	-2.2	-0.25 vs. 11	0

slr1819	hypothetical protein	50	-1.5	1 vs. 18	0
slr1820	hypothetical protein	66	1.9	1 vs. 13	0
slr1821	hypothetical protein	122	-1.8	9 vs. 23	0
slr1826	hypothetical protein	45	2.1	11.75 vs. 23	0
slr1827	hypothetical protein	30	-2.2	-0.25 vs. 11	0
slr1840	hypothetical protein	85	1.9	3 vs. 13	0
slr1841	probable porin; major outer membrane protein	37162	-3.3	3 vs. 18	0
slr1847	hypothetical protein	1222	1.5	3 vs. 12.25	0
slr1851	hypothetical protein	730	-2.9	1 vs. 18	0
slr1852	unknown protein	582	1.8	11 vs. 13	0
slr1853	carboxymuconolactone decarboxylase	228	2.1	11.75 vs. 13	0
slr1854	unknown protein	193	2.4	9 vs. 13	0
slr1855	unknown protein	213	1.5	11.75 vs. 13	0
slr1856	phosphoprotein substrate of icfG gene cluster	254	1.0	11.75 vs. 13	0
slr1857	isoamylase	182	1.8	11.75 vs. 13	0
slr1859	anti-sigma f factor antagonist	856	3.1	9 vs. 13	0
slr1594	two-component response regulator PatA subfamily	343	3.6	1 vs. 6	0
slr1861	probable sigma regulatory factor	572	2.8	11 vs. 13	0
slr1862	unknown protein	208	-1.8	-0.25 vs. 6	0
slr1863	unknown protein	171	3.0	9 vs. 13	0
slr1864	hypothetical protein	148	1.7	3 vs. 18	0
slr1865	unknown protein	159	1.9	3 vs. -0.25	0
slr1866	unknown protein	204	1.9	1 vs. -0.25	0
slr1869	unknown protein	168	1.7	12.25 vs. 23	0
slr1870	hypothetical protein	199	-1.5	1 vs. 12.25	0
slr1874	D-alanine--D-alanine ligase	54	2.2	1 vs. 13	0
slr1875	hypothetical protein	111	2.3	1 vs. 18	0
slr1876	hypothetical protein	17	-1.2	9 vs. 12.25	5.036E-10
slr1880	hypothetical protein	49	1.4	6 vs. 13	0
slr1886	hypothetical protein	861	-4.2	3 vs. 18	0
slr1890	bacterioferritin	251	-1.4	0.25 vs. 13	0
slr1894	probable DNA-binding stress protein	971	2.0	3 vs. 12.25	0
slr1895	hypothetical protein	142	1.8	-0.25 vs. 6	0
slr1900	hypothetical protein	176	1.2	1 vs. 18	0
slr1902	putative transposase [ISY120a: 851653 - 852454]	285	-2.0	1 vs. 13	0
slr1906	hypothetical protein	86	-1.1	3 vs. 13	0
slr1907	hypothetical protein	223	-1.9	3 vs. 23	0
slr1908	probable porin; major outer membrane protein	2647	-2.2	0.25 vs. 13	0

slr1911	hypothetical protein	64	1.5	0.25 vs. 11	0
slr1912	putative PP2C-type protein phosphatase	311	1.7	9 vs. 13	0
slr1913	hypothetical protein	43	1.3	6 vs. 18	0.0000062 14
slr1914	hypothetical protein	206	-2.1	6 vs. 18	0
slr1915	hypothetical protein	679	-2.5	0.25 vs. 18	0
slr1917	hypothetical protein	445	-3.7	6 vs. 18	0
slr1918	hypothetical protein	592	-2.3	6 vs. 18	0
slr1919	hypothetical protein	71	2.3	0.25 vs. 11.75	0
slr1920	unknown protein	177	1.4	6 vs. 12.25	0
slr1927	hypothetical protein	186	2.7	3 vs. 13	0
slr1932	unknown protein	627	-1.7	3 vs. 23	0
slr1934	pyruvate dehydrogenase E1 component. alpha subunit	252	1.9	1 vs. 13	0
slr1939	unknown protein	63	-1.2	6 vs. 23	0
slr1940	periplasmic protein. function unknown	45	-1.2	1 vs. 12.25	0
slr1945	2.3-bisphosphoglycerate-independent phosphoglycerate mutase	528	1.4	1 vs. 13	0
slr1946	hypothetical protein	126	-1.9	11 vs. 23	0
slr1951	hypothetical protein	144	-1.9	6 vs. 18	0
slr1956	unknown protein	92	1.8	1 vs. 13	0
slr1957	hypothetical protein	2639	-3.8	1 vs. 12.25	0
slr1958	unknown protein	352	-2.3	1 vs. 12.25	0
slr1959	unknown protein	67	-1.4	-0.25 vs. 9	0
slr1960	putative transposase [ISY391a(partial copy): 1762937 - 1763383]	111	-2.5	1 vs. 13	0
slr1962	probable extracellular solute-binding protein	89	-1.2	11 vs. 23	0
slr1966	hypothetical protein	94	-1.6	1 vs. 12.25	0
slr1968	unknown protein	98	-2.5	1 vs. 18	0
slr1666	pleiotropic regulatory protein homolog	336	1.0	23 vs. 13	0
slr1970	hypothetical protein	146	-1.5	9 vs. 13	0
slr1971	hypothetical protein	35	-1.6	3 vs. 13	0
slr1974	GTP binding protein	167	-1.8	3 vs. 18	0
slr1693	two-component response regulator PatA subfamily	216	1.1	9 vs. 0.25	0
slr1977	hypothetical protein	20	-1.5	3 vs. 13	0
slr1978	hypothetical protein	59	1.1	1 vs. 23	0
slr1980	unknown protein	82	2.3	3 vs. 23	0
slr1694	expression activator appA homolog	157	1.0	12.25 vs. 23	0
slr1990	hypothetical protein	104	1.5	6 vs. 13	0
slr1760	two-component response regulator	53	2.3	-0.25 vs. 6	0
slr2000	hypothetical protein	18	-2.0	11.75 vs. 18	0
slr2003	hypothetical protein	142	1.8	1 vs. 13	0
slr2004	periplasmic protein. function unknown	222	1.9	6 vs. 18	0
slr2005	periplasmic protein. function unknown	146	-2.1	9 vs. 23	0

slr2006	hypothetical protein	22	2.3	9 vs. 13	0
slr2008	hypothetical protein	58	1.1	11.75 vs. 23	8.353E-08
slr1975	N-acylglucosamine 2-epimerase	116	2.3	1 vs. 13	0
slr2025	hypothetical protein	378	1.2	1 vs. 12.25	0
slr2036	putative transposase [ISY203a: 573408 - 574580]	24	2.8	9 vs. 23	0
slr2037	unknown protein	42	2.6	9 vs. 18	0
slr2038	hypothetical protein	17	1.4	3 vs. 11.75	3.738E-09
slr1983	two-component hybrid sensor and regulator	252	-1.5	-0.25 vs. 6	0
slr2042	hypothetical protein	25	-1.0	11 vs. 23	4.314E-09
slr2043	zinc transport system substrate-binding protein	20	1.5	3 vs. 13	6.91E-12
slr2044	zinc transport system ATP-binding protein	14	1.5	3 vs. 13	4.065E-13
slr2045	zinc transport system permease protein	92	1.7	3 vs. 18	0
slr2047	PhoH like protein	91	-1.1	11 vs. 23	0
slr2048	periplasmic protein. function unknown	100	2.2	1 vs. 13	0
slr2052	hypothetical protein	371	-2.9	1 vs. 13	0
slr2053	putative hydrolase	47	-1.1	11 vs. 13	0
slr2057	water channel protein	2756	3.3	11.75 vs. 18	0
slr2059	iron-sulfur cluster binding protein homolog	79	-1.1	3 vs. 13	0
slr2060	hypothetical protein	45	-1.6	6 vs. 13	0
slr2062	putative transposase [ISY052a: 1420842 - 1422331]	275	-1.5	1 vs. -0.25	0
slr2074	similar to mannose-1-phosphate guanylyltransferase	121	1.2	0.25 vs. 11	2.061E-10
slr2077	probable ABC transporter. periplasmic binding protein	107	1.1	6 vs. 12.25	0
slr2078	hypothetical protein	30	-1.1	1 vs. 12.25	0
slr2079	putative glutaminase	497	1.7	11.75 vs. 18	0
slr2080	hypothetical protein	388	1.0	11 vs. 23	4.065E-13
slr2084	hypothetical protein	123	-1.2	1 vs. 13	0
slr2095	putative transposase [ISY120c: 1561629 - 1562430]	163	-1.4	1 vs. 13	1.162E-07
slr2024	two-component response regulator CheY subfamily	130	1.2	6 vs. 18	0
slr2041	probable two-component response regulator	148	-1.2	3 vs. 18	0
slr2101	hypothetical protein	78	-1.2	6 vs. 12.25	0
slr2103	hypothetical protein	76	1.6	1 vs. 13	0
slr2100	two-component response regulator	33	1.1	-0.25 vs. 9	0
slr2107	probable polysaccharide ABC transporter permease protein	16	-2.3	-0.25 vs. 12.25	0
slr2108	probable polysaccharide ABC transporter ATP binding subunit	167	-2.3	1 vs. 11	0
slr2110	unknown protein	154	2.0	6 vs. 18	0
slr2111	unknown protein	52	-1.9	-0.25 vs. 6	0
slr2112	putative transposase [ISY100o: 1626093 - 1627038]	9	2.4	9 vs. 18	0.000001846
slr2114	perosamine synthetase	74	-1.7	-0.25 vs. 9	0

slr2115	unknown protein	506	-2.3	-0.25 vs. 6	0
slr2116	probable glycosyltransferase	583	2.6	6 vs. 18	0
slr2117	hypothetical protein	663	-2.9	-0.25 vs. 6	0
slr2118	unknown protein	155	4.0	6 vs. 18	0
slr2120	hypothetical protein	36	-1.2	6 vs. 13	0
slr2121	hypothetical protein	17	-1.3	6 vs. 23	0.0000003 23
slr2126	probable glycosyltransferase	479	1.8	6 vs. 23	0
slr2128	hypothetical protein	145	-1.2	1 vs. 13	5.185E-09
slr2131	RND multidrug efflux transporter	73	2.1	0.25 vs. 12.25	0
slr2132	phosphotransacetylase	35	-3.8	0.25 vs. 13	0
slr2136	GcpE protein homolog	122	1.1	23 vs. 13	0
slr2143	L-cysteine/cystine lyase	40	1.2	1 vs. 13	0
slr2144	periplasmic protein. function unknown	95	1.8	18 vs. 11	0
sml0009	similar to virulence-associated protein VapC	218	2.2	9 vs. 23	0
sml0010	putative transposase	28	4.0	9 vs. 23	0
sml0011	hypothetical protein	21122	-1.9	12.25 vs. 18	0
sml0012	hypothetical protein	1123	-1.1	1 vs. 13	0
sml0013	hypothetical protein	447	-1.5	-0.25 vs. 9	0
smr0002	putative transposase [ISY100v: 3095975 - 3096319. join 3097194 - 3097362. join 3098314 - 3098743]	17	3.8	6 vs. 18	0.0003997
smr0013	hypothetical protein	159	2.7	9 vs. 23	0
smr0015	hypothetical protein	115	1.0	23 vs. 13	0.0475930 47
ssl0105	hypothetical protein	454	1.1	3 vs. 13	1.219E-12
ssl0242	hypothetical protein	132	1.2	3 vs. 11.75	0
ssl0258	hypothetical protein	301	1.9	6 vs. 23	0
ssl0259	hypothetical protein	434	1.9	6 vs. 18	0
ssl0294	hypothetical protein	450	1.3	0.25 vs. 12.25	0
ssl0312	hypothetical protein	450	-1.1	1 vs. 9	1.764E-09
ssl0323	unknown protein	144	2.9	1 vs. 23	0
ssl0331	hypothetical protein	168	2.0	6 vs. 23	0
ssl0350	unknown protein	940	-1.9	-0.25 vs. 11.75	0
ssl0352	hypothetical protein	1039	2.0	0.25 vs. 12.25	0
ssl0353	hypothetical protein	201	-1.9	11 vs. 23	0
ssl0385	hypothetical protein	295	-1.7	1 vs. -0.25	0
ssl0426	putative transposase [ISY100t(partial copy): 141097 - 141410]	45	-1.6	-0.25 vs. 9	0
ssl0438	similar to 50S ribosomal protein L12	118	1.0	6 vs. 11.75	4.154E-10
ssl0461	hypothetical protein	260	1.3	11.75 vs. 18	0
ssl0467	unknown protein	288	2.3	0.25 vs. 13	0
ssl0483	hypothetical protein	3438	1.8	6 vs. 18	0

ssl0564	transcriptional regulator	88	2.1	6 vs. 13	0
ssl0738	unknown protein	51	3.3	9 vs. 18	0
ssl0739	hypothetical protein	33	3.5	9 vs. 18	0
ssl0750	unknown protein	72	-1.4	1 vs. 13	0
ssl0787	unknown protein	190	1.2	23 vs. 13	0
ssl0788	hypothetical protein	311	-1.5	11 vs. 23	0
ssl0832	hypothetical protein	498	-3.9	1 vs. 13	0
ssl0900	hypothetical protein	86	-1.1	6 vs. 13	0
ssl1004	hypothetical protein	255	-1.5	3 vs. 18	0
ssl1046	hypothetical protein	2512	-4.8	0.25 vs. 12.25	0
ssl1047	hypothetical protein	332	-1.2	3 vs. -0.25	0
ssl1263	hypothetical protein	2947	1.5	11.75 vs. 23	0
ssl1300	hypothetical protein	306	-2.2	1 vs. 13	0
ssl1326	unknown protein	308	1.4	6 vs. 23	2.845E-12
ssl1328	hypothetical protein	128	-1.2	1 vs. 12.25	0
ssl1376	hypothetical protein	347	-2.8	-0.25 vs. 9	0
ssl1377	hypothetical protein	181	-2.6	-0.25 vs. 6	0
ssl1378	hypothetical protein	169	-2.7	-0.25 vs. 9	0
ssl1464	unknown protein	38	1.3	0.25 vs. 11.75	0.016157687
ssl1498	hypothetical protein	2057	-4.9	-0.25 vs. 6	0
ssl1507	putative transposase [ISY508a: 1710788 - 1711753]	104	2.0	6 vs. 23	0
ssl1520	unknown protein	948	-4.9	3 vs. 13	0
ssl1533	unknown protein	5289	-4.4	1 vs. 13	0
ssl1577	hypothetical protein	28	-2.2	1 vs. 13	0
ssl1690	hypothetical protein	895	-1.9	6 vs. 18	0
ssl1707	hypothetical protein	78	1.8	1 vs. 13	0
ssl1762	hypothetical protein	17633	3.6	-0.25 vs. 6	0
ssl1792	hypothetical protein	34	2.4	3 vs. 23	0
ssl1807	hypothetical protein	422	-2.5	3 vs. 23	0
ssl1918	hypothetical protein	83	1.7	9 vs. 18	0
ssl1920	putative transposase [ISY523l(partial copy): 520871 - 521420]	53	1.4	9 vs. 18	0.00007372
ssl1923	hypothetical protein	128	1.1	9 vs. 13	0.0001372
ssl2064	hypothetical protein	153	-2.1	-0.25 vs. 9	0
ssl2065	unknown protein	149	1.7	3 vs. 23	0
ssl2069	hypothetical protein	105	2.7	-0.25 vs. 6	0
ssl2100	unknown protein	97	1.1	3 vs. 18	9.33E-08
ssl2138	unknown protein	198	2.9	6 vs. 23	0
ssl2148	hypothetical protein	340	-1.7	9 vs. 18	0
ssl2153	probable ribose phosphate isomerase B	16	1.9	11 vs. 23	0.028861305
ssl2162	unknown protein	524	2.9	-0.25 vs. 11.75	0

ssl2245	unknown protein	6131	2.2	1 vs. 13	0
ssl2250	bacterioferritin-associated ferredoxin	246	-1.6	1 vs. 23	0
ssl2380	unknown protein	10470	1.5	3 vs. 0.25	0
ssl2384	unknown protein	881	-2.4	0.25 vs. 11.75	0
ssl2420	unknown protein	228	-2.2	-0.25 vs. 12.25	0
ssl2501	unknown protein	20196	-4.8	3 vs. 18	0
ssl2559	ferredoxin	163	1.9	1 vs. -0.25	0
ssl2595	hypothetical protein	177	2.5	3 vs. 18	0
ssl2648	hypothetical protein	229	-1.3	1 vs. 11	0
ssl2717	hypothetical protein	131	-2.0	23 vs. 13	0
ssl2733	hypothetical protein	571	-1.6	1 vs. 11	0
ssl2749	hypothetical protein	110	2.2	3 vs. 13	0
ssl2781	hypothetical protein	223	1.8	6 vs. 18	0
ssl2789	similar to resolvase	17	2.4	3 vs. -0.25	0.0002424
ssl2807	hypothetical protein	92	1.1	0.25 vs. 11.75	0.001736
ssl2814	unknown protein	800	3.9	1 vs. 12.25	0
ssl2823	hypothetical protein	133	1.3	9 vs. 13	0
ssl2874	hypothetical protein	317	1.5	0.25 vs. 11.75	0
ssl2920	hypothetical protein	248	-3.9	-0.25 vs. 6	0
ssl2921	hypothetical protein	229	4.0	3 vs. 23	0
ssl2999	hypothetical protein	260	-2.1	1 vs. 13	0
ssl3044	probable ferredoxin	241	4.2	1 vs. 12.25	0
ssl3127	similar to permease protein of ABC transporter	15	-2.9	3 vs. -0.25	4.065E-13
ssl3142	unknown protein	43	1.5	0.25 vs. 11.75	0.001212
ssl3177	hypothetical protein	1183	1.3	3 vs. 13	0
ssl3222	unknown protein	113	1.3	9 vs. 23	0
ssl3291	hypothetical protein	740	1.6	1 vs. 13	0
ssl3382	hypothetical protein	206	-1.3	-0.25 vs. 9	6.268E-07
ssl3389	hypothetical protein	311	-2.4	3 vs. 18	0
ssl3410	unknown protein	335	-1.2	0.25 vs. 12.25	0
ssl3446	hypothetical protein	251	3.9	-0.25 vs. 12.25	0
ssl3451	hypothetical protein	108	2.2	3 vs. 13	0
ssl3549	hypothetical protein	309	-1.4	3 vs. -0.25	0
ssl3573	hypothetical protein	149	-1.6	3 vs. -0.25	0
ssl3649	putative transposase [ISY120d(partial copy): 604956 - 605288]	217	-1.1	1 vs. 9	5.284E-12
ssl3692	hypothetical protein	101	-1.5	1 vs. -0.25	0
ssl3712	hypothetical protein	71	2.0	1 vs. 13	0
ssl3719	hypothetical protein	21	1.6	6 vs. 18	0.0000930 2
ssl3769	unknown protein	1212	2.6	-0.25 vs. 9	0

ssl3803	hypothetical protein	1300	1.6	3 vs. 13	0
ssl3829	hypothetical protein	40	2.1	6 vs. 0.25	0
ssr0109	hypothetical protein	334	-1.6	3 vs. 23	0
ssr0335	unknown protein	370	1.5	6 vs. 12.25	0
ssr0336	hypothetical protein	575	1.3	6 vs. 12.25	0
ssr0349	hypothetical protein	301	2.2	12.25 vs. 23	0.00002182
ssr0511	unknown protein	786	-1.0	1 vs. 23	0.00001991
ssr0536	unknown protein	3742	-1.6	1 vs. 9	0
ssr0550	hypothetical protein	184	1.7	1 vs. 13	0
ssr0657	hypothetical protein	68	-2.1	9 vs. 18	0
ssr0663	hypothetical protein	55	-1.5	1 vs. 23	0.000001923
ssr0692	hypothetical protein	42493	-4.3	1 vs. 13	0
ssr0693	unknown protein	363	-2.2	1 vs. 12.25	0
ssr0706	unknown protein	181	1.4	6 vs. 12.25	0
ssr0756	hypothetical protein	596	1.5	6 vs. 23	0
ssr0757	hypothetical protein	397	-1.2	1 vs. 18	0
ssr0759	unknown protein	252	-1.3	11.75 vs. 18	0
ssr0761	hypothetical protein	278	-1.0	1 vs. 9	0.001959
ssr0817	putative transposase [ISY352g: 3511668 - 3512290. join 3513238 - 3514051]	79	-1.4	1 vs. 23	0.0009891
ssr0854	hypothetical protein	57	-1.3	1 vs. 23	0.02077716
ssr0871	putative transposase [ISY352e: 2921301 - 2921595. join 3108631 - 3109754]	428	-1.9	1 vs. 13	0
ssr1038	unknown protein	2566	-4.6	1 vs. 13	0
ssr1041	hypothetical protein	47	1.8	3 vs. 23	3.729E-09
ssr1049	unknown protein	94	-1.8	1 vs. 12.25	0
ssr1155	hypothetical protein	449	-1.2	1 vs. 12.25	0
ssr1169	stress induced hydrophobic peptide homolog	2909	-1.4	6 vs. 18	0
ssr1175	putative transposase [ISY100v: 3095975 - 3096319. join 3097194 - 3097362. join 3098314 - 3098743]	91	2.0	9 vs. 23	0
ssr1238	hypothetical protein	416	-1.3	3 vs. -0.25	0
ssr1251	hypothetical protein	577	-5.3	0.25 vs. 12.25	0
ssr1256	hypothetical protein	95	-2.5	1 vs. 13	0
ssr1258	hypothetical protein	355	3.2	3 vs. 23	0
ssr1260	hypothetical protein	711	3.0	6 vs. 23	0
ssr1274	unknown protein	8	-5.6	-0.25 vs. 11.75	0.0001857
ssr1375	hypothetical protein	551	-2.0	18 vs. 11	0
ssr1407	hypothetical protein	330	-2.1	3 vs. 13	0
ssr1473	hypothetical protein	187	-2.9	-0.25 vs. 11	0
ssr1527	probable molybdopterin [MPT] converting factor. subunit 1	724	3.1	1 vs. 18	0

ssr1528	hypothetical protein	349	2.3	3 vs. 11.75	0
ssr1552	hypothetical protein	725	1.1	1 vs. 9	0
ssr1558	hypothetical protein	66	2.2	11.75 vs. 23	0
ssr1562	hypothetical protein	1158	-3.0	1 vs. 12.25	0
ssr1698	hypothetical protein	38	4.1	1 vs. 13	0
ssr1766	hypothetical protein	396	-1.1	1 vs. 23	3.881E-08
ssr1768	unknown protein	502	-1.1	1 vs. 9	0
ssr1853	unknown protein	164	-1.4	1 vs. 6	0
ssr2009	hypothetical protein	29	1.5	6 vs. 18	0.001771
ssr2016	hypothetical protein	268	5.8	0.25 vs. 11	0
ssr2047	hypothetical protein	400	-1.2	1 vs. 13	4.065E-13
ssr2049	unknown protein	161	-1.8	-0.25 vs. 9	0
ssr2060	unknown protein	101	2.4	9 vs. 13	0
ssr2061	glutaredoxin	546	1.0	3 vs. 13	0
ssr2062	hypothetical protein	1945	-6.6	0.25 vs. 13	0
ssr2066	hypothetical protein	1258	3.7	12.25 vs. 23	0
ssr2067	hypothetical protein	218	-3.8	-0.25 vs. 12.25	0
ssr2078	putative transposase [ISY802b(partial copy): 1384736 - 1385513]	81	-2.3	1 vs. 23	0
ssr2087	hypothetical protein	743	1.4	0.25 vs. 12.25	0
ssr2130	hypothetical protein	182	1.2	6 vs. 13	0
ssr2153	unknown protein	233114	-3.1	6 vs. 23	0
ssr2194	unknown protein	24	1.9	-0.25 vs. 6	1.951E-09
ssr2201	unknown protein	454	-1.1	1 vs. 18	6.178E-08
ssr2227	putative transposase	783	-6.0	3 vs. 23	0
ssr2317	unknown protein	88	-1.4	1 vs. -0.25	0
ssr2333	unknown protein	41	-2.1	11.75 vs. 23	0
ssr2406	unknown protein	108	-1.4	-0.25 vs. 12.25	0
ssr2422	unknown protein	80	-1.6	1 vs. 13	0
ssr2549	unknown protein	159	-1.6	6 vs. 18	0
ssr2551	hypothetical protein	22	1.5	-0.25 vs. 9	0.0233661 11
ssr2553	unknown protein	24	6.3	1 vs. -0.25	0
ssr2554	hypothetical protein	422	-1.6	1 vs. -0.25	0
ssr2611	hypothetical protein	293	1.1	1 vs. 13	0
ssr2615	hypothetical protein	156	1.8	9 vs. 23	0
ssr2708	hypothetical protein	55	-1.2	3 vs. 12.25	4.195E-10
ssr2710	hypothetical protein	111	-2.4	6 vs. 18	0
ssr2723	hypothetical protein	335	-1.0	3 vs. -0.25	0
ssr2754	hypothetical protein	721	-1.1	1 vs. 18	2.664E-09
ssr2781	hypothetical protein	176	1.1	1 vs. 13	0
ssr2787	unknown protein	67	-2.2	1 vs. 23	0

ssr2806	hypothetical protein	83	-2.4	0.25 vs. 12.25	0
ssr2843	hypothetical protein	66	-2.1	6 vs. 23	0
ssr2899	putative transposase [ISY523m(partial copy): 1483390 - 1484062]	47	2.4	-0.25 vs. 6	0
ssr2912	unknown protein	78	-2.8	9 vs. 23	0
ssr2962	hypothetical protein	239	-2.2	1 vs. 12.25	0
ssr2972	unknown protein	66	-1.5	1 vs. 18	0
ssr2975	unknown protein	107	-2.1	-0.25 vs. 6	0
ssr2998	hypothetical protein	3251	2.1	3 vs. 12.25	0
ssr3000	hypothetical protein	76	-3.2	-0.25 vs. 6	0
ssr3122	hypothetical protein	297	-1.3	-0.25 vs. 11.75	0
ssr3129	unknown protein	568	-4.3	1 vs. 18	0
ssr3159	unknown protein	57	1.9	6 vs. 23	0
ssr3184	4Fe-4S type iron-sulfur protein	507	-2.2	6 vs. 23	0
ssr3188	hypothetical protein	107	-1.6	9 vs. 23	0
ssr3189	hypothetical protein	6952	-1.1	0.25 vs. 13	0
ssr3402	unknown protein	178	1.6	6 vs. 18	0
ssr3409	hypothetical protein	44	1.4	-0.25 vs. 9	1.219E-12
ssr3410	hypothetical protein	63	-1.5	6 vs. 18	0
ssr3452	putative transposase [ISY352a(partial copy): 572672 - 572905]	104	-1.7	0.25 vs. 12.25	0
ssr3465	unknown protein	87	-2.0	1 vs. 13	0
ssr3532	unknown protein	851	-1.2	1 vs. 11	0
ssr3550	hypothetical protein	87	-1.7	3 vs. 11.75	0
ssr3570	unknown protein	206	-2.2	0.25 vs. 11.75	0
ssr3571	hypothetical protein	804	-1.8	1 vs. 13	0
ssr3572	hypothetical protein	1102	-1.5	1 vs. 13	0
ssr3588	hypothetical protein	192	-1.4	11.75 vs. 18	0
ssr3589	hypothetical protein	228	-1.4	11.75 vs. 18	0
sll7001	putative transposase [ISY391e(partial copy): 166 - 1298]	23	-2.4	-0.25 vs. 11.75	2.678E-09
sll7002	putative transposase [ISY391e(partial copy): 166 - 1298]	56	-2.7	-0.25 vs. 6	0
sll7003	plasmid stability protein	23	-1.4	0.25 vs. 13	0.03077284
sll7009	unknown protein	15	2.4	6 vs. 18	0
sll7027	unknown protein	11	2.4	1 vs. 23	0.01319839
sll7028	hypothetical protein	99	1.5	3 vs. 18	0
sll7029	hypothetical protein	34	1.9	1 vs. 18	0
sll7030	hypothetical protein	210	2.5	1 vs. 23	0
sll7031	hypothetical protein	123	1.9	1 vs. 13	0
sll7033	hypothetical protein	66	2.2	9 vs. 23	0
sll7043	unknown protein	32	2.2	9 vs. 23	0

sll7047	hypothetical protein	230	-1.8	6 vs. 13	0
sll7055	unknown protein	29	-2.4	1 vs. 12.25	0
sll7062	unknown protein	560	4.0	12.25 vs. 23	0
sll7063	unknown protein	308	3.1	12.25 vs. 23	0
sll7064	unknown protein	147	5.0	12.25 vs. 23	0
sll7065	unknown protein	68	4.8	12.25 vs. 23	0
sll7066	unknown protein	119	4.5	12.25 vs. 23	0
sll7067	unknown protein	398	-5.3	1 vs. 12.25	0
sll7069	hypothetical protein	44	3.8	11.75 vs. 18	0
sll7070	unknown protein	165	-4.1	-0.25 vs. 12.25	0
sll7085	unknown protein	215	-2.7	1 vs. 11	0
sll7086	unknown protein	29	-3.5	3 vs. 12.25	0
sll7087	unknown protein	61	-2.8	3 vs. 12.25	0
sll7089	unknown protein	76	-3.2	0.25 vs. 13	0
sll7090	unknown protein	96	-4.6	1 vs. 12.25	0
sll7106	exodeoxyribonuclease V. alpha chain	5	-1.4	-0.25 vs. 11	0.0005927
slr7005	integrase/recombinase	16	-3.6	1 vs. 13	0
slr7010	unknown protein	29	1.3	11 vs. 23	0
slr7011	unknown protein	29	1.1	11 vs. 23	0
slr7012	hypothetical protein	25	1.2	6 vs. 23	3.813E-07
slr7013	hypothetical protein	12	1.5	11 vs. 23	4.045E-07
slr7014	unknown protein	22	2.1	9 vs. 23	0
slr7023	hypothetical protein	13	-1.8	3 vs. 13	0
slr7026	unknown protein	277	1.2	6 vs. 12.25	0
slr7032	hypothetical protein	216	-2.0	-0.25 vs. 9	0
slr7041	probable growth inhibitor. PemK-like protein	42	1.3	11 vs. 23	3.252E-12
slr7049	resolvase	8	-2.1	-0.25 vs. 9	0.003521
slr7054	unknown protein	33	-1.0	6 vs. 12.25	0
slr7057	unknown protein	278	-1.1	1 vs. 13	3.249E-07
slr7058	hypothetical protein	192	-3.0	6 vs. 13	0
slr7059	hypothetical protein	195	1.2	-0.25 vs. 6	0
slr7068	hypothetical protein	37	1.1	11.75 vs. 18	7.838E-09
slr7071	hypothetical protein	41	-1.6	1 vs. 12.25	0
slr7076	hypothetical protein	755	-2.9	0.25 vs. 11.75	0
slr7080	unknown protein	87	1.4	0.25 vs. 13	0
slr7081	unknown protein	18	-1.1	3 vs. 12.25	0
slr7082	unknown protein	14	1.2	6 vs. 23	0.0000683
slr7088	hypothetical protein	143	-2.3	1 vs. 13	0

slr7091	hypothetical protein	121	-5.2	1 vs. 12.25	0
slr7092	hypothetical protein	64	4.0	11.75 vs. 23	0
slr7094	hypothetical protein	151	-1.4	6 vs. 0.25	0
slr7095	hypothetical protein	83	-1.6	6 vs. 0.25	0
slr7096	hypothetical protein	39	-1.0	3 vs. 0.25	0.048946991
slr7099	unknown protein	32	-1.9	-0.25 vs. 9	0
slr7100	unknown protein	45	1.6	0.25 vs. 13	0
slr7102	hypothetical protein	34	1.4	1 vs. 23	0
ssl7004	probable plasmid stability protein	34	-1.6	0.25 vs. 13	0.001234
ssl7021	unknown protein	77	-1.0	1 vs. 11	0.0004924
ssl7046	hypothetical protein	59	1.4	9 vs. 23	0.00002623
ssl7048	hypothetical protein	12	-2.0	3 vs. 23	0.010734235
ssl7051	unknown protein	73	-5.8	6 vs. 18	0
ssl7053	hypothetical protein	15	-3.9	6 vs. 23	0
ssl7074	hypothetical protein	268	-1.7	1 vs. 13	0
ssr7017	hypothetical protein	48	-1.9	-0.25 vs. 6	0
ssr7018	unknown protein	3459	-1.4	1 vs. 18	0
ssr7036	unknown protein	5625	-1.4	0.25 vs. 13	0
ssr7040	probable cell growth regulatory protein	57	2.0	6 vs. 23	0
ssr7072	hypothetical protein	71	-1.6	-0.25 vs. 9	0
ssr7079	unknown protein	49	1.4	6 vs. 12.25	0.000003291
ssr7093	hypothetical protein	106	3.9	11 vs. 23	0
sll8002	hypothetical protein	39	-1.4	0.25 vs. 13	0
sll8004	hypothetical protein	42	-1.5	3 vs. 13	0
sll8006	type I restriction-modification system. S subunit	462	-1.9	1 vs. 13	0
sll8007	unknown protein	213	-1.9	1 vs. 13	0
sll8012	unknown protein	66	-1.3	6 vs. 13	0
sll8017	unknown protein	262	-1.6	3 vs. 12.25	0
sll8018	hypothetical protein	64	-1.0	1 vs. 9	8.129E-13
sll8019	hypothetical protein	41	1.7	9 vs. 18	0
sll8020	hypothetical protein	20	-1.2	6 vs. 23	7.666E-10
sll8025	hypothetical protein	5	3.7	1 vs. 23	0.0009272
sll8034	2-nitropropane dioxygenase	28	-2.9	6 vs. 18	0
sll8035	hypothetical protein	10	-2.8	3 vs. -0.25	0
sll8040	unknown protein	40	-1.2	1 vs. 11	0
sll8043	putative transposase [ISY100y: 38542 - 39487]	22	-2.0	18 vs. 11	1.28E-10
sll8048	hypothetical protein	40	1.2	6 vs. 23	0
sll8049	type I site-specific deoxyribonuclease chain R	71	-1.1	6 vs. 23	0
slr8016	plasmid partitioning protein. ParB	46	-1.2	-0.25 vs. 9	0
slr8021	hypothetical protein	26	-1.9	6 vs. 18	0

slr8023	probable esterase	37	-1.7	3 vs. 18	0
slr8026	transcriptional regulatory protein MarR family	2089	-2.2	0.25 vs. 11.75	3.531E-08
slr8029	resolvase	16	-1.0	23 vs. 13	0.0000129
slr8036	probable acetyltransferase	372	-2.2	3 vs. 18	0
slr8038	WD-repeat protein	272	-2.9	6 vs. 23	0
slr8044	unknown protein	28	1.6	9 vs. 23	0
slr8045	putative transposase [ISY100x: 40984 - 41929]	24	-2.6	18 vs. 11	1.626E-12
ssl8003	unknown protein	55	-1.6	11.75 vs. 13	2.886E-11
ssl8005	hypothetical protein	164	-1.6	23 vs. 13	0
ssl8008	hypothetical protein	315	-2.3	3 vs. 13	0
ssl8028	hypothetical protein	101	1.5	11 vs. 23	1.069E-09
ssl8041	transposase	106	3.0	3 vs. 18	0
ssr8047	unknown protein	52	-2.4	-0.25 vs. 9	0
sll5002	unknown protein	510	1.7	3 vs. 13	0
sll5003	hypothetical protein	55	1.3	9 vs. 23	0
sll5006	unknown protein	20	1.8	11.75 vs. 23	5.077E-10
sll5014	similar to maturase	52	2.6	6 vs. 12.25	0
sll5026	hypothetical protein	42	1.5	9 vs. 23	0
sll5028	hypothetical protein	66	-1.4	0.25 vs. 11.75	1.616E-08
sll5030	hypothetical protein	123	1.3	6 vs. 23	0
sll5032	hypothetical protein	38	1.3	6 vs. 18	0.0000012 69
sll5033	hypothetical protein	44	-1.7	-0.25 vs. 6	0
sll5034	hypothetical protein	92	1.0	3 vs. 13	0
sll5035	transcriptional regulatory protein ArsR family	63	-2.2	18 vs. 11	0
sll5036	sulfide-quinone reductase	10	-1.3	3 vs. 23	0.00624
sll5041	putative transposase [ISY523u: 38789 - 39659]	24	1.1	6 vs. 11.75	0.003387
sll5042	probable sulfotransferase	22	1.4	3 vs. 18	1.011E-09
sll5046	unknown protein	39	1.4	1 vs. 13	0
sll5048	probable glycosyltransferase	50	-1.6	6 vs. 13	0
sll5050	probable glycosyltransferase	30	-1.2	-0.25 vs. 6	0
sll5052	similar to exopolysaccharide export protein	28	1.2	9 vs. 12.25	0
sll5059	two-component response regulator	73	1.1	9 vs. 13	0
sll5061	hypothetical protein	525	-2.0	1 vs. -0.25	0
sll5062	unknown protein	48	2.3	11 vs. 23	0
sll5066	probable plasmid partitioning protein. ParA family	15	3.5	3 vs. 18	0
sll5069	unknown protein	73	-2.3	6 vs. 23	0
sll5075	hypothetical protein	408	1.0	9 vs. 23	0.0000024 72
sll5076	hypothetical protein	62	1.6	9 vs. 18	0

sll5081	hypothetical protein	62	-2.9	-0.25 vs. 11	0
sll5083	unknown protein	274	1.4	9 vs. 23	0
sll5084	probable plasmid partitioning protein. ParB	100	1.4	11.75 vs. 23	0
sll5089	unknown protein	15	-1.5	6 vs. 11.75	2.154E-11
sll5090	unknown protein	34	2.1	11.75 vs. 23	0
sll5097	hypothetical protein	71	-2.3	1 vs. 13	0
sll5104	arsenate reductase	100	1.6	6 vs. 18	0
sll5109	unknown protein	23	-1.7	6 vs. 18	0
sll5122	SOS mutagenesis and repair. UmuC protein homolog	5	-1.3	3 vs. 12.25	0.004675
sll5123	SOS mutagenesis and repair. UmuD protein homolog	11	-1.5	-0.25 vs. 13	0.0001359
sll5128	unknown protein	195	1.8	3 vs. 23	0
sll5130	hypothetical protein	29	2.6	3 vs. 13	0
sll5132	hypothetical protein	51	1.7	3 vs. -0.25	0
slr5010	integrase/recombinase	58	-2.9	3 vs. 13	0
slr5012	hypothetical protein	80	1.5	11 vs. 23	0
slr5013	unknown protein	28	-2.5	-0.25 vs. 9	0
slr5016	unknown protein	85	1.4	6 vs. 23	0
slr5017	hypothetical protein	100	-1.6	-0.25 vs. 9	8.129E-13
slr5021	hypothetical protein	115	-2.1	3 vs. 13	0
slr5022	probable aminotransferase	24	1.0	6 vs. 23	0.009235
slr5023	hypothetical protein	74	-1.4	-0.25 vs. 9	0
slr5024	hypothetical protein	135	2.1	6 vs. 23	0
slr5029	putative transposase [ISY391d(partial copy): 31333 - 32206]	194	-1.4	1 vs. 23	0.0000621 4
slr5037	hypothetical protein	141	2.6	1 vs. 12.25	0.0000369 5
slr5051	unknown protein	126	-1.3	-0.25 vs. 13	0
slr5055	similar to UDP-N-acetyl-D-mannosaminuronic acid transferase	19	-1.3	3 vs. 18	0
slr5056	probable glycosyltransferase	25	-1.2	6 vs. 18	0
slr5077	hypothetical protein	158	-2.2	1 vs. 13	0
slr5082	hypothetical protein	124	-2.4	3 vs. 13	0
slr5085	unknown protein	9	2.4	11.75 vs. 23	0.0006267
slr5087	hypothetical protein	143	1.0	6 vs. 23	0
slr5088	probable short-chain dehydrogenase	94	-1.1	-0.25 vs. 9	0
slr5101	hypothetical protein	186	-1.4	1 vs. 12.25	0
slr5102	hypothetical protein	58	1.2	6 vs. 23	2.524E-10
slr5105	plasmid partitioning protein. ParA family	23	2.4	6 vs. 18	4.065E-13
slr5111	unknown protein	1441	-3.3	0.25 vs. 12.25	0
slr5112	unknown protein	236	-3.4	0.25 vs. 11.75	0
slr5116	hypothetical protein	70	2.1	3 vs. -0.25	0

slr5118	hypothetical protein	96	-1.7	1 vs. 13	0
slr5119	hypothetical protein	434	-1.8	1 vs. 13	0
slr5124	hypothetical protein	93	-2.3	1 vs. 13	0
slr5126	unknown protein	837	1.3	6 vs. 23	0
slr5127	unknown protein	229	-1.9	-0.25 vs. 6	0
ssl5001	unknown protein	84	2.0	3 vs. 12.25	0
ssl5015	unknown protein	39	1.8	6 vs. 23	0
ssl5065	unknown protein	15	-2.5	-0.25 vs. 9	0.0000221 6
ssl5068	unknown protein	18	2.6	-0.25 vs. 6	0
ssl5070	unknown protein	669	-2.0	3 vs. 0.25	0
ssl5091	unknown protein	11	-6.6	-0.25 vs. 11	1.759E-09
ssl5095	hypothetical protein	61	-1.1	18 vs. 11	0.0003881
ssl5096	unknown protein	20	-1.9	1 vs. 11	2.317E-08
ssl5098	unknown protein	346	-3.4	1 vs. 12.25	0
ssl5103	unknown protein	48	2.6	3 vs. 23	0
ssl5113	unknown protein	254	-1.5	1 vs. 13	0
ssl5114	unknown protein	112	1.1	-0.25 vs. 6	8.129E-13
ssl5129	hypothetical protein	40	2.4	1 vs. -0.25	0
ssr5009	unknown protein	142	1.6	-0.25 vs. 11.75	0
ssr5011	hypothetical protein	41	-1.8	1 vs. 13	0
ssr5020	hypothetical protein	69	1.9	1 vs. 23	0.000829
ssr5074	unknown protein	145	-1.5	-0.25 vs. 9	1.626E-12
ssr5106	hypothetical protein	13	2.4	6 vs. 18	6.007E-08
ssr5117	hypothetical protein	114	1.1	6 vs. 23	0
ssr5120	unknown protein	235	-1.5	0.25 vs. 13	0
ssr5121	hypothetical protein	593	1.8	11 vs. 23	0
sll6010	unknown protein	70	-2.5	6 vs. 13	0
sll6017	hypothetical protein	311	-1.8	1 vs. 13	0
sll6036	chromosome partitioning protein. ParA family	62	2.1	6 vs. 23	0
sll6069	unknown protein	68	-2.5	6 vs. 13	0
sll6076	hypothetical protein	312	-1.8	1 vs. 13	0
sll6093	chromosome partitioning protein. ParA family	41	2.2	6 vs. 0.25	0
sll6098	hypothetical protein	130	1.2	9 vs. 23	0
slr6005	unknown protein	8	-2.5	3 vs. -0.25	0
slr6006	unknown protein	4	-1.7	6 vs. 23	8.536E-12
slr6008	unknown protein	11	1.7	11.75 vs. 23	0
slr6009	unknown protein	6	-2.1	3 vs. 12.25	0
slr6011	probable nuclease	34	1.5	12.25 vs. 23	0
slr6012	unknown protein	922	-5.3	1 vs. 12.25	0
slr6013	unknown protein	655	-3.9	-0.25 vs. 12.25	0

slr6014	unknown protein	721	3.7	11.75 vs. 23	0
slr6015	unknown protein	379	-3.4	23 vs. 13	0
slr6016	unknown protein	515	-3.0	-0.25 vs. 11	0
slr6021	unknown protein	78	1.3	6 vs. 0.25	0.000001204
slr6022	unknown protein	25	-2.0	3 vs. 23	0
slr6029	hypothetical protein	27	1.2	0.25 vs. 13	0.0005039
slr6034	cytidine deaminase	88	1.1	11.75 vs. 18	2.032E-12
slr6037	arsenate reductase	243	2.2	3 vs. 23	0
slr6038	hypothetical protein	84	2.0	3 vs. 13	0
slr6039	hypothetical protein	316	3.6	-0.25 vs. 11	0
slr6040	two-component response regulator	148	3.2	-0.25 vs. 11	0
slr6041	two-component sensor histidine kinase	131	-2.4	3 vs. 23	0
slr6042	probable cation efflux system protein. czcB homolog	64	-2.0	3 vs. 0.25	0
slr6043	probable cation efflux system protein. czcA homolog	56	2.3	0.25 vs. 12.25	0
slr6044	hypothetical protein	213	3.1	0.25 vs. 13	0
slr6045	unknown protein	67	1.5	9 vs. 23	0.000012606
slr6047	hypothetical protein	109	-2.5	1 vs. 12.25	0
slr6049	hypothetical protein	296	-1.8	1 vs. 13	0
slr6050	hypothetical protein	475	-2.9	-0.25 vs. 11	0
slr6051	hypothetical protein	434	-3.3	-0.25 vs. 11	0
slr6056	probable transcriptional regulator	144	2.3	6 vs. 23	0
slr6057	hypothetical protein	190	1.1	6 vs. 11.75	0
slr6064	unknown protein	7	-1.9	3 vs. 23	0
slr6065	unknown protein	4	-1.9	3 vs. -0.25	4.739E-07
slr6067	unknown protein	13	2.4	11.75 vs. 23	0
slr6068	unknown protein	6	-1.4	1 vs. 12.25	8.007E-11
slr6070	probable nuclease	35	1.5	12.25 vs. 23	0
slr6071	unknown protein	925	-5.3	1 vs. 12.25	0
slr6072	unknown protein	656	3.8	12.25 vs. 23	0
slr6073	unknown protein	725	-3.8	-0.25 vs. 11.75	0
slr6074	unknown protein	378	-3.4	-0.25 vs. 13	0
slr6075	unknown protein	512	-2.9	-0.25 vs. 11	0
slr6080	unknown protein	78	1.4	6 vs. 18	1.492E-09
slr6081	unknown protein	24	-2.0	3 vs. 18	0
slr6088	hypothetical protein	24	-1.5	3 vs. 23	0.002368
slr6090	unknown protein	32	1.4	6 vs. 13	0

slr6095	type I restriction-modification system. M subunit (fragment)	36	-1.8	-0.25 vs. 9	0
slr6096	type I restriction-modification system. M subunit (fragment)	3	-2.6	-0.25 vs. 9	0.0000033 58
slr6097	type I site-specific deoxyribonuclease	328	1.8	6 vs. 23	0
slr6100	hypothetical protein	47200	-2.1	1 vs. 18	0
slr6103	hypothetical protein	182	-1.2	-0.25 vs. 9	0
slr6104	hypothetical protein	790	1.9	6 vs. 0.25	0
slr6106	hypothetical protein	43	-3.7	-0.25 vs. 6	0
slr6107	hypothetical protein	15	-1.1	1 vs. 13	0.0000037 22
slr6108	hypothetical protein	109	-1.5	-0.25 vs. 6	0
ssl6018	unknown protein	131	2.4	3 vs. -0.25	0
ssl6023	unknown protein	139	1.8	6 vs. 23	0
ssl6035	unknown protein	38	-3.5	-0.25 vs. 6	0
ssl6077	unknown protein	129	2.7	3 vs. -0.25	0
ssl6082	unknown protein	133	1.9	6 vs. 23	0
ssl6092	unknown protein	33	-2.2	-0.25 vs. 6	0
ssr6002	unknown protein	58	3.5	9 vs. 0.25	0
ssr6003	unknown protein	80	-3.3	-0.25 vs. 9	0
ssr6019	unknown protein	2447	-2.2	1 vs. 13	0
ssr6030	unknown protein	830	2.1	3 vs. 13	0
ssr6032	hypothetical protein	10	-3.4	6 vs. 23	0.001427
ssr6046	hypothetical protein	620	-4.7	1 vs. 12.25	0
ssr6048	unknown protein	530	-1.9	1 vs. 12.25	0
ssr6078	unknown protein	2444	-2.2	1 vs. 13	0
ssr6089	unknown protein	1089	1.7	1 vs. 13	0
ssr6099	unknown protein	158	-2.5	-0.25 vs. 12.25	0

ABBREVIATIONS

ePBR: phenometrics environmental photobioreactor, PBR: photobioreactor, ZT: zeitgeber time (hours past dawn), OD_{750}: optical density (absorption) at 750 nm, chl *a*: chlorophyll *a*, TOC: total organic carbon, TN: total nitrogen, OCP: orange carotenoid protein, NPQ: non-photochemical quenching, RM-ANOVA: Repeated Measurement Analysis of Variance, P-I: Photosynthesis versus irradiance, DCMU: 3-(3,4-dichlorophenyl)-1,1-dimethylurea, PSII: photosystem II: AET, alternative electron transport. ATP: Adenosine triphosphate NADPH: Nicotinamide adenine dinucleotide phosphate, RUBISCO: Ribulose-1,5-bisphosphate carboxylase/oxygenase, RPKM: reads per kilobase transcript per million, Ci: inorganic carbon.